EFFICIENT RELAY SELECTION TECHNIQUES FOR D2D COMMUNICATION UNDER USER MOBILITY AND PRESENCE OF OBSTACLES

By

Durgesh Singh

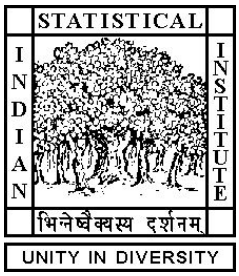

A thesis submitted in partial fulfillment of the requirements
for the degree of *Doctor of Philosophy* in *Computer Science*
at *Indian Statistical Institute*

Supervisor:

Prof. Sasthi C. Ghosh

Advanced Computing & Microelectronics Unit
Indian Statistical Institute
203 B.T. Road, Kolkata-700108

December 2021

To my Parents..

Acknowledgement

First and foremost, I am very thankful to my supervisor Prof. Sasthi C. Ghosh for accepting me as a student and giving me his guidance at every step of my life whether personal or professional. Sir has been a source of inspiration to do my work honestly and with zeal. I acknowledgment him for shaping my research orientation. When I joined him as Ph.D., I had zero knowledge about research, with his patient and motivation, I have come this far.

I would like to thank Dr. Arpan Chattopadhyay for giving me a chance to work with him, where I learned new technical skills. I thank all the professors of my department and during my M.Tech course Prof. Aditya Bagchi, Prof. Arijit Bishnu, Prof. Arijit Ghosh, Prof. Ansuman Banerjee, Prof. Bhabani P Sinha, Prof. Bhargab B. Bhattacharya, Prof. Debapriyo Majumdar, Prof. Diganta Mukherjee, Prof. Kishan C. Gupta, Prof. Krishnendu Mukhopadhyaya, Prof. Mandar Mitra, Prof. Nabanita Das, Prof. Sandip Das, Prof. Sasanka Roy, Prof. Sourav Chakraborty, Prof. Subhas Chandra Nandy, Prof. Susmita Sur-Kolay, Prof. Swapan K. Parui, Prof. Utpal Garain, for being available to me whenever I needed them. Kindly forgive me if I have missed some names. Their invaluable advice and visionary thoughts always intrigued me to learn more. The journey to my thesis, being away from my home, would not have been easy if they would not have been there. I would like to express my gratitude to late Prof. C. A. Murthy, whose zeal, applying innovative ideas, and impeccable teaching skills always made look big things simpler and which eventually enlightened my thought process.

I thank all the research scholars Gopi, Shankar, Dhrub da, Subhasis da, Subhankar, Uma Kant, Sameer Desai, Jayant Jha, Gopal, Kanishka, Sumit, Joginder, and rest all for making the environment full of knowledge with their discussions and lively which was an apt working condition. I thank all the non-teaching staff of the ACMU office and the institution for felicitating my work with their cooperation and processing all the help smoothly. I thank institution for providing the fellowship which never let me feel the financial stress. I thank the environment of this institution, greenery around it and the various trees in the campus have always captivated my attention and will make me remember this campus forever. I thank the administration, Dean Sir, CE Sir Brig J N Pandey (Retd), Mr. Utpal Mahto, Bappa da, and all others for all the help and allowing me to stay in the campus during covid times which made me submit my work on time. I thank my hostel mates and friends Archan, Abanti, Ashwin, Harmender, Ranjan, Subhadeep, Sanjana, and rest all for making me feel happy whenever I felt sad or were going through ups and downs during my Ph.D. tenure. We spent some of my life's most constructive and information rich discussions which involved long duration sessions related to mathematics and variety of interesting areas.

I want to thank my father Master Warrant Officer (retd.) Bhupesh Singh, whose stories and anecdotes on various scientists since childhood has raised my interest in pursuing research some day in my life. I would like to acknowledge the constant motivation and sacrifice by my mother (Mrs. Rambha Singh) since childhood which helped me come this far, my brother (Dr. Brijesh Singh) and sister (Smriti Singh) for being constant source of support and cherishing me love when I needed the most. I would like to acknowledge and thank my wife Dr. Vandana Singh whose constant support and motivation since start of my Ph.D. days, and believing in me has helped me reach this far. We spent long discussions, cherishable, intellectual, brain storming and interesting sessions related to almost every aspect of life on tea together. Last but not the least, I am very grateful to my sweet little daughter (Dhrivika Singh) who turned 16 months while writing this acknowledgnment. She has been a very important source of my happiness. She has taught me to keep on rising again after a fall, while she was learning to walk.

Abstract

Formalization of device to device (D2D) communication and millimeter wave (mmWave) technology into 5G and beyond cellular networks has given rise to novel challenges of multitude dimensions. Relay selection problem (RSP) is one such fundamental challenge in D2D communication where a user equipment (UE) acts as a relay to divert the communication path between two communicating UEs when they are not in vicinity of each other or when outages occur due to blockages. In this thesis, we developed several relay selection algorithms considering the mobility of the UEs as well as the presence of obstacles.

We first developed a network-assisted stochastic integer programming (SIP) model to incorporate uncertainty in network parameters due to UE's mobility. By utilizing the SIP model, we developed a greedy metric which is computed locally at each node on per-hop basis. This metric predicts the network parameters for upcoming *global* time instants based on information available at the current global time instant. We have developed relay selection algorithms for both network-assisted and device-controlled scenarios of D2D communication using the developed greedy metric. Here, we have considered the mobility of UEs, but presence of obstacles is not considered.

Next, we considered the RSP in the presence of obstacles. Since mmWave suffers from severe penetration losses, a given relay link might get disconnected easily, especially by dynamic obstacles which may change their positions abruptly. We developed a network-assisted probabilistic model which captures the mobility related parameters of UEs and dynamic obstacles by sensing via radars. A detailed analysis for capturing the dynamic obstacles using geometry is presented and an algorithm to select best relay which maximizes average data rate is developed. Here, the orientation in motion of dynamic obstacles is assume to be known at the base station (BS).

Orientation of the motion of dynamic obstacles is very difficult to measure accurately at the BS as it may *vary rapidly* compared to that of the speed and also the obstacles are not usually connected to the BS. We developed a network-assisted model to consider the scenarios where the orientation information is *unknown*. Using simple and innovative geometric techniques, we derived expressions for probability of blockages and based on them developed a relay selection algorithm.

The relay initially provided by the BS at global time instants may get blocked by unknown dynamic obstacles in near future during *local* time instants, thus leading to huge packet loss and delay. Dynamic obstacles may cause abrupt variations in channel quality and deferring to the BS for an appropriate solution would incur extra delay. Hence, a decision is made locally by source UE: i) to stop communication on the current relay and switch to a new relay by performing *directional search* in its vicinity, or ii) to continue on the current relay. For the former case, directional search comprises the exploration phase when a new relay is selected. Since the newly selected relay at the exploration phase itself is

vulnerable to blockages, it must be ensured that frequent relay switching is minimized while selecting a relay, as switching has a significant delay overhead. The UE has to locally decide during exploration phase: i) do not select the new relay link as it is likely to be obstructed and go for exploration on another relay link, ii) select the new relay link as it is likely to be free of obstacles and choose it for data transmission, or iii) send more probe packets as decision cannot be made at the current exploration phase and go for further exploration on the same relay link. Both decision problems are modeled using partially observable Markov decision process (`POMDP`) framework. The channel quality is learned via acknowledgments (`ACKs`) which are also vulnerable to blockages. Optimal threshold policy is derived for both problems. Later, we gave easy to use stationary policies, which is based on the number of successive `ACK` successes or `ACK` failures.

Through extensive simulations, we validated our theoretical findings. Our approaches outperform various other classical and state of art approaches.

PUBLICATIONS FROM THE CONTENT OF THE THESIS

Journal

- **D. Singh** and S. C. Ghosh, "Mobility-Aware Relay Selection in 5G D2D Communication Using Stochastic Model," in **IEEE Transactions on Vehicular Technology**, vol. 68, no. 3, pp. 2837-2849, March 2019.

Conference

- **D. Singh**, A. Chattopadhyay and S. C. Ghosh, "Local Relay Selection in Presence of Dynamic Obstacles in Millimeter Wave D2D Communication" in **55th IEEE International Conference on Communications (IEEE ICC)**, Montreal, QC, Canada, pp. 1–6 2021.
- **D. Singh**, A. Chattopadhyay and S. C. Ghosh, "Distributed Relay Selection in Presence of Dynamic Obstacles in Millimeter Wave D2D Communication" in **54th IEEE International Conference on Communications (IEEE ICC)**, Dublin, Ireland, pp. 1–6, 2020.
- **D. Singh** and S. C. Ghosh, "Network-Assisted D2D Relay Selection Under the Presence of Dynamic Obstacles" in **44th IEEE Conference on Local Computer Networks (IEEE LCN)**, Osnabrueck, Germany, pp. 129–132, 2019.
- **D. Singh** and S. C. Ghosh, "A distributed algorithm for D2D communication in 5g using stochastic model" in **16th IEEE International Symposium on Network Computing and Applications, (IEEE NCA)**, Cambridge, MA, USA, pages 459—466, 2017.

Manuscript submitted

- **D. Singh**, A. Chattopadhyay and S. C. Ghosh, "To Continue Transmission or to Explore Relays: Millimeter Wave D2D Communication in Presence of Dynamic Obstacles". (Submitted to **IEEE Transactions on Mobile Computing**. submission manuscript id: TMC-2021-08-0649).

Acronyms and Notations

QoE	Quality of Experience
UE	User Equipment
D2D	Device to Device
BS	Base Station
QoS	Qualtiy of Service
mmWave	millimeter wave
MIMO	multi input multi out
POMDP	partially observable Markov decision process
SIP	stochastic integer program
MINLP	mixed integer non linear program
CF	connectivity factor
DC-OC	Direct Communication-Operator Controlled
DR-OC	Device Relaying-Operator Controlled
DC-DC	Direct Communication-Device Controlled
DR-DC	Device Relaying-Device Controlled
SINR	Signal to noise ratio
LOS	Line of Sight
NLOS	Non line of sight
AODV	Adhoc on demand distance vector
LTE-A	Long term evolution-Advanced
PL	Path loss
PLE	Path loss exponent
CSI	Channel state information
RREQ	Route request
RREP	Route reply
NCF	Network assisted connectivity factor
DC-DCF	Device controlled distributed connectivity factor
PPP	Poisson point process
RSS	Received signal strength
CBF	contention based forwarding
ACK	Acknowledgment

$t, t+1, \cdots,$	Discretized global time instants.
Δt	Duration between consecutive time instants t and $t+1$.
l	Discretized local time instants.
δ	Duration between consecutive local time instants.
$G^t(N^t, E^t)$	Network graph at time t with nodes set N^t and edge set E^t.
(i, j)	Link between nodes/UEs i and j.
C_{ij}^t	Capacity of link (i, j) at time t.
ξ_{ij}^{t+1}	Conditional probability that link will be connected at time $t+1$ given it was connected at t.
$adj^t(i)$	Function that returns set of neighboring nodes of UE i at time t.
V_i^t	Speed of UE i at time t.
$\overrightarrow{V_i^t}$	Velocity of UE i at time t.
θ_i^t	Orientation of UE i at time instant t.
$\overrightarrow{T}_i^t$	Position vector of UE i at time instant t.
d_{ij}^t	Euclidean distance between UEs i and j at time instant t.
$\mathbb{K}$	Set of dynamic obstacles.
K	Total number of dynamic obstacles.
$\mathbb{R}$	Set of static obstacles.
R	Total number of static obstacles.
I_{ij}^{t+1}	Indicator Random variable capturing blockage of link (i, j) at $t+1$.
Q_{ij}^{t+1}	Received power at UE j from UE i at $t+1$.
$\overline{pl}_{ij}^{t+1}$	Received power component due to fading signal at $t+1$.
$\overline{pp}_{ij}^{t+1}$	Received power component due to penetration loss from obstacle at $t+1$.
Γ_p	Penetration loss from the blocking obstacle.
κ_{ij}	Threshold on received power for required communication on link (i, j).
$\mathbb{U}^i$	Viable set for UE i given by BS.
b_l^j	Belief of link j at local time instant l.
$\Phi(\cdot, \cdot)$	Bayesian Estimator function for the belief.
ζ	Cost of exploration of a new relay link.
$\mathbb{H}_l^j$	History vectors of ACKs for link j at local time instant l.
$J_l(\cdot)$	Cost function for the dynamic program at local time instant l

Contents

List of Tables

List of Figures

Chapter 1

Introduction

1.1 Background

There is an exponential surge in mobile users due to rapid emergence of media rich applications involving streaming of video and multimedia files. This has dramatically increased the data rate requirements in recent past and will be a major concern for near future too [2, 3]. Media-rich mobile applications like tele-presence and 3D holography will require data rates which can not be met by previous generation technologies like 4G networks [1]. Similarly, a compulsory data rate of 1.78 and 3.56 *Gbps* is required by applications like uncompressed video streaming [3]. Along with these bandwidth-intensive applications, new applications are emerging with rapid speed which require strict constraints on delay, higher data rate, robust and reliable network, lower power consumption and promise high quality of experience (QoE) to users [4, 1, 5, 2, 6]. To meet these requirements, 5G and beyond cellular networks have been proposed. Device to device (D2D) communication in 5G is a paradigm shift in cellular networks where devices or user equipments (UEs) in vicinity can communicate among each other with or without involving the base station (BS). D2D communication helps to meet aforementioned challenges along with spectrum reuse, offloading of overloaded BS, utilizing contextual information like location of UEs, enhancing connectivity at the cell edge and forming adhoc networks to provide connectivity when the BS is not present (e.g., in war fields) or destroyed in natural calamities (e.g., earthquake, hurricane, tsunami, flood, etc.) [4, 1, 5, 2, 6].

1.1.1 D2D Communication

In D2D communication, proximity mobile UEs in cellular network can communicate with each other with or without the need of the BS. The concept of D2D communication is already realized with standards like Bluetooth (IEEE 802.15.1), Zigbee (IEEE 802.15.4), Wi-Fi (IEEE 802.11) which utilizes frequencies in unlicensed band [1, 7, 2]. Operations in unlicensed band may not provide guarantee on the QoS requirements of mobile users compared to cellular

networks due to uncontrolled interference in unlicensed band. D2D communication brings in the concept of relays where a relay helps in passing on the data towards the destination node. To guarantee the QoS requirements, the D2D communication must be included in cellular networks standards under licensed band. Fixed relaying is included for 4G long term evolution advanced (LTE-A) cellular standard [8]. However, fixed relaying may not provide the full benefits like utilizing available communication space between two nodes which are in vicinity of each other. This brings in the concept of device relaying where a given device/UE may act as relay. This type of communication may take place with or without assistance from the BS depending upon the need of the application under consideration.

The architecture that supports D2D communication and used in this thesis is primarily based on two tiers namely macro-cell and device tiers [1]. The macro-cell tier consists of the conventional cellular architecture where base station communicates in the licensed bandwidth with the UEs. The device tier consists of UEs taking part in D2D communications. Here, proximity devices or UEs can communicate directly among themselves *with* or *without* the help of a BS which are referred as *operator-controlled* (OC) and *device-controlled* (DC) respectively. In both OC and DC categories, UEs can either directly send data to the destination (DC-OC & DC-DC [1] shown in Figure 1.1(i) & 1.1(iii) respectively) or can send data through intermediate UEs acting as relays (DR-OC & DR-DC [1] shown in Figure 1.1(ii) & 1.1(iv) respectively) to further transfer the data to the destination. In DR-DC and DC-DC there is no control of the base station for link establishment.

The D2D communication can be further classified as underlay or overlay to the BS depending upon the frequency re-use factor. In underlay scenario, a D2D pair shares resources with the cellular users while in overlay scenario a given D2D pair is allocated dedicated frequency band either inside the licensed band (*in-band*) or unlicensed band (*out-band*). In the underlay scenario, the D2D users might interfere with the conventional cellular users since the frequency is re-used. The *in-band* overlay scenario reserves additional licensed frequency for D2D communication which might be under-utilized if the reserved frequencies are not used for longer time period since licensed band is costlier. In the case of *out-band* overlay scenario, the frequency used is allocated from the unlicensed spectrum which is usually free of cost, however they might suffer from severe interference from other transmitters transmitting in the same frequency band. This introduces uncontrolled interference in device controlled scenario of D2D communication. In this thesis, we are dealing with the communication in device tier of the given network architecture involving in-band or out-band overlay type of communications.

1.1.2 mmWave Communication and Obstacles

Due to emergence of bandwidth-intensive applications, there is an urge to find new solutions to satisfy their required data rate need [3]. Recently, millimeter wave (mmWave) is widely studied for short range D2D communication [9] due to their high available bandwidth and

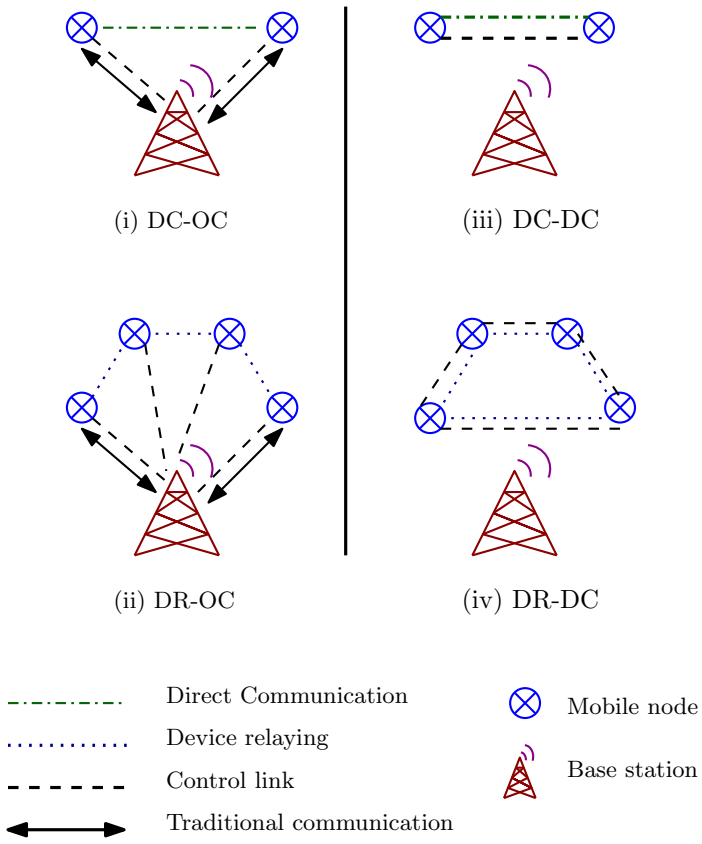

Figure 1.1: D2D architecture

capacity. mmWave is a band of radio frequencies in electromagnetic spectrum lying in range of 30 to 300 GHz. Due to very high frequency of mmWave, it suffers from higher propagation losses. However, it is compensated by using directional antenna arrays which focus the transmit beams towards the direction of the destination UE. The transmit and receive antenna gains are increased by placing a large number of antennas in a small region owing to mmWave's smaller wavelength. These multi-input multi-output (MIMO) antennas make the directional communication possible using beam-forming techniques [10].

However, mmWave channels are very much susceptible to the blockage by obstacles due to very high penetration loss [11, 3]. For example, penetration losses of about 40 dB for outdoor tinted glass at 28 GHz mmWave and 178 dB from a 10 cm brick wall at 40 GHz are mentioned in [11] and [12] respectively. This indicates that even a line of sight (LOS) communication for a given D2D link may get blocked [13, 14] by obstacles due to very high penetration loss of mmWave. Hence, it renders mmWave unsuitable in presence of such obstacles which may completely block the mmWave signal.

Searching or discovering neighboring UEs in order to establish new mmWave D2D links by the source UE requires some significant delay because mmWave beams are directional and narrow which takes some time in order to discover neighboring UEs in all directions. This is in contrast to traditional micro-waves of cellular networks which are broad-casted and

hence the delay required in establishing the link in neighborhood is negligible. One of the technique is to sequentially search the space in all directions to align transmitter and receiver beams (*beam alignment*). This overall process of beam alignment is termed as the *exploration phase* [15, 16]. Beam alignment is an important step before establishing a D2D communication link since even a small mis-alignment in transmitter and receiver beams may cause huge drop in signal quality. It has been experimentally shown in [17] that the orientation of a handset relative to the body or hand can cause very rapid fluctuations in signal quality even resulting in call drops. Different approaches for the alignment of transmitter and receiver beams can be found in [18] and references therein.

1.1.3 Relay Selection

To implement D2D efficiently, one has to solve several issues like service and peer discovery, resource allocation, mode selection, channel quality estimation, relay selection and power usage [1, 5, 2, 19, 20, 7, 21, 22, 23] among others. Relay selection is one of the most fundamental and challenging topic inherent to D2D communication. In the relay selection problem, appropriate UEs are chosen to transfer data packets from source to destination nodes or UEs when they are not in vicinity of each other or the communication path is blocked by some static or dynamic obstacle. Relays help in utilizing the available communication space between any two given UEs which can potentially participate in D2D communication. In network assisted scenario, relays help in connecting the mobile nodes at the cell edge with the network, where the network reachability is poor. In this scenario, relays are also useful in offloading the overloaded BS. In both network assisted and device controlled scenarios of mmWave D2D communication, D2D links are of short range and directional in nature and thus the multi-hop data transmission introduced by relaying UEs helps in mitigating the interference at the nodes locally. In addition, mmWave D2D links support applications requiring very high data rate given their applicability to short range communications. Here source UE, destination UE, the relaying UEs as well as obstacles may be mobile which makes the relay selection problem very challenging. One of the objective in this problem is to minimize the average delay while keeping the packet loss under control which is directly dependent on the selection of appropriate UE relays.

1.2 Motivation

1.2.1 Mobility of UEs

Efficient selection of an appropriate relaying UE/node is directly dependent on various network parameters like connectivity, capacity of links, packet loss, delay and throughput. These parameters are inherently dependent on temporal and spatial behavior of the mobile nodes. Unpredictable mobility makes it hard to decide whether a given node is a good relay at the moment of its discovery [24]. This shows that we must have to account for the

dynamic nature of mobile nodes which brings stochastic elements in this type of networks. Mobile nodes taking part in D2D communication send each other some information in the form of packets over the communication channel. Time is discretized as t, $t+1$, $\cdots$, where Δt is the small time difference between t and $t+1$. The challenge arises due to the fact that nodes may change their position from a time instant t to the next time instant $t+1$. Thus data packets transferred at time t may get lost at time $t+1$ while they are still in transit, due to the mobility of nodes. We are considering that for a little time difference Δt, there can be large impact on the distance and signal to noise plus interference ratio (SINR) after the link is established, depending on the velocity of the mobile users. A lot of research has been done to optimize one or more aforementioned objectives which considers only a snapshot of the network, which is inadequate when considering the velocity of nodes. Since the link quality between two nodes is not directly visible to the BS, and mobility of nodes can lead to exponential performance degradation depending upon average users' speed, global optimum solution when available to the mobile nodes may become less useful [25]. Thus we need to develop a framework based on predicting the future information by capturing various mobility related parameters locally. Most of the works consider mobility implicitly and hence the performance is tightly coupled with the considered mobility model [26]. Hence there is a need to model the mobility of nodes explicitly. Distribution of distance between nodes is analyzed in [27, 28] because distance between nodes is one of the parameters involved in computations of SINR. The analysis based on distance distribution might not dwell to practical solution when devices follow heterogeneous mobility settings with different speed ranges [29]. Hence there is a need to develop a metric which incorporates heterogeneous mobility of nodes into account explicitly.

1.2.2 Vulnerability of relays in presence of dynamic obstacles

Relays are useful when there is outage due to mobility of nodes as explained above. In addition, relays are also useful in diverting the communication path to mitigate the effects of outages due to blockages especially in mmWave D2D links. Various studies [30, 31, 32, 33, 34, 27] exist in literature to mitigate obstacle's severe effect. However, these studies take into account the static nature of obstacles which may not be true in practice where there may be dynamic obstacles moving throughout the given service region. The problem arising due to uncertainty caused by dynamic obstacles becomes more challenging when the UEs participating in the D2D communication are also in motion [35]. Note that even static obstacles become dynamic relative to moving UEs acting as source, destination or relays. Hence the relaying UEs which are also in motion might themselves get vulnerable to blockage by some obstacles. The authors in [14] showed a significant drop in data rate even when a pedestrian act as a blockage. For mmWave communication, capturing dynamic obstacles is a challenging task whose information may not be available apriori to the local nodes.

1.2.3 Challenges in capturing dynamic obstacles effectively

The speed and orientation of dynamic obstacles need to be computed in order to capture their effects on D2D links. In network assisted mode of D2D communication, where BS assists the devices in forming D2D links, to measure position, speed and orientation of the UEs and dynamic obstacles which effects D2D links, radars can be employed [36, 37], or vision cameras [14, 38] can be used to keep track of obstacles. However, capturing the instantaneous speed using these techniques is easy compared to measuring the instantaneous orientation in motion of obstacles accurately. This is due to the fact that the orientation of dynamic obstacles might change abruptly compared to the change in speed for a very small time duration. Capturing the orientation in motion of dynamic obstacle is also challenging due to the fact that they might not be connected to the network in comparison to UEs which are connected to the BS and thus can send regular update about their mobility related parameters. In such scenarios where the orientation in motion of the dynamic obstacles is *unknown*, capturing the effects of dynamic obstacles on mmWave D2D links is a challenging task.

1.2.4 Local proactive decisions to minimize delay in case of blockage

Initially, the BS may suggest source UE to continue communication via some D2D relay. However, with time the relay link suggested by the BS might deteriorate in quality causing severe packet loss for that D2D relay link. Thus there would be a problem of deciding whether to stop communication on that chosen mmWave D2D relay link in case of successive packet losses *or* whether to continue the transmission over it. Since the BS might undergo some delay in acquiring the local channel state information from the UEs, and, in addition, by the time UEs get global solution, it may become less useful due to change in positions of the UEs and dynamic obstacles. Hence, in case of successive packet losses, aforementioned decision must be made locally in a proactive manner. There can be other parameters local to a UE (like battery, channel availability, perceived throughput etc.) which may further create problems in implementing the global solution [25]. The authors in [37, 36] used radar to capture the movement of UEs and obstacles. Mobility related parameters of dynamic obstacles are not known a priori. Vision cameras and machine learning (ML) techniques were used by the authors in [39, 40, 14, 38] for tracking obstacle's spatio-temporal behavior. However all these require either expensive hardware or *high processing time* and *energy usage*. These might be apt at the BS but not at the UE which needs a local solution in an online fashion. The ML based solution in [40] might need re-training when there is a change in the environment. Moreover, it requires that the link breakage event must follow some well defined pattern with some known distribution. However, due to the presence of obstacles, variations in link quality behavior is abrupt. So these factors may not be perfectly modeled as also argued in [41], thus requiring an online and proactive approach. We aim to learn the dynamics of the environment at the UE locally in a timely manner. To account for the

dynamic obstacles locally, partially observable Markov decision process (POMDP) [42, 43, 44] can be used in modeling the variations in unobserved D2D links. Note that in such an environment where dynamic obstacles are present, even the acknowledgments (ACKs) can get lost due to the presence of dynamic obstacles.

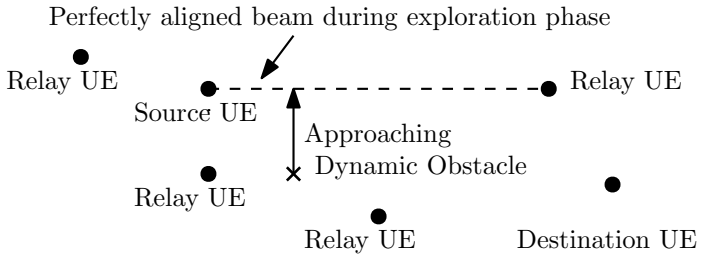

Figure 1.2: Perfectly aligned beam of source-destination during exploration susceptible for blockage due to dynamic obstacles.

1.2.5 Minimizing frequency in relay switching locally

In the aforementioned scenario, after making the decision of stopping communication on the current relay link due to occurrence of successive packet losses caused by blockage from dynamic obstacle, a new relay link in the source UE's vicinity is chosen by undergoing *exploration* phase. The exploration time which involves a directional search has a substantial delay (ranging from few microseconds to 10 ms [15]). Since there is presence of dynamic obstacles in the environment, newly selected relay links are also vulnerable to get blocked by those obstacles, even when the source and relay beams are perfectly aligned as shown in Figure 1.2. Also, the relay links which are selected based on highest data-rate may not be the best [39] as the relay itself may have higher chances of getting blocked. This might lead to frequent relay exploration and switching which causes increased delay, energy consumption and probably outage leading to call drops. Hence the frequency in relay switching must be minimized in order to satisfy the QoE of mobile users. This problem of relay selection during exploration phase is also challenging because the blockage occurs at the data transmission time (100-1000 times higher than exploration time) whereas decision of relay selection must be made at the exploration phase itself. Here also, the decision to explore and select a relay during exploration phase has to be made locally because exchange of channel state information with the BS might cause extra delay [45] along with delay in exploration phase.

1.3 Scope, Contributions and Outline of the Thesis

We have considered outages due to both mobility of nodes as well as due to blockage from static and dynamic obstacles on a mmWave D2D link while studying the problem of relay selection in D2D communication. Theoretical results have been shown for various cases involving both network assisted and device controlled scenarios. First, we focus on the

problem of relay selection considering the mobility of nodes and later we derive solutions for the relay selection problem considering the presence of obstacles in mmWave D2D link.

1.3.1 Propositions and the Methodology

For the problem of relay selection considering the mobility of nodes, we need to consider the mobility of nodes explicitly which brings stochastic elements into the network related parameters, thus affecting the network performance. We developed a generic metric termed connectivity factor (CF) which captures the heterogeneous mobility of devices and can be applied to both LOS and NLOS scenarios. To compute CF, either we need to know the distributions of mobility related parameters or knowing only the expectation and variance of these parameters is sufficient when the distributions are not known. This metric can then be applied to devise the relay selection algorithms for both network assisted and device controlled scenarios. To model this problem, stochastic integer programming is used which incorporates the uncertainty caused in network related parameters due to mobility of nodes explicitly. The performance of our algorithms are validated through extensive simulations and where they outperform other approaches.

Next, we looked into the relay selection problem where presence of obstacles in mmWave D2D link is considered. Dynamic obstacles may abruptly change their position blocking the communication path of a newly selected relay, thus making the relay selection problem more challenging. For the network assisted scenarios, we developed relay selection algorithm by capturing the presence of such dynamic obstacles effectively. We developed a probabilistic model which captures the mobility related parameters of UEs and dynamic obstacles. We utilized simple and innovative geometric techniques to derive expressions for probability of blockages and using them developed relay selection algorithms.

For the device controlled scenarios, the relay initially provided by the BS at global time instants may get blocked by unknown dynamic obstacles in near future during *local* time instants, thus leading to huge packet loss and delay. Hence a decision must be made either to continue on the current relay or explore another new relay. The extra delay incurred due to directional search performed during exploration phase for the mmWave antenna must be taken into account while making such a decision. We derived optimal threshold policies which take the decisions by counting only the number of successive ACK failures. Moreover, the newly selected relay at the exploration phase itself is vulnerable to blockages due to dynamic obstacles. It must be ensured that frequent relay switching is minimized while selecting a relay, as switching has a significant delay overhead. Here also, optimal threshold policies are derived where a decision of selecting or not selecting a given relay under exploration is made based on counting the number of successive ACK successes or ACK failures. Both decision problems are modeled using partially observable Markov decision process (POMDP) framework. The channel quality is learned via acknowledgments (ACKs) which are also vulnerable to blockages. Through extensive simulations, we validated our theoretical

findings. Our approaches outperform various other classical and state of art approaches.

1.3.2 Contributions and Outline of the thesis

To incorporate the uncertainty in various network parameters due to mobility of nodes, we first developed a network assisted stochastic integer programming (SIP) model. This model predicts the network parameters for upcoming time instance based on information available at current time instance. The SIP model is then converted to an equivalent deterministic mixed integer non-linear program (MINLP) model and then we proved its hardness result. By exploiting the constraints of MINLP, we developed a distributed greedy metric termed as *connectivity factor* (CF) which is calculated locally at each node on per-hop basis. It captures the nodes' mobility and hence takes care of link reliability which in turn controls packet loss and delay considering the interference at each node. It can be computed in $O(n)$ time, where n is the number of transmitters interfering with the given link. Our approach is applicable to any mobility model with relevant distributions of mobility parameters known. This is because CF is generic in nature which captures the heterogeneous mobility of devices and can be applied to both line of sight (LOS) and non-line of sight (NLOS) scenarios. We constructed perceived graph based on CF values to devise network assisted and device controlled relay selection algorithms for given source-destination pairs. This is shown in detail in Chapter 3. Along with this chapter, Chapters 4 and 5 also consider the mobility of nodes in part for the relay selection problem for mmWave D2D communication.

Along with the mobility of UEs, the relay selection problem in mmWave D2D communication must take into account the presence of static and dynamic obstacles. We devised different strategies in Chapters 4-7 for the relay selection problem considering blockages due to obstacles depending upon whether it is network assisted scenario or device controlled scenario.

Chapters 4 and 5 consider the network assisted scenario for the relay selection problem in mmWave D2D communication. In Chapter 4, we have developed a probabilistic model for relay selection which considers both moving UEs and dynamic obstacles. Then we have analyzed the probability of dynamic obstacles blocking a link in 3D Euclidean space by exploiting the information from MIMO radar connected to the base station. Finally, using this information, we have developed unique strategies based on simple geometry to find the best relay which maximizes the expected data rate. This is a network assisted strategy which assumes that the speed and orientation of both UEs and moving obstacles are known with high probability at the BS.

In Chapter 5, we have considered the scenario where orientations in motion of dynamic obstacles are *unknown*. This is due to the fact that the dynamic obstacles might not be connected to network in contrast to UEs which are well connected to the BS whose mobility related parameters can be acquired easily. Also, radars can be used to sense the speed and orientation of dynamic obstacles, but the variations in orientation of motion can

be sudden and abrupt in comparison to variations in their speed. This information is of utmost importance in order to capture dynamic obstacle's effects on a given mmWave D2D link which might get blocked by such obstacles. Here also, we formulated the problem in a probabilistic framework considering the fact that orientation in motion of dynamic obstacles is *unknown*, whereas, their speed is known along with known mobility parameters of UEs. The blockage probabilities are computed based on geometry which gives an unified and elegant approach applicable to general scenario of motion of UEs, i.e., given two UEs, either both UEs are static, or only one of them is moving, or both of them are moving. We have proposed solutions to find the best next hop direct/relay D2D node using assistance from the BS using the above mentioned approach.

In Chapters 6 and 7, we have looked at the relay selection problem locally at the UEs considering the presence of dynamic obstacles in mmWave D2D link. Also, we have assumed that there is no extra hardwares like radars or vision cameras available at the UEs for tracking obstacles.

The local channel condition of D2D relay initially given by the BS deteriorates gradually with time due to presence of dynamic obstacles and moving UEs. In such cases, a new relay needs to be chosen appropriately to stop potential heavy packet loss in further local time instances. In order to choose the appropriate relay node locally, first it must be ascertain that after how much successive packet losses one should go for exploring other good relay. In other words, the UE needs to make the decision locally, whether to *stop* communication on the current relay link or to *continue* communication on the current relay link undergoing successive packet loss. These decisions have to be made *locally* since D2D channel condition is local to UEs and propagating the quality of the D2D channel to BS by UEs may incur extra delay. We seek to learn the presence of obstacles in D2D channels using the finite horizon POMDP framework which helps in modeling the uncertainty introduced in link quality due to presence of obstacles. The objective here is to minimize the cost incurred due to delay when channel quality deteriorates due to successive packet losses, by making UEs choose locally the best possible decision between i) to stop communication on the current link and switch to another good relay link by exploring other possible UEs in its locality, or ii) to continue transmission on the current relay link itself. We showed that the optimal policy is a threshold based policy which checks whether a certain belief probability exceeds a threshold. The policy maps belief to the given set of actions. This is a non-trivial result that required proof of several interesting intermediate results. Our optimal policy can be implemented locally at each UE, thereby facilitating distributed implementation. The threshold policy is further reduced to counting the number of successive ACK failures, which is a simple and easy to implement and based on which UE can make appropriate decision locally. Chapter 6 describes our derived solution in great detail.

Furthermore, after making the decision to switch to another good relay as in the above mentioned problem, potential UEs in vicinity of the source UE must be explored in order

to select a new relay when the current link gets blocked. Frequent relay switching must be avoided which leads to call drops and high energy consumption. In Chapter 7 of this thesis, we have proposed the idea of reducing frequency in relay exploration and switching and thus average end-to-end delay (in seconds) at the expense of additional exploration time units (few milliseconds) during beam alignment. The source UE locally chooses that *action* among given set of actions at the exploration phase which minimizes the future expected cost which would be incurred to compensate for the delay due to packet loss: i) stop exploration on current link as it would become *bad* in near future, or ii) choose the current link under exploration for data transmission, or iii) transmit further probe packets to test the quality of D2D channel since current information is not enough to make a decision. The problem is formulated as a finite horizon POMDP. The model learns the channel quality in an online fashion using ACKs information which can also get lost due to blockage. The model does not require to undergo a training phase and hence suitable when there is a change in the environment. Here also, we showed that the optimal policy is threshold type policy which tells the UE to take appropriate decision locally. This is a non-trivial result that required proof of several interesting intermediate results. Our optimal policy can be implemented locally at each UE, thereby facilitating distributed implementation. Later, the threshold policy for the problem is further reduced to counting the number of successive ACK successes or ACK failures, which is simple and easy to implement solution.

In Chapter 8, we give the conclusion of works reported in this thesis and also some future works in this direction are mentioned.

The related literature is given in Chapter 2. The thesis is divided into three parts. Part I considers mobility of UEs in both network assisted and device controlled scenarios of D2D communication comprising of Chapter 3, part II considers network assisted scenario for mmWave D2D communication considering both mobility of UEs and dynamic obstacles comprising of Chapters 4 and 5. Part III considers device controlled scenario for mmWave D2D communication considering presence of dynamic obstacles in local D2D relay links comprising of Chapters 6 and 7. Bibliography is provided at the end of the thesis.

Chapter 2

Literature Review

Mobility of UEs

D2D communication in 5G is studied by several authors recently [4, 1, 5, 2]. The authors in [1] gave a two-tier architecture of 5G D2D communication. In *device tier*, proximity devices communicate directly among themselves with or without the need of a BS. Whereas, in *macro tier*, devices take part in conventional cellular communication. In [5, 7, 2, 21, 46, 22, 23], the authors discuss various issues and challenges in 5G D2D communication which are to be met for its successful implementation. Various optimization frameworks [47, 48, 49, 50] have been proposed for solving the challenges in D2D communication. An optimization framework for resource allocation problem is given in [47, 48]. Performance of D2D communication using a stochastic geometry analysis is done in [49]. A simple 5G D2D network design has been developed in [50] as an MINLP to minimize the average network delay. A cross layer network assisted relay selection scheme for D2D communication in LTE-A is developed in [51]. Outage probability analysis of full duplex relay assisted D2D network is done in [52]. All these works consider a snapshot of the network and do not consider the mobility of the nodes adequately, thus they are more suitable for stationary D2D users as argued in [26]. Effects of user mobility in D2D network is considered in [28] by using stochastic geometry tools. Stochastic geometry has been used to analyze the transmission capacity for relay assisted D2D network [53]. The authors in [27] have used stochastic geometry for improving the coverage and spectral efficiency of millimeter wave (mmWave) D2D communication. The authors in [26] stated that optimization methods and stochastic geometry are not able to provide appropriate tools to capture the nodes' mobility and change in network topology adequately. The authors in [54] showed how chance constrained programming (CCP) is helpful in predicting uncertain scenarios with some guarantee of success for autonomous vehicles path planning and thus claiming the usefulness of CCP. The author in [55] considered various telecommunication problems where stochastic optimization is used as a method to tackle uncertainty due to mobility of nodes.

Mobility can play an important role to ensure the performance of several network related

parameters [56, 57]. In [57], the authors surveyed the mobility models in vehicular adhoc network. Role of mobility on the behavior of energy and bandwidth efficiency has been discussed in [58] and node density has been considered to account for mobility. The authors in [59] concluded that mobility doesn't affect the performance of network much where mobile users are pedestrians. The authors in [60] discussed smart mobility solutions which reduces the signaling overhead for low speed mobile users. However, mobility can lead to exponential performance degradation depending upon node's speed as mentioned in [25]. The authors in [25] gave a network assisted method where the global optimum solution may or may not be used by nodes based upon local information. This method is not applicable in the device-controlled mode, where nodes may move independently without any support from BS. The authors in [61, 62] considered the mobility of nodes in terms of the contact time where contact time denotes the duration for which two nodes are within the transmission range of each other. The authors in [62] developed a distributed transmission strategy where the nodes use the local information opportunistically to choose the next hop node based on the contact time distribution. They emphasized on transmission of a single copy of a message to reduce the communication overhead. The authors in [26] argued that metric considering mobility implicitly (contact time) is tightly coupled with mobility models. Thus the performance of such metrics may be qualitatively different for various mobility models even when nodes have same average speed. They emphasized the importance of explicit mobility modeling which incorporates the user's movement directly into the optimization framework.

There is a need to develop metrics that should address the dynamic parameters due to mobility of nodes, not only for the network assisted case but also for the purely distributed case. There are several metrics described in literature and few to mention are in [63, 64, 24] to select the next hop, but they do not consider the mobility of nodes adequately. The authors in [65] argued that most of the studies give emphasis on network assisted approach and develop system centric metrics. Hence they developed a user centric metric but it also does not capture the mobility factor into account. SINR is a user centric metric which can be used to decide if a link should be active or not. But the authors in [66] discussed that SINR calculated in snapshot of network cannot be a good metric to predict link reliability due to the reason of mobility of nodes. Thus, it is required that mobility should be taken into account while computing the SINR values for the upcoming time instances. Distance between nodes is one of the parameters involved in computations of SINR. Distribution of distance between nodes is considered and analyzed in [27, 28] using stochastic geometry tools. The analysis based on distance distribution might dwell to an impractical solution when devices follow heterogeneous mobility settings with different speed ranges [29]. Supporting this argument, the authors in [67] studied and validated the impact of non-uniformly distributed users on the performance of 5G ultra dense networks. In this thesis, we have developed a distributed greedy metric which incorporates heterogeneous mobility of nodes into account

explicitly. The proposed metric not only takes care of the reliability of the link for the upcoming time instances but also predicts the variation in SINR and hence capacity of the link under consideration. This work is shown in great detail in Chapter 3.

Blockage due to Obstacles

High available bandwidth and short range transmission of mmWave is a attractive choice for D2D communication [9, 68]. However severe penetration loss of mmWave make it susceptible to very high blockage from various obstacles [13, 14, 69, 70], thus requiring an almost LOS communication path. This raises challenges while selecting relays in mmWave D2D communication, which have been studied recently in various works. Survey of mmWave communication can be found in [71] and the references therein. Most of the works [31, 32, 33, 34, 72, 27] deals with static obstacles. However, presence of dynamic obstacles in D2D channel make it more susceptible to unprecedented change in the link's quality. The authors in [14] showed a moving pedestrian acting as a source of blockage may cause significant drop in data rate. In network assisted mode, to capture the effects of obstacles, radars which uses Doppler effect can be used to track these obstacles. In wireless communication, it has been studied to synchronize wireless sensor nodes [73], to recognize human gesture [74], to locate people [75] and recently studied in [76] for search and rescue operations to locate trapped people in natural disasters. High reflection coefficient of mmWave in outdoor materials [11] makes them suitable for utilizing the Doppler effect phenomenon as in radars. Blockage detection performance of radars co-deployed with cellular system is analyzed in [37]. Recently, efforts have been made to leverage the MIMO radar along with mmWave communication system [77]. MIMO radar has also been the focus of recent study to get more accurate information of position of objects [78, 79]. In this thesis, we have developed a network assisted probabilistic model which captures the mobility related parameters of both UE and dynamic obstacles by utilizing the information sensed via radars. This model is then used to compute the blockage probability of any given link by dynamic obstacles using simple geometry. Later, we devised a relay selection algorithm to select the best relay which maximizes average data rate. This work is given in more detail in Chapter 4.

Also, the authors in [17] experimentally showed that the orientation of a handset relative to the body or hand can cause very rapid fluctuations in signal quality even resulting in call drops. Radars were used in [36] to keep track of obstacles and UEs to devise relay selection techniques. Vision cameras and machine learning (ML) techniques are used by the authors in [39, 40, 14, 38] for tracking obstacle's behavior which is used in predicting future data rates for a longer time horizon in the relay selection problem. Above techniques might not give accurate information of the instantaneous orientations of obstacles since they might change direction abruptly compared to that of the speed. The authors in [68] provided a solution which uses smart antennas at the blockage which helps in diverting the

communication through it. This might not be possible to put hardware on each moving obstacles and moreover, all dynamic obstacles might not be connected to the BS. The authors in [80] devised an infrastructure based relay selection technique for mmWave D2D communication. The relays placement is fixed and might need to be updated depending upon variations in signal caused due to presence of obstacles as the orientation of the obstacles is not considered. The authors in [41] devised an online relay selection technique considering dynamic blockage where the relays are unmanned autonomous vehicles (UAV). Here the relays have freedom to move in 3D space as when needed for a given source destination pair. However, in absence of UAV, for the UEs which act as relays and whose motion cannot be controlled, above mentioned solution might not be useful. The authors in [81] considered dynamic blockage and devised an N^{th} best routing technique. In case of dynamic blockage, the next best relay route among N best relays is chosen to avoid sudden call drops. This analysis considers static obstacles and chooses the next best relay when the current relay suffers blockage due to dynamic obstacles and UE mobility. However, due to motion of UEs and obstacles the channel information of N^{th} best relay might be outdated after some time instants and performance of the network might deteriorate due to dynamic obstacles. Hence there is a need to actively sense and analyze the presence of dynamic obstacles. In this thesis we have developed an analytical framework where the orientation in motion of the dynamic obstacles is unknown. A probabilistic analysis is presented using innovative idea from geometry. Geometry has also been used previously in [82, 36]. The authors in [82] used geometric analysis to characterize directional mmWave NLOS based on first order reflections. However, we developed a probabilistic model which uses geometry to provide probability expressions of blockage for a given link by dynamic obstacles considering the fact that the orientation in motion of these obstacles is *unknown*. Later, we have developed a relay selection technique using the above derived probability expression and the model. This work is shown in more detail in Chapter 5.

The change in mmWave D2D link quality is highly abrupt and depends upon the presence of dynamic obstacles which may not follow any prior known distribution. This change in link quality needs to be propagated [45] to the BS which might cause extra delay. Hence, as mentioned before, by the time this change is propagated to the BS and a global solution is provided by the BS, it might become less useful due to UE dynamics [83] and moving obstacles. Hence in these scenarios, a local solution needs to be provided at each UE. Also, at each UE it might not be possible to deploy extra hardware like Radars or vision cameras. The presence of obstacles and its tracking somehow needs to be learned [70]. For local solutions, placement of Radars or vision cameras might not work if the channel condition changes abruptly and processing time is too high. Also, the authors in [40] provided ML based solution to measure the link qualities for D2D relay selection problem in vehicular networks, however it might require to re-train the model when there is change in the environment. In such cases the link breakage event must follow some well defined pattern

with some known distribution. However, due to presence of dynamic obstacles, variations in link quality behavior is abrupt, making it difficult to perfectly model the environment as also argued in [41], thus requiring an online approach. The authors in [39] mentioned an online ML technique at the network which learns about the dynamics of the environment for enabling beam training to prevent blockages. However in this work we aim to learn the dynamics of environment locally. Enabling diversity [84] and multiplexing techniques along with the multi-beam reflection [85] are another options to efficiently utilize the highly available space through multi-beam communication paths. However to utilize its full potential, besides requiring extra resources and capturing bandwidth, it must also be ensured that individual components of the multi-beam path must also be free of the obstacles.

To account for the uncertainty in D2D links due to dynamic obstacles locally, POMDP [42, 43, 44] can be used in modeling the channel variations in unobserved D2D links. It has been used widely in many areas like scheduling, multichannel access, relay selection [86, 87, 88, 42, 89, 90, 91, 92] among others. The problem of whether to transmit or not in case of packet loss was first studied in a classical paper [93] which experimentally studied when to transmit or suspend transmission based on past estimates of success or failure transmission in order to save energy in transmitting packets which are going to get lost at the expense of little decrement in throughput. This was analytically studied by the authors in [86] using the POMDP framework. The authors assumed that the feedback is perfect, which might not be true due to presence of dynamic obstacles. In another work [90], the authors used POMDP to model the environment considering various types of feedback. It lacks to consider the cost due to delay induced by directional mmWave exploration. In case of blockage by dynamic obstacles, a new relay is chosen by exploring relay links through beam-forming [15, 16] which are in the source UE's vicinity. This involves a directional search of new relay and has a considerable delay. Detailed techniques for beam-alignment and beam-management under various scenarios can be found in [18]. The new relaying UE must be chosen carefully during exploration time (ranging from few microseconds to 10 ms [15] for short range), because it may get blocked during data transmission time (100-1000 times higher than exploration time) due to presence of dynamic obstacles, even when the source and relay beams are perfectly aligned to achieve highest data rate. It has been shown by the authors in [39] that the relay links selected based on highest data-rate may not be the best as it may have higher chances of getting blocked. This might lead to frequent relay exploration and switching resulting in increased delay, energy consumption and call drops. Hence, the problem of deciding to select any given relay during exploration should be dealt locally considering the presence of dynamic obstacles. In this thesis, we deal with two sequential decision problems. The first one is to make a local decision when packet loss occurs: whether to stop communication on the current relay link and explore and switch to a new relay link, or to continue the communication on the current relay link. The second decision problem deals with minimizing frequent relay switching in case the decision in

previous problem was to stop communication on the current relay link and explore and switch to a new relay link. Both of these problems are modeled using POMDP framework and optimal threshold policies are derived respectively in Chapters 6 and 7.

Part I

Mobility of UEs in Both Network Assisted and Device controlled scenarios of D2D communication

Chapter 3

Mobility Aware D2D Relay Selection using Stochastic Model

Much of the content of this chapter is copied from my own papers[1,2] *with the permission of my co-author Sasthi C. Ghosh. Even though the paper can be found in the literature, it is copied here so that I can make minor changes and clarifications for the convenience of the reader.*

In the relay selection problem appropriate relay nodes are chosen to transfer data packets from source to destination nodes when they are not in vicinity of each other. Here source node, destination node as well as the relay nodes all denote the `UEs` which may be mobile. When the source and destination are not in vicinity of each other, the intermediate relay nodes receive the data packets from the sending node and forward it to an appropriate next hop node which can be another relay or the destination node. Time is discretized as t, $t+1$, $\cdots$, where Δt is the small time difference between t and $t+1$. The challenge arises due to the fact that nodes may change their position from a time instant t to the next time instant $t+1$. Thus data packets transferred at time t may get lost at time $t+1$ while they are still in transit, due to the mobility of nodes. We are considering that for a little time difference Δt, there can be a large impact on the distance and `SINR` after the link is established, depending on the velocity of the mobile users. The objective could be to optimize various network parameters like capacity of links, packet loss, delay and throughput. These parameters are inherently dependent on temporal and spatial behavior of the mobile nodes. A lot of research has been done to optimize one or more aforementioned objectives which considers only a snapshot of the network [47, 48, 49, 50, 51, 52], which is inadequate when considering the velocity of nodes [26]. Since the mobility of nodes can lead to exponential performance degradation depending upon average users' speed, global optimum solution obtained by

[1]D. Singh and S. C. Ghosh. Mobility-aware relay selection in 5g d2d communication using stochastic model, IEEE Transactions on Vehicular Technology, 68(3):2837–2849, 2019.

[2]D. Singh and S. C. Ghosh. A distributed algorithm for d2d communication in 5g using stochastic model, IEEE 16th International Symposium on Network Computing and Applications (NCA), pages 1–8, 2017.

the BS, when available to the mobile nodes may become less useful [25]. Thus we need to develop a framework based on predicting the future information by capturing various mobility related parameters *locally*. Most of the works consider mobility *implicitly* [61, 62] and hence the performance is *tightly coupled* with the considered mobility model [26]. Hence there is a need to model the mobility of nodes *explicitly*. Note that different nodes may have different mobility patterns. This heterogeneity must also be captured while computing the SINR. Thus instantaneous SINR cannot be a good metric. Hence, we need a metric which can predict channel parameters (e.g., SINR) for the upcoming time instance $t+1$ which should be computed at the current time t and should also consider the heterogeneous mobility of nodes. We have developed such a metric and shown its computations along with its computational efficiency in the analysis section.

The organization of the chapter is as follows:

- We have developed a SIP model to capture the dynamic network parameters by incorporating node's mobility explicitly (section 3.1).
- We have converted the developed SIP to its equivalent deterministic MINLP and proved its NP-hardness (section 3.2).
- We have developed a distributed greedy metric termed as *connectivity factor* (CF) by exploiting the constraints of MINLP model, which captures the reliability and expected capacity of the links. This metric is computed locally at current time instance t which consists of the predicted information for the upcoming time instance $t+1$ with some probabilistic guarantee. We have shown that CF for a link can be computed in $O(n)$ time where n is the number of transmitters interfering to that link. CF is generic in nature which captures the heterogeneous mobility of devices and can be applied to both LOS and NLOS scenarios. To compute CF, either we need to know the distributions of mobility related parameters or knowing only the expectation and variance of these parameters is sufficient when the distributions are not known (section 3.3).
- We have constructed a `perceived graph` using the CF metric. Perceived graph consists of the predicted information for the upcoming time instance $t+1$ which is computed at the current time instance t. Then we developed relay selection strategies for both the network assisted and the device controlled scenarios using perceived graph (section 3.4).
- We have validated the performance of our algorithm through extensive simulations and the results are compared with a recent algorithm based on AODV as described in [94] (section 3.5).

The conclusion is mentioned in section 3.6.

3.1 Stochastic Integer Programming Formulation of the Problem

We consider a service region served by a single BS where mobile devices or UEs are sending information to each other in the form of packets using wireless communication channels. We assume that mobile devices are moving independently and have the capability to establish links among themselves for D2D communications. Time is discretized and a mobile device may change its position from a time instant t to the next time instant $t+1$, where Δt is the small time difference between t and $t+1$. A graph $G^t = (N^t, E^t)$ is used to represent the mobile network at a particular time instant t, where N^t is the set of all nodes representing mobile devices and E^t is the set of all edges which represents links between the nodes which are in transmission range of each other at time t. There is a single static BS which is connected to all user devices in the given service region. Each link (i, j) at time t has a capacity C_{ij}^t for sending the data packets. Links may not be symmetrical due to presence of interference and uncertain wireless channels due to node's mobility. We are considering the general case, where Γ is set of source, destination and demand triplets $< s_\zeta, r_\zeta, h_\zeta >$. Here h_ζ is the demand supplied by source node s_ζ to destination r_ζ. Let $F_{ij}^t(\zeta)$ be the flow from node i to j for the source-destination pair $\zeta \in \Gamma$ at time t, an integer quantity which represents the number of packets transferred. Let ξ_{ij}^{t+1} be the conditional probability that link (i, j) is active at time $t+1$ given that the link was active at time t. Let us define e_{ij}^t as a Boolean variable whose value is 1, if there is an edge between nodes i and j at time t, and 0, otherwise. Now ξ_{ij}^{t+1} can be defined as follows:

$$\xi_{ij}^{t+1} = P\{e_{ij}^{t+1} = 1 | e_{ij}^t = 1\},\ \forall (i,j) \in E^t. \tag{3.1.1}$$

We assume that the network exhibits short range dependent characteristics. The average network delay t_s at each hop for the traffic exhibiting short range dependent characteristics can be computed as [50], [95]:

$$t_s \equiv \frac{1}{\lambda^t} \sum_{(i,j)\in E^t} \left[\frac{\lambda_{ij}^t}{\chi_{ij}^t - \lambda_{ij}^t} \right]$$

where $\lambda_{ij}^t = \sum_{\zeta\in\Gamma} F_{ij}^t(\zeta)$ is the average traffic on link (i, j) at time t, $\chi_{ij}^t = C_{ij}^t$ is the service capacity of link (i, j) at time t and $\lambda^t = \sum_{\zeta\in\Gamma} h_\zeta$ is the total demand in the network.

We will give a SIP model whose objective is to minimize average network delay per hop while keeping the link failure probability below a predefined threshold. Let α_{ij} be the threshold on allowable link failure probability for link (i, j). We define an optimization variable ω_{ij}^t, a Boolean variable which denotes those links (i, j) that are selected at time t for flow of traffic among possible set of available links in E^t. We can say that if at time t, $e_{ij}^t = 1$ and link (i, j) is selected for flow of packets, then $\omega_{ij}^t = 1$ else $\omega_{ij}^t = 0$. We also

define a constant $\mathfrak{M}$ which denotes the total number of available channels with the BS. The SIP formulation for a multiple source-destination pair is as follows:

$$Minimize\ t_s \tag{3.1.2}$$

$$\sum_{j:(i,j)\in E^t} F_{ij}^t(\zeta) - \sum_{i:(j,i)\in E^t} F_{ji}^t(\zeta) = \begin{cases} h_\zeta, & \text{if } i = s_\zeta \\ -h_\zeta, & \text{if } i = r_\zeta, \zeta \in \Gamma \\ 0, & \text{otherwise} \end{cases} \tag{3.1.3}$$

$$\sum_{\zeta\in\Gamma} F_{ij}^t(\zeta) \leq E[C_{ij}^{t+1}] \cdot \omega_{ij}^t, \forall (i,j) \in E^t \tag{3.1.4}$$

$$F_{ij}^t(\zeta) \geq 0,\ \forall (i,j) \in E^t,\ \zeta \in \Gamma \tag{3.1.5}$$

$$\sum_{(i,j)\in E^t} \omega_{ij}^t \leq \mathfrak{M} \tag{3.1.6}$$

$$P\{e_{ij}^{t+1} = 1 | e_{ij}^t = 1\} \geq (1 - \alpha_{ij}) \cdot \omega_{ij}^t, \forall (i,j) \in E^t \tag{3.1.7}$$

$$\omega_{ij}^t \in \{0,1\},\ \forall (i,j) \in E^t \tag{3.1.8}$$

The flow constraint (3.1.3) signifies the amount of flow coming in is same as the amount of flow going out at time t at a particular node except for source and destination nodes. The capacity constraint (3.1.4) signifies that total flow on link (i,j) at time t cannot exceed the expected capacity $E[C_{ij}^{t+1}]$ of that link at the next time instance $t+1$. Constraint (3.1.5) signifies that flow at a link cannot be negative. Constraint (3.1.6) signifies that there can be at most $\mathfrak{M}$ links chosen for flow of traffic at time instance t as there are $\mathfrak{M}$ available channels. Constraint (3.1.7) captures the conditional probability of link reliability for the next time instance $t+1$ given that it is active at the current time instance t. It checks if the link breakage probability satisfies the given threshold α_{ij}. Depending upon this constraint, we decide at time t to choose the appropriate link in the source-destination path for next time instance $t+1$. Hence, this gives a guarantee over the link reliability probability.

In the next section, we will derive a way to convert the SIP to its equivalent MINLP. We will also prove that the converted MINLP is NP-hard.

3.2 Converting SIP to its equivalent MINLP

A classical way of solving an optimization problem with probabilistic constraints is to first convert the probabilistic constraints into its equivalent deterministic constraints and then solve the optimization problem involving deterministic constraints only. Before converting constraint (3.1.7) to its equivalent deterministic form, we first need to take into account the attenuation factors that affect the signal quality, which in turn affect the reliability of a link. The attenuation factors may be dependent on the device's mobility and other

environmental factors which needs to be incorporated in our stochastic framework. Let us denote the overall attenuation by Ω_{ij}^t, which is a random variable capturing the randomness of the signal power and in turn the capacity of link (i, j) at time t, assuming noise is constant for the channel. We can say that if $\Omega_{ij}^t \leq \gamma$, then then $e_{ij}^t = 1$ else $e_{ij}^t = 0$, where γ is a predefined threshold which determines the connectivity between two nodes. Now we will proceed to define the expectation $\mu_{ij}^t = E[\Omega_{ij}^t]$ and standard deviation $\sigma_{ij}^t = \sqrt{var(\Omega_{ij}^t)}$, where $var(\Omega_{ij}^t)$ is variance of Ω_{ij}^t. We assume these values are known for current time instance t. Assuming that link (i, j) is selected at time t ($\omega_{ij}^t = 1$), constraint (3.1.7) can be re-written as:

$$P\{\Omega_{ij}^{t+1} \leq \gamma | \Omega_{ij}^t \leq \gamma\} \geq 1 - \alpha_{ij} \quad \forall (i, j) \ \in E^t. \tag{3.2.1}$$

Here Ω_{ij}^{t+1} represents the attenuation factor for link (i, j) in the next instance $t + 1$. This is important because it gives a relationship of signal strength of mobile nodes for the upcoming time instance $t + 1$ which is computed at the current time instance t.

Remark 3.2.1. *When two random variables X and Y are independent then we can say their conditional probability satisfies $P(X|Y) = P(X)$.*

Using remark 3.2.1 and the previous assumption that nodes are moving independently, we can say that Ω_{ij}^{t+1} and Ω_{ij}^t are independent and we can again rewrite constraint (3.2.1) as:

$$P\{\Omega_{ij}^{t+1} \leq \gamma\} \geq 1 - \alpha_{ij} \quad \forall (i, j) \ \in E^t. \tag{3.2.2}$$

Using mean and variance of Ω_{ij}^{t+1}, we can convert probabilistic constraint (3.2.2) into its equivalent deterministic one using the approach stated in [96]. From constraint (3.2.2), we get,

$$P\left\{\frac{\Omega_{ij}^{t+1} - \mu_{ij}^{t+1}}{\sigma_{ij}^{t+1}} > \frac{\gamma - \mu_{ij}^{t+1}}{\sigma_{ij}^{t+1}}\right\} \leq \alpha_{ij}. \tag{3.2.3}$$

Remark 3.2.2. *If X is a random variable with mean ν and variance s^2, then for any real number $c > 0$, one-sided Chebyshev inequality (Cantelli's inequality) [97] can be stated as:*

$$P\left\{\frac{X - \nu}{s} > c\right\} \leq \frac{1}{1 + c^2}.$$

Using remark 3.2.2 with $c = \frac{\gamma - \mu_{ij}^{t+1}}{\sigma_{ij}^{t+1}}$, constraint (3.2.3) becomes

$$P\left\{\frac{\Omega_{ij}^{t+1} - \mu_{ij}^{t+1}}{\sigma_{ij}^{t+1}} > \frac{\gamma - \mu_{ij}^{t+1}}{\sigma_{ij}^{t+1}}\right\} \leq \frac{1}{1 + \left(\frac{\gamma - \mu_{ij}^{t+1}}{\sigma_{ij}^{t+1}}\right)^2}. \tag{3.2.4}$$

Now constraints (3.2.3) and (3.2.4) implies $\frac{1}{1+\left(\frac{\gamma-\mu_{ij}^{t+1}}{\sigma_{ij}^{t+1}}\right)^2} \leq \alpha_{ij}$, which implies,

$$\mu_{ij}^{t+1} + \sigma_{ij}^{t+1}\sqrt{\frac{1-\alpha_{ij}}{\alpha_{ij}}} \leq \gamma. \tag{3.2.5}$$

We can now replace probabilistic constraint (3.1.7) with its equivalent deterministic constraint (3.2.5) and get two new constraints:

$$\mu_{ij}^{t+1} + \sigma_{ij}^{t+1}\sqrt{\frac{1-\alpha_{ij}}{\alpha_{ij}}} \leq \gamma + (1-\omega_{ij}^{t}) \cdot L_{inf}, \forall (i,j) \in E^t \tag{3.2.6}$$

$$\mu_{ij}^{t+1}, \sigma_{ij}^{t+1} \geq 0, \forall (i,j) \in E^t. \tag{3.2.7}$$

Here L_{inf} is a very large number representing positive infinity.

After converting the probabilistic constraint (3.1.7) in `SIP` formulation to its equivalent deterministic form, the final `MINLP` can be stated as: Minimize objective function (3.1.2) subject to the constraints (3.1.3)-(3.1.6), (3.2.6)-(3.2.7) and (3.1.8).

Proposition 3.2.1. *The MINLP formulated above is NP-Hard.*

Proof. Let us define a well known decision flow problem (ϱ) on graph $H(\hat{V}, \hat{E})$ with source and sink vertices as $\hat{s}$ and $\hat{r}$, capacity $C(e) \in Z^+$ and price $p(e), \forall e \in \hat{E}$. Demand is $B \in Z^+$ and there is a bound $M' \in Z^+$ on the total price of selected edges. Problem ϱ is defined as: is there a flow function $f : \hat{E} \to Z^+$ satisfying the following constraints:

$$\sum_{(i,j)\in\hat{E}} f(i,j) - \sum_{(j,i)\in\hat{E}} f(j,i) = 0, \ \forall \ i,j \in \hat{V} \setminus \{\hat{s}, \hat{r}\} \tag{3.2.8}$$

$$\sum_{(i,\hat{r})\in\hat{E}} f(i,\hat{r}) - \sum_{(\hat{r},i)\in\hat{E}} f(\hat{r},i) = B \tag{3.2.9}$$

$$0 \leq f(e) \leq C(e) \tag{3.2.10}$$

$$\sum_{e:f(e)>0, e\in\hat{E}} p(e) \leq M'. \tag{3.2.11}$$

In [98], it is stated that problem ϱ is NP-complete even when $p(e) \in \{0,1\}\ \forall e \in \hat{E}$.

Let us consider a decision version of `MINLP`, where we want to find if such a flow exists or not which satisfies the respective constraints. Let us assume that constraints (3.2.6)-(3.2.7) always satisfied assuming γ is very large number. Flow constraints (3.1.3) in `MINLP` is equivalent to constraints (3.2.8) and (3.2.9) in problem ϱ. Also capacity constraint (3.1.4) and non-negativity constraint (3.1.5) in `MINLP` are equivalent to constraint (3.2.10) in problem ϱ. In problem ϱ, $p(e) \in \{0,1\}\ \forall e \in \hat{E}$ implies whether an edge is selected or not. Thus constraint (3.2.11) of problem ϱ implies number of selected edges is bounded by M' which

is again equivalent to constraint (3.1.6) and (3.1.8) of our MINLP when $M' = \mathfrak{M}$. Hence we can say that problems ϱ can be reduced to the decision version of our MINLP and hence both are equivalent. This implies the developed optimization problem MINLP is NP-hard. □

Though our MINLP will give optimum solution but it will take considerable amount of time to produce solution because of the computational complexity of the problem. However, we can carefully exploit the constraints (3.1.4) (capacity constraint) & (3.2.6) (link breakage constraint) of MINLP to develop a greedy metric which can be used to produce a heuristic solution to transfer packets from source to destination. In the next section, we will derive the greedy metric from these two constraints and will show its efficient computation.

3.3 Greedy Metric & its Computation

Greedy Metric

Constraint (3.1.4) signifies the upper bound on the expected flow in the next time instance $t+1$, which is calculated at the current time instance t. We are considering this constraint because both communicating nodes are moving and thus interference dynamics from neighboring nodes are highly unpredictable which might reduce the data rate substantially. Hence, higher capacity at time t may not imply that the capacity requirements will be satisfied at the next time instance $t+1$. Constraint (3.2.6) signifies that the probability of a link which was present at time t will also be present in time $t+1$. Lesser the value on the left hand side of constraint (3.2.6), higher is the probability of the link to be connected at time $t+1$. By combining these two constraints, for each link (i,j) at time $t+1$, we define the greedy metric termed as connectivity factor (CF) and denoted by Λ_{ij}^{t+1} as follows:

$$\Lambda_{ij}^{t+1} = \frac{E[C_{ij}^{t+1}]}{\left(\mu_{ij}^{t+1} + \sigma_{ij}^{t+1}\sqrt{\frac{1-\alpha_{ij}}{\alpha_{ij}}}\right)} \tag{3.3.1}$$

Since this metric is applied to each link (i,j), it is computed at each node locally using the link related information from their respective neighboring nodes. If Λ_{ij}^{t+1} has higher value, then link (i,j) has higher chance of being chosen. Let us denote the numerator and denominator of CF as $\Im_{ij}^{t+1}$ and $\wp_{ij}^{t+1}$ respectively for all link (i,j) at time $t+1$. The numerator $\Im_{ij}^{t+1}$ decides the time it will take to transfer the packets because it represents the expected capacity of the link. Denominator $\wp_{ij}^{t+1}$ signifies link breakage condition. For a link (i,j) to exist at time $t+1$ with probability $1-\alpha_{ij}$, $\wp_{ij}^{t+1} \leq \gamma$ must be satisfied. If $\wp_{ij}^{t+1}$ has lower value, then it implies lower chance of link breakage which in turn means higher reliability of the link's existence for the next time instance $t+1$. All of these values are computed at the current time instance t.

In the analysis of the following subsections, we will show how to compute efficiently the

CF metric by incorporating the predicted information for the upcoming time instance $t+1$ on the link (i,j) under consideration. This analysis also shows how CF metric captures the local information when the mobile nodes can have heterogeneous mobility models.

Computations of μ_{ij}^{t+1}

To compute the components of CF value for a link, we will need to take into account the SINR values that each node receives from its neighbors because it is an important factor which gives information about the signal strength and link's capacity. Estimating SINR becomes critical due to mobility of nodes which effects the signal strength as well as interference from other nodes in proximity. We can say that two nodes i and j are connected at time t, if $S_{ij}^t \geq S_{th}$, where S_{ij}^t is the received SINR at time t and S_{th} is the threshold on minimum SINR required for a link to be considered as active. Since nodes i and j are moving, by the time they start communicating, the computed S_{ij}^t value may change by next time instance $t+1$. We need to model SINR and related parameters in terms of speed and direction of nodes which is developed in this and subsequent sections. We are giving a general network model which can take care of mobility of nodes irrespective of the mobility model chosen for the nodes.

We define attenuation factor as the inverse of SINR value between two links (i,j): $\Omega_{ij}^t = \frac{1}{S_{ij}^t}$ at time t, which is a random variable capturing the randomness of the signal power and in turn the capacity of link (i,j) at time t, assuming noise is constant for the channel. Now using this notation we can say that if $\Omega_{ij}^t \leq \gamma$, then there is an edge between nodes i and j, where $\gamma = \frac{1}{S_{th}}$. We will compute μ_{ij}^{t+1} of Ω_{ij}^t using the SINR expression at time t as stated below:

$$S_{ij}^t = \frac{Q_{ij}^t}{N_{th} + \mathbb{I}_{ij}^t}. \tag{3.3.2}$$

Here Q_{ij}^t is the power received by node j from node i, $\mathbb{I}_{ij}^t$ is the interference received on link (i,j) at time t and N_{th} is the thermal noise which is assumed to be constant. Both Q_{ij}^t and $\mathbb{I}_{ij}^t$ depend on the path loss (PL) model. PL is a function of distance and shadowing factors which both can be random [99]. We use the PL model given by [99, 100] which can be stated as follows:

$$Q_{ij}^t = P_i^t \cdot \mathfrak{K} \cdot \left(\frac{d_0}{d_{ij}^t}\right)^{\rho} \cdot \psi \tag{3.3.3}$$

Here P_i^t is the power transmitted by node i at time t. Here, $\mathfrak{K} = G_t \cdot G_r \cdot \left(\frac{\lambda}{4\pi d_0}\right)^2$ is a unit-less parameter which depends on the antenna characteristics and the average channel attenuation, G_t and G_r are the antenna gains at the transmitter and receiver respectively which is assumed to be constant for the analysis, $\lambda = c/f$ is the wavelength, c is the speed of light and f is the frequency. $\mathfrak{K}$ is assumed to be constant in the analysis. Here, d_0 is a reference distance for the antenna far-field, d_{ij}^t is the distance between nodes i and j at time t, ρ is the path loss exponent (PLE) and ψ is the shadowing random variable.

Shadowing component is random and can have any well known distribution p_ψ (e.g., log normal distribution [99]). Note that the ρ and ψ can take values depending upon whether LOS or NLOS communication takes place. We define Q_{ij}^{t+1} as the power received by node j from node i at the next time instance $t+1$ as follows:

$$Q_{ij}^{t+1} = P_i^t \cdot \mathfrak{K} \cdot \left(\frac{d_0}{d_{ij}^{t+1}}\right)^\rho \cdot \psi \tag{3.3.4}$$

Here Q_{ij}^{t+1} is a time dependent random variable which depends upon d_{ij}^{t+1} as well as the shadowing effect.

Now we will look into the denominator part of the SINR expression in equation (3.3.2) for the next time instance $t+1$: $N_{th} + \mathbb{I}_{ij}^{t+1}$. Here $\mathbb{I}_{ij}^{t+1}$ is the interference seen at the link (i,j) at time $t+1$ which can be expressed as:

$$\mathbb{I}_{ij}^{t+1} = \sum_{\forall k, k \neq i} Q_{kj}^{t+1}. \tag{3.3.5}$$

Now we can express Ω_{ij}^{t+1} as follows:

$$\Omega_{ij}^{t+1} = \frac{1}{S_{ij}^{t+1}} = \frac{N_{th} + \sum_{\forall k, k \neq i} Q_{kj}^{t+1}}{Q_{ij}^{t+1}}. \tag{3.3.6}$$

Assuming all devices transmit with the same power (i.e., $P_i^t = P,\ \forall i \in N^t$), the above expression can be simplified using equation (3.3.4) as:

$$\Omega_{ij}^{t+1} = \frac{\frac{N_{th}}{P \cdot \mathfrak{K} \cdot \psi} + \sum_{\forall k, k \neq i} \left(\frac{d_0}{d_{kj}^{t+1}}\right)^\rho}{\left(\frac{d_0}{d_{ij}^{t+1}}\right)^\rho}. \tag{3.3.7}$$

Equation (3.3.7) is used to find out the expectation and standard deviation of Ω_{ij}^{t+1} for the next time instance $t+1$. This calculation is made at the current time instance t. Note that ψ depends upon material of medium and assumed to be independent of time and in turn independent of d_{ij}^{t+1}. Let us represent the numerator and denominator of equation (3.3.7) by Ψ_n and Ψ_d respectively. Ψ_n is made up of two components $\frac{N_{th}}{P \cdot \mathfrak{K} \cdot \psi}$ and $\sum_{\forall k, k \neq i} \left(\frac{d_0}{d_{kj}^{t+1}}\right)^\rho$. Let us denote them by Ψ_{n1} and Ψ_{n2} respectively.

Remark 3.3.1. *If two random variables X and Y are independent then their measurable functions f(X) and g(Y) are also independent random variables.*

Proposition 3.3.1. *Ψ_n and Ψ_d are independent random variables.*

Proof. Ψ_n has two components Ψ_{n1} & Ψ_{n2}. Now both are independent to each other since random variables ψ and d_{kj}^{t+1} are independent. Since Ψ_{n1} is a function of ψ and Ψ_{n2} is a

function of d_{kj}^{t+1}, we can say that Ψ_{n1} and Ψ_{n2} are also independent using remark 3.3.1.

Note that Ψ_d is the function of random variable d_{ij}^{t+1}. Also, Ψ_n consists of Ψ_{n1} and Ψ_{n2} which are functions of two independent random variables ψ and d_{kj}^{t+1} respectively. Now we can see that Ψ_{n2} is calculated for the values of $\frac{d_0}{d_{kj}^{t+1}}$ for all k where $k \neq i$. So we can say that d_{kj}^{t+1} is independent of d_{ij}^{t+1}. Hence Ψ_n and Ψ_d are independent random variables. □

Therefore using above proposition we can say that the random variables in the equation (3.3.7) are independent of each other.

Remark 3.3.2. *if X and Y are two independent random variables then $E[X/Y] = E[X] \cdot E[1/Y]$.*

Remark 3.3.3. *if $X_1, X_2 \cdots, X_n$ are random variables then $E[X_1 + X_2 + \cdots + X_n] = E[X_1] + E[X_2] + \cdots + E[X_n]$.*

By taking expectation on both sides of equation (3.3.7) and using remarks 3.3.2 and 3.3.3, we get:

$$\mu_{ij}^{t+1} = \left(\frac{N_{th}}{P \cdot \mathfrak{K}} \cdot E\left[\frac{1}{\psi}\right] + \sum_{\forall k, k \neq i} E\left[\left(\frac{d_0}{d_{kj}^{t+1}}\right)^{\rho}\right]\right) \cdot E\left[\left(\frac{d_{ij}^{t+1}}{d_0}\right)^{\rho}\right]. \tag{3.3.8}$$

We will now find out $E\left[\left(\frac{d_{ij}^{t+1}}{d_0}\right)^{\rho}\right]$. Let us say nodes i and j have speed V_i^t & V_j^t with known distributions f_{V_i} in $[V_i^{min}, V_i^{max}]$ and f_{V_j} in $[V_j^{min}, V_j^{max}]$ respectively. Their angle of movements θ_i^t & θ_j^t are assumed to have known distributions f_{θ_i} & f_{θ_j} in $[-\pi, \pi]$ respectively. The positions of nodes i and j at current time instance t are (x_i^t, y_i^t) & (x_j^t, y_j^t) respectively. Let us denote their positions at next time instance $t+1$ as (x_i^{t+1}, y_i^{t+1}) and (x_j^{t+1}, y_j^{t+1}) respectively. Then the distance d_{ij}^{t+1} between them at time $t+1$ can be expressed as:

$$d_{ij}^{t+1} = \sqrt{(y_j^{t+1} - y_i^{t+1})^2 + (x_j^{t+1} - x_i^{t+1})^2}$$

where, $x_j^{t+1} = x_j^t + V_j^t \Delta t \cos\theta_j^t$, $y_j^{t+1} = y_j^t + V_j^t \Delta t \sin\theta_j^t$, $x_i^{t+1} = x_i^t + V_i^t \Delta t \cos\theta_i^t$ and $y_i^{t+1} = y_i^t + V_i^t \Delta t \sin\theta_i^t$. Here Δt is the small time difference between t and $t+1$. Expression for d_{ij}^{t+1} is dependent on four independent random variables V_i^t, V_j^t, θ_i^t & θ_j^t. Since we know the probability distribution functions (`pdfs`) of all of them, we can find $E\left[\left(\frac{d_{ij}^{t+1}}{d_0}\right)^{\rho}\right]$ as follows:

$$E\left[\left(\frac{d_{ij}^{t+1}}{d_0}\right)^{\rho}\right] = \int_{-\pi}^{\pi}\int_{-\pi}^{\pi}\int_{V_j^{min}}^{V_j^{max}}\int_{V_i^{min}}^{V_i^{max}} \left(\frac{d_{ij}^{t+1}}{d_0}\right)^{\rho} \cdot f_{V_i} \cdot f_{V_j} \cdot f_{\theta_i} \cdot f_{\theta_j} \quad dV_i^t dV_j^t d\theta_i^t d\theta_j^t. \tag{3.3.9}$$

Using the similar approach, $E\left[\left(\frac{d_0}{d_{ij}^{t+1}}\right)^{\rho}\right]$ can also be calculated. Similarly, $E[\frac{1}{\psi}]$ can be

calculated as follows:

$$E\left[\frac{1}{\psi}\right] = \int_{-\infty}^{\infty} \left(\frac{1}{\psi}\right) \cdot p_{\psi}. \tag{3.3.10}$$

Hence we can calculate the value of μ_{ij}^{t+1} as in equation (3.3.8).

Computations of σ_{ij}^{t+1}

We will use the similar approach as in previous subsection to calculate σ_{ij}^{t+1} of Ω_{ij}^{t+1} from its variance $var\{\Omega_{ij}^{t+1}\}$ as:

$$\sigma_{ij}^{t+1} = \sqrt{var\{\Omega_{ij}^{t+1}\}}. \tag{3.3.11}$$

By taking variance both sides in equation (3.3.7), we get:

$$var\{\Omega_{ij}^{t+1}\} = var\left\{ \frac{\frac{N_{th}}{P \cdot \Re \cdot \psi} + \sum_{\forall k, k \neq i} \left(\frac{d_0}{d_{kj}^{t+1}}\right)^{\rho}}{\left(\frac{d_0}{d_{ij}^{t+1}}\right)^{\rho}} \right\} \tag{3.3.12}$$

Remark 3.3.4. *if X and Y are two independent random variables then $var\{X/Y\} = E[X^2] \cdot E[1/Y^2] - E[X]^2 \cdot E[1/Y]^2$.*

Remark 3.3.5. *if $X_1, X_2 \cdots, X_n$ are independent random variables then $var\{X_1 + X_2 + \cdots + X_n\} = var\{X_1\} + var\{X_2\} + \cdots + var\{X_n\}$.*

As mentioned earlier, Ψ_n and Ψ_d are independent random variables. So using remark 3.3.4, equation (3.3.12) can be written as:

$$var\left\{\frac{\Psi_n}{\Psi_d}\right\} = \left\{ E[\Psi_n^2] \cdot E\left[\frac{1}{\Psi_d^2}\right] - E[\Psi_n]^2 \cdot E\left[\frac{1}{\Psi_d}\right]^2 \right\}.$$

Since $\Psi_n = \Psi_{n1} + \Psi_{n2}$, using remark 3.3.2 and 3.3.3, we can write above expression as:

$$\begin{aligned} var\left\{\frac{\Psi_n}{\Psi_d}\right\} = & \left\{ \left(E[\Psi_{n1}^2] + E[\Psi_{n2}^2] + 2 \cdot E[\Psi_{n1}] \cdot E[\Psi_{n2}] \right) \cdot E\left[\frac{1}{\Psi_d^2}\right] \right. \\ & \left. - \left(E[\Psi_{n1}]^2 + E[\Psi_{n2}]^2 + 2 \cdot E[\Psi_{n1}] \cdot E[\Psi_{n2}] \right) \cdot E\left[\frac{1}{\Psi_d}\right]^2 \right\}. \end{aligned} \tag{3.3.13}$$

Substituting the values of Ψ_{n1}, Ψ_{n2}, Ψ_d and using remark 3.3.3, we can write above expres-

sion as:

$$
\begin{aligned}
var\left\{\frac{\Psi_n}{\Psi_d}\right\} =& \Bigg\{\left(\frac{N_{th}^2}{P^2\cdot\mathfrak{K}^2}\cdot E\left[\frac{1}{\psi^2}\right] + E\left[\left(\sum_{\forall k,k\neq i}\left(\frac{d_0}{d_{kj}^{t+1}}\right)^{\rho}\right)^2\right]\right. \\
&+ 2\cdot\frac{N_{th}}{P\cdot\mathfrak{K}}\cdot E\left[\frac{1}{\psi}\right]\cdot\sum_{\forall k,k\neq i}E\left[\left(\frac{d_0}{d_{kj}^{t+1}}\right)^{\rho}\right]\Bigg)\cdot E\left[\left(\frac{d_{ij}^{t+1}}{d_0}\right)^{2\rho}\right] \\
&- \left(\frac{N_{th}^2}{P^2\cdot\mathfrak{K}^2}\cdot E[\frac{1}{\psi}]^2 + E\left[\sum_{\forall k,k\neq i}\left(\frac{d_0}{d_{kj}^{t+1}}\right)^{\rho}\right]^2\right. \\
&\left.+ 2\cdot\frac{N_{th}}{P\cdot\mathfrak{K}}\cdot E\left[\frac{1}{\psi}\right]\cdot\sum_{\forall k,k\neq i}E\left[\left(\frac{d_0}{d_{kj}^{t+1}}\right)^{\rho}\right]\right)\cdot E\left[\left(\frac{d_{ij}^{t+1}}{d_0}\right)^{\rho}\right]^2\Bigg\}. \qquad (3.3.14)
\end{aligned}
$$

The term $E\left[\left(\sum_{\forall k,k\neq i}\left(\frac{d_0}{d_{kj}^{t+1}}\right)^{\rho}\right)^2\right]$ in right hand side of equation (3.3.14) is quadratic and hence requires $O(n^2)$ time for computation. All other terms require $O(n)$ computation time. Here n is the number of transmitters interfering with the link (i,j). We assume that simple mathematical computations like addition and multiplication require $O(1)$ time. We will now show that this quadratic term can also be computed in linear time as stated in proposition 3.3.2 below.

Remark 3.3.6. *If $var(A)$ and $E[A]$ are respectively the variance and expectation of a random variable A, then we can say that $E[A^2]$=$var(A)$+$E[A]^2$.*

Proposition 3.3.2. *$var\left\{\frac{\Psi_n}{\Psi_d}\right\}$ in equation (3.3.14) can be computed in linear time.*

Proof. We can see that the term $E\left[\left(\sum_{\forall k,k\neq i}\left(\frac{d_0}{d_{kj}^{t+1}}\right)^{\rho}\right)^2\right]$ is making the computation of equation (3.3.14) quadratic by involving quadratic terms. Using remark 3.3.6 we can re-write this term as follows:

$$
E\left[\left(\sum_{\forall k,k\neq i}\left(\frac{d_0}{d_{kj}^{t+1}}\right)^{\rho}\right)^2\right] = var\left\{\sum_{\forall k,k\neq i}\left(\frac{d_0}{d_{kj}^{t+1}}\right)^{\rho}\right\} + E\left[\sum_{\forall k,k\neq i}\left(\frac{d_0}{d_{kj}^{t+1}}\right)^{\rho}\right]^2. \qquad (3.3.15)
$$

Using remarks 3.3.6, 3.3.5 and 3.3.3 we can re-write above as follows:

$$
\begin{aligned}
E\left[\left(\sum_{\forall k,k\neq i}\left(\frac{d_0}{d_{kj}^{t+1}}\right)^{\rho}\right)^2\right] =& \sum_{\forall k,k\neq i}\left\{E\left[\left(\frac{d_0}{d_{kj}^{t+1}}\right)^{2\rho}\right] - E\left[\left(\frac{d_0}{d_{kj}^{t+1}}\right)^{\rho}\right]^2\right\} \\
&+ \left(\sum_{\forall k,k\neq i}E\left[\left(\frac{d_0}{d_{kj}^{t+1}}\right)^{\rho}\right]\right)^2. \qquad (3.3.16)
\end{aligned}
$$

Now we can see that the right hand side of equation (3.3.16) can be solved in $O(n)$ time. This expression can be substituted in equation (3.3.14) to make its overall computation linear. □

Finally, σ_{ij}^{t+1} in equation (3.3.11) can be computed in linear time using equation (3.3.14).

Computations of $E[C_{ij}^{t+1}]$

The capacity of link (i,j) at the next time instance $t+1$ can be expressed using Shannon's theorem as:

$$C_{ij}^{t+1} = B \cdot \log_2(1 + S_{ij}^{t+1}) \tag{3.3.17}$$

$$= B \cdot \log_2 \left(\frac{N_{th} + \mathbb{I}_{ij}^{t+1} + Q_{ij}^{t+1}}{N_{th} + \mathbb{I}_{ij}^{t+1}} \right). \tag{3.3.18}$$

Here, B is the bandwidth of the signal, S_{ij}^{t+1} is the `SINR` on link (i,j) at time $t+1$. Taking expectation on both sides yield:

$$E[C_{ij}^{t+1}] = B \cdot E\left[\log_2 \left(\frac{N_{th} + \mathbb{I}_{ij}^{t+1} + Q_{ij}^{t+1}}{N_{th} + \mathbb{I}_{ij}^{t+1}} \right) \right]. \tag{3.3.19}$$

Substituting equations (3.3.4) & (3.3.5) in equation (3.3.19), we get:

$$\begin{aligned} E[C_{ij}^{t+1}] =& B \cdot E\left[\log_2 \left(\frac{N_{th}}{P \cdot \mathfrak{K} \cdot \psi} + \sum_{\forall k} \left(\frac{d_0}{d_{kj}^{t+1}} \right)^{\rho} \right) \right] \\ & - B \cdot E\left[\log_2 \left(\frac{N_{th}}{P \cdot \mathfrak{K} \cdot \psi} + \sum_{\forall k, k \neq i} \left(\frac{d_0}{d_{kj}^{t+1}} \right)^{\rho} \right) \right]. \end{aligned} \tag{3.3.20}$$

Let us denote $X = \frac{N_{th}}{P \cdot \mathfrak{K} \cdot \psi} + \sum_{\forall k} \left(\frac{d_0}{d_{kj}^{t+1}} \right)^{\rho}$ and $Y = \frac{N_{th}}{P \cdot \mathfrak{K} \cdot \psi} + \sum_{\forall k, k \neq i} \left(\frac{d_0}{d_{kj}^{t+1}} \right)^{\rho}$. Assume that there are n transmitters which are interfering to link (i,j). We can see that computing $E[\log_2(X)]$ requires computation of n different d_{kj}^{t+1} components corresponding to each of n interfering transmitters. Since computing each of d_{kj}^{t+1} requires evaluating a 4 dimensional integration, thus computation of $E[\log_2(X)]$ requires computing a $4n$ dimensional integration. Using the following remark, we can reduce the computation of $E[\log_2(X)]$ to n number of 4 dimensional integrations, which is computationally better than computing a $4n$ dimensional integration.

Remark 3.3.7. *If $Z \geq 1$ is a random variable with expectation $E[Z]$ and variance $var(Z)$ respectively, then $\ln(Z)$ around $E[Z]$ can be approximated using Taylor series as:*

$$\ln(Z) = \ln(E[Z]) + \frac{Z - E[Z]}{E[Z]} - \frac{(Z - E[Z])^2}{2 \cdot E[Z]^2} + \cdots$$

Neglecting higher order terms and taking expectation on both side in above yields,

$$E[\ln(Z)] \approx \ln(E[Z]) - \frac{var(Z)}{2 \cdot E[Z]^2}. \tag{3.3.21}$$

Now using remark (3.3.7), we can re-write $E[\log_2(X)]$ in terms of $\ln(E[X])$, $var(X)$ and $E[X]$, all of which can be computed in linear time. Similar argument holds for $E[\log_2(Y)]$ as well. Hence computation of $E[C_{ij}^{t+1}]$ takes linear time. Thus μ_{ij}^{t+1}, σ_{ij}^{t+1} and $E[C_{ij}^{t+1}]$ all can be computed in linear time.

Till now we have discussed how to compute the `CF` metric in a generic sense. For specific cases like `mmWave` communication, the G_t and G_r can be computed by incorporating the additional gain of the directional antenna arrays, as stated in the following remark. Accordingly the `CF` metric for such cases can be computed by using these values.

Remark 3.3.8. *Short range `D2D` communication involving `mmWave` channel usually employs directional antenna arrays with beam-forming capabilities which increases transmitter and receiver antenna gains (G_t & G_r) to compensate for high propagation loss [10]. For a uniform planar square antenna array composed of L_p elements, antenna gains can be written as [10]:*

$$G_x = \begin{cases} G_{ml} & \text{if } \theta \leq \phi/2 \\ G_{sl}, & \text{otherwise} \end{cases} \tag{3.3.22}$$

where $x = \{t, r\}$ is subscript for transmitter & receiver, $G_{ml} = L_p$ is the main-lobe gain, $G_{sl} = 1/\sin^2(3\pi/2\sqrt{L_p})$ is the side-lobe gain, $\phi = \sqrt{3}/\sqrt{L_p}$ is the beam-width, and $\theta \in [-\pi, \pi]$ is the angle off the boresight direction. Mobility of devices would make them go out of each other's range, hence at every such instance the alignment of transmitter-receiver pair needs to be done. However, this alignment overhead is in order of hundreds of micro seconds even for extremely narrow beams of width=1° as mentioned and validated in [101]. Since the data transmission time duration is in order of seconds, we can consider the alignment overhead to be negligible. So we are assuming that the transmitter-receiver pairs are perfectly aligned to obtain the maximum power gain as also done in [10]. In the simulation section, we have shown the effect of directionality on the end to end delay for different network loads in Figure 3.6.

3.4 Relay Selection Strategy

In this section, we will first construct a perceived network graph based on Λ_{ij}^{t+1} values. Then we will discuss the associated relay node selection strategy to find the source-destination path for both network assisted as well as distributed cases. We will describe the relay selection for all four types of `D2D` communication as shown in Figure 1.1.

3.4.1 Perceived Graph

We will now calculate Λ_{ij}^{t+1} values in algorithm 1 using the values of μ_{ij}^{t+1}, σ_{ij}^{t+1} and $E[C_{ij}^{t+1}]$ computed in previous section. This algorithm uses constraint (3.2.5) to compute Λ_{ij}^{t+1} as shown in line 5. Note that the reliability with certain guarantee (α_{ij}) is ensured by the

condition $\wp_{ij} \leq \gamma$ in this line. Each node runs this algorithm locally and shares Λ_{ij}^{t+1} values with the BS using channel state information (CSI) at current time instance t. These information are used at the BS to construct a *perceived graph* $G_{per}^{t+1}(N^{t+1}, \hat{E}^{t+1})$ as shown in algorithm 2. In G_{per}^{t+1}, $N^{t+1} = N^t$ and $\hat{E}^{t+1} \subseteq E^t$ such that $\Lambda_{ij}^{t+1} \geq 0$ & $(i,j) \in E^t$. Note that edges are not symmetric due to mobility and interference among nodes. It is also important to note that the perceived graph leverages the property of Λ_{ij}^{t+1} which keeps the delay and packet loss information for the upcoming time instance in a per hop basis. So G_{per}^{t+1} contains the information for the next time instance $t+1$ which is calculated at the current time instance t.

Algorithm 1: CF_Computation Algorithm

input : i, γ, α_{ij}, μ_{ij}^{t+1}, σ_{ij}^{t+1}, $E[C_{ij}^{t+1}]$

n_i; *//adjacent node set for current node i*
$\Lambda_{ij}^{t+1} \leftarrow (-1)$;
for $\forall j \in n_i$ **do**
  $\wp_{ij}^{t+1} := \left(\mu_{ij}^{t+1} + \sigma_{ij}^{t+1}\sqrt{\frac{1-\alpha_{ij}}{\alpha_{ij}}}\right)$;
  if $\wp_{ij}^{t+1} <= \gamma$ **then**
    $\Lambda_{ij}^{t+1} = \frac{E[C_{ij}^{t+1}]}{\wp_{ij}^{t+1}}$;
  end
end
return Λ_{ij}^{t+1};

Algorithm 2: Construct_Perceived_Graph Algorithm

input : $G^t(N^t, E^t)$, Λ_{ij}^{t+1}

$\hat{E}^{t+1} \leftarrow 0$;
for $\forall i \in \{1, 2, \cdots, N^t\}$ **do**
  for $\forall j \in \{1, 2, \cdots, N^t\}$ **do**
    if $(E^t[i][j] = 1)$ & $(\Lambda_{ij}^{t+1} \geq 0)$ **then**
      $\hat{E}^{t+1}[i][j] = 1$;
    end
  end
end
return $G_{per}^{t+1}(N^{t+1}, \hat{E}^{t+1})$;

The perceived graph (G_{per}^{t+1}) can be used for both *network assisted* and *distributed* scenarios. In the network assisted (DR-OC & DC-OC) scenario, when the BS is acting as the controller for forming the links among the nodes, this graph can be used by BS to predict with some success guarantee (depending upon α_{ij}) to establish a source-destination path. Since Λ_{ij}^{t+1} values are calculated locally for each link (i,j) on a per hop basis, we can also

use this metric in the distributed case in which nodes are moving in an adhoc manner without any BS assistance. Nodes in this setting will share the information among themselves as done in *route finding* phase of classical AODV protocol. In this scenario we assume that there are multiple route reply packets and the source node will wait for maximum of ϵ_t time after getting the first route reply packet to make decisions for the best path among all the available paths. This will essentially simulate a perceived graph which will give approximate solution restricted by ϵ_t time. This is elaborated in the next section.

3.4.2 Route Selection Algorithm

3.4.2.1 Operator Controlled (DR-OC & DC-OC)

In this mode, BS has complete topology information of the network and is responsible for finding a source-destination path. In DC-OC, data can be transferred directly to the destination when it is in vicinity of the source node. Otherwise, devices act as relays (DR-OC) and we need to choose the best relaying nodes along the path such that they minimizes overall packet loss and average delay.

If we choose a path with least average delay, it may not be the most reliable path, causing a lot of re-transmissions of data packets due to packet loss. If we choose a path with the highest reliability but with little consideration on the expected capacity, the selected path may cause higher delay. Hence, we need to choose a path which considers both reliability and expected capacity which has precisely been considered by our CF metric (Λ_{ij}^{t+1}). We can see that choosing the *widest path* in the perceived graph takes care of both reliability and delay. The widest path P_W^ζ for a source-destination pair $\zeta \in \Gamma$ is the path having maximum *width*, where width of a path P^ζ is defined as $\min_{\forall(i,j)\in P^\zeta}\{\Lambda_{ij}^{t+1}\}$. The widest path P_W^ζ of the perceived graph $G_{per}^{t+1}(N^{t+1}, \hat{E}^{t+1})$ can be found using a variation of Dijkstra's shortest path algorithm which runs in $O(|\hat{E}^{t+1}| \cdot \log(|N^{t+1}|))$ time. We term the procedure to compute widest path as WP(). Procedure WP() returns P_W^ζ and the bottleneck capacity $min\_cap\_P_W^\zeta = \min_{\forall(i,j)\in P_W^\zeta}\{C_{ij}^t\}$.

So the overall relay selection algorithm can be described as follows. Suppose a sending node s_ζ wants to send h_ζ packets to r_ζ. If they are in vicinity of each other, then DC-OC is activated and the BS instructs s_ζ to directly transfer packets to r_ζ in the current time instance t. If the capacity of the link is not sufficient, then the communication takes place in the next time instance and so on until h_ζ packets are transferred. If s_ζ and r_ζ are not in vicinity of each other, then BS assists for DR-OC type of communication where intermediate nodes act as relays for source-destination path. BS constructs the perceived graph at every time instance t using algorithm 2 and uses WP() routine to find the corresponding widest path. Nodes in the chosen path are directed by BS to transfer data packets bounded by $min\_cap\_P_W^\zeta$ using send_pkts_OC() function. Acknowledgments of successful packet delivery are handled by this function. One or more links in this path may break while the packets are in transit leading to packet loss. Also, not all of the packets may be transferred

to the destination due to capacity limitations of links in the path at the current time instance t. Hence an intermediate node i may posses the packets of the source node s_ζ after the time instance t ends. This procedure is shown in algorithm 3 which runs at `BS` for every time instance t until the destination receives all the packets.

Algorithm 3: Network assisted connectivity factor (`NCF`) Algorithm

input : $G^t(N^t, E^t)$, $\Gamma < s_\zeta, r_\zeta, h_\zeta >$

$G^{t+1}_{per}(N^{t+1}, \hat{E}^{t+1})$=$Construct\_Perceived\_Graph()$;
for $i = \{1, 2, \cdots, N^t\}$ **do**
  for $\forall \zeta \in \Gamma$ **do**
    if $(i \leftarrow \ sending\_node)$ **then**
      $(P^\zeta_W, min\_cap\_P^\zeta_W) \leftarrow WP(G^{t+1}_{per}, i, r_\zeta)$;
      $send\_pkts\_OC(P^\zeta_W, min\_cap\_P^\zeta_W)$;
      if $Packets\{r_\zeta\} == h_\zeta$ **then**
        remove ζ from Γ;
      end
    end
  end
end

3.4.2.2 Device Controlled (`DR-DC & DC-DC`)

In this mode, nodes themselves control the link establishment as they are not assisted by `BS`. Since they don't have the knowledge of complete network topology, so finding widest path in distributed fashion is a challenge. We will leverage the path finding techniques in adhoc networks known as `AODV` [64] for this purpose. In `AODV` there is a route finding phase in which source node floods a route request (`RREQ`) packet in the network. When `RREQ` reaches destination, a route reply (`RREP`) packet is sent back to source node from destination forming a source-destination path. We are considering a variant of `AODV` described in [94] which assumes that multiple `RREP` packets arrive at the source in the increasing order of the delay. In our route selection scheme we are storing the width of a path in the corresponding `RREP` packet instead of the delay. The source node after receiving the first `RREP` packet, holds the transmission of data for maximum of ϵ_t time. This is to ensure that the source node gets the `RREP` packet for a path $P^\zeta_W(\epsilon_t)$ which has maximum width among all the `RREPs` arrived at the source node during ϵ_t time and it is selected for the communication. This essentially constructs a perceived graph in a distributed fashion. Note that $P^\zeta_W(\epsilon_t)$ might not be the best path globally which was selected in the operator controlled mode because here the path chosen will have the width restricted by ϵ_t time. The function call `path_DC()` is used to find $P^\zeta_W(\epsilon_t)$ which essentially calls the route finding phase routines `RREQ` and `RREP`. Λ^{t+1}_{ij} is input to this function which is calculated as described in algorithm 1.

So the overall relay selection algorithm can be described as follows. Suppose node s_ζ wants to send h_ζ packets to r_ζ. The data transmission can take place directly if they are in vicinity of each other (`DC-DC`). If s_ζ and r_ζ are not in vicinity of each other (`DR-DC`), node s_ζ will check if it has the corresponding $P_W^\zeta(\epsilon_t)$ path using `path_exists_DC()` function, otherwise it finds this path using `path_DC()` function. Packets are sent via $P_W^\zeta(\epsilon_t)$ in a distributed fashion using `send_pkts_DC()` function call which also handles the acknowledgments of the successful packet delivery. Here also packet loss may occur due to one or more links failure or the capacity limitations of the links in $P_W^\zeta(\epsilon_t)$. Hence an intermediate relay node i may posses some packets of node s_ζ which are left unsent to node r_ζ at the end of time t. These packets will be transferred to the destination at the next time instance $t+1$ and so on until destination receives all the packets. This procedure is shown in algorithm 4 which runs at every time instance t at every node which has data to be sent.

Algorithm 4: Device controlled distributed connectivity factor (`DC-DCF`) Algorithm

input : i, ϵ_t, Λ_{ij}^{t+1}, $\Gamma < s_\zeta, r_\zeta, h_\zeta >$

```
1  if (i ← sending_node) then
2      for ∀ζ ∈ Γ do
3          if (i ≠ r_ζ) then
4              if (path_exists_DC(i, r_ζ)) then
5                  send_pkts_DC(P_W^ζ(ε_t));
6              end
7              else
8                  P_W^ζ(ε_t) = path_DC(i, r_ζ, Λ_ij^{t+1}, ε_t);
9                  goto Line 4;
10             end
11         end
12     end
13 end
```

3.5 Experiment and Results

Simulation Parameters

Simulation parameters are mostly taken from [102], [103]. Through simulations we are trying to analyze the strength of the proposed greedy metric and the associated algorithms. We are initially distributing 30 nodes uniformly in a 100×100 m^2 area. Nodes are moving independently following random walk mobility model with a speed uniformly distributed in $[0, V_{max}]$ m/s, where $V_{max} \in \{5, 8, 10, 12\}$ and their angle of motion is uniformly distributed in $[-\pi, \pi]$. Note that we have used random walk mobility model for computing μ_{ij}^{t+1}, σ_{ij}^{t+1} and $E[C_{ij}^{t+1}]$ in our simulation. However, similar approach can be extended for other

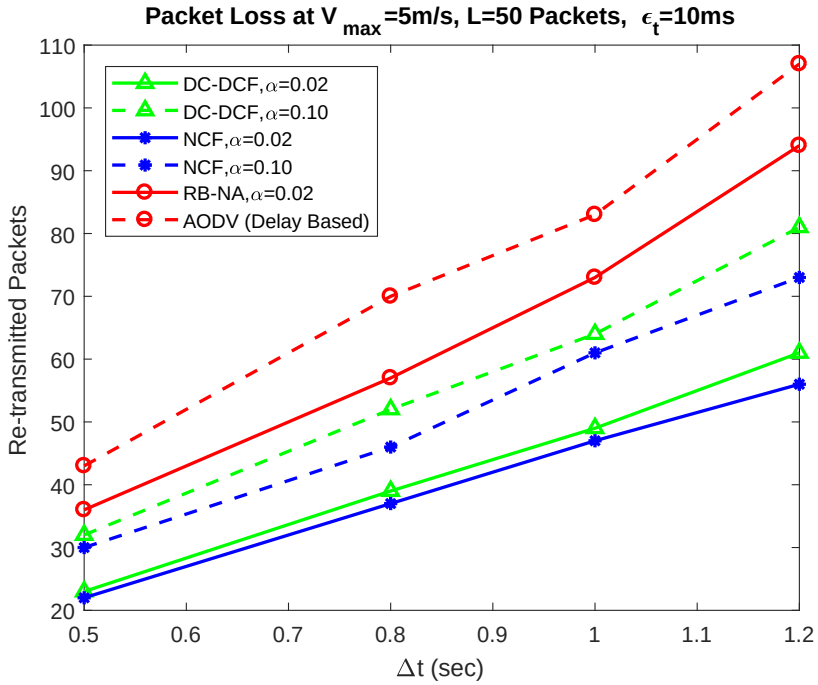

Figure 3.1: Depiction of the effects of Δt on packet loss.

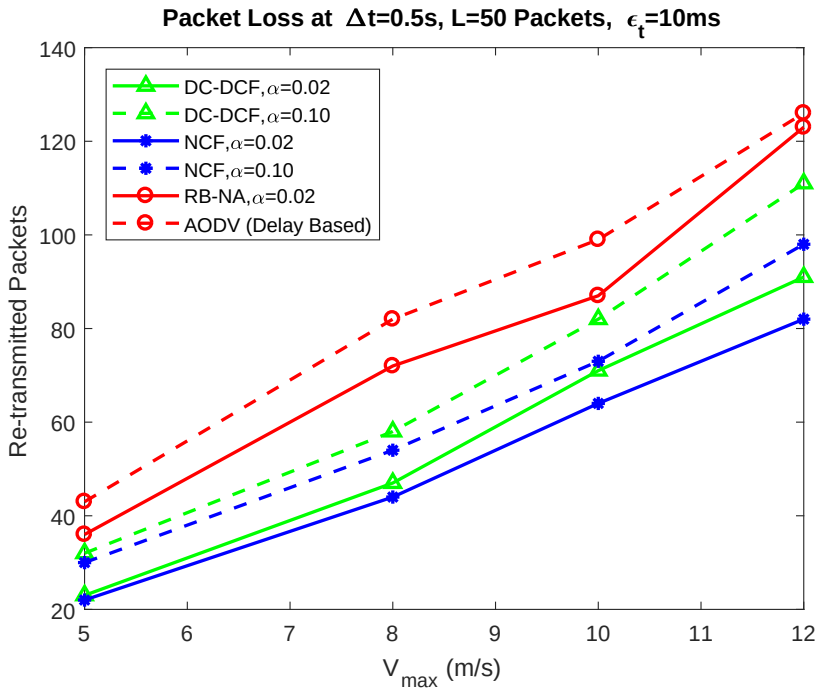

Figure 3.2: Depiction of the effects of variation in maximum speed on packet loss.

mobility models as long as the `pdfs` of the corresponding mobility parameters are known. We are assuming that at any instance of time the number of node are always 30 in the simulation region and all the nodes are capable of participating in `D2D` communication.

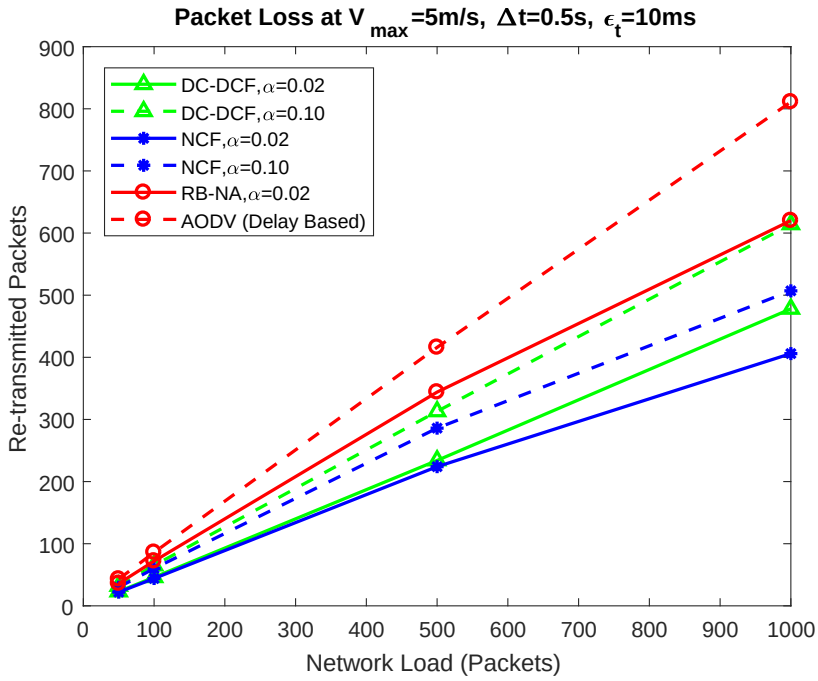

Figure 3.3: Depiction of the effects of network load on packet loss.

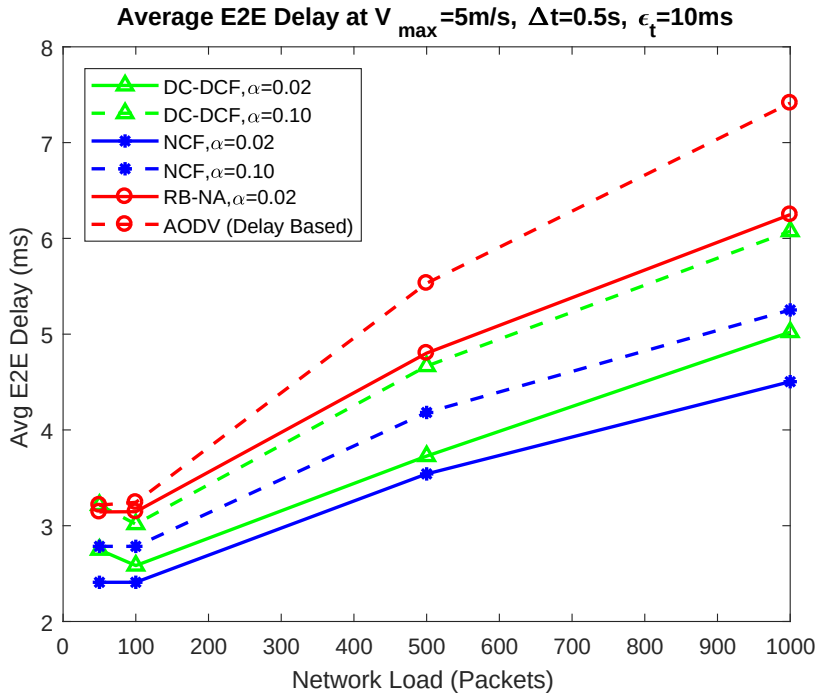

Figure 3.4: Depiction of the effects of network load on average end to end delay per packet.

We have considered a single source-destination pair having a load (denoted here by L for simplicity) of $L \in \{50, 100, 500, 1000\}$ packets, where a packet is of size 100 bytes. We have considered $\Delta t = \{0.5, 0.8, 1.0, 1.2\}$ s, admissible error rate $\alpha_{ij} = \{0.02, 0.10\}$ and

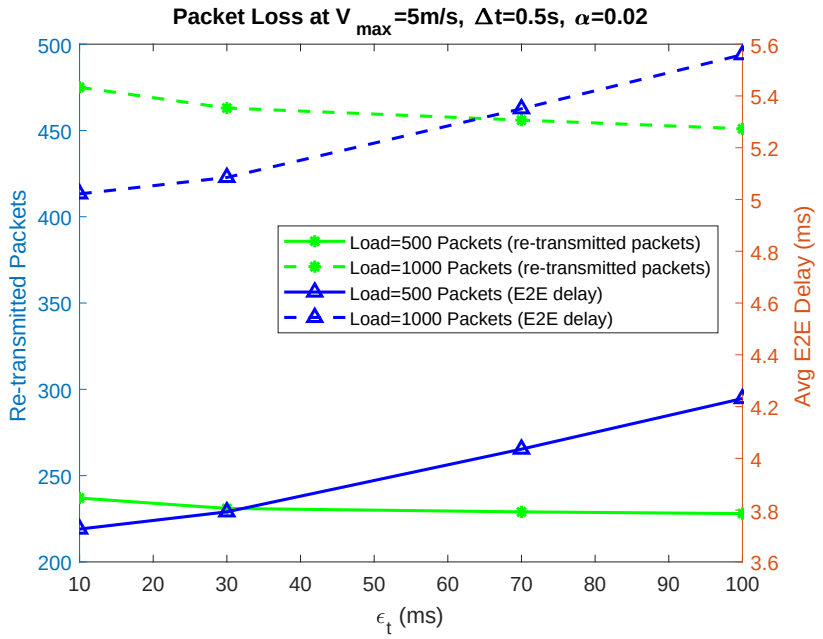

Figure 3.5: Depiction of the effects of variation of ϵ_t on packet loss and average end to end delay per packet in DC-DCF for $\alpha = 0.02$.

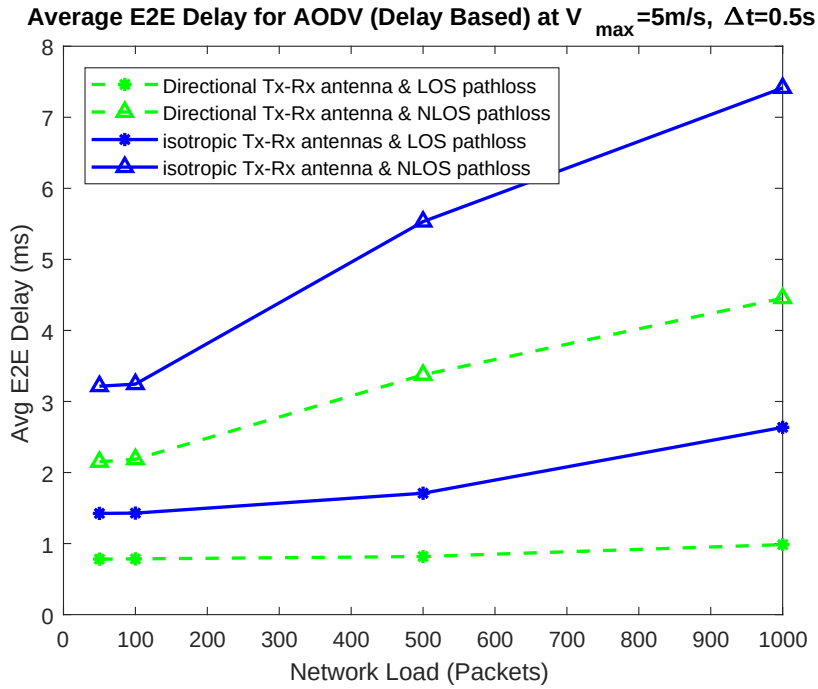

Figure 3.6: Effects of isotropic & directional antennas for 61 GHz mmWave for both LOS & NLOS scenarios.

$\epsilon_t = \{10, 30, 70, 100\}$ ms in our simulation. We have considered path loss model as given in [102] for non-line of sight (NLOS) scenario of an urban model for 61 GHz millimeter wave. The corresponding parameters are: path loss exponent ρ is 4.49, signal bandwidth is

20 MHz and standard deviation of log-normal shadowing component (σ_ψ) in dB is 4.0 dB. The maximum transmission power of a D2D user device is 24 dBm, the thermal noise density is -174 dBm/Hz [103] and hence $N_{th} = 2 \cdot 10^{-10.4}$ mW. We have used Shannon's capacity for each link (i, j) at time t to compute C_{ij}^t.

We have compared our algorithms NCF & DC-DCF with reliability based (RB-NA) & delay based (AODV) algorithms. The RB-NA approach is a network assisted algorithm where the path with the highest reliability is chosen. The reliability of a path P is defined as $\min_{(i,j)\in P} \frac{1}{\wp_{ij}^{t+1}}$ where $\wp_{ij}^{t+1}$ is the denominator of CF metric. The AODV in our experiment is based on the least delay path as discussed in [94].

Experimental Results & Analysis

We have run the experiment using the simulation environment mentioned in the previous subsection and taken the average of the results of around 30000 runs. We have written our own $C++$ custom code and run them on a GNU 4.8 compiler on Intel core $i7$ machine.

We have analyzed the effect of different parameters like Δt, V_{max}, L, ϵ_t and α_{ij} on packet loss and average end to end delay per packet. Figures 3.1, 3.2 and 3.3 depict results of varying Δt, V_{max} and L on the packet loss due to mobility keeping all other corresponding parameters fixed as shown in respective figures. Note that packet re-transmission is caused due to packet loss. Figure 3.4 depicts the result of varying L on the average E2E delay per packet, keeping other parameters fixed as shown in this figure. Average E2E delay is defined as the average transmission time for a packet to reach the destination, ignoring the propagation and processing delays. Since we have considered only one source destination pair in our simulation study for simplicity, we have neglected the queuing delay.

The following observations can be made from Figures 3.1-3.3: 1) *effects of varying* α: NCF and DC-DCF with $\alpha = 0.02$ have lesser packet loss than NCF and DC-DCF with $\alpha = 0.10$ respectively. This is because the admissible error rate α plays an important role in determining the link reliability and which in turn affects the packet loss. Higher values of α implies lesser reliability on link existence for the next time instance as compared to lower value of α. 2) *Effects of assistance from the BS*: NCF with $\alpha = 0.02$ and $\alpha = 0.10$ have lesser packet loss than DC-DCF with $\alpha = 0.02$ and $\alpha = 0.10$ respectively. This is due to the fact that NCF is network assisted approach and BS have complete network topology information. Hence BS can select the best suitable source-destination path and thus gets a better performance as compared to DC-DCF which is a distributed approach, which lacks the complete network topology information. 3) Both NCF and DC-DCF outperform RB-NA and AODV due to the fact that later two algorithms respectively consider reliability and capacity factors individually, whereas both these factors are taken care by our algorithms.

It can be observed in Figure 3.4 that similar behavior as in case of packet loss happens in terms of average E2E delay for all the three points mentioned in previous paragraph. The reason is that additional time is required to compensate for the re-transmitted packets.

Additionally, we can observe the behavior specific to Figure 3.1: packet loss is increasing as Δt increases. This is due to the fact that the distance ($V\Delta t$) between the nodes increases with Δt and hence the chance of packet loss also increases.

Also, Figure 3.2 depicts that increasing V_{max} causes more packet loss because the distance $V\Delta t$ between nodes increases with increasing speed. Higher speed causes the node to quickly go out of the range of the nearby nodes which are transmitting packets, hence causing higher packet loss.

Figure 3.3 depicts that the packet loss is increased as the number of packets transferred is increased. Higher the number of packets, more chances are to split the packets in multiple next hops, causing a higher chance of overall packet loss due to mobility of nodes.

It can be also observed in Figure 3.4 that the delay increases with the network load because the packet loss increases along with network load and thus the total time to compensate for the re-transmission of packets causes rise in average `E2E` delay.

Figure 3.5 shows the effect of increasing the wait time ϵ_t for `DC-DCF` on packet loss as well as average `E2E` delay for $L = \{500, 1000\}$ packets keeping other parameters fixed as shown. We can see the trade-off between delay and re-transmission of packets, as ϵ_t increases, packet re-transmission is reduced but the average `E2E` delay increases and vice versa. This is because as ϵ_t increases, the devices get higher chance to select a better path which reduces average packet loss but it incorporates more delay because of higher ϵ_t.

From the results shown in Figures 3.1-3.5, we can see $\Delta t * V$ is an important factor in which both Δt and V have effects on packet loss which helps in choosing the best next hop node. High $\Delta t * V$ value causes higher packet loss. Higher speed V of nodes may end up in breakage of links causing more packet loss. If Δt is high, it causes more packets to be sent which in turn, may cause more packet loss. We need to look at an appropriate $\Delta t * V$ value such that the capacity of link is satisfied along with speed to ensure the packets loss is affordable. We cannot control the speed of nodes but we can surely control Δt value. In other words, we can determine Δt value at which our algorithms should be executed to ensure the packet loss is kept below a threshold. Also, in case of `DC-DCF` we have to choose a value of ϵ_t which have moderate packet loss probability as well as appropriate minimum delay as there is a trade-off between them.

Figure 3.6 shows the effect of using isotropic and directional antennas under both `LOS` and `NLOS` settings. For directional antennas, we have considered number of antenna elements $L_p = 4$ [10]. Thus we get main-lobe gain $G_{ml} = 4$, side-lobe gain $G_{sl} = 2$ and beam-width $\phi = 0.866$ using equation (3.3.22). Interference is caused due to the side-lobe power from the transmitting devices over the link under consideration. Using these values, we have computed the `SINR`. For `NLOS`, `PL` parameters are same as in previous results (ρ & σ_ψ are 4.49 & 4.0 dB respectively) and for `LOS`, ρ & σ_ψ are 1.88 & 1.2 dB respectively [102]. Figure 3.6 shows the end to end delay versus network load for both isotropic & directional antennas under both `NLOS` & `LOS` settings. It can be observe that the performance of

directional antennas in LOS setting is overall best as expected. Similarly the performance of LOS setting is better than the NLOS setting.

3.6 Conclusion

We have developed an operator controlled SIP model to minimize the average network delay while keeping the packet loss under control by capturing the effect of mobility of nodes. After converting the SIP to its equivalent MINLP and proving its NP-hardness, we derived a distributed greedy metric CF by exploiting constraints of MINLP. CF computed at current time instance t captures the per-hop delay and reliability by incorporating channel uncertainty by modeling dynamic and unpredictable SINR for next time instance $t+1$ using the nodes' mobility. We have shown the efficient computations of CF which is applicable for any mobility models as long as the pdfs of the corresponding mobility parameters are known. Using the locally computed CF values we constructed a operator controlled perceived graph at current time t which holds information for the upcoming time instance $t+1$. This graph is used to find the appropriate source-destination path by using a widest path algorithm based on CF values. Similarly for device controlled case, this graph is constructed by waiting for ϵ_t time at the source node after it receives first RREP packet during route finding phase. Simulations have been performed to show that the proposed network assisted and distributed relay selection algorithms outperform the reliability and delay based approaches. Depending on the average velocity of nodes, we can tune the parameters Δt and ϵ_t such that both packet loss and delay are satisfied according to the need of an application.

Part II

Network Assisted Scenario for mmWave D2D communication

Chapter 4

Network Assisted D2D Relay Selection Under the Presence of Dynamic Obstacles

Much of the content of this chapter is copied from my own paper[3] *with the permission of my co-author Sasthi C. Ghosh. Even though the paper can be found in the literature, it is copied here so that I can make minor changes and clarifications for the convenience of the reader.*

Recently, `mmWave` is widely studied for short range `D2D` communication [9] due to their high available bandwidth and capacity. Although `mmWave` suffer from higher propagation loss characteristics, it is compensated by placing a large number of antennas in a small region owing to their smaller wavelength, which in turn increases the antenna gains at transmitter and receiver. These multi-input multi-output (`MIMO`) antennas make the directional communication possible using beam-forming techniques [10]. However, `mmWave` channels are very much susceptible to the blockage by obstacles due to very high penetration loss. For example, penetration losses of about 40 dB for outdoor tinted glass at 28 GHz `mmWave` and 178 dB from a 10 cm brick wall at 40 GHz are mentioned in [11] and [12] respectively. This requires almost a `LOS` communication for a given `D2D` link. Hence along with the mobility of `UEs` which was analyzed in Chapter 3, presence of obstacles also severely effects the network parameters in mmWave `D2D` communication. Note that there exist studies which consider reflected waves for short range `D2D` communication as in [104], but we focused on `LOS` communication in this work. Relays can be used to divert the communication path to mitigate the effects of outages due to blockages. The problem becomes more challenging when the obstacles are also in motion (dynamic obstacles) along with the moving UEs.

To account for the dynamic nature of the obstacles we have leveraged the information

[3] D. Singh and S. C. Ghosh. Network-assisted D2D relay selection under the presence of dynamic obstacles. In 44th IEEE Conference on Local Computer Networks (LCN), pages 129–132, 2019.

from Radars which uses Doppler effect to sense the presence of obstacles along with their movement speed and orientation. We assume that the BS is equipped with radars which helps in capturing the movement of dynamic obstacles with very high accuracy. It is also assumed that the BS knows the mobility related parameters of UEs. We first design a probabilistic model which uses simple geometric techniques to compute the link blockage probability due to dynamic obstacles. Then using this geometric analysis, we develop an algorithm to choose the best relay from the set of available relays which can provide the maximum expected data rate. Finally, we have compared and shown that our algorithm outperforms traditional approaches which do not consider the effect of dynamic obstacles.

The organization of this chapter is as follows: System model is described in section 4.1. The problem formulation is provided in section 4.2. Effects of mobility of UE and obstacles over D2D link in relay selection problem is analyzed in section 4.3. Simulations results are provided in section 4.4, followed by the conclusions in section 4.5.

4.1 System Model

Network

We are considering a service region occupied with mobile nodes which can form D2D communication and a single base station (BS). We are considering specifically the operator-controlled (network-assisted) scenario of device-tier of 5G D2D architecture mentioned in [1] and shown in figure 4.1, where the BS assists UEs for either a direct connection between them or through a potential UE relay to forward data to the destination. Time is discretized as t, $t+1$, $t+2$, ..., where Δt is the small time difference between the current time instance t and the next time instance $t+1$. At time instant t, the connectivity of the mobile nodes or UEs is represented as a graph $G^t(N^t, E^t)$, where N^t represents the set of UEs and E^t represents the set of edges. Here an edge (i, j) between two UEs $i \in N^t$ and $j \in N^t$ represents that they can communicate to each other. For a node $i \in N^t$, $adj^t(i)$ is the set of all neighbors of node i at time t. We assume that UEs are moving independently and the links are formed independently of each other. We are considering device-tier of the aforementioned D2D architecture, hence we are assuming that UEs have the capability to form mmWave D2D link among themselves for D2D communication in out-band or in-band overlay scenarios such that they are not interfered from the cellular users. Node $i \in N^t$ is moving with velocity vector $\overrightarrow{V}_i^t$. We denote speed, angle of elevation and azimuth angle of node i at time t as V_i^t, α_i^t and β_i^t respectively, which are known at the BS. For each node $i \in N^t$, its acceleration is 0 for Δt time duration (speed is unchanged for Δt duration). We are considering nodes as point objects in 3D Euclidean space. Position vector of node i is defined as $\overrightarrow{T_i^t} : (x_i^t, y_i^t, z_i^t)$ at time t. Euclidean distance between nodes i and j moving with

speeds V_i^t & V_j^t respectively is denoted as d_{ij}^t. Hence d_{ij}^{t+1} can be computed as:

$$d_{ij}^{t+1} = \sqrt{(z_j^{t+1} - z_i^{t+1})^2 + (y_j^{t+1} - y_i^{t+1})^2 + (x_j^{t+1} - x_i^{t+1})^2}$$

where,

$$x_i^{t+1} = x_i^t + V_i^t \Delta t \cos\alpha_i^t \sin\beta_i^t;\ x_j^{t+1} = x_j^t + V_j^t \Delta t \cos\alpha_i^t \sin\beta_i^t$$

$$y_i^{t+1} = y_i^t + V_i^t \Delta t \cos\alpha_i^t \cos\beta_i^t;\ y_j^{t+1} = y_j^t + V_j^t \Delta t \cos\alpha_i^t \cos\beta_i^t$$

$$z_i^{t+1} = z_i^t + V_i^t \Delta t \sin\alpha_i^t;\ z_j^{t+1} = z_j^t + V_j^t \Delta t \sin\alpha_i^t$$

Note that azimuth angle is measured with respect to positive y-axis (north direction when

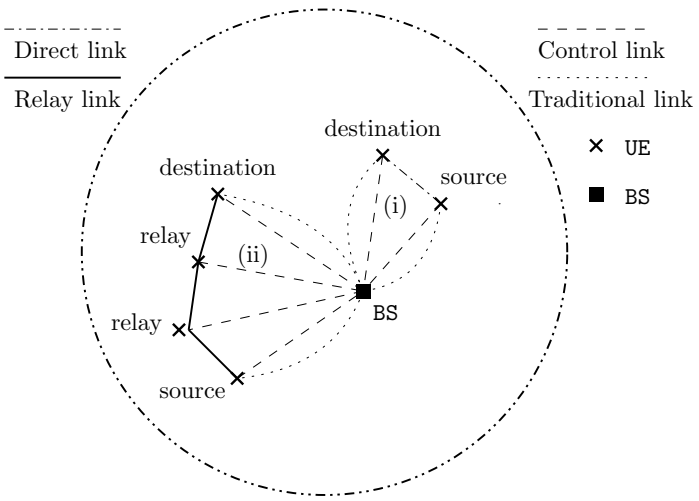

Figure 4.1: Network-assisted device-tier architecture for D2D communication [1]

look from top into the x-y plane) and elevation angle is measured with respect to the x-y plane (horizon) as shown in figures 4.2(i)-(ii). Elevation and azimuth angles are two important parameters which signify respectively height of the reflecting objects and their orientation with respect to the positive y-axis direction (north direction) on the given plane. Azimuth angle along with round trip delay of reflected wave gives the position of object at current time instance in x-y plane. Note that UEs could be tracked easily as they are connected to BS, however it is difficult to track other dynamic objects which are not connected to BS like vehicles and people. We are assuming that the BS has MIMO radar capability that can be used to measure α_i^t, β_i^t and round trip delay using Doppler effect. Here α_i^t and β_i^t signify the moving direction of UEs in 3D Euclidean space, round trip delay helps to measure the distance r_i^t of node i from the BS at time t and Doppler shift measures the speed of node i. Note that r_i^t and r_j^t can be used to measure positions $\overrightarrow{T_i^t}$ and $\overrightarrow{T_j^t}$ of nodes i and j respectively with respect to the BS. Hence, we can measure distance d_{ij}^t between nodes i and j.

Obstacles

We are considering that a link $(i, j) \in E^t$ can be obstructed by some static and dynamic obstacles. The dynamic obstacles may not be communicating with the BS, which might bring difficulty in tracking them. Hence, we are using radar leveraged BS which can detect the presence of obstacles with some probability of success as discussed in [37], where the obstacles are treated as line Boolean model with their centers distributed according to independent homogeneous Poisson point process (PPP) with density λ_o. The length and orientation of each obstacle are uniformly distributed and written as η_k and θ_k respectively. We denote $\mathbb{K} = \{1, 2, \cdots, K\}$ as the set of dynamic obstacles which are moving independent of each other, where K is the maximum number of obstacles present in the given region. There are some radars located in that area and radar locations are also independent homogeneous PPP with density λ_R. The presence of an obstacle k is detected with the closest radar with detection probability p_k^t at time t as mentioned in [37]. For analysis, we are considering the center of the dynamic obstacle $k \in \mathbb{K}$ as a point object with position vector $\overrightarrow{T_k^t} : (x_k^t, y_k^t, z_k^t)$. Similarly there are a total of R static obstacles and an static obstacle $l \in \mathbb{R}$ remains stationary throughout the experiment. Hence its position can be represented as: $\overrightarrow{T_l} : (x_l, y_l, z_l)$. Their positions can be pre-computed in a lookup table and can be easily verified for their interference with a communicating D2D link. Let us denote I_{ij}^{t+1} as the indicator variable representing if any obstacle $k \in \mathbb{R} \cup \mathbb{K}$ blocks link (i, j) under consideration when communication takes place during time interval Δt from the current time instant t to the next time instant $t + 1$:

$$I_{ij}^{t+1} = \begin{cases} 0, & \text{if } (i,j) \ \textit{is not blocked by any obstacle } k \in \mathbb{R} \cup \mathbb{K} \textit{ at time } t+1 \\ 1, & \text{otherwise} \end{cases} \tag{4.1.1}$$

mmWave Channel

We are considering a simple sectored antenna array model for both transmitters and receivers. For a uniform planar square antenna array composed of L_p elements, antenna gains can be written as [105]:

$$G_x = \begin{cases} G_{ml} & \text{if } \theta \leq \phi/2 \\ G_{sl}, & \text{otherwise} \end{cases} \tag{4.1.2}$$

where $x = \{t, r\}$ is subscript for transmitter & receiver, $G_{ml} = L_p$, G_{sl} and ϕ are main-lobe gain, side-lobe gain and beam-width respectively. Here $\theta \in [-\pi, \pi]$ is the angle off the boresight direction. We are assuming that the transmitter-receiver pairs are perfectly aligned to obtain the maximum power gain [10]. Alignment overhead is in order of hundreds of micro seconds even for extremely narrow beams of width=1° as mentioned and validated in [101] which can be neglected with respect to communication time in order of seconds.

For a link $(i, j) \in E^t$, where node i is the transmitter and j is receiver, the received

signal to noise ratio (SNR) can be computed as $S_{ij}^{t+1} = \frac{Q_{ij}^{t+1}}{N_{th}}$, where N_{th} is the constant thermal noise, Q_{ij}^{t+1} is the signal strength received at j from i at time $t+1$ in presence of obstacles. We are considering both the large scale fading path loss as well as path loss due to penetration from the obstacles. Here Q_{ij}^{t+1} consists of these two components and can be defined as [99, 100]:

$$Q_{ij}^{t+1} = \overline{pl}_{ij}^{t+1} \cdot \overline{pp}_{ij}^{t+1} \tag{4.1.3}$$

where $\overline{pl}_{ij}^{t+1} = P_i^t \cdot \mathfrak{K} \cdot \left(\frac{d_0}{d_{ij}^{t+1}}\right)^{\rho} \cdot \psi$ is a component of the received power due to fading of signal and $\overline{pp}_{ij}^{t+1} = \frac{1}{\Gamma_p}$ is the component of received power due to penetration loss because of obstacle's presence in link (i, j). Here P_i^t is the transmitted power from node i at time t and $\mathfrak{K} = G_t \cdot G_r \cdot \left(\frac{\lambda}{4\pi d_0}\right)^2$ is a constant. Here G_t and G_r are the transmitter & receiver antenna gains respectively which are assumed to be constant over time, λ is the wavelength and d_0 is a reference distance for the antenna far-field. Here d_{ij}^{t+1} is the distance between nodes i and j at time $t+1$, ρ is the PLE and ψ is the shadowing random variable. We also assume P_i^t to be constant for each transmitting node. Γ_p is the penetration loss from the blocking obstacle. We are assuming that the penetration loss by a single obstacle $\Gamma_p \to \infty$ [101] and thus even a presence of single obstacle may break the connectivity of the given mmWave link. Later, I_{ij}^{t+1} is computed by making use of this fact. This implies an LOS path is required between two D2D nodes for successful communication.

4.2 Problem Formulation & Probabilistic Model

Suppose a mobile node i transmits at time t to another mobile node j (relay or destination node) by forming a link (i, j). The transmission takes place for Δt duration till the next time instance $t+1$. The link may be disconnected due to mobility of the nodes or may be blocked by some obstacle during this Δt duration. Let us define e_{ij}^t as a Boolean variable whose value is 1, if there is an edge between nodes i and j at time t, and 0, otherwise. Here an edge between two nodes represents that they are within the communication range of each other and there is no obstacle between them. Our problem is to find out those links which are connected at current time instant t (i.e., $e_{ij}^t = 1$) and have the higher probability of being connected for the next time instant $t+1$ while the communication takes place. Our objective is to maximize the expected data rate while taking care of packet loss and average delay. For a given node i, we want to find a node $j \in adj^t(i)$ for relaying the packets such that the following objective is satisfied:

$$\arg\max_j E[C_{ij}^{t+1}], j \in adj^t(i) \tag{4.2.1}$$

where, $E[\cdot]$ denotes the expectation, C_{ij}^{t+1} denotes the capacity of link (i, j) at the next time instance $t+1$. Thus $E[C_{ij}^{t+1}]$ signifies the expected data rate available till next time

instance $t+1$. Let us define ξ_{ij}^{t+1} as the probability that link (i,j) will be connected at time $t+1$ given it was connected at current time instance t:

$$\xi_{ij}^{t+1} = P\{e_{ij}^{t+1} = 1 | e_{ij}^{t} = 1\},\ \forall (i,j) \in E^t. \tag{4.2.2}$$

Now, we can write $E[C_{ij}^{t+1}] = \xi_{ij}^{t+1} \cdot C_{ij}^{t} + (1 - \xi_{ij}^{t+1}) \cdot C_{ij}^{t}$. We know that with probability $(1-\xi_{ij}^{t+1})$, link (i,j) is going to fail at the next time instance $t+1$, hence $C_{ij}^{t+1} = 0$. Hence, our objective reduces to:

$$E[C_{ij}^{t+1}] = \xi_{ij}^{t+1} \cdot C_{ij}^{t}. \tag{4.2.3}$$

ξ_{ij}^{t+1} captures the link breakage probability during the transmission time Δt considering nodes mobility as well as static and dynamic obstacles for the upcoming time instance $t+1$. Note that ξ_{ij}^{t+1} is computed at current time instance t. It is evident that e_{ij}^{t+1} and e_{ij}^{t} are independent as nodes i and j are moving independently and also K obstacles are moving independently of each other. The independence of e_{ij}^{t+1} and e_{ij}^{t} also arises from the fact that even for two static nodes i and j which are connected at time t, may get disconnected at upcoming time instance $t+1$ due to blockage from independently moving obstacles. Hence we may reduce equation (4.2.2) to:

$$\xi_{ij}^{t+1} = P\{e_{ij}^{t+1} = 1\}. \tag{4.2.4}$$

To satisfy equation (4.2.4), the SNR received at node j from node i must be greater than a minimum threshold S_{ij}^{th}. The threshold S_{ij}^{th} denotes the required SNR of the given link (i,j) depending upon the type of communication used (e.g., voice, video call etc.). So equation (4.2.4) reduces to:

$$\xi_{ij}^{t+1} = P(S_{ij}^{t+1} \geq S_{ij}^{th}). \tag{4.2.5}$$

Since S_{ij}^{t+1} is a function of Q_{ij}^{t+1}, for the upcoming time instance $t+1$, S_{ij}^{t+1} depends on (i) $\overline{pl_{ij}^{t+1}}$ and (ii) $\overline{pp_{ij}^{t+1}}$. Now we can compute $\overline{pp_{ij}^{t+1}}$ using the indicator random variable I_{ij}^{t+1} as stated in equation (4.1.1). Hence we can express equation (4.2.5) as a joint distribution of $\overline{pl_{ij}^{t+1}}$ and I_{ij}^{t+1}:

$$\xi_{ij}^{t+1} = P(\overline{pl_{ij}^{t+1}} \geq \kappa_{ij}, I_{ij}^{t+1} = 0) \tag{4.2.6}$$

where κ_{ij} is the threshold on received power to satisfy the given data-rate requirements and I_{ij}^{t+1} indicates that the link is not blocked in the upcoming time instant $t+1$. We can write equation (4.2.6) as a conditional probability expression:

$$\xi_{ij}^{t+1} = P(\overline{pl_{ij}^{t+1}} \geq \kappa_{ij} | I_{ij}^{t+1} = 0) \cdot P(I_{ij}^{t+1} = 0) \tag{4.2.7}$$

The first term of right hand side in above equation signifies the probability of packet loss due to node's mobility when there is no obstacle and the second term takes care of probability that whether any obstacle interferes with the given link till the next time instance $t+1$.

Now in subsequent sections we will show how to compute these two terms.

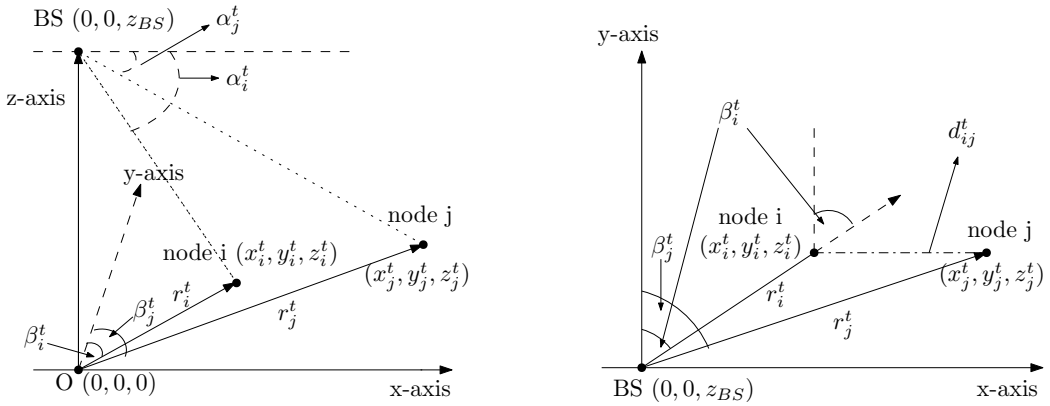

(i) Side-View (ii) Top-View

Figure 4.2: Position and orientation of `UEs` for side and top views with respect to `BS`.

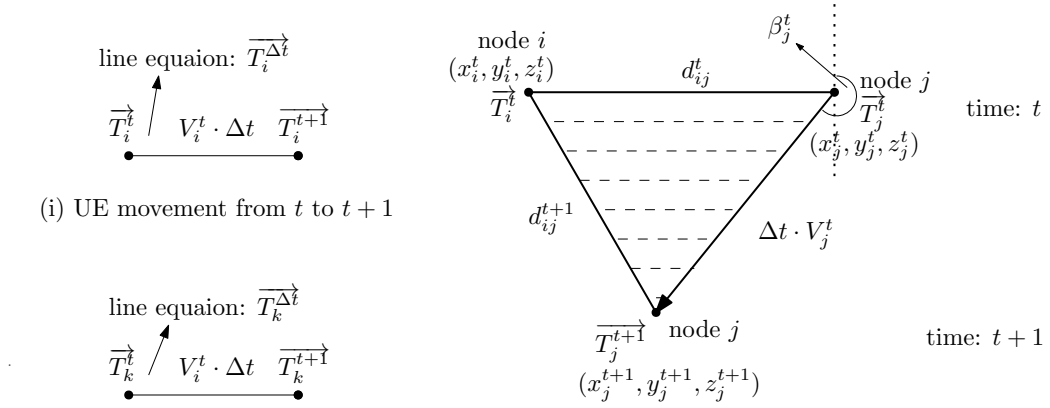

(i) UE movement from t to $t+1$

(ii) Obstacle movement from t to $t+1$

(iii) Node i is static and j is moving.

Figure 4.3: Representation of path of movement for `UEs` and dynamic obstacle.

4.3 Analysing Effects of Mobility and Obstacles in Relay Selection

We are exploiting the information from the radar linked with the `BS` to locate the `UEs` and moving obstacles. The positions are first find out and $P(\overline{pl_{ij}^{t+1}} \geq \kappa_{ij} | I_{ij}^{t+1} = 0)$ is computed based on it. Then using geometrical analysis, we compute $P(I_{ij}^{t+1} = 0)$. Finally, we develop an algorithm using the analysis to determine the best relay node among the potential relays considering both static and dynamic obstacles.

4.3.1 Finding Positions and Movements of Nodes and Obstacles

BS will store the location of moving UEs and obstacles using the analysis as shown in figures 4.2(i)-(ii). Figure 4.2(i) shows the side-view and figure 4.2(ii) shows its top-view indicating distance d_{ij}^t between nodes i and j. BS of height z_{BS} is located at $(0, 0, z_{BS})$, nodes i & j are located at (x_i^t, y_i^t, z_i^t) & (x_j^t, y_j^t, z_j^t) at time t respectively. We can find out the positions of node i:

$$x_i^t = r_i^t \cos\alpha_i^t \sin\beta_i^t; y_i^t = r_i^t \cos\alpha_i^t \cos\beta_i^t; z_i^t = z_{BS} - r_i^t \sin\alpha_i^t$$

Similarly we can compute the positions of static and dynamic obstacles. Once the respective positions are known, we need to analyze if the links formed at time t are going to be obstructed by any obstacle for Δt time duration till the time instance $t+1$ or not. To do so, we need to look into the path of a moving object (UE or dynamic obstacle) for Δt duration as follows: a moving UE i positioned at $\overrightarrow{T_i^t}$ at time t will move with velocity V_i^t for duration of Δt to arrive at new location $\overrightarrow{T_i^{t+1}}$ at time $t+1$. This movement for a short time duration Δt is a straight line as shown in figure 4.3(i). The equation of this line segment is:

$$\mu \cdot \overrightarrow{T_i^{t+1}} + (1-\mu) \cdot \overrightarrow{T_i^t} = \overrightarrow{T_i^{\Delta t}} \tag{4.3.1}$$

where, $\mu \in (0, 1)$. Similarly the motion path of a dynamic obstacle $k \in \mathbb{K}$ as shown in figure 4.3(ii) can be written as:

$$\mu \cdot \overrightarrow{T_k^{t+1}} + (1-\mu) \cdot \overrightarrow{T_k^t} = \overrightarrow{T_k^{\Delta t}} \tag{4.3.2}$$

where, $\mu \in (0, 1)$. Static obstacle $l \in \mathbb{R}$ is assumed to be positioned as $\overrightarrow{T_l}$ which is stationary throughout the experiment.

We can compute d_{ij}^{t+1} using $\overrightarrow{T_i^{t+1}}$ and $\overrightarrow{T_j^{t+1}}$. Then using this value, we can compute $\overline{pl_{ij}^{t+1}}$ for a given realization of ψ and respective PLEs. Hence $P(\overline{pl_{ij}^{t+1}} \geq \kappa_{ij} | I_{ij}^{t+1} = 0)$ can be computed as:

$$P(\overline{pl_{ij}^{t+1}} \geq \kappa_{ij} | I_{ij}^{t+1} = 0) = \begin{cases} 1, & \text{if } \overline{pl_{ij}^{t+1}} \geq \kappa_{ij} \\ 0, & \text{otherwise.} \end{cases} \tag{4.3.3}$$

It signifies the minimum received signal criteria between UEs to satisfy the respective minimum data rate requirement of link (i, j) given that there are no interfering obstacles. In the next section, we will compute $P(I_{ij}^{t+1} = 0)$.

4.3.2 Analyzing Blockage Due to Obstacles

We must capture the location of static obstacles and motion path of dynamic obstacles in order to find $P(I_{ij}^{t+1} = 0)$ as:

$$P(I_{ij}^{t+1} = 0) = \prod_{l \in \mathbb{R}} \prod_{k \in \mathbb{K}} p_k^t \cdot P_{ij\_k}^{int} \cdot P_{ij\_l}^{int}. \tag{4.3.4}$$

where p_k^t is the detection probability of dynamic obstacle $k \in \mathbb{K}$ at time t. $P_{ij\_k}^{int}$ and $P_{ij\_l}^{int}$ are the probabilities that the link under consideration is not blocked by any of the obstacles in the set $\mathbb{K}$ and $\mathbb{R}$ respectively. Here p_k^t can be computed as stated in section 4.1. We will now calculate $P_{ij\_k}^{int}$ and $P_{ij\_l}^{int}$ for various possible cases.

4.3.2.1 Both nodes are stationary

In this case, for nodes i and j, $\overrightarrow{T_i^t} = \overrightarrow{T_i^{t+1}}$ and $\overrightarrow{T_j^t} = \overrightarrow{T_j^{t+1}}$ and hence the equation of line $\overrightarrow{T_{ij}}$ connecting them can be expressed as:

$$\mu \cdot \overrightarrow{T_i^t} + (1-\mu) \cdot \overrightarrow{T_j^t} = \overrightarrow{T_{ij}},\ \forall \mu \in (0,1). \tag{4.3.5}$$

Now we need to capture the potential obstacles which might hinder the communication between nodes i and j positioned at $\overrightarrow{T_i^t}$ and $\overrightarrow{T_j^t}$. If none of the static obstacles $l \in \mathbb{R}$ positioned at $\overrightarrow{T_l}$ satisfy equation (4.3.5), then $P_{ij\_l}^{int} = 1$ otherwise $P_{ij\_l}^{int} = 0$. For all dynamic obstacles $k \in \mathbb{K}$, we have to find whether the equation of their motion path $\overrightarrow{T_k^{\Delta t}}$ (equation (4.3.2)) intersects with $\overrightarrow{T_{ij}}$ (equation (4.3.5)). Hence we can find,

$$P_{ij\_k}^{int} = \begin{cases} 1, & \text{if } \overrightarrow{T_k^{\Delta t}} \textit{ do not intersect } \overrightarrow{T_{ij}}, \forall k \in \mathbb{K} \\ 0, & \text{otherwise} \end{cases} \tag{4.3.6}$$

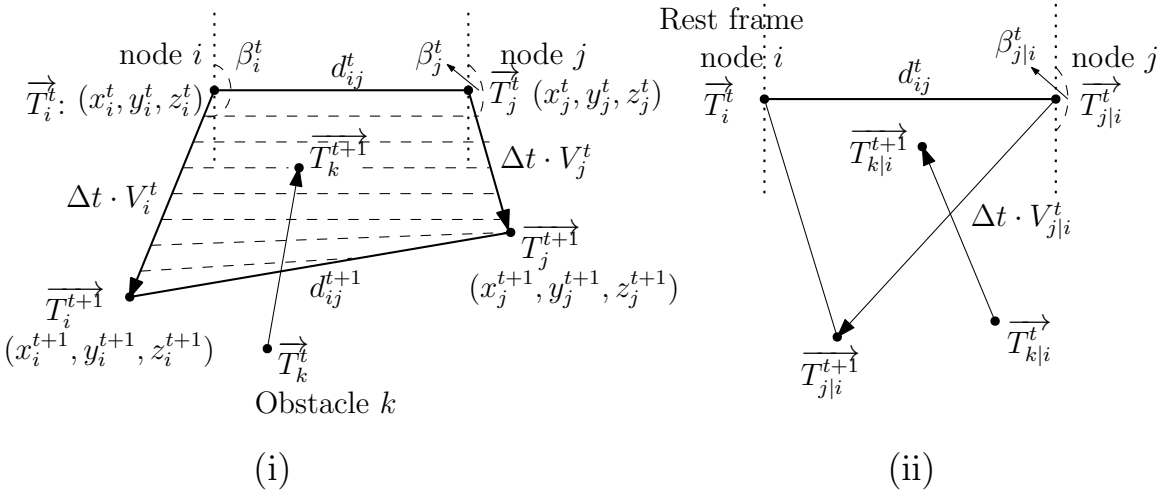

Figure 4.4: (i) Representation of both nodes moving in a skew path and obstacle k (ii) Relative motion of node j and obstacle k relative to node i.

4.3.2.2 One of the two nodes is moving

Let us assume that node i is stationary node and j is the moving node. We can categorize it into two cases: first is a special case when the BS detects that node j is moving towards

or away from the stationary node i where the angle of movement is 180° or 0° respectively with respect to line $\overrightarrow{T_i^t}\overrightarrow{T_j^t}$. In this case, node j's movement forms a straight line with respect to the stationary node i for duration Δt denoted as $\overrightarrow{T_{ij}^{\Delta t}} = \overrightarrow{T_i^t}\overrightarrow{T_j^{t+1}}$. For static obstacles again if none of $l \in \mathbb{R}$ satisfy line $\overrightarrow{T_{ij}^{\Delta t}}$, then $P_{ij\_l}^{int} = 1$ otherwise $P_{ij\_l}^{int} = 0$. For dynamic obstacles, we need to find out if any obstacle $k \in \mathbb{K}$ blocks the communication between nodes i and j by verifying if k's motion path equation $\overrightarrow{T_k^{\Delta t}}$ intersects $\overrightarrow{T_{ij}^{\Delta t}}$ or not. Thus for dynamic obstacles we can compute:

$$P_{ij\_k}^{int} = \begin{cases} 1, & \text{if } \overrightarrow{T_k^{\Delta t}} \textit{ do not intersect } \overrightarrow{T_{ij}^{\Delta t}}, \forall k \in \mathbb{K} \\ 0, & \text{otherwise} \end{cases} \tag{4.3.7}$$

The second case is described when node j moves at angle relative to node i other than that from the set $\{0°, 180°\}$. This case is described in figure 4.3(iii). Initially at time t, node j is inside the range of node i at a distance of d_{ij}^t when no obstacles were present. By the next time instance $t+1$, node j will cover a distance of $\Delta t \cdot V_j^t$ from its initial point $\overrightarrow{T_j^t}$. As mentioned in equation (4.3.1), $\overrightarrow{T_j^{\Delta t}} = \overrightarrow{T_j^t}\overrightarrow{T_j^{t+1}}$ denotes the line segment representing the movement of node j for the duration of Δt time. In the mentioned figure, arrow denotes the direction of motion of node j. The shaded region denotes a bounded region $B_{ij}^{\Delta t}$ formed by three vertices $\overrightarrow{T_i^t}$, $\overrightarrow{T_j^t}$ and $\overrightarrow{T_j^{t+1}}$ during time Δt. Since three points define a unique plane in 3D Euclidean space, points in $B_{ij}^{\Delta t}$ are coplanar and the equation of the plane denoted as $P_1^{\Delta t}$ is:

$$(\overrightarrow{T_p^{\Delta t}} - \overrightarrow{T_i^t}) \cdot ((\overrightarrow{T_j^{t+1}} - \overrightarrow{T_i^t}) \times (\overrightarrow{T_j^t} - \overrightarrow{T_i^t})) = 0 \tag{4.3.8}$$

where $\times$ denotes vector cross product, $\overrightarrow{T_p^{\Delta t}}$ denotes the position vector (x^t, y^t, z^t). The shaded region covers the entire possible area where communication between nodes i and j takes place. We also call this region $B_{ij}^{\Delta t}$ as the *communication region* which might be vulnerable due to presence of obstacles. For static obstacle l, $\forall l \in \mathbb{R}$, we need to check if point $\overrightarrow{T_l}$ satisfies equation (4.3.8) or not. If it does not satisfy then there is no blockage from it. Otherwise, we need to check if it lies inside the bounded region $B_{ij}^{\Delta t}$ or not. If it lies inside then $P_{ij\_l}^{int} = 1$, otherwise $P_{ij\_l}^{int} = 0$. For each dynamic obstacle $k \in \mathbb{K}$, we need to check whether the line segment $\overrightarrow{T_k^{\Delta t}}$ intersects with the given plane $P_1^{\Delta t}$ in equation (4.3.8). For this, we need to consider three possible cases:

1. $\overrightarrow{T_k^{\Delta t}}$ does not intersect with plane $P_1^{\Delta t}$ and in this case is parallel to plane.
2. $\overrightarrow{T_k^{\Delta t}}$ lies on plane $P_1^{\Delta t}$.
3. $\overrightarrow{T_k^{\Delta t}}$ intersects plane $P_1^{\Delta t}$ on a point. In this case it crosses the plane.

Let us say $\hat{k}^{\Delta t}$ represents the unit vector (direction vector) of the line representing the obstacle's movement $(\overrightarrow{T_k^{\Delta t}})$ and $\overrightarrow{u}^{\Delta t} = (\overrightarrow{T_j^{t+1}} - \overrightarrow{T_i^t}) \times (\overrightarrow{T_j^t} - \overrightarrow{T_i^t})$ denotes the normal vector to

plane $P_1^{\Delta t}$. To categorize all the above mentioned cases, we need to find the dot product of $\hat{k}^{\Delta t}$ and $\overrightarrow{u}^{\Delta t}$, if it is 0 then $\overrightarrow{u}^{\Delta t}$ and $\hat{k}^{\Delta t}$ are orthogonal and hence the plane is parallel to $\overrightarrow{T_k^{\Delta t}}$. In this case there are two possibilities, first $\overrightarrow{T_k^{\Delta t}}$ may lie outside plane and is parallel to the plane (case i) and second when $\overrightarrow{T_k^{\Delta t}}$ lies on the plane (case ii). To further distinguish between these two, we need to find dot product of $(\overrightarrow{T_i^t} - \overrightarrow{T_k^t})$ and $\overrightarrow{u}^{\Delta t}$. If this value is 0 then line is contained in the plane (case ii) otherwise line is outside the plane (case i). For case i, when line $\overrightarrow{T_k^{\Delta t}}$ is outside the plane and parallel to it then obstacle k does not interfere with the communication region. For case ii, $\overrightarrow{T_k^{\Delta t}}$ lies inside plane $P_1^{\Delta t}$ and hence has the possibility of interfering with the bounded region (which is the communication region). Now in this case, we need to figure out if obstacle's line equation $\overrightarrow{T_k^{\Delta t}}$ lies inside this region or not. To check this we perform the following two step procedure for all the dynamic obstacles $k \in \mathbb{K}$:

step a. Check if moving obstacle's line equation $\overrightarrow{T_k^{\Delta t}}$ intersects with any of the three sides of the bounded region $B_1^{\Delta t}$, i.e., $\overrightarrow{T_i^t}\overrightarrow{T_j^t}$, $\overrightarrow{T_i^t}\overrightarrow{T_j^{t+1}}$ or $\overrightarrow{T_j^t}\overrightarrow{T_j^{t+1}}$.

step b. If step a is successful, it implies obstacle k interferes with $B_{ij}^{\Delta t}$. Otherwise, we need to check if line $\overrightarrow{T_k^{\Delta t}}$ is either completely inside or outside $B_{ij}^{\Delta t}$. For this, we will check for any one of the points either $\overrightarrow{T_k^t}$ or $\overrightarrow{T_k^{t+1}}$ of motion path of dynamic obstacle k lies inside or outside $B_{ij}^{\Delta t}$. If that point lies inside then whole line segment describing the motion path of dynamic obstacle lies inside $B_{ij}^{\Delta t}$ otherwise it lies outside. If it lies inside then it interferes with the communication region during Δt time, otherwise not.

For case iii, if the dot product $\hat{k}^{\Delta t} \cdot \overrightarrow{u}^{\Delta t}$ is not 0 then line $\overrightarrow{k}^{\Delta t}$ crosses plane $P_1^{\Delta t}$ and they intersect at one point (case iii). We need to check if this point of intersection lies inside bounded region $B_{ij}^{\Delta t}$. If so then obstacle k interferes the communication region of nodes i and j, otherwise there is no interference. Based on above discussion, we can calculate $P(I_{ij}^{t+1} = 0)$ as follows:

$$P_{ij\_k}^{int} = \begin{cases} 1, & \text{if } \overrightarrow{T_k^{\Delta t}} \textit{ do not interfere } B_{ij}^{\Delta t}, \forall k \in \mathbb{K} \\ 0, & \text{otherwise} \end{cases} \tag{4.3.9}$$

4.3.2.3 Both nodes are moving

In this case both nodes i and j are moving from time t to $t+1$. Based on their relative angle of motion we can categorize them into two cases, first when they both are moving towards or away from each other (relative angle of movement $\in \{0°, 180°\}$). This case is similar to that of the previous section except here node i is also moving. But here too, both nodes will form a straight line and hence we need to simply check if any obstacle is intersecting it. Hence this is solved in similar way as mentioned in the previous section.

For the second case when nodes i and j are *not* moving towards or away from each other, there are two possibilities: case i) all four points are co-planar and case ii) they are not co-planar. Case i) is formed when either both nodes i & j are moving parallel to each other or when they are intersecting each other's motion path. The path formed by them is not co-planar when the respective equations of their motion paths are skew (i.e., they neither intersect nor are parallel to each other) as shown in figure 4.4(i). To check for this categorization, we need to form a plane equation with any three points out of the given four points and then check if the fourth point lies inside this plane equation or not. Now to check whether an obstacle interferes with the communication region, we will first give a solution for the non co-planar case and then generalize it to the co-planar case.

For case ii), where motions paths $\overrightarrow{T_i^{\Delta t}}$ and $\overrightarrow{T_j^{\Delta t}}$ are skew, we compute the relative position and velocity of node j with reference to the other node i which is kept at rest. Relative position is computed as $\overrightarrow{T}^t_{j|i} = \overrightarrow{T}^t_j - \overrightarrow{T}^t_i$ and relative velocity is computed as $\overrightarrow{V}^t_{j|i} = \overrightarrow{V}^t_j - \overrightarrow{V}^t_i$, where the magnitude speed is denoted as $V^t_{j|i}$. This is shown in figure 4.4(ii) which is reduced from figure 4.4(i), where node j is moving with reference to the fixed node i. This in turn gives three points $\overrightarrow{T}^t_{i|i}$, $\overrightarrow{T}^t_{j|i}$ and $\overrightarrow{T}^{t+1}_{j|i}$ from which we can form the equation of a unique plane which will give a new communication region bounded by these three points. We will also compute the relative positions of all static and dynamic obstacles and relative velocities of dynamic obstacles with respect to the fixed node i. Now this reduces to the problem of verifying if any of these obstacles are interfering with the communication region. This verification can be done exactly as explained in the previous section.

Using same approach we can proceed for case i) when the four points are co-planar. The only difference that arises here is that the resulting relative positions lie in the same plane which contains all four points. Whereas, for the non co-planar case the resulting relative positions might shift the plane according to vector difference of their velocities and positions. Using these analysis, we now give the relay selection algorithm.

4.3.3 Relay Selection Algorithm

Using the above analysis, we present our dynamic-obstacle (`D-Obs`) based relay selection algorithm in algorithm 5. For a given sending node i, we will choose the relay among the nodes in $adj^t(i)$ which gives the best expected data rate. The probability that a link connected at current time instance t is still connected for the next time instance $t+1$ is calculated from the analysis section which considers all the possible cases of movements of `UEs` and moving obstacles as done in line 5. From line 6-8 we get the relay node (denoted as $chosen\_j$) with the best average data-rate. Function $begin\_transmission(i, chosen\_j)$ transmits the data from node i to the chosen relay node $chosen\_j$. This process repeats for all sending nodes $i \in N^t$. Line 5 takes $O(R+K)$ computation time for a pair of sending and relaying nodes, where R and K are number of static and dynamic obstacles. For a given

sending node i, to choose the best relay node, our algorithm takes $O(n(R+K))$ running time, where n is the number of adjacent nodes to node i.

Algorithm 5: D-Obs Algorithm

input : $G(N^t, E^t)$,κ_{ij}, $\mathbb{K}$, $\mathbb{R}$

for $\forall i \in N^t$ **do**
  if *i is sending node* **then**
    $max\_j = 0$;
    for $\forall j \in (adj^t(i))$ **do**
      $temp = P(\overline{pl_{ij}^{t+1}} \geq \kappa_{ij} | I_{ij}^{t+1} = 0) \cdot P(I_{ij}^{t+1} = 0) \cdot C_{ij}^t$;
      if $max\_j \leq temp$ **then**
        $max\_j = temp$;
        $chosen\_j = j$;
      end
    end
    $begin\_transmission(i, chosen\_j)$
  end
end

4.4 Experiment and Results

4.4.0.1 Simulation Environment

We are initially distributing 30 `UEs` uniformly in a 200 $m \times 200$ m square area. Throughout the experiment these nodes remain within the service region. For simulation purpose, we assumed that `UEs` and obstacles are placed on the ground (i.e. x-y plane) ignoring z-axis. Each node is moving with speed uniformly in range $[0, V_{max}]$ m/s, for $V_{max} \in \{5, 10, 15, 20\}$ and angle in range $[-\pi, \pi]$. In the experiment, Δt which is measured in seconds, takes value from the set $\{0.5, 1, 1.5, 2\}$. Nodes are using directional transmitter and receiver antennas for 60 GHz frequency with $L_p = 4$, such that $G_r = G_t = 6$ dB and we are considering a scenario where `LOS PLE` is 2.5 and zero mean log-normal shadowing random variable with standard deviation 3.5 [10, 106]. Thermal noise density is -174 dBm/Hz [103] and devices are using 18 dBm transmit power. Capacity of each link (i, j) at time t is $C_{ij}^t = B \cdot \log_2(1 + S_{ij}^t)$ $bits/sec$, where $B = 20$ MHz is bandwidth and `SNR` threshold S_{ij}^{th} is taken to be 20 dB [107]. We are assuming fixed packet length of 65535 *bytes*. There are static and dynamic obstacles initially distributed uniformly in the environment. Number of static obstacles $R = 10$ is fixed throughout the experiment, whereas number of dynamic obstacles K varies in range $\{0, 10, 20, 30\}$. For all of the cases, dynamic obstacles are moving with a speed uniformly distributed in range $[0, 10]$ m/s. Radars are deployed in the region with $\Lambda_R = 0.001$ [37]. We assume a single source-destination pair for simplicity and all other devices may act as relay. We are comparing the results of our algorithm with metrics

based on RSS and a contention based forwarding (CBF) approach [108] which select relay node based on signal strength and shortest distance from destination respectively.

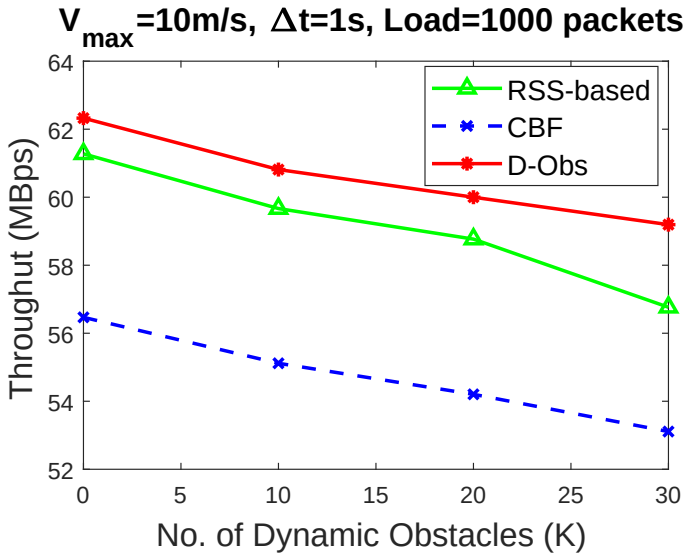

Figure 4.5: K vs avg. throughput.

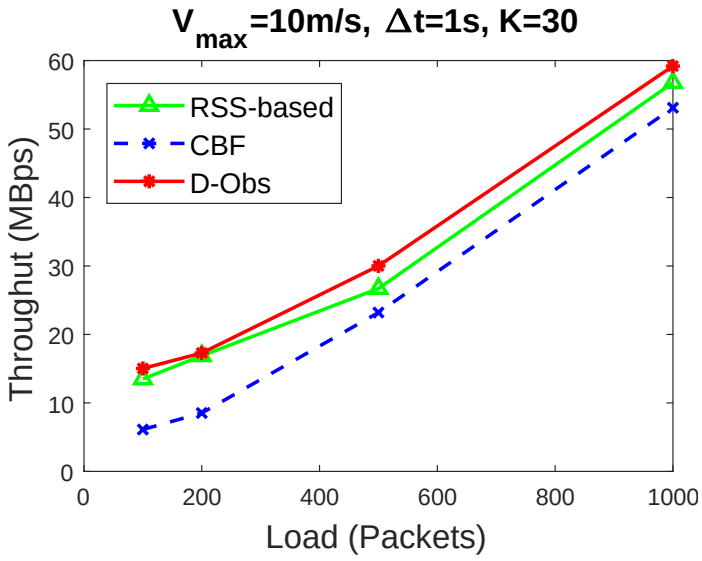

Figure 4.6: Load vs avg. throughput.

4.4.0.2 Experimental Results & Analysis

We have written our own C++ custom code and run them on a GNU 4.8 compiler on Intel core $i7$ machine using the simulation environment mentioned in previous section and taken the average of the results of about 10000 runs.

Figure 4.5 depicts the effect of varying K on average throughput keeping other parameters fixed as mentioned in the figure. Average throughput decreases rapidly for RSS and CBF

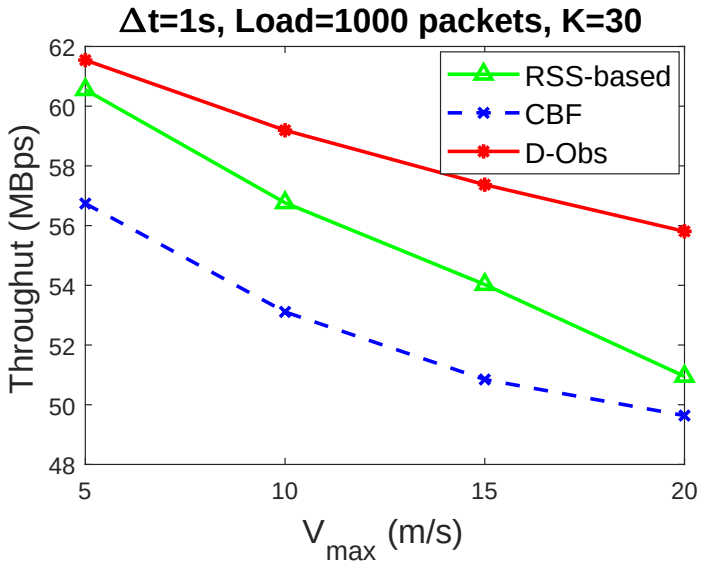

Figure 4.7: V_{max} vs avg. throughput.

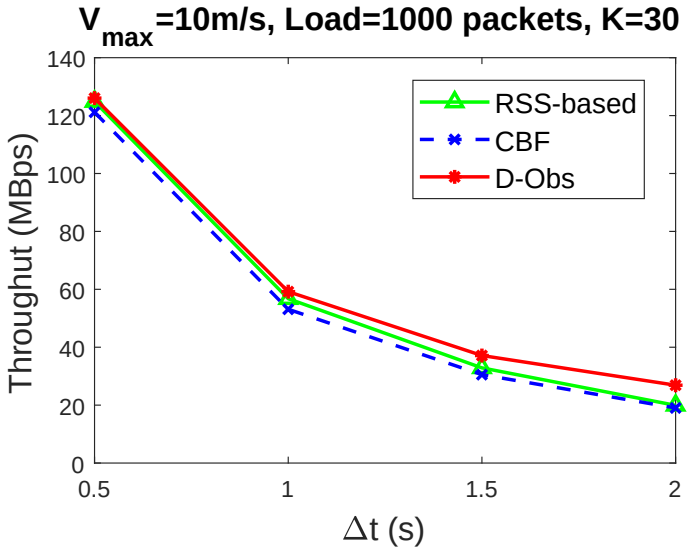

Figure 4.8: Δt vs avg. throughput.

based approaches as compared to `D-Obs` algorithm, because both of them neither consider mobility nor obstacle and forward packets solely based on signal strength and distance from destination respectively. As a result the packet loss is also very high in both `RSS` and `CBF` based approaches as compared to `D-Obs` algorithm as shown in figure 4.9. Packet loss in `CBF` approach is higher than `RSS` because it chooses a relay based on its closer distance to the destination in which case the chosen relay `UE` can be far from the transmitting `UE` which may increase the chance of blockage from static & dynamic obstacles. Also signal strength could be low causing a high end to end delay if packet loss occurs.

Figure 4.6 depicts the effect of varying network load on average throughput keeping

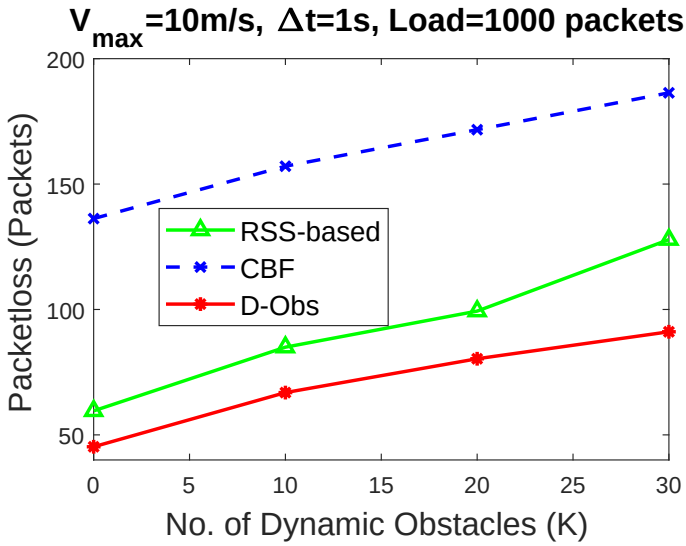

Figure 4.9: K vs avg. packetloss.

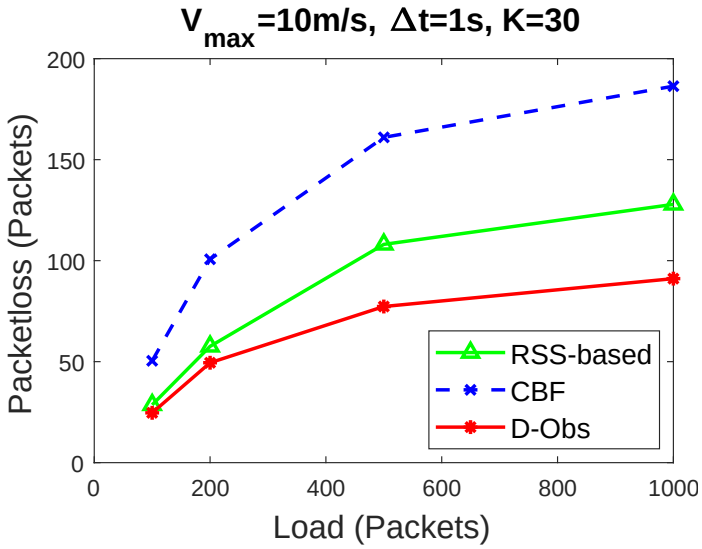

Figure 4.10: Load vs avg. packetloss.

other parameters fixed as mentioned in the figure. Here again average throughput for both `RSS` and `CBF` based approaches are lower as compared to `D-Obs` algorithm, because of the same reasons as mentioned above. As the number of packets to be sent increases, the chance of packets loss also increases due to mobility as well as obstacles which is shown in figure 4.10.

Figure 4.7 depicts the effect of varying V_{max} on average throughput keeping other parameters fixed as mentioned in the figure. Here as the speed increases, the performance of `RSS` and `CBF` deteriorate more rapidly as compared to `D-Obs` because with higher speed, nodes can move longer distance giving more chance for static and dynamic obstacle to interfere with them. Higher speed also causes more packet loss due to mobility as nodes may

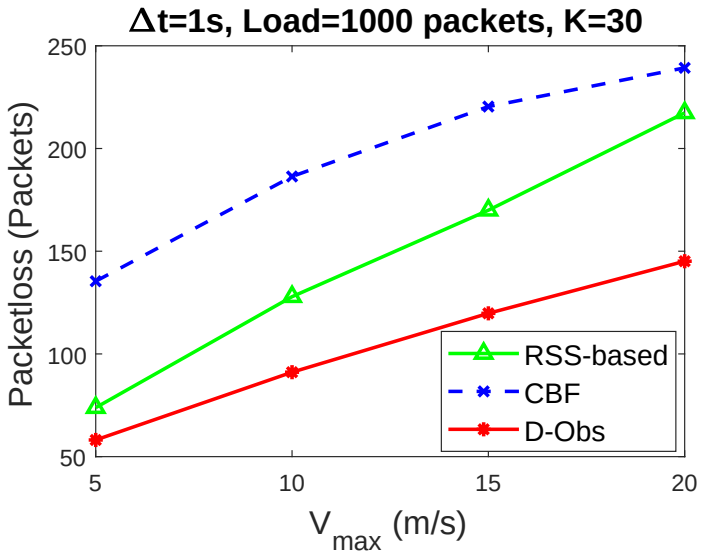

Figure 4.11: V_{max} vs avg. packetloss.

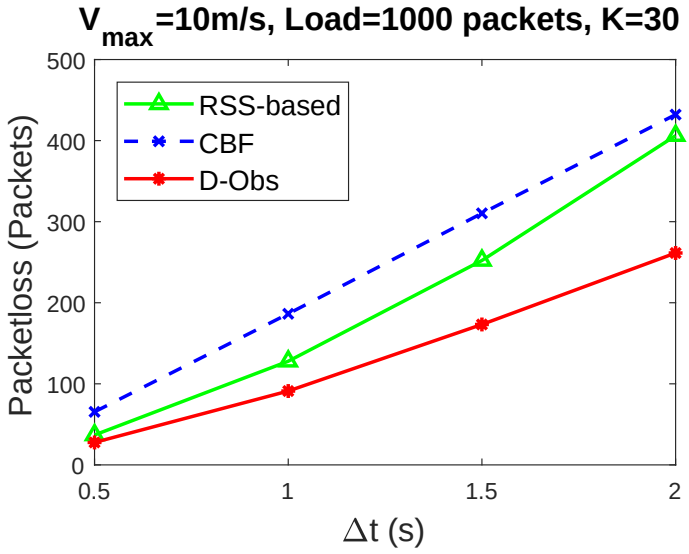

Figure 4.12: Δt vs avg. packetloss.

go out of range of each other quickly. The corresponding packet loss graph is shown in figure 4.11.

Figure 4.8 depicts the effect of varying Δt on average throughput keeping other parameters fixed as mentioned in the figure. Here also, we can see that increasing Δt results in poor performance of `RSS` and `CBF` compared to `D-Obs`. This is because, with higher Δt, nodes can move longer distance causing increase in chances of blockage by static and dynamic obstacles which in turn causes more packet loss. Also longer distance may cause packet loss due to mobility. The packet loss graph is shown in figure 4.12.

4.5 Conclusion

We formulated the problem of relay selection by capturing the effects of both obstacles and node's mobility. We optimized throughput by taking care of packet loss and average delay. To capture the motion of dynamic obstacles, we leveraged the radar employed with base station which would detect them with certain probability. Later, we used geometrical analysis to derive unique solutions for computing the best relay node. In simulations, we have shown the effects of both obstacles and node's mobility on throughput as well as packet loss. Results show that `D-Obs` outperforms other classical algorithms by appropriately capturing the effects of obstacles and node's mobility.

Chapter 5

Network Assisted D2D Relay Selection in the Presence of Dynamic Obstacles with Unknown Orientation

In the previous chapter, we saw that the mobility parameters of dynamic obstacles, if not captured efficiently, might cause packet loss, delay and hence deterioration of QoS. Therefore, in order to capture the effects of these arbitrary moving obstacles, instantaneous position and velocity (speed and orientation) of UEs and dynamic obstacles must be tracked. However, a dynamic obstacle's motion is hard to predict as they are not connected to the BS. In contrast, UEs are well connected to the network and can periodically send their movement information to the BS with very high accuracy. Even though speed of dynamic obstacles can be measured with some accuracy, their orientation might be unknown or very difficult to measure. The change in orientation of movement might be very rapid as compared to that of change in speed for a small time duration. Solutions using smart antennas at blockages to divert communication through moving obstacles was provided by the authors in [68], however it might not be possible to place such antennas on every moving obstacle. Radars might be employed [36, 37], or vision cameras might be used [38] to capture the mobility related parameters of these obstacles. However, sensing the speed of these obstacles with very high accuracy is much easier compared to their orientation of motion as orientation in motion may change rapidly and arbitrarily comparatively to the change in speed of their motion. Machine learning techniques can be used to predict the blockage by such moving obstacles [14], however, these models need to be re-trained again when there is a change in dynamic obstacle's motion pattern, which would consume significant time. Hence there is a need to study the movement of dynamic obstacles which will capture the uncertainty in network parameters posed due to unknown orientation of

dynamic obstacles. In the previous chapter, we did a probabilistic analysis using geometry to devise relay selection techniques considering dynamic obstacles, however the uncertainty in obstacle's orientation was not considered.

In this chapter, we are investigating the relay selection problem in network assisted mmWave D2D communication where dynamic obstacles have *unknown* orientation. An appropriate UE acting as relays has to be selected considering the effects of dynamic obstacles on mmWave D2D links in order to maximize data rate by minimizing packet loss and delay. Here speed of `UEs` and obstacles are known at the BS but *instantaneous orientation* of dynamic obstacles are *unknown* to the BS. The information of mobility parameters of UEs for the next time instant is propagated to the BS at the current time instant. A geometric interpretation for the problem is given which further elaborates the formulated problem. Later, a probabilistic analytical framework is developed using geometry to compute blockage probability across all possible scenarios of movements of UEs. This analysis is then used in devising a relay selection strategy.

System model and problem formulation are given in Sections 7.1 and 7.2 respectively. Link blockage probabilities analysis is done in Sections 5.3 and 5.4. The relay selection algorithm is given in Section 5.5. Simulation results and conclusions are given respectively in Sections 5.6 and 7.5.

5.1 System Model & Notations

We are considering a service region equipped with a millimeter wave base station. Time is discretized as t, $t+1$, $t+2$,$\cdots$ and Δt is the small time difference between t and $t+1$. A graph $G^t \cup \mathfrak{B}$ is used to represent the service region, where $G^t = (N^t, E^t)$ represents network graph where E^t is set of edges among UEs which are also termed as nodes (N^t) at time instant t. Here $\mathfrak{B}$ represents a singleton set signifying the BS which assists the `D2D` communication among nodes. We are using the operator controlled scenario of the device-tier of 5G `D2D` architecture mentioned in [1]. We are assuming that UEs take part in `D2D` communication using out-band or in-band overlay scenarios such that they are not interfered from the cellular users. E^t is the set of all edges which represents links between the nodes which are in transmission range of each other at time t and $adj^t(i)$ is the set of neighboring nodes of the node $i, \forall i \in N^t$ at time t. Here, (i, j) denotes the D2D link formed between nodes i and j. At time t, each node $i \in N^t$ is moving with certain speed V_i^t and orientation θ_i^t till time $t+1$. Position of the nodes i and j at time t are denoted as $\overrightarrow{T}_i^t : (x_i^t, y_i^t)$ and $\overrightarrow{T}_j^t : (x_j^t, y_j^t)$ respectively. Nodes are moving independently of each other and the links among them are formed independently of each other. It is assumed that at time instant t, BS knows nodes' speed, position and orientation with very high accuracy as the nodes are connected to the BS. However all of these parameters are subject to change with time. It is assumed that the acceleration is 0 for Δt time duration (speed is unchanged

for Δt duration). Let us denote d_{ij}^t as the Euclidean distance between node i and j at time t. Their respective speed and direction are V_i^t & V_j^t and θ_i^t & θ_j^t at time t.

A link $(i,j) \in E^t, \forall i,j \in N^t$ is formed between transmitting UE i and receiving UE j if the signal to noise ratio (`SNR`) denoted as S_{ij}^{t+1}, is above a required data rate threshold S_{ij}^{th}. We can write $S_{ij}^{t+1} = \frac{Q_{ij}^{t+1}}{N_{th}}$, where N_{th} is the thermal noise and is assumed to be constant. Q_{ij}^{t+1} is the received signal strength (`RSS`) at time $t+1$ at node j from node i which can be computed as [99, 100]:

$$Q_{ij}^{t+1} = P_i^t \cdot \mathfrak{K} \cdot \left(\frac{d_0}{d_{ij}^{t+1}}\right)^{\rho} \cdot \psi \cdot \frac{1}{\Gamma_p} \tag{5.1.1}$$

where P_i^t is constant transmitted power from node i at time t, $\mathfrak{K} = G_t \cdot G_r \cdot \left(\frac{\lambda}{4\pi d_0}\right)^2$ is a unit-less constant, G_t and G_r are the constant antenna gains at the transmitter and receiver respectively, λ is the wavelength, d_0 is a reference distance for the antenna far-field, d_{ij}^{t+1} is the distance between nodes i and j at time $t+1$, ρ is the path loss exponent (`PLE`) and ψ is the shadowing random variable which can have any well known distribution p_ψ (e.g., log normal distribution [99]). Γ_p is the penetration loss from the blocking obstacle. We are assuming that the penetration loss by a single obstacle $\Gamma_p \to \infty$ and thus even a single obstacle may break the given `mmWave` D2D link. Hence `LOS` communication is required between any two `D2D` nodes. Initially, transmitter and receiver are assumed to be perfectly aligned at any given time and ready for communication [10].

There are a total of K dynamic obstacles in the service region which belong to set $\mathbb{K} = \{1, 2, \cdots, K\}$. A given link (i,j) formed at time t can be obstructed by any dynamic obstacles $k \in \mathbb{K}$ during Δt duration till time instant $t+1$ with certain probability $p_{k\_ij}^{t+1}$ (which is computed in the analysis). A dynamic obstacle k is moving with speed V_k^t at time t and assumed to be a point object along with nodes for the sake of analysis. The orientation angle of obstacle k is denoted as θ_k^t and is unknown at current time instant t. It is chosen uniformly in $[-\pi, \pi]$ with `pdf`:

$$f_{\theta_k^t} = \frac{1}{2\pi}, -\pi \leq \theta_k^t \leq \pi.$$

We define I_{ij}^{t+1} as the random variable indicating link (i,j) obstruction by the obstacles present in the service region. Since each obstacle k has a probability $p_{k\_ij}^{t+1}$ of interfering with a given link (i,j), we can say:

$$P(I_{ij}^{t+1} = 0) = \prod_{k=1}^{K} (1 - p_{k\_ij}^{t+1}) \tag{5.1.2}$$

If $P(I_{ij}^{t+1} = 0) = 1$ then the link (i,j) is not obstructed by any obstacle for the upcoming time instant, otherwise the link is obstructed by at least one obstacle $k \in \mathbb{K}$ with some positive probability.

Now let us define few more notations: ξ_{ij}^{t+1} is denoted as the conditional probability that link (i,j) is active at time $t+1$ given that the link was active at time t. Let us define e_{ij}^{t} as a Boolean variable whose value is 1, if there is an edge between nodes i and j at time t, and 0, otherwise. Now ξ_{ij}^{t+1} can be defined as follows:

$$\xi_{ij}^{t+1} = P\{e_{ij}^{t+1} = 1 | e_{ij}^{t} = 1\},\ \forall (i,j) \in E^t. \tag{5.1.3}$$

Here ξ_{ij}^{t+1} computed at the current time instant takes care of the nodes mobility as well as dynamic obstacles for the upcoming time instant $t+1$. This in turn depends on S_{ij}^{t+1} which is varying due to mobility of nodes and dynamic obstacles.

5.2 Problem Formulation & Probabilistic Model

A node i transmits some data to another node j at time t. The link (i,j) is established at time t which was free of any obstacles, however it may get blocked by some moving obstacle while the transmission is in process during Δt duration till time instant $t+1$. We are considering the problem of choosing the best `D2D` direct/relay nodes locally at current time instant t such that the local throughput at each node is maximized while considering the nodes' mobility as well as dynamic obstacles in the `mmWave` channel for the upcoming time instant $t+1$. Speed and orientation of nodes are known, however, only speed of dynamic obstacles are known but their orientation is unknown at the BS. The presence of dynamic obstacles in a given link may break the connection for the upcoming time instant $t+1$. For a given sending node $i \in N^t$, we can formally write the objective as:

$$\arg\max_{j} E[C_{ij}^{t+1}], \forall j \in adj^t(i), \tag{5.2.1}$$

where $E[C_{ij}^{t+1}]$ denotes mathematical expectation of capacity of link (i,j) till the upcoming time instant $t+1$ which can be expanded as $E[C_{ij}^{t+1}] = \xi_{ij}^{t+1} \cdot C_{ij}^{t} + (1-\xi_{ij}^{t+1}) \cdot 0$, where ξ_{ij}^{t+1} is the probability that the link established at time t will still be connected till time $t+1$. Hence we can say that with probability $(1-\xi_{ij}^{t+1})$, $C_{ij}^{t} = 0$. This is because if link is disconnected, then the capacity of that link is zero. Hence we can say that $E[C_{ij}^{t+1}] = \xi_{ij}^{t+1} \cdot C_{ij}^{t}$. Links among nodes are formed independently, nodes and obstacles are moving independently and also it is given that at time t, link (i,j) is connected, i.e., $P(S_{ij}^{t} \geq S_{th}) = 1$. Hence, we can say $\xi_{ij}^{t+1} = P(S_{ij}^{t+1} \geq S_{th})$, where $P(S_{ij}^{t+1} \geq S_{th})$ represents the probability that S_{ij}^{t+1} is greater than the required data rate threshold S_{th}. This signifies that for a successful link formation, the `SNR` received must be greater than a minimum threshold value S_{th} till the next time instant $t+1$. We know that S_{ij}^{t+1} is a function of Q_{ij}^{t+1} which in turn is a function of d_{ij}^{t+1} and I_{ij}^{t+1}. The indicator function I_{ij}^{t+1} captures the blockage of link (i,j) by any obstacles from time t till time $t+1$. Keeping all others terms in Q_{ij}^{t+1} constant, we can now

say that for a successful link formation, ξ_{ij}^{t+1} is reduced to:

$$\xi_{ij}^{t+1} = P(d_{ij}^{t+1} \leq \gamma, I_{ij}^{t+1} = 0) \tag{5.2.2}$$

where γ is the threshold on distance between nodes i and j denoting the maximum permissible distance between them to form a communication link. We can reduce equation (5.2.2) as:

$$\xi_{ij}^{t+1} = P(d_{ij}^{t+1} \leq \gamma | I_{ij}^{t+1} = 0) \cdot P(I_{ij}^{t+1} = 0) \tag{5.2.3}$$

In the next section, we will show the computation of ξ_{ij}^{t+1} for a link (i, j) at time t till upcoming time instant $t + 1$. Now we will show the geometrical interpretation of ξ_{ij}^{t+1}.

Geometrical Interpretation of ξ_{ij}^{t+1}

First term $P(d_{ij}^{t+1} \leq \gamma | I_{ij}^{t+1} = 0)$ of equation (5.2.3) represents the probability that link (i, j) is connected till time $t + 1$ given that there are no obstacles present. This implies that node j must not go out of communication range (distance at-most γ) of node i for time duration Δt (from current time instant t to next time instant $t + 1$). The area of communication region of nodes i and j during Δt time duration which is susceptible to blockage by obstacles is called the *vulnerable region*. All possible scenarios of *vulnerable region* is shown in Figure 5.1. We also denote line segment as $\overrightarrow{T}_{ij}^{t}$ which is formed by end points $\overrightarrow{T}_{i}^{t}$ and $\overrightarrow{T}_{j}^{t}$. The parametric equation of this line segment is:

$$\overrightarrow{T}_{ij}^{t} = \lambda \overrightarrow{T}_{i}^{t} + (1 - \lambda) \overrightarrow{T}_{j}^{t} \tag{5.2.4}$$

where, $\lambda \in (0, 1)$. Similarly, we can define $\overrightarrow{T}_{ik}^{t}$ for line segment formed by end points $\overrightarrow{T}_{i}^{t}$ and $\overrightarrow{T}_{k}^{t}$. Also the *line* joining points i and j is denoted as the line ij.

The second term $P(I_{ij}^{t+1} = 0)$ of ξ_{ij}^{t+1} represents the probability that link (i, j) would not be obstructed by any obstacle. For a given obstacle $k \in \mathbb{K}$, speed of obstacle is known and its orientation is unknown, hence obstacle k centered at $\overrightarrow{T}_{k}^{t}$, may go anywhere in $[-\pi, \pi]$ represented by $C_k^{\Delta t}$ as shown in Figure 5.2(a). The example is shown for a specific case where node i is static and node j is in motion. However, this may be extended to the other general cases mentioned in Figure 5.1. In the given example, *obstacle k may obstruct link (i, j) if it lies inside vulnerable region of nodes i and j*. The probable movement of obstacle k is represented as a circle of radius $V_k^t \cdot \Delta t$ (denoted as $C_k^{\Delta t}$) as shown in Figure 5.2(a). The circle $C_k^{\Delta t}$ is centered at $T_k^t : (x_k^t, y_k^t)$ whose equation can be written in parametric form as:

$$x_k^{t+1} = x_k^t + (V_k^t \Delta t)\cos(\theta_k^t); y_k^{t+1} = y_k^t + (V_k^t \Delta t)\sin(\theta_k^t) \tag{5.2.5}$$

where $\theta_k^t \in (-\pi, \pi)$.

Figures 5.2(b) and 5.2(c) shows two different realizations at time instant $t + 1$ of the obstacle's movement presented in Figure 5.2(a). In Figure 5.2(b), obstacle do not interfere

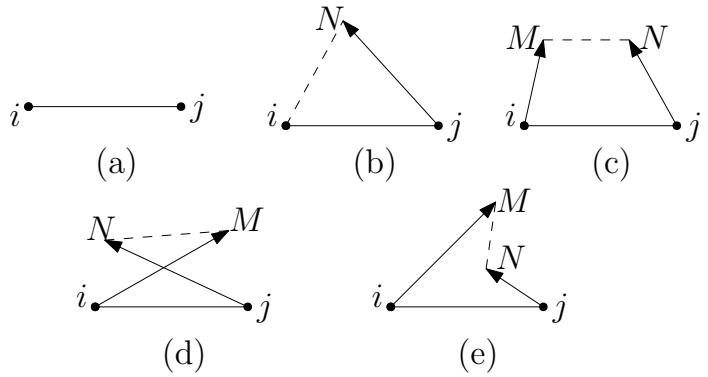

Figure 5.1: Schematic representation of vulnerable region when (a) both node are static, (b) one of the nodes is moving and (c)-(e) both nodes are moving. Bounded region represents the communication zone which constitute the *vulnerable region*.

with the link (i, j) for duration Δt. However, in Figure 5.2(c), obstacle is interfering with the link (i, j) for duration Δt and thus causing packet loss and delay. Here we assume that if an obstacle's path lies inside the vulnerable region then the obstacle would block that link. Now in next section, the respective probabilities $P(d_{ij}^{t+1} \leq \gamma | I_{ij}^{t+1} = 0)$ and $P(I_{ij}^{t+1} = 0)$ are computed using geometry for all possible cases.

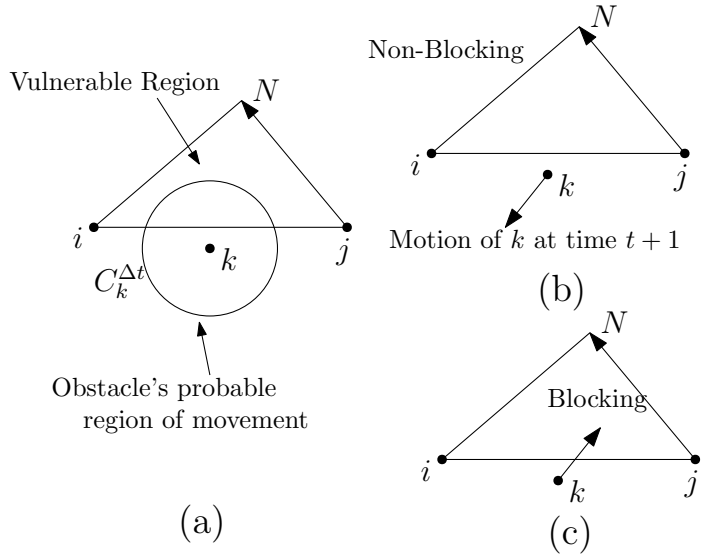

Figure 5.2: (a) Vulnerable region shown for a specific case where node i is static node j is mobile. Non blocking and blocking realizations of (a) is shown respectively in (b) and (c) at time $t + 1$.

5.3 Computation of $P(d_{ij}^{t+1} \leq \gamma | I_{ij}^{t+1} = 0)$

We will compute the probability of link (i, j) connectivity till time instant $t + 1$ given that there are no obstacle present.

If nodes i and j are static then distance between them is constant for Δt duration. If they are already connected at time t, they would be connected till next time instant $t+1$ given that there is no obstacle. Hence, for this case $P(d_{ij}^{t+1} \leq \gamma | I_{ij}^{t+1} = 0) = 1$ otherwise it is 0.

For both the cases, when node i is static and node j is moving and the case when both of them are moving, initially at time t, node j is inside the range of the node i at a distance of $d_{ij}^{t} < \gamma$. During Δt duration, node j may get out of communication range depending upon its movement. Since we can find out d_{ij}^{t+1} for the next time instant $t+1$, the probability of nodes i and j going out of each other's range can be calculated as follows:

$$P(d_{ij}^{t+1} \leq \gamma | I_{ij}^{t+1} = 0) = \begin{cases} 1, & \text{if } d_{ij}^{t+1} \leq \gamma \\ 0, & \text{otherwise.} \end{cases} \tag{5.3.1}$$

5.4 Computation of $P(I_{ij}^{t+1} = 0)$

To compute $P(I_{ij}^{t+1} = 0)$, we need to take into account the effect of each obstacle $k \in \mathbb{K}$ on the given link (i, j) during time duration Δt which is given by the probability $p_{k\_ij}^{t+1}$. Nodes i and j are positioned at $\overrightarrow{T}_i^t$ and $\overrightarrow{T}_j^t$ respectively. Obstacle $k \in \mathbb{K}$ positioned at $\overrightarrow{T}_k^t$ can lie anywhere on circumference of the circle $C_k^{\Delta t}$ at time $t+1$ which denotes its probable movement. We need to check if the given vulnerable region under consideration is affected by the obstacle's probable movement and then compute $p_{k\_ij}^{t+1}$ for all possible cases. The analysis computing the probability of blockage is shown for just one obstacle k. However, same analysis is applicable for all obstacles as they are moving independently.

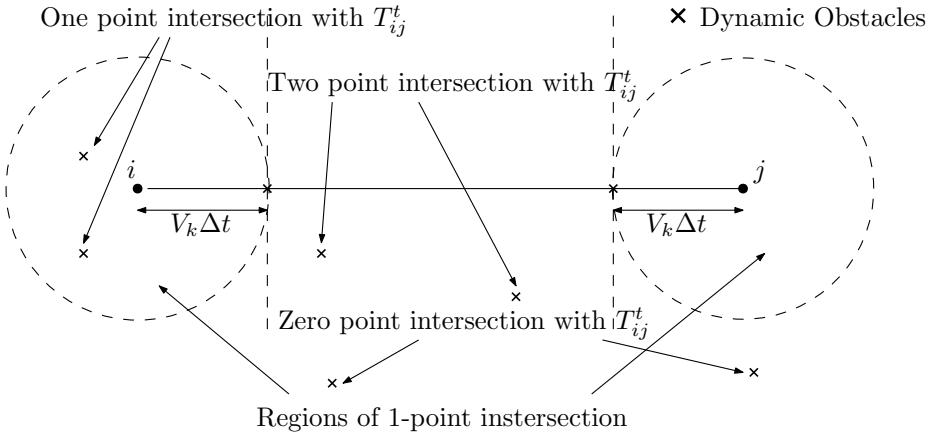

Figure 5.3: Both nodes i and j are static.

5.4.1 Both nodes are static

Here the two UEs i and j are static (shown in Figure 5.3) and are initially connected at time instant t through link (i, j) represented by line segment $\overrightarrow{T_{ij}^{\Delta t}}$ as aforementioned in

equation (5.2.4). Similarly, the equation of circle showing possible movement of obstacle k for duration of Δt time is given in equation (5.2.5). After solving equations (5.2.4) and (5.2.5) for λ, we get number of intersection points of circle $C_k^{\Delta t}$ with the line segment T_{ij}^t (when $\lambda \in (0,1)$). Let us define this number of intersection points as Ψ which may take values in $\{0,1,2\}$. 1) If the value of Ψ is 0 then obstacle k may or may not interfere with link (i,j) for Δt duration depending upon if both T_i^t and T_j^t lie inside circle $C_k^{\Delta t}$ (defined as indicator random variable $\mathbb{F} = 1$) or not ($\mathbb{F} = 0$). 2) If Ψ is 1 then obstacle k interfere with link (i,j) for Δt duration and intersect at one point on the line segment T_{ij}^t. 3) If Ψ is 2 then obstacle k interfere with link (i,j) for Δt duration and intersect at two points on the line segment T_{ij}^t. Note that Ψ wont be greater than 2 since a line can cross a circle at at-most 2 points. The probability of blocking the link is computed in the following Proposition 5.4.1.

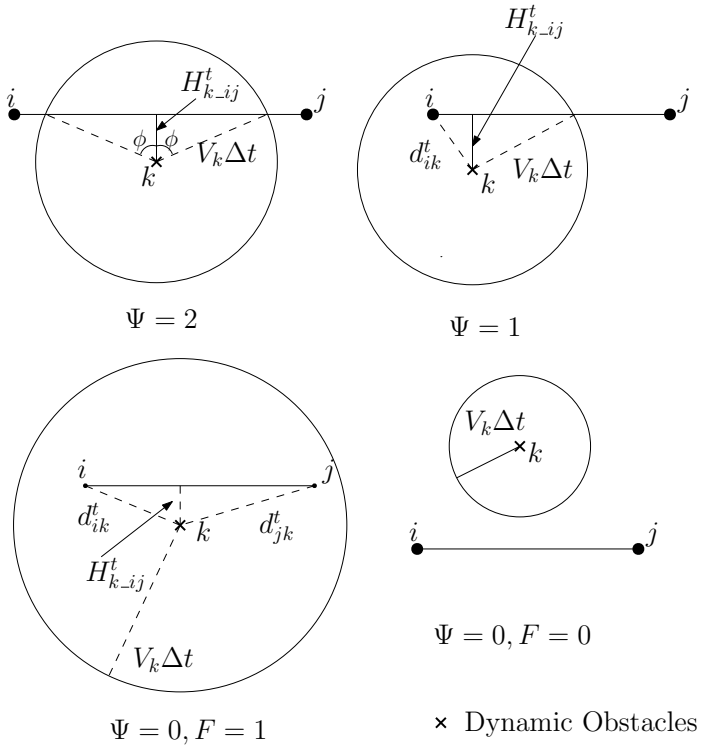

Figure 5.4: Computing blockage probability for both node static case.

Proposition 5.4.1. *For a given link (i,j) between static nodes i and j, blockage probability*

$p^{t+1}_{k\_ij}$ *due to obstacle* $k \in \mathbb{K}$ *with unknown orientation is given by*

$$p^{t+1}_{k\_ij} = \begin{cases} \dfrac{\cos^{-1}\left(\frac{H^t_{k\_ij}}{V^t_k}\right)}{\pi}, & \Psi = 2 \\ \dfrac{abs\left((\text{-}1)^a \cos^{-1}\left(\frac{H^t_{k\_ij}}{\min(d^t_{ik}, d^t_{jk})}\right) + \cos^{-1}\left(\frac{H^t_{k\_ij}}{V^t_k}\right)\right)}{2\pi}, & \Psi = 1 \\ \dfrac{abs\left((-1)^b \cos^{-1}\left(\frac{H^t_{k\_ij}}{d^t_{ik}}\right) + (-1)^c \cos^{-1}\left(\frac{H^t_{k\_ij}}{d^t_{jk}}\right)\right)}{2\pi}, & \Psi = 0,\ \mathbb{F} = 1 \\ 0, & \Psi = 0,\ \mathbb{F} = 0 \end{cases} \tag{5.4.1}$$

where $H^t_{k\_ij}$ *is the Euclidean distance from* T^t_k *to the line segment* T^t_{ij}, $abs(\cdot)$ *denotes the absolute value function. Here* a *is* 0 *or* 1 *depending upon whether* $\angle kxy$ *is acute or obtuse respectively, where* x=i *and* y=j *if* $d^t_{ik} < d^t_{jk}$, *otherwise* x=j *and* y=i. *Similarly,* b *is* 0 *or* 1 *depending upon whether* $\angle kij$ *is acute or obtuse respectively, and* c *is* 0 *or* 1 *depending upon whether* $\angle kji$ *is acute or obtuse respectively.*

Proof. Figure 5.3 shows all possible scenarios when both UEs are static. Appropriate positions of the dynamic obstacle k is shown with respect to Ψ which is the number of points of intersection of line segment $\overrightarrow{T}^{\Delta t}_{ij}$ with $C^{\Delta t}_k$. The analysis for respective cases is shown in figure 5.4.

For the case $\Psi = 2$, blockage probability can be computed as: $p^{t+1}_{k\_ij}$=ϕ/π. Now we can derive ϕ=$\cos^{-1}\left(\frac{H^t_{k\_ij}}{V^t_k \Delta t}\right)$, where, $H^t_{k\_ij}$ as defined earlier, is the shortest distance of point $\overrightarrow{T}^t_k$ from line segment $\overrightarrow{T^t_{ij}}$. Hence

$$p^{t+1}_{k\_ij} = \frac{\cos^{-1}\left(\frac{H^t_{k\_ij}}{V^t_k \Delta t}\right)}{\pi}.$$

Similarly, for the case when $\Psi = 1$, if $\overrightarrow{T^{\Delta t}_i}$ is inside $C^{\Delta t}_k$ then probability of blockage is

$$\frac{abs\left((-1)^a \cos^{-1}\left(\frac{H^t_{k\_ij}}{d^t_{ik}}\right) + \cos^{-1}\left(\frac{H^t_{k\_ij}}{V^t_k \Delta t}\right)\right)}{2\pi}.$$

Here, $a = 1$ if $\angle kij$ is obtuse, otherwise, $a = 0$ and $abs(\cdot)$ denotes the absolute value function. If for this case ($\Psi = 1$), $\overrightarrow{T}^{\Delta t}_j$ is inside $C^{\Delta t}_k$ then probability of blockage is

$$\frac{abs(\left((-1)^a \cos^{-1}\left(\frac{H^t_{k\_ij}}{d^t_{jk}}\right) + \cos^{-1}\left(\frac{H^t_{k\_ij}}{V^t_k \Delta t}\right)\right)}{2\pi}.$$

Here, $a = 1$ if $\angle kji$ is obtuse, otherwise, $a = 0$.

Proceeding in the similar manner for the case when $\Psi = 0, \mathbb{F} = 1$ as shown in Figure

5.4, the probability of blockage can be directly computed as

$$\frac{abs\left((-1)^b \cos^{-1}\left(\frac{H^t_{k\_ij}}{d^t_{ik}}\right) + (-1)^c \cos^{-1}\left(\frac{H^t_{k\_ij}}{d^t_{jk}}\right)\right)}{2\pi}.$$

Here, if $\angle kij$ is obtuse then $b = 1$, otherwise $b = 0$. If $\angle kji$ is obtuse then $c = 1$, otherwise $c = 0$. Note that, if one of the angle $\angle kij$ is obtuse then other angle $\angle kji$ would be acute and vice versa. Note that both angles could not be obtuse (thus, a and b must not take value 1 simultaneously). However note that both angles may be acute (thus, a and b can take value 0 simultaneously).

For the case when $\Psi = 0, \mathbb{F} = 0$, probability of blockage is 0, since obstacle k is not going to interfere with the link (i, j). □

5.4.2 One of the node is moving

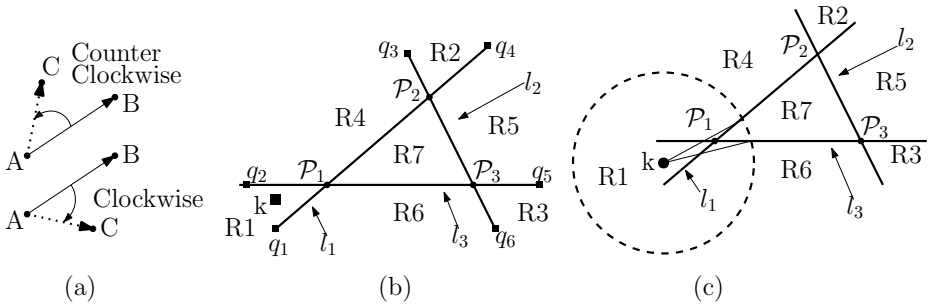

Figure 5.5: (a) Direction of point C with respect to line AB (b) All possible sub-regions when one of the nodes is moving and form a triangular communication zone. (c) Specific case where obstacle k residing in sub-region R_1 may block the communication zone from two sides l_1 and l_3 of the triangular vulnerable region.

In this case, node i is static and j is moving with speed V^t_j. We first define a method to identify the location of obstacle around the vulnerable region. Let us consider a point C whose tilt from a line AB needs to be found out which is defined as the direction towards which the point C is facing from line AB. We define *sign(BA, CA)* as the function computing the sign of cross product of two vectors BA and CA across the pivot A as shown in Figure 5.5(a). The pivot is point of reference from where the tilt of a given point is measured with respect to the given line passing through it. *sign(BA, CA)* will be positive $(+)$ or it will be negative $(-)$ depending upon whether point C is towards counter-clockwise or clockwise direction of line AB respectively. In our problem, in order to find out probability of blockage by obstacle k (position as described earlier is $\overrightarrow{T}^t_k$) in the vulnerable region, we have to consider various sub-regions in the vulnerable region with obstacle's initial position as shown in Figure 5.5(b). There are three lines considered as line $l_1 : [\mathcal{P}_1, \mathcal{P}_2]$, $l_2 : [\mathcal{P}_2, \mathcal{P}_3]$, and $l_3 : [\mathcal{P}_3, \mathcal{P}_1]$ with end points denoted in respective square brackets. The pivots are

denoted as $\mathcal{P}_1$, $\mathcal{P}_2$, and $\mathcal{P}_3$ respectively for lines l_1, l_2, and l_3 as shown in the figure. For example, in order to find out the tilt of point k (in sub-region defined by $q_1\mathcal{P}_1q_2$ as shown in the figure) with respect to line l_1, l_2 and l_3 (respectively on pivots $\mathcal{P}_1$, $\mathcal{P}_2$ and $\mathcal{P}_3$), we would calculate $s_1 = sign(l_1, \overrightarrow{T}^t_{\mathcal{P}_1 k})$, $s_2 = sign(l_2, \overrightarrow{T}^t_{\mathcal{P}_2 k})$, and $s_3 = sign(l_3, \overrightarrow{T}^t_{\mathcal{P}_3 k})$. Combination of $< s_1, s_2, s_3 >$ triplets *uniquely* define the presence of k in a particular sub-region where it resides. The final result is shown in Table 5.1, where we can distinguish among various sub-regions. The column s_1, s_2, and s_3 denote signs representing the tilt of point k with respect to lines l_1, l_2, and l_3 respectively. The first column defines the sub-region where point k resides. In the first row, where the triplets are $< +, -, - >$, defines the presence of point k in sub-region R_1. Currently, while deriving this table, we assume that point k do not lie on any of the lines and this specific condition would be dealt later. Since we know all the line equations as described in previous section, we can find out the sub-region where k is present. Note that the relative choice of lines and respective pivot points inherently decides the values given in Table 5.1. Hence we first design a method to select the lines and relative pivot points in order to make the Table 5.1 values constant across all the possible cases in upcoming sections as well.

Method to choose pivot points and lines: We choose the first pivot point such that it has the minimum y co-ordinate value among three points of the triangle. If two vertex have same y co-ordinate values then we choose the one with least x-value to be the first pivot point ($\mathcal{P}_1$). Then we move in clockwise direction to choose the second pivot point. The line between the first pivot point and second pivot point is chosen to be the first line l_1. Then we again move in clockwise direction to choose the third pivot point and the line between second ($\mathcal{P}_2$) and third pivot point ($\mathcal{P}_3$) is the second line l_2. The remaining line is designated as the third line l_3. Similarly the sub-regions are defined as shown in the figure. For example, R_1 is the sub-region formed by the intersection of l_1 and l_3 and which is opposite to l_2. Similarly all other sub-regions are defined relative to lines and their intersections to make the notion of sub-regions uniform across all scenarios. Hence using this strategy we can utilize Table 5.1 across all possible scenarios.

Sub-region	s_1	s_2	s_3	Sub-region	s_1	s_2	s_3
R_1	$+$	$-$	$+$	R_5	$-$	$+$	$-$
R_2	$+$	$+$	$-$	R_6	$-$	$-$	$+$
R_3	$-$	$+$	$+$	R_7	$-$	$-$	$-$
R_4	$+$	$-$	$-$				

Table 5.1: Identifying sub-regions of obstacle k at time t when one of the node is moving.

Handling boundary conditions: In order to complete the above design for finding sub-regions where an obstacle might be present, we need to describe appropriate boundary conditions. As shown in Figure 5.5(b), points marked as $q_1 - q_6$ show the probable presence of obstacles which constitute boundary cases. For example, let us take point q_1 on line l_1 as shown in Figure 5.5(b). This point is neither on clockwise $(-)$ nor on counter-clockwise $(+)$ side of line l_1. The $sign(l_1, \overrightarrow{T}^t_{\mathcal{P}_1 q_1})$ function won't give the tilt of point q_1 in this case and hence we won't be able to apply the mapping given in Table 5.1. We can observe that when an obstacle is present at point q_1, it would enter the vulnerable region only from side denoted by line l_3 (i.e., from sub-region R_6). Hence, we would modify our design for such cases by returning $-$ (negative sign denoting clockwise direction), when function $sign(l_1, \overrightarrow{T}^t_{\mathcal{P}_1 q_1})$ is executed. Now the triplet for the point q_1 can be written as $< -, -, + >$ which corresponds to sub-region R_6, hence verifying our observation. This implies that in order to compute the blockage probability due to obstacle present at point q_1, we need to compute the blockage probability relative to line l_3. Similarly, we can see for other cases: for point q_4 on line l_1 as shown in Figure 5.5(b), returned triplet would be $< -, +, - >$, which corresponds to sub-region R_5. This is also verified from the observation of the figure that obstacle would enter from the side l_2 corresponding to sub-region R_5. Similarly for point q_5 on line l_3 we can give the triplet as: $< -, +, - >$ which corresponds to sub-region R_5 which is also verifiable from the observation in the Figure 5.5(b). Similarly other mentioned boundary cases, we can get unique triplets of signs corresponding to the sub-regions from where the obstacle would enter the vulnerable region.

Computing blockage probability due to dynamic obstacle: Now we give the algorithm to compute the blockage probability $p^{t+1}_{k\_ij}$ for an obstacle k on link (i, j) for the duration Δt. Note that for the case when i and j move in a straight line, the probability of blockage by k is computed in same manner as mentioned in Proposition 5.4.1. We will now consider the other scenarios where i and j form a triangular vulnerable region during Δt time duration. We will identify the sub-region of presence of obstacle k (positioned at $\overrightarrow{T}^t_k$). In sub-region R_7, k would block the entire vulnerable region, hence for this case $p^{t+1}_{k\_ij} = 1$. All the sub-regions mentioned are mutually exclusive. For sub-regions R_4, R_5, and R_6, the obstacle k blocks the communication from the respective lines (lines l_1, l_2 and l_3) only. For this case we can use the same method to calculate $p^{t+1}_{k\_ij}$ as described previously in Proposition 5.4.1. The sub-regions R_1, R_2, and R_3 are *critical regions* from where the obstacle k would block link (i, j) from two different sides of the triangular vulnerable region as shown in Figure 5.5(c). For example, the presence of obstacle k in R_1 might block the communication from line l_1 and line l_3. Here we need to take the unions of the events constituting blockage from obstacle on these two lines of the vulnerable region. Note that for computing the blockage probability on a line, we use the method described in Proposition 5.4.1. First let us denote $f\_static(X_1, k)$ as a function call which executes the algorithm mentioned in Proposition 5.4.1. Here X_1 denotes the line segment which is going

to be blocked by obstacle k. The return value of this function is in $[0, 1]$. The blockage probability $p_{k\_ij}^{t+1}$ due to obstacle $k \in \mathbb{K}$ is given below:

step i. Find out sub-region R for obstacle k.

step ii. If $R = R_7$, then $p_{k\_ij}^{t+1} = 1$. Else if, $R = R_4$, or $R = R_5$, or $R = R_6$, then $p_{k\_ij}^{t+1}$ is $f\_static(X_1, k)$, where $X_1 = l_1$, $X_1 = l_2$, or $X_1 = l_3$ for $R = R_4$, $R = R_5$, or $R = R_6$ respectively. This function is computed according to Proposition 5.4.1.

step iii. Else, when $R = R_1$, or $R = R_2$, or $R = R_3$, $p_{k\_ij}^{t+1} = f\_static(X_1, k) + f\_static(X_2, k)$, where X_1 and X_2 are the two sides of the triangular region going to be blocked by the obstacle k. Here $< X_1, X_2 >$ takes values in $< l_1, l_3 >$, $< l_1, l_2 >$, and $< l_2, l_3 >$ respectively for the cases when $R = R_1$, $R = R_2$, and $R = R_3$. Note that the sum of the two values returned by function calls would not exceed 1. This is because the line segments taken as arguments in these function call lie in exclusive sub-regions as already mentioned before.

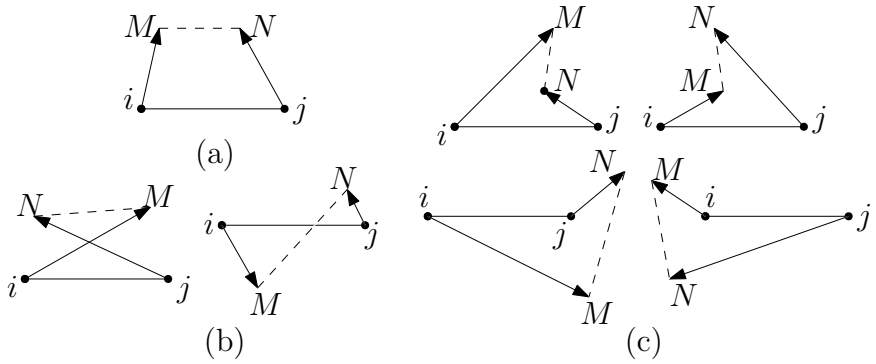

Figure 5.6: Various sub-classes when both nodes are moving.

5.4.3 Both nodes are moving

This case is shown in Figure 5.6 where nodes i and j both are moving with speeds V_i^t and V_j^t respectively. As shown in this figure, we denote M and N as the location of node i and j at time instant $t + 1$ respectively. This case is divided into 3 main sub-classes as depicted in the Figure 5.6(a)-(c). We develop a solution which abstracts the selection of sub-regions in the vulnerable region using the notion of pivots and lines formed by these pivots to include all possible motion of nodes for all the three sub classes. We first describe the method to differentiate among these cases. Later, we give the method to compute the blockage probability $p_{k\_ij}^{t+1}$ due to an obstacle $k \in \mathbb{K}$ using the method as described for the scenario when only one of the nodes is moving as mentioned in the previous subsection.

5.4.3.1 Differentiating among various sub-classes when both nodes are moving

If either *line segments* $\overrightarrow{T}^t_{iM}$ and $\overrightarrow{T}^{t+1}_{iN}$ or *line segments* $\overrightarrow{T}^t_{ij}$ and $\overrightarrow{T}^{t+1}_{MN}$ intersect with each then this scenario is represented by Figure 5.6(b) and denoted as sub-class(b) of this case where both nodes are moving. When point M lies in $\triangle ijN$, or point N lies in $\triangle ijM$, or point i lies in $\triangle MjN$, or point j lies in $\triangle iMN$, then in that case the scenario is depicted in Figure 5.6(c) and denoted as sub-class (c). Otherwise, the scenario would be depicted by Figure 5.6(a) which is denoted as sub-class (a).

5.4.3.2 Computation of $p^{t+1}_{k\_ij}$ for sub-class (a)

After identifying the scenarios based on sub-classes as mentioned above, we first describe the method for computing $p^{t+1}_{k\_ij}$ for sub-class (a) which is shown in Figure 5.6(a). Here also, we need to determine the sub-region where the obstacle lies. Before describing the rule which describes the sub-region for the given obstacle and the corresponding probability of blockage, let's first describe the necessary steps required to make the presented design applicable throughout any general scenario of motion of `UEs` for sub-class (a).

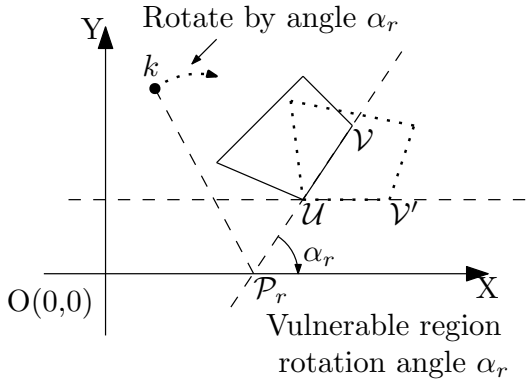

Figure 5.7: Geometric rotation of the vulnerable region to fix its representation across all possible movements of `UEs` in sub-class (a)

Fix the representation of vulnerable region for general scenarios involving movement of `UEs`: Let $\mathcal{U}$ denotes the bottom and leftmost pivot among four points (i, j, M, and N). And, let $\mathcal{V}$ denotes the first point in counter-clockwise direction. This is shown in Figure 5.7. Let α_r denotes the angle that line $\mathcal{UV}$ subtends on X-axis as shown in Figure 5.7. Point $\mathcal{P}_r$ is the point of intersection of line $\mathcal{UV}$ and X-axis. The vulnerable region is rotated by angle α_r in clockwise direction with respect to point $\mathcal{P}_r$. This process in turn makes the side of the vulnerable region represented by points $\mathcal{U}$ and $\mathcal{V}$ parallel to X-axis which is shown by dotted lines in Figure 5.7. Here, the obstacle k is also rotated by angle α_r in clockwise direction with respect to point $\mathcal{P}_r$. These operations require $O(1)$ time for each given obstacle. Note that this operation has to be performed for all the obstacles present in the region. If the line formed by points $\mathcal{U}$ and $\mathcal{V}$ are parallel to X-axis, then

there is no need to perform the geometric rotations either for the vulnerable region or the obstacle. By doing this process we achieve the uniformity in region finding algorithm and respective blockage probability computation across all possible general movement of UEs for this sub-class.

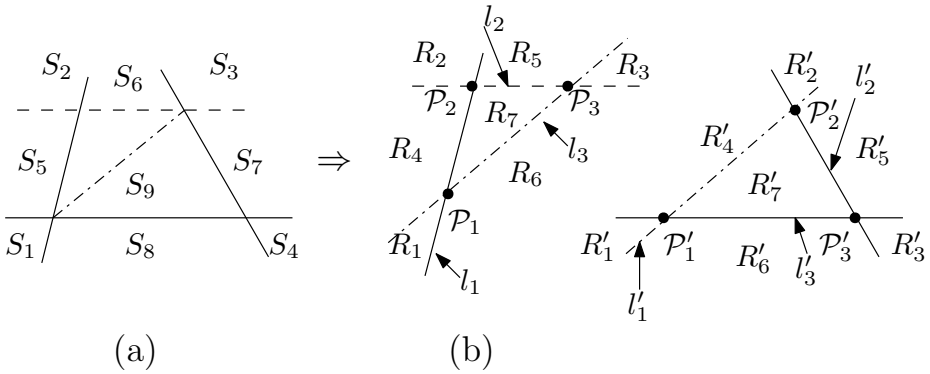

Figure 5.8: Sub class (a) when both nodes are moving.

Sub-region	Rule	X_1	X_2
S_1	$R_1 \cup R'_1$	l_1	l'_3
S_2	R_2	l_1	l_2
S_3	$R'_2 \cup R_3$	l_2	l'_2
S_4	R'_3	l'_2	l'_3
S_5	$R_4 - R'_1$	l_1	*null*
S_6	$R_5 - R'_2$	l_2	*null*
S_7	$R'_5 - R_3$	l'_2	*null*
S_8	$R'_6 - R_1$	l'_3	*null*
S_9	$R_7 \cup R'_7$	$\times$	$\times$

Table 5.2: Identifying sub-regions of obstacle k and arguments of function calls computing the blockage probability when both nodes are moving for sub-class (a).

Rule to find the sub-region of obstacle k and corresponding blockage probability: After we have fixed the representation of the vulnerable region, we describe the rules to find sub-region of the obstacle and compute the corresponding blockage probability.

As shown in Figure 5.6(a), the vulnerable region is a quadrilateral which is partitioned into 2 triangular vulnerable regions $\triangle\mathcal{P}_1\mathcal{P}_2\mathcal{P}_3$ and $\triangle\mathcal{P}'_1\mathcal{P}'_2\mathcal{P}'_3$. Here $\mathcal{P}_1$, $\mathcal{P}_2$, $\mathcal{P}_3$, $\mathcal{P}'_1$, $\mathcal{P}'_2$, and $\mathcal{P}'_3$ are respective pivots in the above mentioned two triangles. These are found out using the method described in previous sub-section. Similarly, lines $l_1 : [\mathcal{P}_1, \mathcal{P}_2]$, $l_2 : [\mathcal{P}_2, \mathcal{P}_3]$, $l_3 : [\mathcal{P}_3, \mathcal{P}_1]$, $l'_1 : [\mathcal{P}'_1, \mathcal{P}'_2]$, $l'_2 : [\mathcal{P}'_2, \mathcal{P}'_3]$, and $l'_3 : [\mathcal{P}'_3, \mathcal{P}'_1]$ are described as in previous sub-section formed by respective pivot points written in square brackets. We can run the sub-region finding algorithm of previous sub-section in both of the triangular vulnerable regions. The presented design finds the sub-region in two triangles individually where the given obstacle k lies at time t. The rule for finding sub-regions in the quadrilateral vulnerable region is summarized in Table 5.2 which is verified by observation and can be checked easily. We can simply calculate the probability of blockage by obstacle k as follows: When obstacle is in sub-region S_9, then blockage probability is 1. For other cases the blockage probability is computed as: $f\_static(X_1, k) + f\_static(X_2, k)$. The values of the arguments X_1 and X_2 are summarized in Table 5.2. Here X_1 and X_2 are the arguments which represent lines which are going to be blocked from obstacle k. For the cases where there is only one line (X_1) which is going to be blocked by obstacle k, the value of the other argument X_2 is mentioned to be *null* in the respective column given in Table 5.2 and $f\_static(X_2, k)$ would not be executed for this case. For the specific case of sub-region S_9, the blockage probability is 1, hence the value in respective arguments column in Table 5.2 is marked by $\times$ which signifies that the argument values are not applicable for this particular case. Here, the returned value of $f\_static(X_1, k) + f\_static(X_2, k)$ would not exceed 1 for the cases shown in Table 5.2 because the arguments X_1 and X_2 together take lines which belong to exclusive sub-regions of the quadrilateral. Hence the regions of the circle $C_k^{\Delta t}$ lying in these sub-regions do not overlap while computing the blockage probability for this sub-class (a).

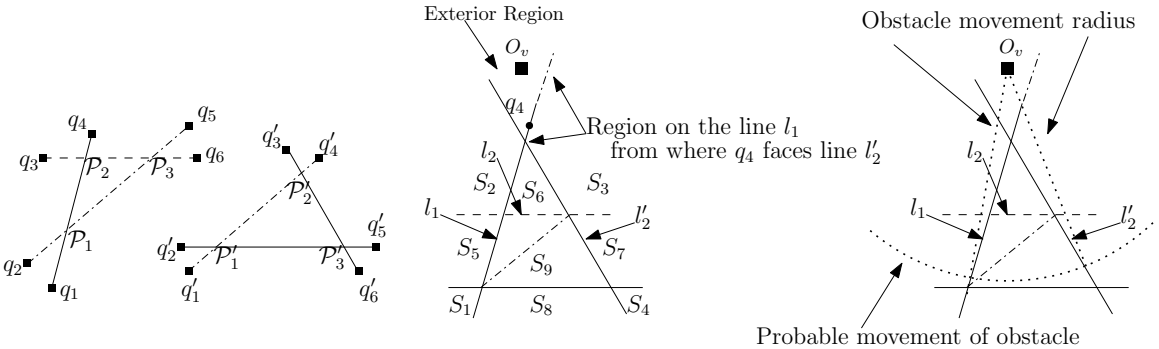

Figure 5.9: Boundary cases for sub-class (a)

Boundary conditions: Since, we are merging the results of two different triangular regions of the given quadrilateral vulnerable region, we need to look for the cases constituting boundary conditions. Here these boundary points also follow the similar notations as was used for the case where only one of the nodes was moving in previous sub-section. Let

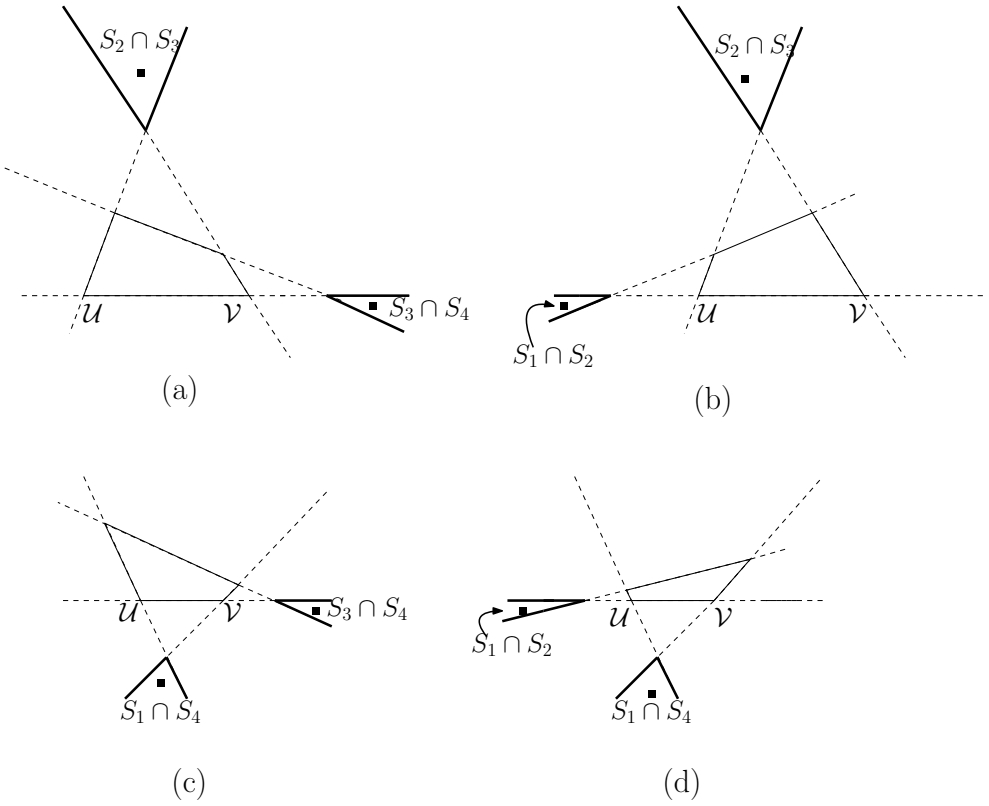

Figure 5.10: Boundary cases for sub-class (a) where obstacle lies in the *exterior region*

us first define the *exterior region* as the outer region of the quadrilateral, which is formed when any of its two opposite sides are extended and they intersect at a point as shown in Figure 5.9(b). This region is opposite to that side of the quadrilateral which is nearest to the point of intersection of the aforementioned two sides. We now describe four types of boundary points: For the first type, the obstacle lies in the exterior region but *not* on any extended sides in that region, for example point O_v as shown in Figure 5.9(b), second type of point lies in the exterior region and only on the extended side of the quadrilateral, for example, point q_4 on line l_1 as shown in Figure 5.9(b) represents this case. The third and fourth types of points do not lie in exterior region and belong respectively to the sets $\mathcal{X} = \{q_4, q_1, q_3, q_6, q_2', q_3', q_5', q_6'\}$ and $\mathcal{Y} = \{q_2, q_1', q_5, q_4'\}$ as shown in Figure 5.9(a).

For the first type of boundary points, the obstacle at point O_v can block the vulnerable region from both sides l_1 and l_2' along with the side l_2 which it is facing. This region where O_v lies, is identified as $S_2 \cap S_3$ because both S_2 and S_3 regions are common to the location where O_v lies. General cases of such points are shown in the Figure 5.10. The rule to locate respective boundary case sub-region is also mentioned in Figure 5.10. We will now give steps to compute the blockage probability for the specific case when the obstacle lies at O_v. Obstacle k at O_v can block the vulnerable zone from l_2, l_1 and l_2'. Hence the blockage probability can be computed: $f\_static(l_1, k) + f\_static(l_2, k) + f\_static(l_2', k)$ as shown in

Figure 5.9(c). Note that the summation of the returned value of these three function calls would not exceed 1 because they compute probabilities of blockage in different exclusive regions where the regions of $C_k^{\Delta t}$ do not overlap as shown in Figure 5.9(c). Similar approach is used for other scenarios as well.

Now, let us look at the second type of boundary point q_4 which is shown in Figure 5.9(b). This point lies in the exterior region on the line segment l_2. It is easy to observe that one of the line vulnerable to blockage would be l_2 (lying in $\triangle\mathcal{P}_1\mathcal{P}_2\mathcal{P}_3$). Also, for this case when obstacle k is lying on q_4, there is one more possibility of blockage of vulnerable region from another side l_2' of the quadrilateral which is lying in the other triangular region $\triangle\mathcal{P}_1'\mathcal{P}_2'\mathcal{P}_3'$ (shown in Figure 5.9 (b)). For the third type of scenario, the point $q_4 \in \mathcal{X}$ do not lie in the exterior region. The rule for finding this condition uses the following steps: If point q_4 is on line l_1, and it belongs to sub-region R_4', then it does not face the line l_2' otherwise if point q_4 lies in sub-region R_2', then it directly faces line l_2'. Hence the probability of blockage can be computed as $f\_static(l_2, k) + f\_static(r, k)$. Here, r is l_2' if q_4 faces the line l_2' otherwise r is $null$. Here also when r is l_2', the sum of the returned function call won't exceed 1 as already explained before. The similar method can be used for other points lying in these two types of regions. For the last type of boundary points belonging to set $\mathcal{Y}$, for example q_2 and q_1' lines vulnerable to blockage are l_1 and l_3 since these points belong to the sub-region S_1. In order to check this condition, we simply need to see whether the obstacle belong to both R_4 (in $\triangle\mathcal{P}_1\mathcal{P}_2\mathcal{P}_3$) and R_6' (in $\triangle\mathcal{P}_1'\mathcal{P}_2'\mathcal{P}_3'$). The probability of blockage by the obstacle lying in S_1 is computed as described earlier. Similarly this strategy is used for the points q_5 and q_4'.

Now we will give the final method which will be used to find out the sub-regions and probability of blockage considering these boundary conditions. We are given the fixed representation of the vulnerable region and the rotated obstacle as input, the steps for the computation of blockage probability is:

i. Locate sub-regions $R_1 - R_7$ and $R_1' - R_7'$ in the two triangles.

ii. Find the sub-regions S_1, S_2, S_3, and S_4 in the quadrilateral.

iii. Perform boundary condition check to locate corresponding sub-regions.

iv. If satisfies boundary check, compute blockage probability using aforementioned strategy.

v. Else Compute blockage probability for obstacle lying in appropriate sub-region $S_1 - S_9$ using aforementioned strategy as mentioned in Table 5.2.

5.4.3.3 Computation of $p_{k\_ij}^{t+1}$ for sub-class (b)

Now we give the method for the sub-class (b) which is shown in Figure 5.6(b). The method to compute blockage probability is similar to above described method with very little difference.

Before describing the rule which describes the sub-region for the given obstacle and the corresponding probability of blockage, let's first describe the necessary steps required to make the presented design applicable throughout any general scenario of motion of `UEs` in this considered sub-class (b).

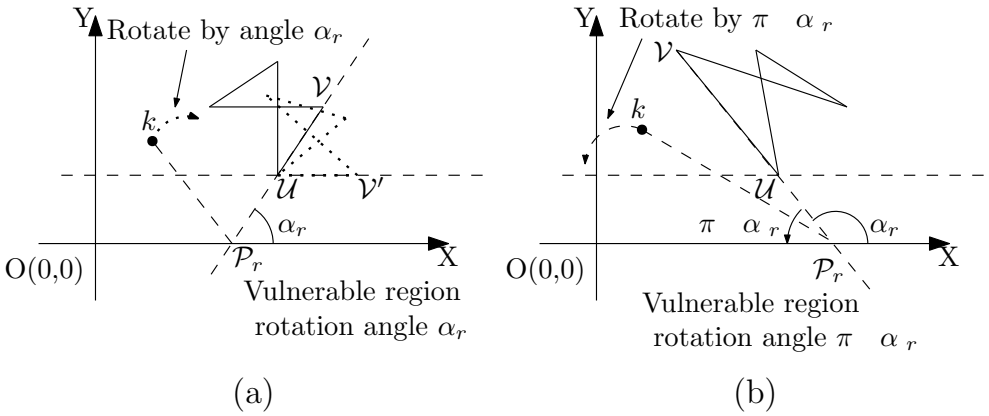

Figure 5.11: Geometric rotation of the vulnerable region to fix its representation across all possible movements of `UEs` in sub-class (b)

Fix the representation of vulnerable region for general scenarios involving movement of `UEs`: There are two different possibilities in this case depending upon whether lines iM and jN are intersecting or lines ij and MN are intersecting as shown in Figure 5.6(b). Here also, we need to find the bottom and left most point denoted as $\mathcal{U}$ as shown in Figure 5.11. We also need to choose the other point $\mathcal{V}$. The rule for choosing $\mathcal{V}$ is as follows: For the case when lines iM and jN are intersecting, if $\mathcal{U}$ is i then $\mathcal{V}$ is M and vice versa, otherwise, if $\mathcal{U}$ is j then $\mathcal{V}$ is N and vice versa. Similarly, for the case when lines ij and MN are intersecting, if $\mathcal{U}$ is i then $\mathcal{V}$ is j and vice versa, otherwise, if $\mathcal{U}$ is M then $\mathcal{V}$ is N and vice versa. Now after getting these two points $\mathcal{U}$ and $\mathcal{V}$, we find the angle formed by the line $\mathcal{UV}$ with the X-axis denoted as α_r as shown in Figure 5.11 (a)-(b). Point $\mathcal{P}_r$ denotes the point of intersection of the line $\mathcal{UV}$ with X-axis. The vulnerable region is rotated along the point $\mathcal{P}_r$ by angle α_r in clockwise direction, if and only if none of the points in the vulnerable region has negative Y-coordinate value after rotation as shown in Figure 5.11(a), otherwise, the vulnerable region is rotated along point $\mathcal{P}_r$ by angle $\pi - \alpha_r$ in counter-clockwise direction as shown in Figure 5.11(b). This process in turn makes the side of the vulnerable region represented by points $\mathcal{U}$ and $\mathcal{V}$ parallel to $X - axis$ which is shown by dotted lines in Figure 5.11(a). Here, the obstacle k is also rotate by angle α_r in clockwise direction with respect to point $\mathcal{P}_r$ or $\pi - \alpha_r$ in counter-clockwise direction with respect to point $\mathcal{P}_r$ depending upon how the vulnerable region is rotate. These operations require $O(1)$ time for each given obstacle. Note that this operation has to be performed for all the obstacles present in the region. If the line formed by points $\mathcal{U}$ and $\mathcal{V}$ are parallel to X-axis, then there is no need to perform the geometric rotations either for the vulnerable region or the obstacle. Here also, this process helps in achieving the uniformity in region finding

algorithm and respective blockage computation across all possible general orientations in motion of UEs for this sub-class.

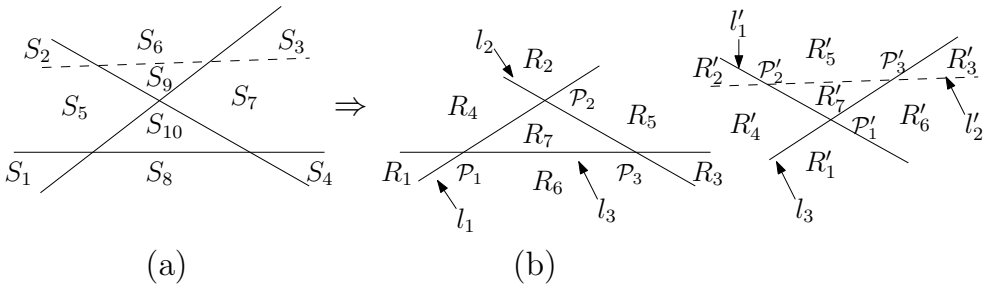

Figure 5.12: Sub class (b) when both nodes are moving.

Sub-region	Rule	X_1	X_2	X_3
S_1	R_1	l_3	l_1	l_1
S_2	R'_2	l_3	l_2	l'_3
S_3	R'_3	l'_2	l'_1	l_1
S_4	R_3	l'_2	l'_3	l_2
S_5	$R_4 \cap R'_4$	l_2	l'_2	$\times$
S_6	R'_5	l'_2	$null$	$\times$
S_7	$R_5 \cap R'_6$	l_2	l'_3	$\times$
S_8	R_6	l_3	$null$	$\times$
S_9	R'_7	$\times$	$\times$	$\times$
S_{10}	R_7	$\times$	$\times$	$\times$

Table 5.3: Identifying sub-regions of obstacle k and arguments of function calls computing the blockage probability when both nodes are moving for sub-class (b).

Rule to find the sub-region of obstacle k and corresponding blockage probability: In order to determine the sub-region where the obstacle lies we give the following approach. As shown in Figure 5.12, the communication region is already divided into 2 triangular regions. Now the triangular regions can be represented as $\triangle\mathcal{P}_1\mathcal{P}_2\mathcal{P}_3$ and $\triangle\mathcal{P}'_1P'_2P'_3$. Similarly, lines $l_1 : [\mathcal{P}_1, \mathcal{P}_2]$, $l_2 : [\mathcal{P}_2, \mathcal{P}_3]$, $l_3[\mathcal{P}_3, \mathcal{P}_1]$, $l'_1 : [\mathcal{P}'_1, \mathcal{P}'_2]$, $l'_2 : [\mathcal{P}'_2, \mathcal{P}'_3]$, and $l'_3 : [\mathcal{P}'_3, \mathcal{P}'_1]$

are described as in previous paragraph formed by respective pivot points written in square brackets. We can run the sub-region finding algorithm of previous sub-section in both of the triangular regions. Here the sub-regions of the vulnerable region are identified by using the rules summarized in Table 5.3. When the obstacle k is in sub-region S_9 or S_{10}, then the blockage probability is 1. For sub-regions S_5-S_8 the blockage probability is computed as: $f\_static(X_1, k) + f\_static(X_2, k)$. The values of the arguments X_1 and X_2 are also summarized in Table 5.3. Here also, the sum of the returned value of the two function calls won't exceed 1 as already explained before. For the remaining sub-regions S_1, S_2, S_3 and S_4, the blockage probability is computed as: $f\_static(X_1, k)+f\_static(X_2, k)+f\_static(X_3, k)$. The values of the arguments X_1, X_2, and X_3 are summarized in Table 5.3. As explained before, the summation of the returned value of these three function calls would not exceed 1. For example, as shown in the Figure 5.14, for region S_1, blockage probability due to obstacle k is computed as: $f\_static(l_3, k) + f\_static(l_1, k) + f\_static(l'_1, k)$. It is clear from the figure that the circular area of do not overlap the vulnerable region by the given computation of blockage probability.

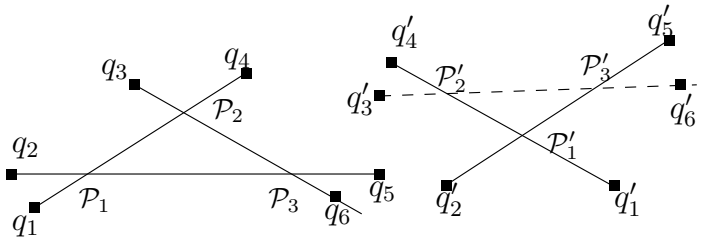

Figure 5.13: Boundary cases for sub-class (b)

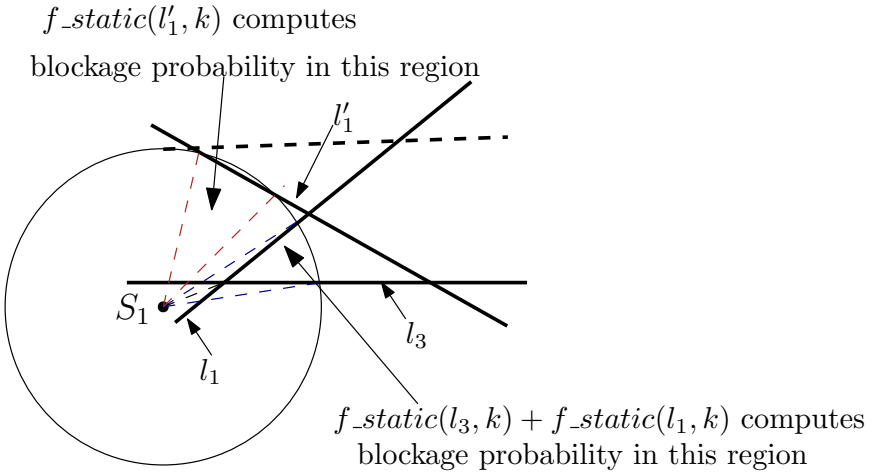

Figure 5.14: Probability of blockage is computed in exclusive sub-regions.

Boundary condition: This is similar to the boundary check mentioned previously for the sub-class (a). Here also we describe four types of boundary points: For the first case, the obstacle lies at any point in the exterior region but *not* on any of the extended

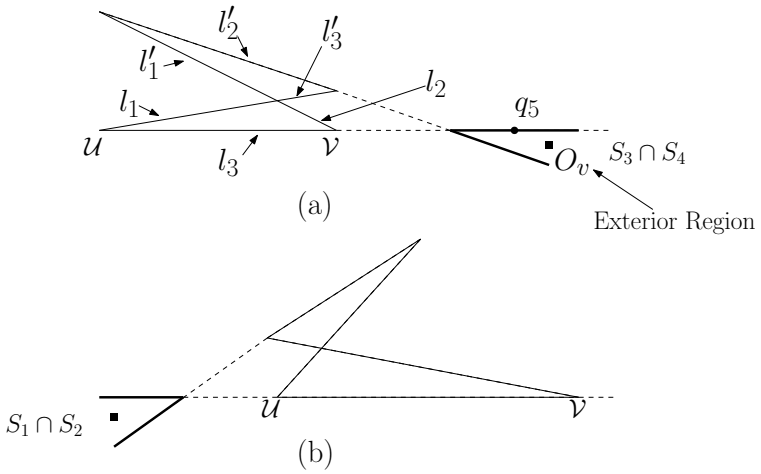

Figure 5.15: Boundary cases for sub-class (b) where obstacle lies in the *exterior region*

lines of the vulnerable region shown in Figure 5.15(a) (point O_v), second type of point lies in the exterior region and only on the line extended from the vulnerable region. Here for example point q_5 as shown in Figure 5.15(a). The third and fourth type of points do not lie in exterior region but belong respectively to the sets $\mathcal{X} = \{q_1, q_2, q_5, q_6, q'_3, q'_4, q'_5, q'_6\}$ and $\mathcal{Y} = \{q'_2, q_3, q_4, q'_1\}$ as shown in Figure 5.13.

For the first type of boundary points, the obstacle k at point O_v can block the vulnerable region from four sides l_2, l_3, l'_2 and l'_3. The region where O_v lies can be identified as $S_3 \cap S_4$ because both S_3 and S_4 regions are common to the location where O_v lies. The other case is presented in the Figure 5.15(b) along with the rule to locate respective location. The blockage probability for case mentioned in the Figure 5.15(a) can be computed: $f\_static(l_2, k) + f\_static(l_3, k) + f\_static(l'_2, k) + f\_static(l'_3, k)$. Note that, here also, the sum of returned values of the function calls would not exceed 1 because the sectors of the circle $C_k^{\Delta t}$ intersecting these lines are exclusive which was similarly shown in Figure 5.14.

Now, let us look at the second type of boundary point q_5 which is shown in Figure 5.15(a). This point lies in the exterior region but on the line l_3. It is easy to observe that three lines vulnerable to this point would be l_2, l'_3 and l'_2. The probability of blockage can be computed as $f\_static(l_2, k) + f\_static(l'_3, k) + f\_static(l'_2, k)$. The returned value would not exceed 1 due to similar reasons mentioned earlier.

For the third type of scenario, the point $q_5 \in \mathcal{X}$ do not lie in the exterior region as shown in 5.13. From this location, obstacle at q_5 may block the communication from lines l_2 and l'_3. The probability of blockage can be computed as $f\_static(l_2, k) + f\_static(l'_3, k)$. The similar method can be used for other obstacle points lying in the set $\mathcal{X}$.

For the last type of boundary points belonging to set $\mathcal{Y}$, for example for points q_2 and q'_1 as shown in Figure 5.13 lines vulnerable to blockage are l_1 and l_3 since these points belong to the sub-region S_1. In order to check this condition, we simply need to see whether the obstacle belong to both R_4 (in $\triangle\mathcal{P}_1\mathcal{P}_2\mathcal{P}_3$) and R'_6 (in $\triangle\mathcal{P}'_1\mathcal{P}'_2\mathcal{P}'_3$). The probability

of blockage by the obstacle lying in S_1 is computed as described earlier. Similarly this strategy is used for the points q_5 and q_4'. The algorithm which will be used to find out the sub-regions and probability of blockage considering these boundary conditions is same as mentioned for the sub-class (a) with difference in the way sub-region finding rules and blockage probabilities are set.

5.4.3.4 Computation of $p_{k\_ij}^{t+1}$ for sub-class (c)

Now we give the method for the sub-class (c) which is shown in Figure 5.6(c). Here also, let's first describe the necessary steps required to make the presented design applicable throughout any general scenario of motion of `UEs` in this considered sub-class (c).

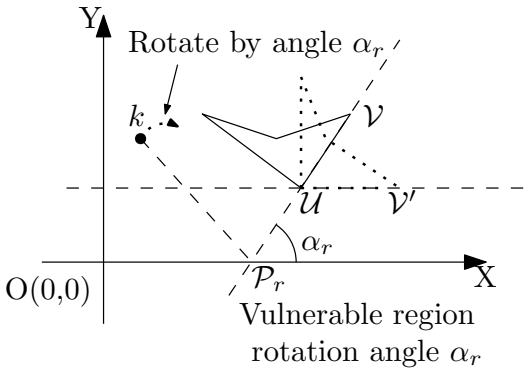

Figure 5.16: Geometric rotation of the vulnerable region to fix its representation across all possible movements of `UEs` in sub-class (c)

Fix the representation of vulnerable region for general scenarios involving movement of `UEs`: We choose one specific point *fork_pivot* which is the point opposite to that point which is making the vulnerable region non-convex. For example, in the Figure 5.17(b), point A is opposite to the point D. We choose A as the *fork_pivot* (termed as F_1). Then we choose next fork_pivots in clockwise order, B as *fork_pivot* F_2 and C as *fork_pivot* F_3. Now using this, we can say that point $\mathcal{U}$ is F_1, $\mathcal{V}$ is F_3 as shown in Figure 5.16. Here also, point $\mathcal{P}_r$ is the intersection point of line $\mathcal{UV}$ and X-axis and angle α_r is formed by line $\mathcal{UV}$ with X-axis. The vulnerable region is rotated by angle α_r in clockwise direction with respect to point $\mathcal{P}_r$. This process in turn makes the side of the vulnerable region represented by points $\mathcal{U}$ and $\mathcal{V}$ parallel to $X-axis$ which is shown by dotted lines in Figure 5.16. Similarly, we rotate the obstacle k by angle α_r in clockwise direction with respect to point $\mathcal{P}_r$. This operation has to be performed for all the obstacles present in the region. If the line formed by points $\mathcal{U}$ and $\mathcal{V}$ are parallel to X-axis, then there is no need to perform the geometric rotations either for the vulnerable region or the obstacle.

Rule to find the sub-region of obstacle k and corresponding blockage probability: In order to determine the sub-region where the obstacle lies we give the following approach. As shown in Figure 5.17 the communication region can be divided into 2 tri-

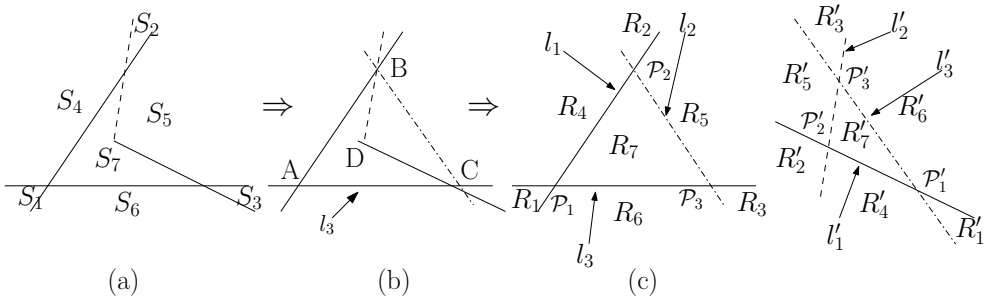

Figure 5.17: Sub class (c) when both nodes are moving.

Sub-region	Rule	X_1	X_2	X_3
S_1	R_1	l_1	l_3	$\times$
S_2	$R_2 - R'_3$	l_1	l'_2	l'_1
S_3	$R_3 - R'_1$	l_3	l'_1	l'_2
S_4	$R_4 \cup R'_3$	l_1	$null$	$\times$
S_5	$R_5 \cup R'_7$	l'_1	l'_2	$\times$
S_6	$R_6 \cup R'_1$	l_3	$null$	$\times$
S_7	$R_7 - R'_7$	$\times$	$\times$	$\times$

Table 5.4: Identifying sub-regions of obstacle k and arguments of function calls computing the blockage probability when both nodes are moving for sub-class (c).

angular regions, the outer triangle $\triangle\mathcal{P}_1\mathcal{P}_2\mathcal{P}_3$ and the inner triangle $\triangle\mathcal{P}'_1\mathcal{P}'_2\mathcal{P}'_3$. Similarly, lines $l_1 : [\mathcal{P}_1, \mathcal{P}_2]$, $l_2 : [\mathcal{P}_2, \mathcal{P}_3]$, $l_3[\mathcal{P}_3, \mathcal{P}_1]$, $l'_1 : [\mathcal{P}'_1, \mathcal{P}'_2]$, $l'_2 : [\mathcal{P}'_2, \mathcal{P}'_3]$, and $l'_3 : [\mathcal{P}'_3, \mathcal{P}'_1]$ are described as in previous paragraph formed by respective pivot points written in square brackets. We can run the sub-region finding algorithm of previous sub-section in both of the triangular regions. The rule for finding sub-regions in the given vulnerable region is summarized in Table 5.4. Here also, we can simply calculate the probability of blockage when obstacle k as follows: When obstacle is in sub-region S_7, then blockage probability is 1. For all other cases *except* S_2 and S_3, the blockage probability is computed as: $f\_static(X_1, k) + f\_static(X_2, k)$. The values of the arguments X_1 and X_2 are summarized in Table 5.4. For the remaining cases S_2 and S_3, the blockage probability is computed as: $f\_static(X_1, k) + f\_static(X_2, k) f\_static(X_3, k)$. The values of the arguments X_1, X_2, and X_3 are summarized in Table 5.4. Here also, the sum of the returned values of these function calls would be less than or equal to 1. This is due to the same reason as mentioned earlier.

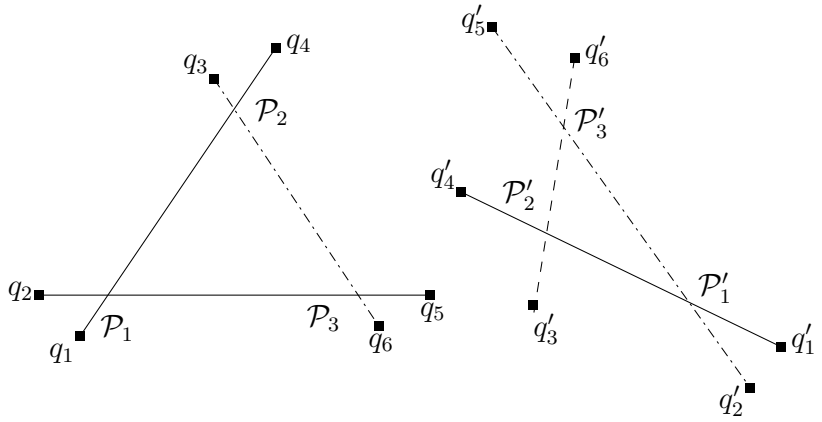

Figure 5.18: Boundary cases for sub-class (c)

Boundary conditions: This is shown in Figure 5.18. In this case, points q_3, q_6, q'_2 and q'_5 do not constitute the boundary conditions since points q_3 and q'_5 belong to sub-region S_4 and points q_6 and q'_2 belong to sub-region S_6. Similarly points q'_3 and q'_4 do not form boundary condition as they belong to either inside vulnerable sub-region S_7 (blockage probability is 1) or outside in sub-regions S_4 or S_6. Points q_1 and q_2 can be dealt in same manner as was described in earlier sub-classes. For point q_4, obstacle would block the given vulnerable region from two sides l'_1 and l'_2. If the obstacle k on q_4 would block only from the side l'_2, then probability of blockage would be $f\_static(l'_2, k)$. Otherwise, if the obstacle k would block from both sides l'_1 and l'_2, then probability of blockage would be $f\_static(l'_2, k) + f\_static(l'_1, k)$. Note that, here also, the function call would return value less than or equal to 1 due to reasons mentioned earlier. This strategy can be similarly applied to all the other points q_5, q'_6 and q'_1. Here also, the algorithm which will be used to find out the sub-regions and probability of blockage considering these boundary conditions is same as mentioned for the sub-class (a) with difference in the way sub-region finding rules and blockage probabilities are set.

5.5 Relay Selection

In this section, we will give a relay selection strategy at the BS for a given source UE using the analysis as shown in algorithm 6. For each given source UE, the best one hop relay UE is chosen which minimizes average packet loss and thus delay considering obstacles. The BS chooses that UE as relay which maximizes local data rate considering the probability of blockage. In the algorithm, function $sort\_descending(\mathbb{S}, Index)$ sorts the vector $\mathbb{S}$ in descending order along with the respective indexes. Function $return()$ gives that adjacent node of i which provides maximum data rate. After the source node transmits its data to the chosen relay node, in the next time instant, relay node becomes the new source node and this process goes on till the data have been transmitted successfully at the destination.

Algorithm 6: Network assisted relay selection Algorithm

input : $G^t(N^t, E^t)$,$\mathbb{K}$,i, $adj^t(i)$, γ

double $temp$=1;
for $j \in adj^t(i)$ **do**
  Compute $P(d_{ij}^{t+1} \leq \gamma | I_{ij}^{t+1} = 0)$;
  $temp$=1;
  for $k \in \mathbb{K}$ **do**
    Compute $p_{k\_ij}^{t+1}$;
    $temp = temp \times (1 - p_{k\_ij}^{t+1})$;
  end
  $P(I_{ij}^{t+1} = 0) = temp$;
  $\mathbb{S}[j]$=$P(d_{ij}^{t+1} \leq \gamma | I_{ij}^{t+1} = 0) \times P(I_{ij}^{t+1} = 0) \times C_{ij}^{t}$;
  $Index[j] = j$;
end
$sort\_descending(\mathbb{S}, Index)$;
return $Index[0]$;

The potential relaying nodes are selected by the BS from a collection of nodes adjacent to the source node and closer to the destination. At each step of selection of one hop relay node, the algorithm takes $O(nK)$ time, where n is the number of nodes in vicinity of the source node and K is number of dynamic obstacles. The BS does this analysis at every time instant t using above mentioned strategy.

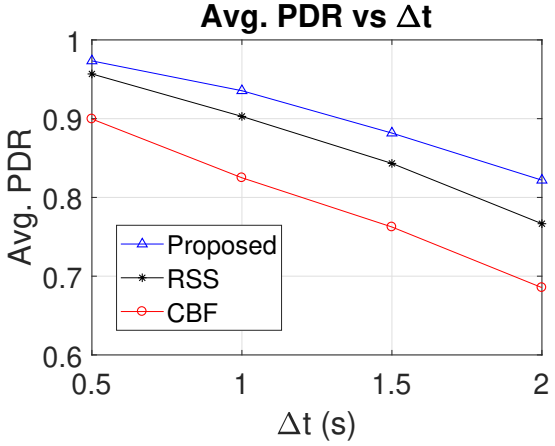

Figure 5.19: Avg. PDR vs Δt.

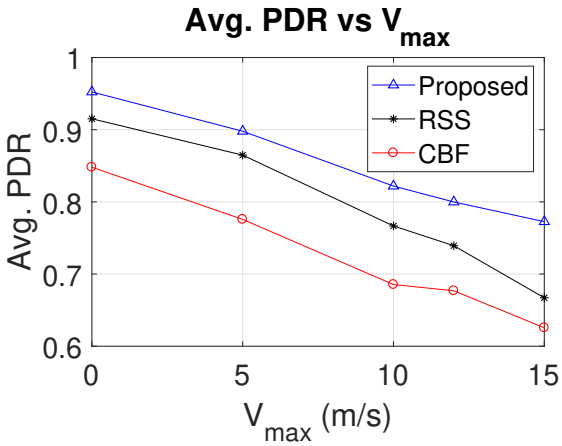

Figure 5.20: Avg. PDR vs V_{max}.

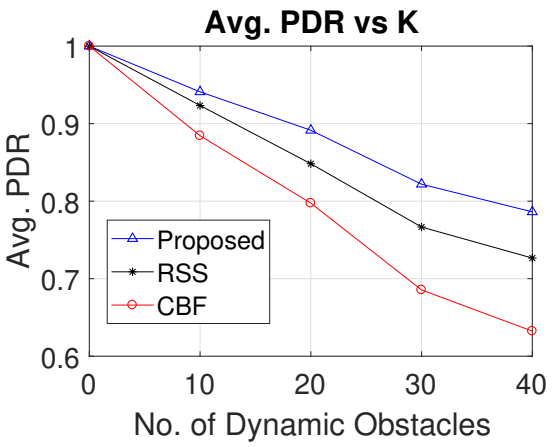

Figure 5.21: Avg. PDR vs K.

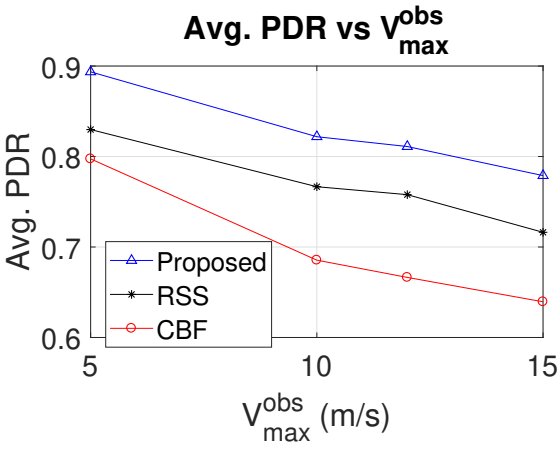

Figure 5.22: Avg. PDR vs V_{max}^{obs}.

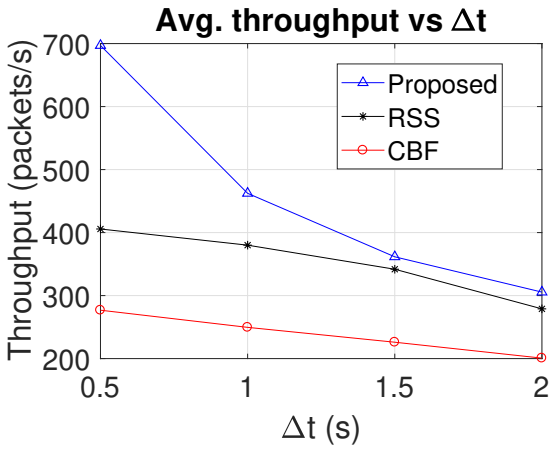

Figure 5.23: Avg. throughput vs Δt.

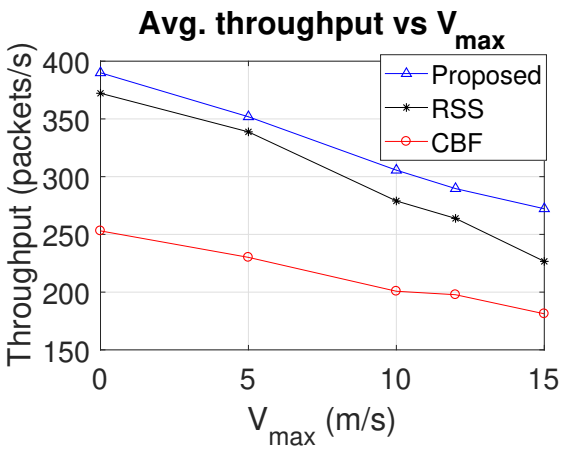

Figure 5.24: Avg. throughput vs V_{max}.

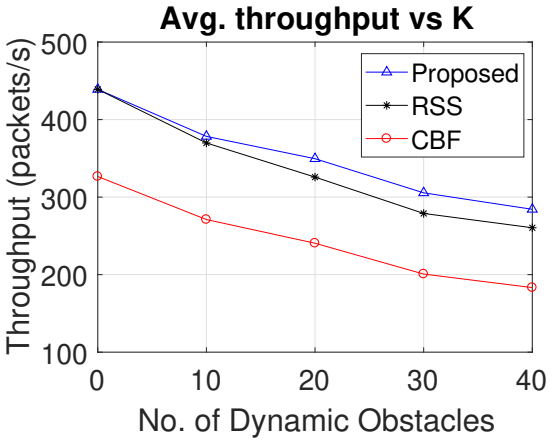

Figure 5.25: Avg. throughput vs K.

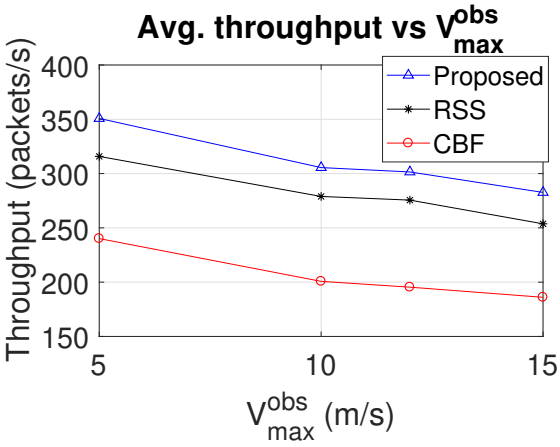

Figure 5.26: Avg. throughput vs V_{max}^{obs}.

5.6 Simulations and Results

5.6.1 Simulation Parameters

We are initially distributing 30 UEs uniformly in a 200 $m \times 200$ m square area. Throughout the experiment these nodes remain within the service region. Each node is moving with speed uniformly in range $[0, V_{max}]$ m/s, for $V_{max} \in \{0, 5, 10, 12, 15\}$ and angle in range $[-\pi, \pi]$, where $V_{max} = 0$ describes the scenario where both UEs are static. In the experiment, Δt which is measured in seconds, takes value from the set $\{0.5, 1, 1.5, 2\}$. Nodes are using directional transmitter and receiver antennas for 60 GHz frequency with $M = 4$, such that $G_r = G_t = 6$ dB and we are considering a scenario where LOS PLE is 2.5 and zero mean log-normal shadowing random variable with standard deviation 3.5 [10, 106]. Thermal noise density is -174 dBm/Hz [103] and devices are using 18 dBm transmit power. Capacity of each link (i, j) at time t is $C_{ij}^t = B \cdot \log_2(1 + S_{ij}^t)$ $bits/sec$, where $B = 20$ MHz is bandwidth and SNR threshold S_{ij}^{th} is taken to be 20 dB [107]. We are assuming fixed packet length of 65535 *bytes*. Network load of maximum 500 packets are transmitted from the source UE. All of the 500 packets might not be received at the destination UE because some packets might get lost due to dynamic obstacles and few may be unsent due to unavailability of the required relay link. There are dynamic obstacles initially distributed uniformly in the environment. The number of dynamic obstacles K varies in range $\{0, 10, 20, 30, 40\}$. Each dynamic obstacle is moving with speed uniformly in range $[0, V_{max}^{obs}]$ m/s, for $V_{max}^{obs} \in \{5, 10, 12, 15\}$ and angle in range $[-\pi, \pi]$. The information of position, speed and orientation of UEs are known at the BS, however only the information about position and speed of obstacles are known and orientation information is *unknown* at the BS. We assume a single source-destination pair for simplicity and all other devices may act as relay.

We have written our own C++ custom code and run them on a GNU 4.8 compiler on Intel core $i7$ machine using the simulation environment mentioned in above. We have run these simulations for 3 hops and taken the average of the results of about 1000 run per-hop. We have analyzed the effects of Δt, V_{max}, K, and V_{max}^{obs} on average packet delivery ratio (PDR) and average throughput. We define PDR as the ratio of packets delivered successfully to that of total packets transmitted. Throughput is defined as the total packets sent successfully per unit time. Here, end to end delay is due to transmission delay and delay incurred due to packet loss. We are ignoring queuing delay for simplicity.

We are comparing the results of our algorithm with metrics based on RSS and a contention based forwarding (CBF) approach [108] which select relay node based on signal strength and shortest distance from destination respectively. Here we are assuming that both RSS based and CBF based algorithms are aware of the mobility of UEs, thus packet losses due to mobility of UEs do not occur. Hence we focus on the packet loss occurring due to presence of dynamic obstacles only. However, note that, awareness of UEs' mobility

would still cause packet loss because full information of dynamic obstacles is not known. Highly mobile nodes would have higher chance to get blocked by dynamic obstacles compared to static nodes because they may traverse a greater area comprising vulnerable region. This has been observed and explained in the next section where results of the simulation are presented.

5.6.2 Simulation Results & Analysis

Figure 5.19 shows the effect of varying Δt on average PDR. Here, $V_{max} = 10\ m/s$, $V_{max}^{obs} = 10\ m/s$, $K = 30$, and as mentioned earlier, maximum network load is 500 packets which is constant throughout the experiment. The figure shows that increasing Δt causes decrease in PDR. This is because, with higher Δt nodes can move longer distances, and hence larger area of vulnerable region will be traversed. This would cause increase in chances of blockage by dynamic obstacles which in turn causes higher packet loss and hence lower PDR. We can see that our method outperforms the mobility aware RSS based and CBF based because our method takes care of the uncertainty in orientation of motion of dynamic obstacles. Large values of Δt cause higher packet loss, and which in turn cause higher end to end delay to compensate for packet loss and hence lower throughput which is shown in Figure 5.23. The insights of results shown in Figure 5.23 are similar to that of Figure 5.19.

Figure 5.20 shows the effect of varying V_{max} on packet loss keeping other parameters fixed: $V_{max}^{obs} = 10\ m/s$, $\Delta t = 2\ s$ and $K = 30$. This figure also shows that increasing V_{max} causes decrease in PDR. The reason is similar to as mentioned in previous paragraph. Increasing V_{max} causes nodes to move longer distances for a given Δt, and hence larger area of vulnerable region will be traversed which would cause increase the chances of blockage by dynamic obstacles. This would in turn cause higher packet loss and hence lower PDR. Our method outperforms the mobility aware RSS based and CBF based because it takes care of the uncertainty in orientation of motion of dynamic obstacles. The throughput is also affected in same manner as described earlier and hence with increasing V_{max}, throughput decreases as shown in Figure 5.24. The insights of results shown in Figure 5.24 are similar to that of Figure 5.20.

Figure 5.21 shows the effect of varying K on packet loss keeping other parameters fixed: $V_{max}^{obs} = 10\ m/s$, $\Delta t = 2\ s$, and $V_{max} = 10\ m/s$. By increasing the parameter K, chances of blockage by dynamic obstacles also increases since more obstacle are present at any given time. Hence, this would cause higher packet loss and hence lower PDR. Here also, our method outperforms the mobility aware RSS based and CBF based because it takes care of the uncertainty in orientation of motion of dynamic obstacles. As shown in Figure 5.25, throughput also decreases as number of dynamic obstacles increases. The insights of results shown in Figure 5.25 are similar to that of Figure 5.21.

Figure 5.22 shows the effect of varying V_{max}^{obs} on packet loss keeping other parameters fixed: $V_{max} = 10\ m/s$, $\Delta t = 2\ s$ and $K = 30$. This figure also, we can see that, increas-

ing value of V_{max}^{obs} would imply decreasing trend in PDR. This is because as the value of V_{max}^{obs} increases, the obstacle would move to longer distances and hence higher chances of penetrating the vulnerable region. This would in turn cause higher chances of packet loss and hence lesser PDR. Since our method takes care of the uncertainty in orientation of motion of dynamic obstacles, it outperforms the mobility aware RSS based and CBF based methods. The throughput is also affected in same manner because PDR is decreasing with V_{max}^{obs}. Hence with increasing V_{max}^{obs}, throughput decreases as shown in Figure 5.26, where insights of the results are similar to that of Figure 5.22.

We observed that the dynamic obstacles have severe effects on the blockage of any given mmWave D2D link. Even the case when both UEs are static, dynamic obstacles have significant impact on the link connectivity. All factors, i.e., discretized time duration Δt, mobility of UEs, number of dynamic obstacles and their speed must be taken into account while analyzing the best relay link. The problem where a chosen relay link become vulnerable to blockage by dynamic obstacles is aggravated when the orientation in motion of these obstacles is unknown as was shown with mobility aware RSS and CBF approaches. We also observe that, for lower values of Δt, the throughput was higher, however with very low value of Δt, signaling overhead might increase due to frequent update of information considering dynamic obstacle's presence. Also with very high value of Δt, the information about dynamic obstacles' presence might get outdated. Hence we need to choose an appropriate value of Δt, for a given environment considering K, V_{max} and V_{max}^{obs}, such that average PDR and throughput is satisfactory for any given use case scenario.

5.7 Conclusion

We formulated the problem of relay selection by capturing the severe effects of dynamic obstacles whose orientation in motion is *unknown*. We have developed an elegant probabilistic framework which is uniform across all the possible scenarios of motion of UEs and hence can be applied with ease. Using the concepts of geometry we derived expressions for the probability of blockage by dynamic obstacles. This is used in our developed framework to derive unique solutions for computing the best relay node which maximizes throughput for each UE. In simulations, we have shown the effects of obstacles on throughput and packet delivery ratio. The uncertainty in link quality induced due to unknown orientation in motion of dynamic obstacles is appropriately captured by our approach. Results show that our algorithm outperforms other classical algorithms.

Part III

Device Controlled Scenario for mmWave D2D communication

Chapter 6

To Continue Transmission or to Explore Relays: Millimeter Wave D2D Communication in Presence of Dynamic Obstacles

Much of the content of this chapter is copied from my own paper[4] *with the permission of my co-authors Arpan Chattopadhyay and Sasthi C. Ghosh. Even though the paper can be found in the literature, it is copied here so that I can make minor changes and clarifications for the convenience of the reader.*

In the previous two chapters, we saw the network assisted mode of operation of mmWave D2D communication where the BS is responsible for controlling links based on the global information it acquired at global time instants. However, D2D links are inherently distributed in nature, i.e., their channel information is local to UEs. Hence the local information must be acquired by the BS which causes some delay. This may cause the information to get outdated in case of presence of dynamic obstacles in the service region. The selected relays are themselves susceptible to blockages due to dynamic obstacles. Hence a relay initially chosen by the BS for transferring data packets between a pair of source-destination UEs may perform poorly over time. This in turn requires a proactive selection of some other relay to avoid further delay and energy consumption while sending packets relentlessly to the destination which are going to get lost anyhow. Also, it must be taken into consideration that mmWave communication is directional in nature and thus requires a significant search cost while finding a relay in vicinity of the source UE.

In this chapter, we address the problem of deciding whether to *stop* communication on a chosen mmWave D2D relay link in case of successive packet losses *or* whether to *continue* the transmission over it, by considering the directional search costs for the new relay as

[4]D. Singh, A. Chattopadhyay, and S. C. Ghosh. Distributed relay selection in presence of dynamic obstacles in millimeter wave d2d communication. In IEEE International Conference on Communications (ICC), pages 1–6, 2020.

well as the presence of dynamic obstacles in the communication path. Here we model this sequential decision problem by a finite horizon POMDP framework while considering a general exploration cost ζ. The D2D link quality is not observable at the current time instant; it can only be observed after taking the decision to transmit packets along a chosen link in the form of ACKs only. Information about dynamic obstacles are *not* known to the BS a priori and it can only be learned by using the feedback from UEs after the communication gets established. We considered the fact that the ACKs can also get lost due to presence of dynamic obstacles, and use conditional belief probability of D2D channel quality given the ACKs history as a sufficient statistic. Optimal threshold policies are derived which map the belief to a set of actions. Additionally, by exploiting the derived policy structure, we obtain a stationary policy which tells the UE when to stop sending packets on the current link and go for exploring new relay links based on the number of consecutive ACK failures. Our optimal policy can be implemented locally at each UE, thereby facilitating distributed implementation. The derived policies capture the trade-off between delay caused due to packet loss and the cost for exploring a new relay link. The theoretical analysis is validated through extensive simulation.

The organization of this chapter as follows. System model is described in section 6.1. The POMDP formulation is provided in section 6.2. Optimal policy structure is derived in section 6.3. Numerical results are provided in section 6.4, followed by the conclusions in section 6.5.

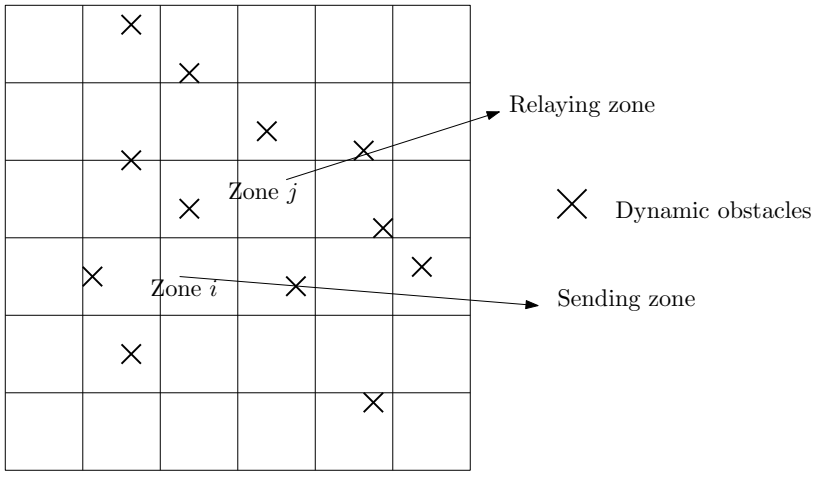

Figure 6.1: Service region divided into zones along with dynamic obstacles.

6.1 System Model

We are considering the device-tier of 5G D2D architecture mentioned in [1], where devices can communicate among themselves with or without the help from BS. The service region is divided into various *zones* or *grids* as shown in figure 6.1 with one BS. Each zone has atleast

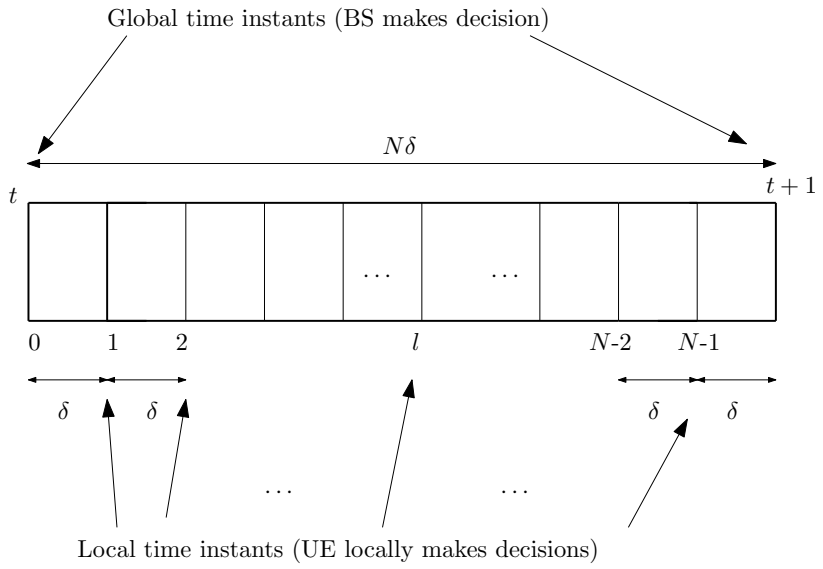

Figure 6.2: Discretized time slots with the smallest slot duration of δ.

one UE which is ready to take part in D2D communication as a relay or source/destination node. The zone where at least one UE wants to transmit data to an UE of some other zone is defined as a *sending zone*. We also define a set of *viable* relay zones ($\mathbb{U}^i$) given by the BS for sending zone i which is nearer to the zone containing the destination UE and is in the communication range of the zone i. When a UE in zone i forms a connection with a UE in another zone $j \in \mathbb{U}^i$, we term this connection as link j. Link is formed between UEs of two zones when they are in communication range of each other and the received signal strength is sufficient for the required data rate. Communication between UEs take place on mmWave channels using directional antennas. The received signal strength (Q_{ij}) on a UE in zone j from a UE in zone i is modeled as [34]:

$$Q_{ij} = \psi_{ij} \cdot P_i \cdot G_t \cdot G_r \cdot PL_{ij} \tag{6.1.1}$$

where, ψ_{ij} is shadowing random variable, P_i is transmit power of UE i, G_t & G_r are transmit and receive beam-forming gains respectively, and PL_{ij} is a distance dependent path loss function.

Time is discretized as $t, t+1, \cdots$ with time duration Δt as shown in figure 6.2. Duration Δt is further sub-divided into various smaller time duration of value δ. We denote each such smaller time duration by l which takes integer values in $[0, N-1]$, where N is represents a positive integer such that $\Delta t = N\delta$. Here δ is the smaller discretized time slot which is assumed to be large enough to send one packet of size L_s bytes. Here, instants $t, t+1, \cdots$ represent the moments when global decisions is given by the BS. At these time instant BS takes the channel state information from all UEs in the service region and gives the decision of best relaying UE of a given zone for a given source UE. Hence, in between two consecutive

time instants when BS can make global decision, a UE can send at-most N packets of size L_s to another UE. Note that at time $l = 0$, the UE chooses the relay link suggested by the BS and at time $l \in \{1, 2, \cdots, N-1\}$, BS has no control over information regarding channel condition local to the UEs. Thus BS do not take part in controlling the links between UEs during two consecutive global time instants. At global time instants, BS sends two types of information to UEs, i) the best relay UE (or node) for a given source UE and ii) viable relaying zones $\mathbb{U}^i$ for given source zone i, hence the zone i may choose an appropriate zone for relaying data from the set $\mathbb{U}^i$.

The service region consists of static and dynamic obstacles which are not known apriori. Also it is assumed that there are no infrastructure support like radars and vision cameras (to identify and track them). The behavior of dynamic obstacles needs to be learned from the received ACKs of sent packets in an on-line fashion. Since mmWaves suffer from severe penetration loss, we assume that presence of even a single static or dynamic obstacle may break an already established D2D link resulting in packet loss. It is assumed that the mobility of UEs in a zone i for $N\delta$ duration do not bring them outside the zone and this do not cause link outage. Hence the only factors responsible for link breakage and packet loss are the presence of obstacles and channel condition due to fading.

The source/relay node may take local decision when the current link quality is not good enough. The node in this case can locally explores and switches to another one-hop node by incurring penalty in terms of delay because a directional search is performed while exploring the neighboring UEs belonging to set $\mathbb{U}^i$. The overall exploration cost for searching a potential relay link is termed ζ. It is assumed that once exploration is complete, channel switching takes negligible time. It is assumed that the beams are perfectly aligned after the exploration phase and we focus on the effects of dynamic obstacles blockage on a given D2D link. The decision of exploration or to continue on the current link after how many successive ACKs failure is to be made at the nodes locally. In the next section we formulate the problem as POMDP.

6.2 Problem Formulation as POMDP

Zone i is the sending zone which contains at least one UE which needs to transmit data to an UE of some other zone $j \in \mathbb{U}^i$ which is termed as link j. Global decision for the best relay is given by the BS at the time instant t to relay data packet till time instant $t + 1$. There are both static and dynamic obstacles present in the environment which causes uncertainty in the channel quality resulting in packet loss and delay. The packet loss and delay needed to be controlled for $N\delta$ duration between the two global time instants t and $t + 1$ at which BS do not have control over the data packets sent. As a result, the packet loss at early time instants may cause high delay and energy wastage if packet loss is not controlled locally. Our problem formulation deals with locally deriving a policy

that dictates sequential actions to be performed based on ACK feedback at each local time instant l. This policy is helpful in deciding when to stop using the current relay when successive packet loss occurs, and to explore new links in order to avoid further packet loss and delay. Hence, our objective is to minimize the delay cost incurred due to packet loss while choosing appropriate relays and keeping the exploring and switching cost as low as possible. We have formulated this problem as a finite horizon POMDP [44] in order to incorporate the uncertainty in channel condition. We will describe the state space, action space, observation, transition probabilistic structure of the problem, respective costs and cost function in upcoming subsections.

For a given sending zone i, the state of relay link $j \in U^i$ is represented as $x_l^j \in \{0, 1\}$. Values of $x_l^j = 1$ and $x_l^j = 0$ signify the relay link j is in good (G) or bad ($\overline{G}$) state respectively. A good state implies that the channel quality is good enough for communication, and a packet is transmitted successfully without getting blocked by obstacles. In a bad state, the channel quality drops and packet loss occurs. The action set $\mathbb{A}$ is defined as {explore & switch to another link ($a_l^j = 0$), transmit on current link (zone) ($a_l^j = 1$)}. The local node in zone i, makes observation at each smaller time instant δ after the packet is sent. This observation is in the form of ACK test which is denoted as $z_l^j \in \{0, 1\}$. Here, $z_l^j = 0$ represents that the acknowledgement is not received for link j because link is bad which causes packet loss, and similarly $z_l^j = 1$ represents that the acknowledgement is received and the link is good and packet is transmitted successfully. We also represent A and $\overline{A}$ as the ACK received or not ($z_l^j = 1$ or $z_l^j = 0$) respectively. Since ACKs are quick and are available in negligible amount of time, for state $x_l^j = 1$ and action $a_l^j = 1$, the observation (ACK) is z_l^j. The ACK may also be uncertain due to the unpredictable behavior of the given channel under consideration.

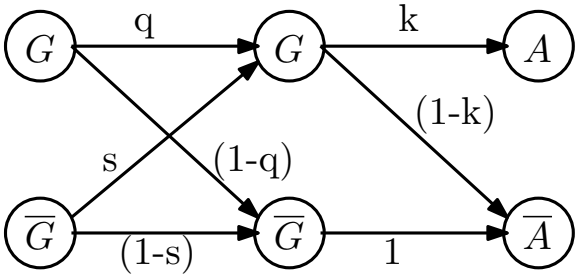

Figure 6.3: Probabilistic structure of the problem at a node locally.

The probabilistic structure of the observation assumed here is shown in figure 6.3 and written as:

$$P(z_l^j = 1|x_l^j = 1) = k; P(z_l^j = 0|x_l^j = 1) = 1 - k$$

$$P(z_l^j = 1|x_l^j = 0) = 0; P(z_l^j = 0|x_l^j = 0) = 1$$

If the system is in bad state with $x_l^j = 0$ at time l, then the probability of obtaining good

observation is zero ($P(z_l^j = 1|x_l^j = 0) = 0$) which is intuitive and obvious. The probabilistic structure assumed for the system state transition is given as:

$$P(x_{l+1}^j = 1|x_l^j = 1) = q; P(x_{l+1}^j = 0|x_l^j = 1) = 1 - q$$

$$P(x_{l+1}^j = 1|x_l^j = 0) = s; P(x_{l+1}^j = 0|x_l^j = 0) = 1 - s$$

Here q, s and $k \in (0, 1)$, respectively represent the probabilities that link is still good, bad link becomes good and the ACK is received successfully when the link is in good state. The transition probability $1 - q$ indicates that the good link becomes bad due to obstacles or signal fading. Similarly $1 - s$ is the probability that bad link is still bad (for obstacles it indicates either obstacle is large in length or moving slowly and effecting the link for longer period). Note that the blockage probability is directly dependent on the dimension, orientation and speed of the obstacle. This is indirectly captured in parameters q, k and s which are learned with time as the model gets more input. The case $q > s$ represents the scenario where the links are positively correlated. Here, chances of good link becoming good in the next time instant is higher than that of a link becoming good from a bad state. Whereas, case $q < s$ represents the scenario where the links are negatively correlated. It denotes the scenario where the chance of bad link becoming good in next time instant is higher than that of a link becoming good from a good state. This case is possible when obstacles are rapidly moving.

For a given relaying zone j, let $\mathbb{H}_l^j = (z_0^j, z_1^j, \cdots, z_l^j)$ denote the information vector available locally to the zone i till smaller time instant l. Let us define b_l as the conditional state distribution acting as the sufficient statistics or belief [44](chapter 5) locally for the given relaying link j as:

$$b_l^j = P(x_l^j = 1|\mathbb{H}_l^j) \tag{6.2.1}$$

This equation signifies the probability that the relaying link is in good state given the previous history information. The belief evolves as:

$$b_{l+1}^j = \Phi(b_l^j, z_{l+1}^j). \tag{6.2.2}$$

Using Baye's rule we get,

$$b_{l+1}^j = \begin{cases} 1, & \text{if } z_{l+1}^j = 1 \\ \frac{[qb_l^j + s(1-b_l^j)](1-k)}{[qb_l^j + s(1-b_l^j)](1-k) + [(1-q)b_l^j + (1-s)(1-b_l^j)]}, & \text{if } z_{l+1}^j = 0 \end{cases} \tag{6.2.3}$$

The cost structure is defined as follows: When packet loss occurs, a fixed cost C is the penalty (in terms of delay) incurred to overcome it. After observing that the current relay link is not good, there may be a need to explore new relay links which might cause some delay and the cost to compensate it. This cost is ζ. If there is no packet loss, then the

cost incurred is 0. Cost of testing for ACK is negligible and hence 0. Here our objective is to derive a decision rule to choose appropriate action (continue with the current relaying zone or explore and switch to some other zone) which leads the system to good state and in turn causes minimum packet loss considering all the required costs. The expected cost is formulated as a dynamic program (DP). At the end of the last period, i.e., $(N-1)th$ period, the expected cost is defined as:

$$J_{N-1}(b^j_{N-1}) = \min\{\zeta, (1 - kb^j_{N-1})C\}. \tag{6.2.4}$$

where $b^j_{N-1} \in (0,1)$ represents the belief of link j at time $N-1$. First term in the above minimization expression is the exploration cost and the second term is the expected cost due to packet loss. Packet loss can be due to two types of events: i) due to the link being in bad state and causing packet loss and ii) when the link is in good state and the ACK is not received due to bad channel quality. For the time instant $l = N-2$, we have,

$$J_{N-2}(b^j_{N-2}) = \min\{\zeta, \gamma_{N-2} + E[J_{N-1}(b^j_{N-1})] \tag{6.2.5}$$

where γ_{N-2} is the expected penalty paid due to packet loss at time $l = N-2$ which is $(1 - kb^j_{N-2})C$. The first term in minimization expression denotes the exploring & switching cost and the second term denotes the cost for continuing in the current relay link. Similarly we can write the dynamic program for the general expression for each $l \in \{0, 1, \cdots, N-2\}$ as:

$$J_l(b^j_l) = \min\{\zeta, \gamma_l + E[J_{l+1}(\Phi(b^j_l, z^j_{l+1}))]\} \tag{6.2.6}$$

where γ_l is the expected penalty paid due to packet loss at time instant l which is $(1-kb^j_l)C$. After solving this DP we will get a policy, based on which the local decision can be made to switch the link or to remain on that link. Hence, for a given relay zone j at time instant l, we minimize the cost $J_l(b_l)$. The derivation of this policy is given in the next section where we derive a policy which maps the belief into action.

6.3 Derivation of the Optimal Policy

6.3.1 Properties of $J_l(b)$

In this subsection, we will explore the properties of the cost function, which will be further exploited to provide a optimal threshold policy in the next subsection.

The expected cost at the end of the $(N-1)th$ period is given by equation (6.2.4). The general expression of cost for the time instant l as mentioned in equation (6.2.6) can be written equivalently as:

$$J_l(b^j_l) = \min\{\zeta, A^j_l(b^j_l)\} \tag{6.3.1}$$

where,

$$A_l^j(b_l^j) = \gamma_l + P(z_{l+1}^j = 1|b_l^j)J_{l+1}(\Phi(b_l^j, 1)) + P(z_{l+1}^j = 0|b_l^j)J_{l+1}(\Phi(b_l^j, 0)) \tag{6.3.2}$$

At the end of time instant l, the local node has calculated b_l that the relay link i is still the good or not and further decides whether to continue on the already selected relay link j or needs to explore and switch to another relay node and incur extra cost ζ. In equation (6.3.1), γ_l indicates the expected penalty incurred due to packet loss and

$$P(z_{l+1}^j = 1|b_l^j)J_{l+1}(\Phi(b_l^j, 1)) + P(z_{l+1}^j = 0|b_l^j)J_{l+1}(\Phi(b_l^j, 0))$$

is the expected cost to be incurred at the upcoming time instant $l + 1$.

For notation simplicity we will now remove the superscript j from each of the respective notations, e.g., we will write b_l^j as b_l and $A_l^j()$ as $A_l()$. Hence $A_l^j(b_l^j)$ is denoted as $A_l(b_l)$.

We can reduce $A_l(b_l)$ in equation (6.3.2) to:

$$\begin{aligned} A_l(b_l) =& (1 - kb_l)C + (b_l q + (1 - b_l)s)kJ_{l+1}(1) \\ &+ (1 - (b_l q + (1 - b_l)s)k)J_{l+1}(\Phi(b_l, 0)) \end{aligned} \tag{6.3.3}$$

We now look into the structure of the cost function. First we will show that functions $A_l(b)$ are piece-wise linear in b in Proposition 6.3.1.

Proposition 6.3.1. *$A_l(b)$ is piece-wise linear and concave in b for each l.*

Proof. We will prove this by first showing that $J_l(b)$ is piece-wise linear and concave for each l using induction. Then we prove our proposition. For time instant $(N - 1)$, we have,

$$J_{N-1}(b) = \min\{\zeta, (1 - kb)C\},$$

which is piecewise linear. For time instant $(N - 2)$, we have,

$$\begin{aligned} J_{N-2}(b) = \quad & \min\{\zeta, (1 - kb)C + (bq + (1 - b)s)kJ_{N-1}(1) \\ & + \min\{(1 - (bq + (1 - b)s)k)\zeta, (1 - (bq + (1 - b)s)k(2 - k))C\}\} \end{aligned} \tag{6.3.4}$$

which is also piece-wise linear and concave since $J_{N-1}(1)$ is constant.

Assuming $J_{l+1}(b)$ is piece-wise linear and concave in b, we can say that for some suitable scalars, $\eta_1, \eta_2, \cdots, \eta_n$ and $\beta_1, \beta_2, \cdots, \beta_n$, $J_{l+1}(b)$ can be written as:

$$J_{l+1}(b) = \min\{\eta_1 + \beta_1 b, \eta_2 + \beta_2 b, \cdots, \eta_n + \beta_n b\}. \tag{6.3.5}$$

We can write $J_l(b)$=min$\{\zeta, A_l(b)\}$. Expanding it using equation (6.3.3), we get:

$$\begin{aligned} J_l(b) = \quad & \min\Bigg\{\zeta, (1-kb)C + (bq+(1-b)s)kJ_{l+1}(1) \\ & + (1-(bq+(1-b)s)k)J_{l+1}\left(\frac{(bq+s(1-b))(1-k)}{1-\{bq+s(1-b)\}k}\right)\Bigg\} \end{aligned} \tag{6.3.6}$$

Putting J_{l+1} from equation (6.3.5) in equation (6.3.6) and simplifying, we get:

$$\begin{aligned} J_l(b) = \quad & \min\{\zeta, (1-kb)C + (bq+(1-b)s)kJ_{l+1}(1) \\ & + \min\{\eta_1(1-\{bq+s(1-b)\}k) + \beta_1(bq+s(1-b))(1-k), \\ & \eta_2(1-\{bq+s(1-b)\}k) + \beta_2(bq+s(1-b))(1-k), \\ & \cdots, \eta_n(1-\{bq+s(1-b)\}k) + \beta_n(bq+s(1-b))(1-k)\}\} \end{aligned} \tag{6.3.7}$$

This is again piece-wise linear and concave in b. Thus the induction is complete.

Now we will show that $A_l(b)$ is also piece-wise linear and concave in b:

$$\begin{aligned} A_l(b) = \quad & (1-kb)C + (bq+(1-b)s)kJ_{l+1}(1) \\ & + (1-(bq+(1-b)s)k)J_{l+1}(\Phi(b,0)) \end{aligned} \tag{6.3.8}$$

The first term $(1-kb)C$ is linear in b. In the second term, $(bq+(1-b)s)k$ is linear in b and $J_{l+1}(1)$ is independent of b, hence overall $(1-kb)C + (bq+(1-b)s)kJ_{l+1}(1)$ is linear in b. Now we prove that $(1-(bq+(1-b)s)k)J_{l+1}(\Phi(b,0))$ is piece-wise linear in b. By putting J_{l+1} from equation (6.3.5) in this expression and simplifying, we get,

$$\begin{aligned} & (1-(bq+(1-b)s)k)J_{l+1}(\Phi(b,0)) \\ & \quad = \min\{\eta_1(1-\{bq+s(1-b)\}k) + \beta_1(bq+s(1-b))(1-k), \\ & \quad\quad \eta_2(1-\{bq+s(1-b)\}k) + \beta_2(bq+s(1-b))(1-k), \cdots, \\ & \quad\quad \eta_n(1-\{bq+s(1-b)\}k) + \beta_n(bq+s(1-b))(1-k)\}. \end{aligned} \tag{6.3.9}$$

Since minimum of finite number of concave function is concave, $A_l(b)$ is piece-wise linear and concave in b for all l.

This proof is similar in spirit to an unsolved exercise given in [44](chapter 5), however the DP and the estimator function of this paper are different from that given in the book. Hence we had to write a complete proof. □

Below lemma is helpful and will be used in determining the monotonicity properties of $A_l(b)$.

Lemma 6.3.1. *If $q > s$ then $\phi(b,0)$ is strictly increasing function of b, otherwise, if $q < s$ then $\phi(b,0)$ is strictly decreasing function of b.*

Proof. We can re-arrange equation (6.2.3) as

$$\Phi(b,0) = \frac{1-k}{k(1-sk-b(q-s)k)} - \frac{1-k}{k}.$$

It is straightforward to see that when $q > s$, then $\Phi(b,0)$ is strictly increasing in b otherwise when $q < s$, $\Phi(b,0)$ is strictly decreasing in b. □

Now we determine the behavior of $A_l(b)$ with b when $q > s$ and $q < s$ separately. First we will look for the case when $q > s$.

Proposition 6.3.2. *For the case when $q > s$ (positively correlated case), $A_l(b)$ is non-increasing with b, i.e., $\forall b, b'$, $0 \leq b < b' \leq 1$, $A_l(b) \geq A_l(b')$.*

Proof. We will prove it using induction. We can see that the base case

$$A_{N-1}(b) = (1-kb)C$$

is linear and non-increasing function in b. Also, we can see

$$\begin{aligned} A_{N-2}(b) &= (1-kb)C + (bq+(1-b)s)kJ_{N-1}(1) \\ &\quad + \min\{(1-(bq+(1-b)s)k)\zeta, (1-(bq+(1-b)s)k(2-k))C\}\} \end{aligned}$$

is piecewise linear and non-increasing function in b. As induction hypothesis, let us assume this is true for $l+1$, that is, $A_{l+1}(b) \geq A_{l+1}(b')$ for all $0 \leq b < b' \leq 1$. Let us now see for l: $A_l(b) = (1-kb)C + (bq+(1-b)s)kJ_{l+1}(1) + (1-(bq+(1-b)s)k)J_{l+1}(\Phi(b,0))$. We can rearrange the terms in this to write as:

$$\begin{aligned} A_l(b) &= C(1-kb) \\ &\quad + (1-(bq+(1-b)s)k)(J_{l+1}(\Phi(b,0)) - J_{l+1}(1)) + J_{l+1}(1) \end{aligned} \tag{6.3.10}$$

In above equation, the term $\Phi(b,0) \leq 1$ because it is a probability term. Function $\Phi(b,0)$ is increasing in b for $q > s$ from lemma 6.3.1. Also, for time instant $l+1$, since $J_{l+1}(b) = \min\{\zeta, A_{l+1}(b)\}$, we can say that $J_{l+1}(b)$ is non-increasing in b due to induction hypothesis. Hence, we can say that $J_{l+1}(\Phi(b,0))$ is also non-increasing in b. Hence, we can say that $J_{l+1}(\Phi(b,0)) - J_{l+1}(1)$ is positive and non-increasing in b. Also the term $(1-(bq+(1-b)s)k)$ is positive ($q > s$) and non-increasing in b. Terms $C(1-kb)$ and $J_{l+1}(1)$ in above equation are non-increasing in b and constant respectively. Hence we can say that $A_l(b)$ is a non-increasing function in b. Hence $A_l(b) \geq A_l(b')$ for all $0 \leq b < b' \leq 1$. □

Next, Proposition 6.3.3 describes the variation of $A_l(b)$ with time l.

Proposition 6.3.3. *For time instants $l \in \{0, 1, \cdots, N-2\}$, $A_l(b)$ is non-increasing with l, i.e., $\forall b \in [0,1]$, $A_l(b) \geq A_{l+1}(b)$.*

Proof. We will first prove $J_l(b) \geq J_{l+1}(b)$, then we will use this to prove $A_l(b) \geq A_{l+1}(b)$. First we start for base case $l = N-1$ and the first term in recursion $l = N-2$:

$$J_{N-1}(b) = \min\{\zeta, (1-kb)C\}$$

and

$$\begin{aligned} J_{N-2}(b) \quad = \quad & \min\{\zeta, (1-kb)C + (bq + (1-b)s)kJ_{N-1}(1) \\ & + \min\{(1-(bq+(1-b)s)k)\zeta, (1-(bq+(1-b)s)k(2-k))C\}\}. \end{aligned}$$

We can easily see that $J_{N-2}(b) \geq J_{N-1}(b)$. We now prove it for first two terms of the recursion $J_{N-2}(b)$ and $J_{N-3}(b)$. We can write $J_{N-3}(b)$ as:

$$\begin{aligned} J_{N-3}(b) &= \min\{\zeta, (1-kb)C + (bq+(1-b)s)kJ_{N-2}(1) + \\ &\quad (1-(bq+(1-b)s)k)J_{N-2}(\Phi(b,0))\} \\ &\geq \min\{\zeta, (1-kb)C + (bq+(1-b)s)kJ_{N-1}(1) + \\ &\quad (1-(bq+(1-b)s)k)J_{N-1}(\Phi(b,0))\} \\ &= J_{N-2}(b) \end{aligned}$$

Hence $J_{N-3}(b) \geq J_{N-2}(b)$. Similarly it proceeds for other l and hence $J_l(b) \geq J_{l+1}(b)$. Now let us see this for $A_l(b)$ using previous proof for $J_l(b)$:

$$\begin{aligned} A_l(b) &= (1-kb)C + (bq+(1-b)s)kJ_{l+1}(1) + \\ &\quad (1-(bq+(1-b)s)k)J_{l+1}(\Phi(b,0)) \\ &\geq (1-kb)C + (bq+(1-b)s)kJ_{l+2}(1) + \\ &\quad (1-(bq+(1-b)s)k)J_{l+2}(\Phi(b,0)) \\ &= A_{l+1}(b) \end{aligned}$$

Hence $A_l(b) \geq A_{l+1}(b)$. □

Propositions 6.3.2 and 6.3.3 together describe the structure of the cost function for $q > s$ case which can be exploited to develop a threshold policy for making decisions of continuing or not on the given link.

Now we determine the behavior of $A_l(b)$ with b when $q < s$ and for cases i) $q \geq 1/2$ and ii) $s \leq 1/2$.

Proposition 6.3.4. *For the case when $q < s$, $A_l(b)$ is non-increasing with b, i.e., $\forall b, b'$, $0 \leq b < b' \leq 1$, $A_l(b) \geq A_l(b')$ for both cases when i) $q \geq 1/2$ and ii) $s \leq 1/2$.*

Proof. We will prove it using induction. We can see from equation (6.2.4) that $J_{N-1}(b) = \min\{\zeta, (1-kb)C\}$ is piecewise linear and non-increasing function in b. Here $A_{N-1}(b) =$

$(1-kb)C$ is non-increasing in b.

As induction hypothesis, we assume that $A_{l+1}(b), A_{l+2}(b), \cdots, A_{N-2}(b)$ are all non-increasing in b. We want to prove that $A_l(b)$ is non-increasing in b. Note that

$$\begin{aligned} A_l(b) &= (1-kb)C + (bq+(1-b)s)kJ_{l+1}(1) \\ &\quad + (1-(bq+(1-b)s)k)J_{l+1}(\Phi(b,0)). \end{aligned} \tag{6.3.11}$$

We can expand it further as:

$$\begin{aligned} A_l(b) &= (1-kb)C \\ &\quad + (bq+(1-b)s)k \min\{\overbrace{\zeta}^{x_1}, \overbrace{A_{l+1}(1)}^{x_2}\} \\ &\quad + \Big(1-(bq+(1-b)s)k\Big) \min\left\{\overbrace{\zeta}^{x_3}, \overbrace{A_{l+1}(\Phi(b,0))}^{x_4}\right\} \end{aligned} \tag{6.3.12}$$

Here also, there are four possible cases due to two minimization expressions in above equation which is due to combinations: $Case\ (i)\ x_1x_3$, $Case\ (ii)\ x_1x_4$, $Case\ (iii)\ x_2x_3$ and $Case\ (iv)\ x_2x_4$.

Case (i)

In this case, we have:

$$A_l(b) = (1-kb)C + (bq+(1-b)s)k\zeta + (1-(bq+(1-b)s)k)\zeta \tag{6.3.13}$$

which can be written further: $A_l(b) = (1-kb)C + \zeta$ which is clearly non-increasing in b.

Case (ii)

We can see that case (ii) is not possible. We can see that $A_{l+1}(1) < A_{l+1}(\Phi(b,0))$ due to induction hypothesis, and $\Phi(b,0) < 1$. Let us assume that $x_1 = \zeta$ is selected from the first minimization term which implies that $\zeta < A_{l+1}(1)$. Now if $x_4 = A_{l+1}(\Phi(b,0))$ is selected from the second minimization term then it implies that $A_{l+1}(\Phi(b,0)) < \zeta$. This in-turn implies $A_{l+1}(\Phi(b,0)) < A_{l+1}(1)$, which is a contradiction due to aforementioned argument. Hence, we can say if $x_1 = \zeta$ is selected from the first minimization, then x_4 cannot be selected from the second minimization term.

Case (iii)

In this case:

$$\begin{aligned} A_l(b) =&(1-kb)C + (bq+(1-b)s)kA_{l+1}(1) + \big(1-(bq+(1-b)s)k\big)\zeta \\ =&C + skA_{l+1}(1) + \zeta - sk\zeta - kb\{C-(s-q)(\zeta - A_{l+1}(1))\} \end{aligned} \tag{6.3.14}$$

Since $s > q$ and $(s-q) \leq 1$, we get that $A_l(b)$ is non-increasing in b provided $\zeta - A_{l+1}(1) \leq C$. For the current combination, $\zeta < A_{l+1}(\Phi(b,0))$ and from induction hypothesis, $A_{l+1}(\Phi(b,0)) \leq A_{l+1}(0)$. This implies $A_{l+1}(0) > \zeta$. Hence to prove $A_l(b)$ is non-increasing in b, it is sufficient to prove that $A_{l+1}(0) - A_{l+1}(1) \leq C$.

From equation (6.3.3) we can write $A_{l+1}(b)$ as:

$$\begin{aligned} A_{l+1}(b) = &(1-kb)C + (bq+(1-b)s)k\min\{\zeta, A_{l+2}(1)\} \\ &+ (1-(bq+(1-b)s)k)\min\{\zeta, A_{l+2}(\Phi(b,0))\} \end{aligned} \tag{6.3.15}$$

Due to the current combination, $\zeta > A_{l+1}(1)$ and from Proposition 6.3.3, $A_{l+1}(1) \geq A_{l+2}(1)$. Hence in the first minimization term $\zeta > A_{l+2}(1)$. For the second minimization term, there are two possible sub-cases in equation (6.3.15): (i) when $\zeta < A_{l+2}(\Phi(b,0))$, and (ii) $\zeta \geq A_{l+2}(\Phi(b,0))$.

For sub-case (i), we have,

$$\begin{aligned} A_{l+1}(b) = &(1-kb)C + (bq+(1-b)s)kA_{l+2}(1) \\ &+ (1-(bq+(1-b)s)k)\zeta \end{aligned} \tag{6.3.16}$$

Now we can say that

$$A_{l+1}(0) - A_{l+1}(1) = \ kC - (s-q)k(\zeta - A_{l+2}(1)).$$

Clearly, $\zeta > A_{l+1}(1)$ as explained above. Hence $A_{l+1}(0) - A_{l+1}(1) < kC \leq C$.

For sub-case (ii), we have,

$$\begin{aligned} A_{l+1}(b) = &(1-kb)C + (bq+(1-b)s)kA_{l+2}(1) \\ &+ (1-(bq+(1-b)s)k)A_{l+2}(\Phi(b,0)) \end{aligned} \tag{6.3.17}$$

Now we can say that

$$\begin{aligned} A_{l+1}(0) - A_{l+1}(1) = kC &+ qk\left\{A_{l+2}\left(\frac{q-qk}{1-qk}\right) - A_{l+2}(1)\right\} \\ &- sk\left\{A_{l+2}\left(\frac{s-sk}{1-sk}\right) - A_{l+2}(1)\right\} \\ &+ A_{l+2}\left(\frac{s-sk}{1-sk}\right) - A_{l+2}\left(\frac{q-qk}{1-qk}\right) \end{aligned} \tag{6.3.18}$$

Since $q < s$ and $A_{l+2}(b)$ is non-increasing function in b (induction hypothesis), we get that $A_{l+2}\left(\frac{s-sk}{1-sk}\right) - A_{l+2}\left(\frac{q-qk}{1-qk}\right) \leq 0$. Also, since $qk < 1$ and $sk < 1$, we can write equation (6.3.18) as,

$$\begin{aligned} A_{l+1}(0) - A_{l+1}(1) &< kC + sk\left\{A_{l+2}\left(\frac{q-qk}{1-qk}\right) - A_{l+2}(1)\right\} \\ &\quad - sk\left\{A_{l+2}\left(\frac{s-sk}{1-sk}\right) - A_{l+2}(1)\right\} \\ &\quad + A_{l+2}\left(\frac{s-sk}{1-sk}\right) - A_{l+2}\left(\frac{q-qk}{1-qk}\right) \\ &< kC + \left\{A_{l+2}\left(\frac{q-qk}{1-qk}\right) - A_{l+2}(1)\right\} \\ &\quad - \left\{A_{l+2}\left(\frac{s-sk}{1-sk}\right) - A_{l+2}(1)\right\} \\ &\quad + A_{l+2}\left(\frac{s-sk}{1-sk}\right) - A_{l+2}\left(\frac{q-qk}{1-qk}\right) \\ &= kC \leq C. \end{aligned} \tag{6.3.19}$$

Hence we can say that $A_l(b)$ is non-increasing in b.

Case (iv)

In this case,

$$\begin{aligned} A_l(b) = (1-kb)C &+ (bq + (1-b)s)kA_{l+1}(1) \\ &+ (1 - (bq + (1-b)s)k)A_{l+1}(\Phi(b,0)). \end{aligned} \tag{6.3.20}$$

Differentiating above equation (6.3.20), we get,

$$\begin{aligned} \frac{d(A_l(b))}{db} = &- kC - (s-q)kA_{l+1}(1) + (s-q)kA_{l+1}(\Phi(b,0)) \\ &+ (1 - (bq + (1-b)s)k)\frac{d(A_{l+1}(\Phi(b,0)))}{d(\Phi(b,0))}\frac{d(\Phi(b,0))}{db} \end{aligned} \tag{6.3.21}$$

where, $\frac{d(\cdot)}{db}$ and $\frac{d(\cdot)}{d(\Phi(b,0))}$ denotes differentiation with respect to b and $\Phi(b,0)$ respectively. We will use subgradients wherever applicable. Re-arranging and simplifying above equation (6.3.21) we get,

$$\frac{d(A_l(b))}{db} = -kC\Big\{1 - \frac{(s-q)\big(A_{l+1}(\Phi(b,0)) - A_{l+1}(1)\big)}{C}\Big\} - \frac{d(A_{l+1}(\Phi(b,0)))}{d(\Phi(b,0))}(s-q)f \tag{6.3.22}$$

where $f = \frac{1-k}{(1-(bq+(1-b)s)k)}$. It can be clearly seen that $f \in (0,1)$ and $0 < (bq+(1-b)s)k < 1$ (since q,s, and $k \in (0,1)$).

Let us first show that $(A_{l+1}(\Phi(b,0)) - A_{l+1}(1)) < kC$. We can also show this for the expression $A_{l+1}(0) - A_{l+1}(1) < kC$ since $A_{l+1}(b)$ attains its maximum value at $b = 0$ due to induction hypothesis. We have already proved $A_{l+1}(0) - A_{l+1}(1) < kC$ in previous $Case(iii)$, sub-case (ii). Since $A_{l+1}(0) \geq A_{l+1}(\Phi(b,0))$, we can also say that

$$A_{l+1}(\Phi(b,0)) - A_{l+1}(1) < kC. \tag{6.3.23}$$

Now let us substitute $A_{l+1}(\Phi(b,0)) - A_{l+1}(1)$ by $k_1 C$ where, $k_1 < k$ and $k_1 \in (0,1)$. We can now reduce equation (6.3.22) as:

$$\frac{d(A_l(b))}{db} = -kC\big\{1 - (s-q)k_1\big\} - \frac{d(A_{l+1}(\Phi(b,0)))}{d(\Phi(b,0))}(s-q)f \tag{6.3.24}$$

Here, $A_{l+1}(\Phi(b,0))$ is piecewise-linear (Proposition 6.3.1) and hence differentiable in each of its sub-domains where it is linear in $\Phi(b,0)$. Also $A_{l+1}(\Phi(b,0))$ is non-increasing with respect to $\Phi(b,0)$, thus $\frac{d(A_{l+1}(\Phi(b,0)))}{d(\Phi(b,0))}$ is negative. First let us expand $A_{l+1}(\Phi(b,0))$ as:

$$\begin{aligned} A_{l+1}(\Phi(b,0)) &= (1 - k\Phi(b,0))C + (\Phi(b,0)q + (1-\Phi(b,0))s)kJ_{l+2}(1) \\ &\quad + (1 - (\Phi(b,0)q + (1-\Phi(b,0))s)k)J_{l+2}(\Phi(\Phi(b,0),0)) \\ &= (1 - k\Phi(b,0))C \\ &\quad + (\Phi(b,0)q + (1-\Phi(b,0))s)k\min\{\zeta, A_{l+2}(1)\} \\ &\quad + (1 - (\Phi(b,0)q + (1-\Phi(b,0))s)k) \\ &\quad \times \min\{\zeta, A_{l+2}(\Phi(\Phi(b,0),0))\}. \end{aligned} \tag{6.3.25}$$

Now $A_{l+1}(1) \geq A_{l+2}(1)$ (due to Proposition 6.3.3), we can say that $A_{l+2}(1) < \zeta$ because $A_{l+1}(1) < \zeta$. Hence in above equation (6.3.25), $\min\{\zeta, A_{l+2}(1)\}$ is equal to $A_{l+2}(1)$. We

can now reduce equation (6.3.25) as:

$$\begin{aligned} A_{l+1}(\Phi(b,0)) = (1-k\Phi(b,0))C + (\Phi(b,0)q + (1-\Phi(b,0))s)kA_{l+2}(1) \\ + (1-(\Phi(b,0)q + (1-\Phi(b,0))s)k) \\ \times \min\{\zeta, A_{l+2}(\Phi(\Phi(b,0),0))\}. \end{aligned} \tag{6.3.26}$$

Now there are two sub-cases in equation (6.3.26) depending upon whether $\zeta \leq A_{l+2}(\Phi(\Phi(b,0),0))$ (sub-case (i)) or $\zeta > A_{l+2}(\Phi(\Phi(b,0),0))$ (sub-case (ii)). Let us look for the first case when $\zeta \leq A_{l+2}(\Phi(\Phi(b,0),0))$.

Sub-case (i):

In this case, $\zeta \leq A_{l+2}(\Phi(\Phi(b,0),0))$, we can expand equation (6.3.26) as follows:

$$\begin{aligned} A_{l+1}(\Phi(b,0)) = (1-k\Phi(b,0))C + (\Phi(b,0)q + (1-\Phi(b,0))s)kA_{l+2}(1) \\ + (1-(\Phi(b,0)q + (1-\Phi(b,0))s)k)\zeta. \end{aligned} \tag{6.3.27}$$

Differentiating above equation (6.3.27) with respect to $\Phi(b,0)$ as follows:

$$\frac{d}{d(\Phi(b,0))}\{(A_{l+1}(\Phi(b,0)))\} = -kC\Big\{1 - \frac{(s-q)}{C}\Big(\zeta - A_{l+2}(1)\Big)\Big\}. \tag{6.3.28}$$

Here also we can say that $\zeta - A_{l+2}(1) < kC$ because we know that $\zeta \leq A_{l+2}(\Phi(\Phi(b,0),0))$ and $A_{l+2}(\Phi(\Phi(b,0),0)) - A_{l+2}(1) < kC$. The later expression $A_{l+2}(\Phi(\Phi(b,0),0)) - A_{l+2}(1) < kC$ can be proved in similar way $A_{l+1}(\Phi(b,0)) - A_{l+1}(1) < kC$ was proved earlier. We can say that $A_{l+2}(0) - A_{l+2}(1) < kC$ in same way as was shown for $A_{l+1}(0) - A_{l+1}(1) < kC$. Now, we know that $A_{l+2}(\Phi(\Phi(b,0),0)) \geq A_{l+2}(1)$ (due to induction hypothesis). Hence we can claim that $A_{l+2}(\Phi(\Phi(b,0),0)) - A_{l+2}(1) < kC$. Now let us substitute $\zeta - A_{l+2}(1)$ by k_2C where, $k_2 < k$ and $k_2 \in (0,1)$. Substituting the result from above equation (6.3.28) in equation (6.3.24), we get,

$$\frac{d(A_l(b))}{db} = -kC\big\{(1-(s-q)k_1) - (1-(s-q)k_2)(s-q)f\big\} \tag{6.3.29}$$

We will show that $k_2 > k_1$ in above equation (6.3.29).

$$\begin{aligned} k_2C = \ & \zeta - A_{l+2}(1) \\ & \geq \zeta - A_{l+1}(1), \text{ since } A_{l+1}(1) \geq A_{l+2}(1) \\ & > A_{l+1}(\phi(b,0)) - A_{l+1}(1), \text{ since } \zeta > A_{l+1}(\phi(b,0)) \\ & = k_1C \end{aligned}$$

Hence we can say that $(1-(s-q)k_1) > (1-(s-q)k_2)(s-q)f$ in equation (6.3.29). Hence overall $\frac{d(A_l(b))}{db}$ in equation (6.3.29) is negative. This shows that for sub-case (i) , $A_l(b)$ is

non-increasing function with respect to b.

Sub-case (ii):

In this case, $\zeta > A_{l+2}(\Phi(\Phi(b,0),0))$, thus we can expand $A_{l+1}(\Phi(b,0))$ in equation (6.3.26) as

$$\begin{aligned} A_{l+1}(\Phi(b,0)) = (1-k\Phi(b,0))C + (\Phi(b,0)q + (1-\Phi(b,0))s)kA_{l+2}(1) \\ + (1-(\Phi(b,0)q + (1-\Phi(b,0))s)k)A_{l+2}(\Phi(\Phi(b,0),0)). \end{aligned} \tag{6.3.30}$$

Differentiating above equation (6.3.30) with respect to $\Phi(b,0)$ and re-arranging as follows:

$$\begin{aligned} \frac{d(A_{l+1}(\Phi(b,0)))}{d(\Phi(b,0))} =& -kC\Bigg\{1 - \frac{(s-q)}{C}\Big(A_{l+2}(\Phi(\Phi(b,0),0)) - A_{l+2}(1)\Big)\Bigg\} \\ &+ (1-(\Phi(b,0)(q-s)+s)k)\frac{d\left(A_{l+2}\left(\Phi\left(\Phi\left(b,0\right),0\right)\right)\right)}{d(\Phi(b,0))} \end{aligned} \tag{6.3.31}$$

We know that $A_{l+2}(\Phi(\Phi(b,0),0)) - A_{l+2}(1) < kC$. Let us substitute $A_{l+2}(\Phi(\Phi(b,0),0)) - A_{l+2}(1)$ by k_3 where $k_3 < k$ and $k_3 \in (0,1)$. Re-writing equation (6.3.31), we get

$$\begin{aligned} \frac{d(A_{l+1}(\Phi(b,0)))}{d(\Phi(b,0))} =& -kC\Big\{1-(s-q)k_3\Big\} \\ &+ (1-(\Phi(b,0)(q-s)+s)k)\frac{d\left(A_{l+2}\left(\Phi\left(\Phi\left(b,0\right),0\right)\right)\right)}{d(\Phi(b,0))} \end{aligned} \tag{6.3.32}$$

Now let us substitute equation (6.3.32) in equation (6.3.24), we get,

$$\begin{aligned} \frac{d(A_l(b))}{db} =& -kC\big\{1-(s-q)(k_1+f)\big\} - kC(s-q)^2k_3f \\ &- \Bigg\{(1-(\Phi(b,0)(q-s)+s)k) \\ &\times \frac{d\left(A_{l+2}\left(\Phi\left(\Phi\left(b,0\right),0\right)\right)\right)}{d(\Phi(b,0))}\Bigg\}(s-q)f \end{aligned} \tag{6.3.33}$$

From equation (6.3.33), we can see that terms

$$(s-q),\ f,\ (1-(\Phi(b,0)(q-s)+s)k) \text{ and } \frac{d\left(A_{l+2}\left(\Phi\left(\Phi\left(b,0\right),0\right)\right)\right)}{d(\Phi(b,0))}$$

are positive. Term

$$\frac{d\left(A_{l+2}\left(\Phi\left(\Phi\left(b,0\right),0\right)\right)\right)}{d(\Phi(b,0))}$$

is positive because $A_{l+2}(\cdot)$ is non-increasing function (due to induction hypothesis) and $\Phi(\cdot,0)$ is decreasing function, hence $A_{l+2}(\Phi(\cdot,0))$ is increasing function. Thus we can say that the term

$$\frac{d\left(A_{l+2}\left(\Phi\left(\Phi\left(b,0\right),0\right)\right)\right)}{d(\Phi(b,0))}$$

is positive. Hence we can say that

$$-\big\{(1-(\Phi(b,0)(q-s)+s)k)\frac{d\left(A_{l+2}\left(\Phi\left(\Phi\left(b,0\right),0\right)\right)\right)}{d(\Phi(b,0))}\big\}(s-q)f$$

is negative in above equation (6.3.33). Let us look at the remaining term

$$-kC\{1-(s-q)(k_1+f)\}-kC(s-q)^2k_3f.$$

We will prove that this term is also negative by proving that $1-(s-q)(k_1+f)>0$ for both cases when i) $q\geq 1/2$ and when ii) $s\leq 1/2$. We can say that for both of these cases, $0<(s-q)f<1/2$, where $0<f<1$. Hence $1>1-(s-q)k_1>1/2$, where $k_1<1$. Thus we can easily see that $1-(s-q)(k_1+f)>0$. Using this fact, we can say that $\frac{d(A_l(b))}{db}$ in equation (6.3.33) is negative implying that $A_l(b)$ is a non-increasing function in b. Thus induction is complete for both cases i) $q\geq 1/2$ and ii) $s\leq 1/2$. □

All these Propositions 6.3.1, 6.3.2, 6.3.3 and 6.3.4 and Lemma 6.3.1 give intermediate results which are useful in proving our Theorem 6.3.1 mentioned in the next subsection. Now we give the following conjecture for the remaining and last case for $q<s$, when $q<1/2$ & $s>1/2$ which is a hard case to prove.

Conjecture 6.3.1. *For the case when $q<s$, and $q<1/2$ & $s>1/2$, $A_l(b)$ is non-increasing with b.*

We believe that this conjecture is true and is also validated through extensive simulations later in the Section 6.4.

6.3.2 Policy Structure

The structure of an optimal policy for our POMDP problem is provided in the following theorem.

Theorem 6.3.1. *The optimal policy for our POMDP problem is a threshold policy. If $\zeta\leq(1-k)C$ then the optimal action is always to explore. For the cases when $q>s$, and $q<s$ (both scenarios when $q\geq 1/2$ and $s\leq 1/2$): When $\zeta>(1-k)C$, at any time instant $l\in\{0,1,\cdots,N-1\}$, the optimal action is to continue transmission on the current relay link if $b_l\geq\alpha_l$, and explore and switch to another better relay link if $b_l<\alpha_l$. Also, the threshold $\alpha_l\in[0,1]$ is non-increasing in l.*

Proof. For the case $\zeta\leq(1-k)C$: First we start for base case $l=N-1$ and the first term in recursion $l=N-2$:

$$J_{N-1}(b)=\min\{\zeta,(1-kb)C\}=\zeta,$$

since $\zeta \leq (1-k)C$. For time instant $N-2$, we have

$$\begin{aligned} J_{N-2}(b) =& \min\{\zeta, (1-kb)C + (bq+(1-b)s)kJ_{N-1}(1) \\ &+ \min\{(1-(bq+(1-b)s)k)\zeta, (1-(bq+(1-b)s)k(2-k))C\}\}. \end{aligned} \tag{6.3.34}$$

We can easily see that $J_{N-2}(b) \leq J_{N-1}(b)$ since $\zeta \leq (1-k)C$. Hence we can conclude that $J_{N-2}(b) = \zeta$. We now check $J_{N-2}(b)$ and $J_{N-3}(b)$. We can write $J_{N-3}(b)$ as:

$$\begin{aligned} J_{N-3}(b) &= \min\{\zeta, (1-kb)C + (bq+(1-b)s)kJ_{N-2}(1)+ \\ &\quad (1-(bq+(1-b)s)k)J_{N-2}(\Phi(b,0))\} \\ &\leq \min\{\zeta, (1-kb)C + (bq+(1-b)s)kJ_{N-1}(1)+ \\ &\quad (1-(bq+(1-b)s)k)J_{N-1}(\Phi(b,0))\} \\ &= J_{N-2}(b) = \zeta \end{aligned}$$

Hence $J_{N-3}(b) = \zeta$. Similarly it proceeds for other l and hence $J_l(b) = \zeta$. Thus cost of exploring in this case when $\zeta \leq (1-k)C$ is always optimal.

For the case when $\zeta > (1-k)C$: Let us see the possible cases which exists for the given DP by fixing $l = N-2$ and at belief probabilities 0 and 1. For $b_{N-2} = 0$, cost ζ of exploration is always optimal if $\zeta \leq C + (1-sk)C$ otherwise continuation is always optimal. For $b_{N-2} = 1$, if $\zeta \leq (1-k)C + (1-qk)C$ then exploration is always optimal. If $\zeta > (1-k)C + (1-qk)C$ then continuing on the current link is the best option and exploring other links is never optimal. Hence we will see the following scenario where we can get the decision criterion for choosing between exploring other links versus continuing on the same relay link. Assuming for $b_{N-2} = 1$, $\zeta > (1-k)C + (1-qk)C$ is satisfied and for $b_{N-2} = 0$, $\zeta \leq C + (1-sk)C$ is satisfied. If this condition is true, then there exists a scalar α_{N-2} with $0 < \alpha_{N-2} < 1$ that determines an optimal policy for the last period as: continue transmission on relay j if $b_{N-2} \geq \alpha_{N-2}$ else stop transmission on relay j and explore and switch to another better relay. Since we are looking for the condition when the communication on given relay link can continue or not. When it cannot be continued then first action is chosen which stops the communication on the current relay link and exploration for new link begins.

Using Proposition 6.3.1, Proposition 6.3.3, Proposition 6.3.2 and Proposition 6.3.4, we can say that the functions $y = \zeta$ and $y = A_l(b_l)$ intersect at a single point and from the DP algorithm in equation (6.3.1), we obtain that the optimal policy for each period is determined by the unique scalars α_l which are such that: $\zeta = A_l(\alpha_l)$. Since we get a single point of intersection which decides the optimal choice for choosing an appropriate option, we can say that the optimal policy for the time period l is given as: continue transmission on relaying zone j if $b_l \geq \alpha_l$, else stop transmission on relaying zone j and explore and switch to another better relay.

Second part of this theorem: Using Propositions 6.3.4, 6.3.3 and 6.3.2, $A_l(b_l)$ are monotonically non-increasing with respect to l. Hence we can say that sequence of α_l is also non-increasing with l (using Proposition 6.3.1 and 6.3.2). □

This theorem do not use the Conjecture 6.3.1 for the proof. However, once this conjecture is proved, its result can be extended to above Theorem 6.3.1. Now, in the Theorem 6.3.1, if $\zeta \leq (1-k)C$ then the UE will only explore all the time in case of packet loss and there would not be any data transmission if packet loss event happens frequently, which is clearly undesirable. We will look for the cases for which $\zeta > (1-k)C$. At $l \to \infty$, α_l converges to some scalar $\overline{\alpha}$, as a decreasing sequence which is bounded below always converges. Hence, for very large horizon length N, the optimal policy can be approximated by a stationary threshold policy with a time-invariant threshold $\overline{\alpha}$.

Case $q > s$: Let us now derive a simplified threshold policy for the case when $q > s$. Note that, if $z_l = 1$, then $b_l = 1$. Hence, without loss of generality, let us assume that $b_0 = 1$. If $z_0 = 0$, then $b_1 = \Phi(b_0 = 1, z_0 = 0) = \frac{q-qk}{1-qk} < 1 = b_0$. Now, it is easy to check that $\Phi(b, 0)$ is a strictly increasing function in b. Hence, $b_2 = \Phi(b_1, 0) < \Phi(b_0, 0) = b_1$. Proceeding in this way, we can show that b_l strictly decreases with l whenever we observe several successive ACK failures. We can define recursively a probability π_m of getting m successive ACK failure as: $\pi_1 = \Phi(1, \overline{A})$, $\pi_2 = \Phi(\pi_1, \overline{A})$, $\cdots$, $\pi_m = \Phi(\pi_{m-1}, \overline{A})$. Let r be the smallest integer such that $\pi_r \leq \overline{\alpha}$. We can further simplify the stationary threshold policy as follows.

Simplified stationary threshold policy ($q > s$): *Let r be the smallest integer such that $\pi_r \leq \overline{\alpha}$. If there are r successive ACK failures, explore and switch to another better relay link, else continue transmission on the current relay link.*

Case $q < s$: As mentioned earlier, for the case when $q < s$ and whether $q \geq 1/2$ or $s \leq 1/2$, the policy is a time-invariant threshold $\overline{\alpha}$ policy. The optimal action at time instant l would be to continue transmission on the current relay link if $b_l \geq \overline{\alpha}$, and explore and switch to another better relay link if $b_l < \overline{\alpha}$.

6.4 Simulation and Results

Simulation Environment

Since D2D communication is suitable for short range only, we consider that the service region comprises of D2D users residing within a small cell of dimension 100 $m \times 100$ m, as also considered in [109, 110]. However it can be extended to the dimensions of macro cell region. We have divided the service region into grid zones each of dimension 10 $m \times 10$ m. Each zone is assumed to have enough UEs to form a D2D link with UEs of other zones. Here 60 GHz mmWave is used and transmitter and receiver antennas with gains $G_r = G_t = 6$ dB are assumed. Data transmission takes place for 1 s with $\delta = 10$ ms, thus there are maximum

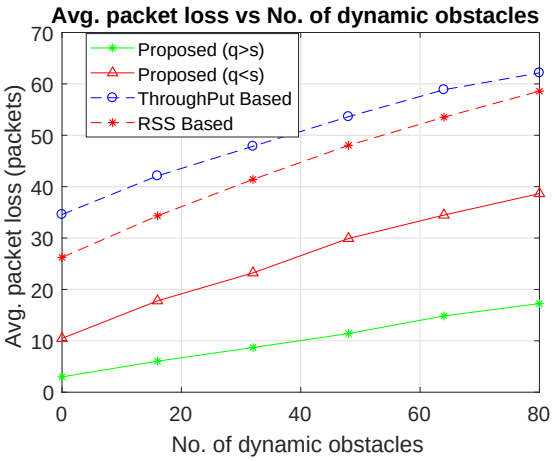

Figure 6.4: Avg. packet loss vs D

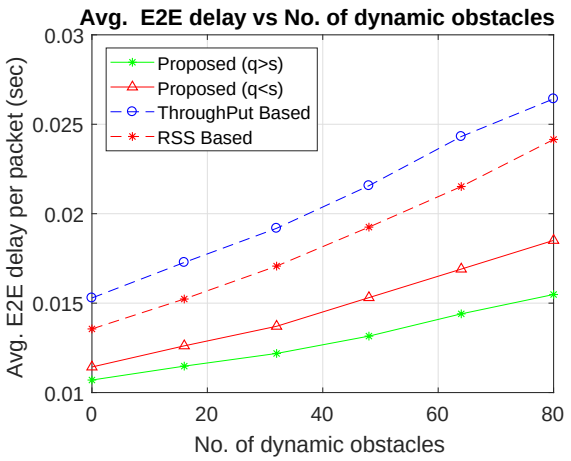

Figure 6.5: Avg. E2E delay per packet vs D

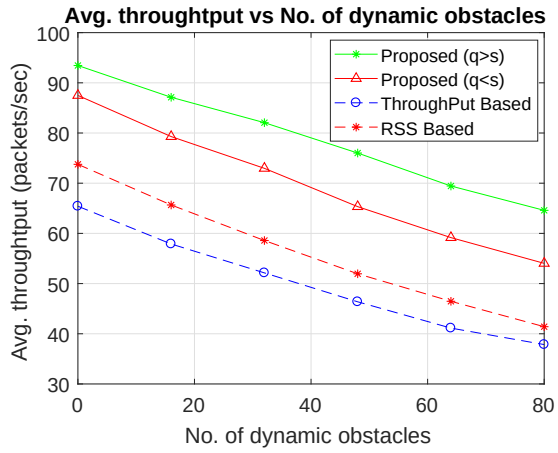

Figure 6.6: Avg. throughput vs D

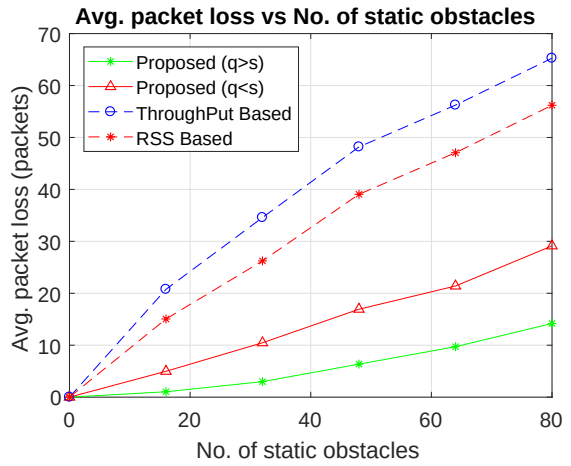

Figure 6.7: Avg. packet loss vs S

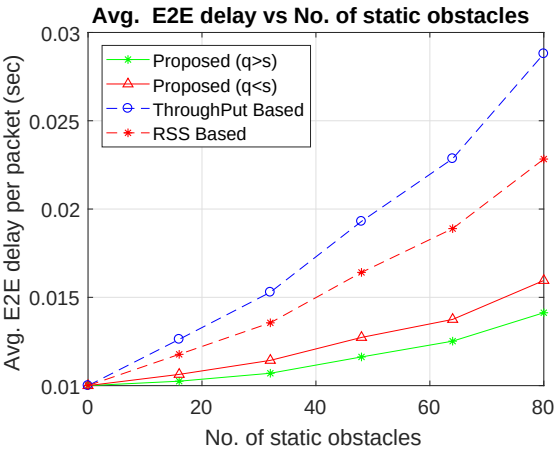

Figure 6.8: Avg. E2E delay per packet vs S

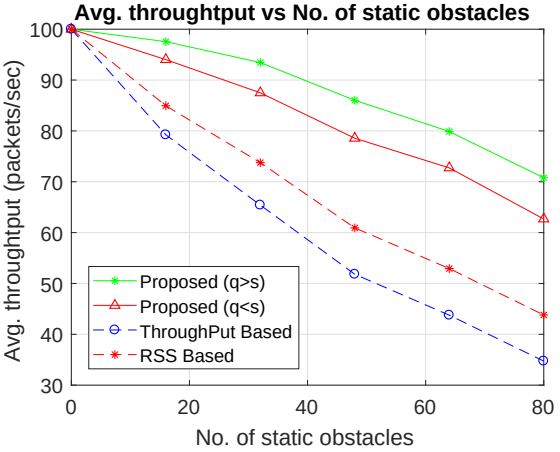

Figure 6.9: Avg. throughput vs S

of 100 packets that can be sent during 1 s local time duration. We are considering a scenario

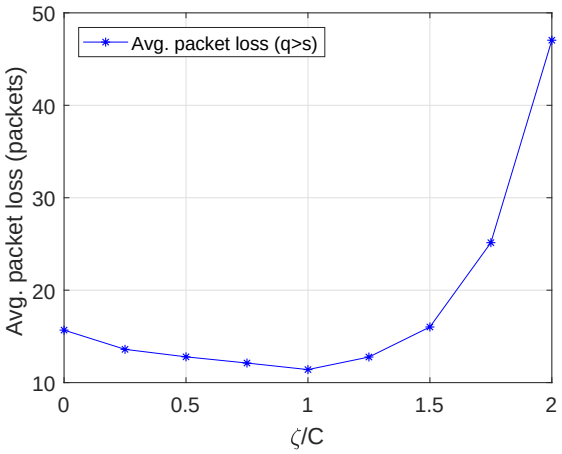

Figure 6.10: Avg. packet loss on varying ζ

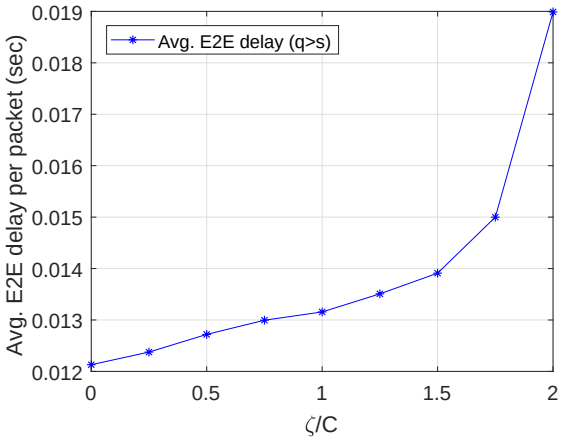

Figure 6.11: Avg. E2E delay per packet on varying ζ

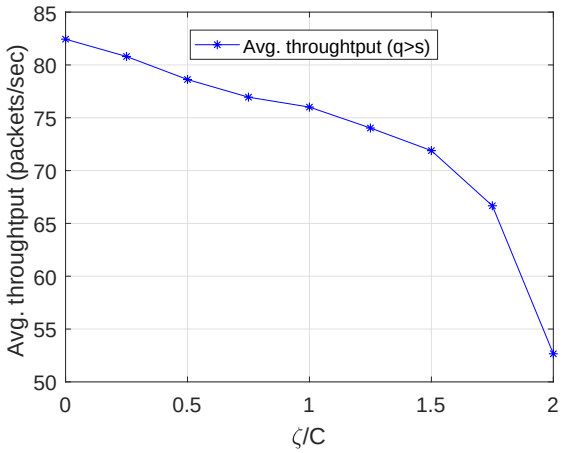

Figure 6.12: Avg. throughput on varying ζ

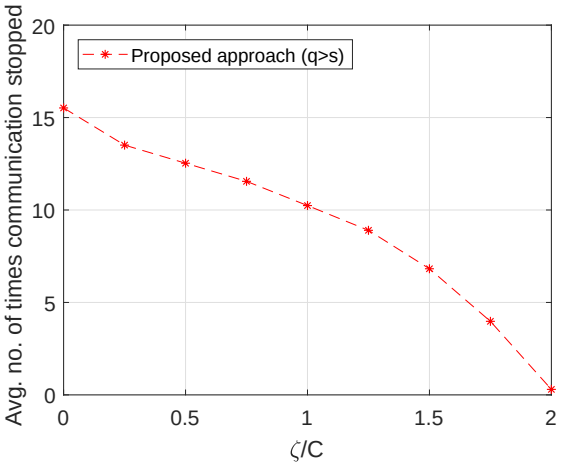

Figure 6.13: Average no. of times the transmission on current link is stopped and new links are explored on varying ζ

where line of sight path loss exponent is 2.5 and log-normal shadowing random variable has zero mean and standard deviation 3.5 [10, 106]. Thermal noise density assumed here is -174 dBm/Hz and transmit power of a UE is 24 dBm. Capacity of each link (i, j) is $B\log_2(1+S_{ij})$ $bits/s$, where $B = 20$ MHz [102] is bandwidth and S_{ij} is the received signal to noise ratio. We are assuming fixed packet length of 65535 $bytes$. There are total S=32 static obstacles placed randomly and D dynamic obstacles present in the environment, where $D \in \{0, 16, 32, 48, 64, 80\}$. Each static obstacle is assumed to be of the dimension of a grid. Hence all communications going via a grid where there is a static obstacle will get blocked. Each dynamic obstacle is moving randomly and independently of each other. We assume a realistic scenario where they follow a random Bernoulli blockage model where with probability p (here we have assumed p=0.7), they may come in between any given

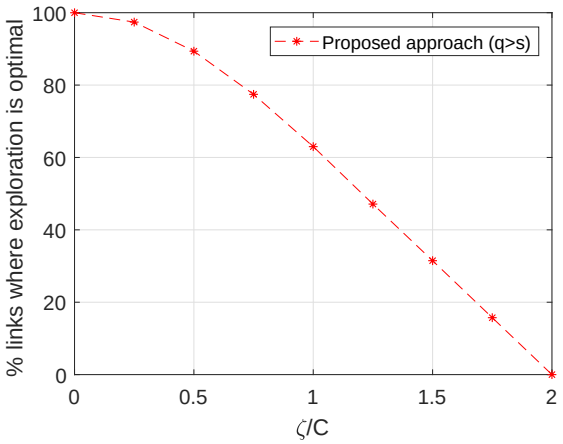

Figure 6.14: Percentage of total available links where exploration is optimal versus varying ζ

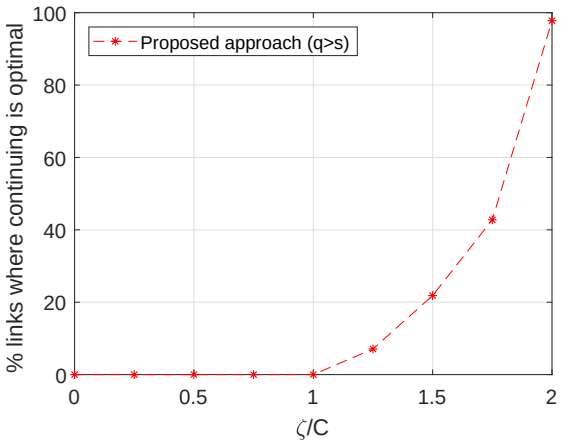

Figure 6.15: Percentage of total available links where continuing is optimal versus varying ζ

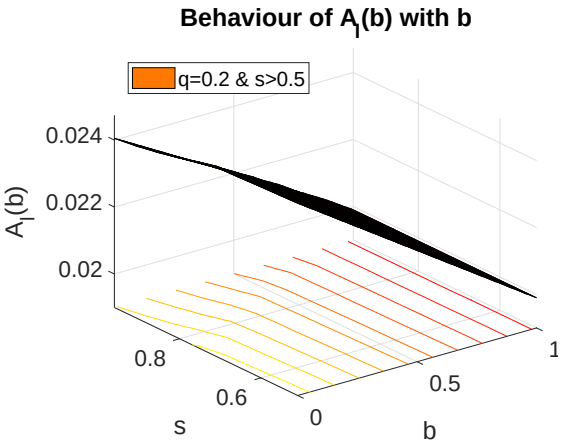

Figure 6.16: Behaviour of $A_l(b)$ with b fixing q=0.2

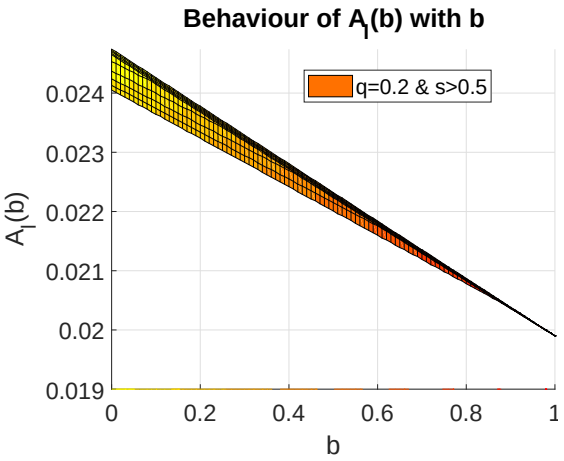

Figure 6.17: $Z-X$ axis view of $A_l(b)$ with b fixing q=0.2

link which is due to their mobility pattern. Once they come in between any given link they would block the link completely with probability 1 and would stay there for some random amount of local time instants which is chosen uniformly in $\{1, 2, \cdots, N-1\}$. Since, at the very start of the experiment the exact values of parameters q, s, and k are unknown to the BS as well as UEs, they need to be estimated along the horizon as communication between nodes take place. For a given link i, let g_i denote the total number of times link i became *good* at time instant $l+1$ given that it was *good* at time instant l. Let G_i represent the total number of times the given link i becomes *good* at time $l+1$ irrespective of whether it was *good* or *bad* at time instant l. Thus we can estimate q empirically by the ratio g_i/G_i. Similarly, this technique is applied to estimate other parameters s, and k at global time instants based on packet loss and ACK success/failure data received from the UEs during local time instants. Through out we maintain the inequality for two different cases when

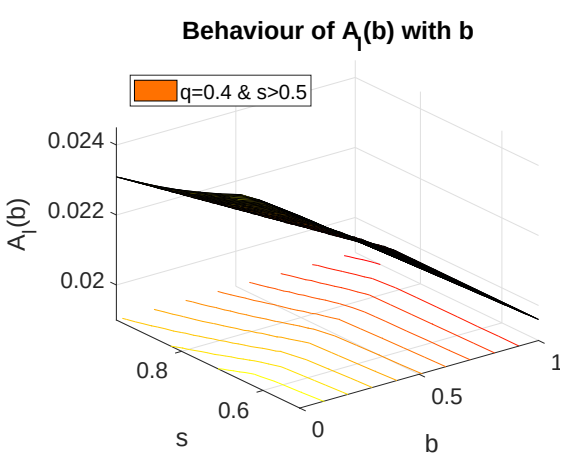

Figure 6.18: Behaviour of $A_l(b)$ with b fixing q=0.4

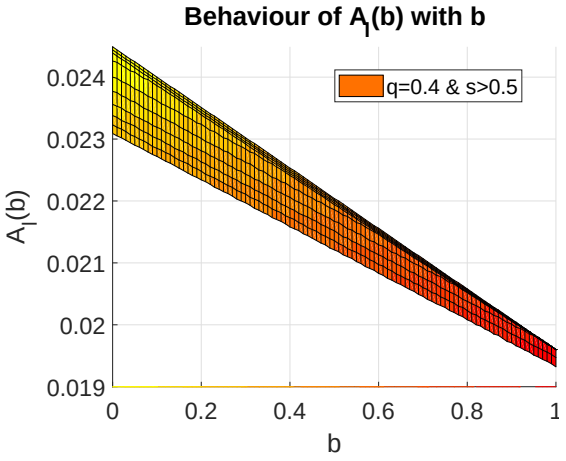

Figure 6.19: $Z - X$ axis view of $A_l(b)$ with b fixing q=0.4

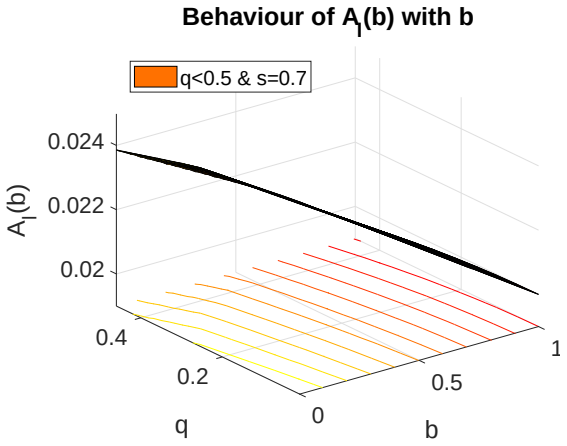

Figure 6.20: Behaviour of $A_l(b)$ with b fixing s=0.7

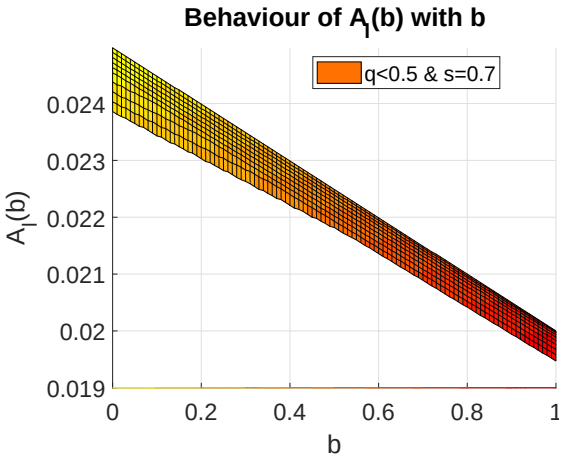

Figure 6.21: $Z - X$ axis view of $A_l(b)$ with b fixing s=0.7

(1) $q > s$ and (2) $q < s$ ((i) $q > 0.5$ and (ii) $s < 0.5$). Once we get estimate of parameters q, s and k, we simply put these values in our model and accordingly can compute the belief probability. Hence we can now apply our main result of Theorem 6.3.1 which simply uses these parameters for finding out the threshold. We are assuming that a given zone i can make connection with another zone out of at-most 8 neighboring zones surrounding it, i.e., $\mathbb{U}^i \leq 8$. We assume a single source-destination pair for simplicity and all other devices in a given zone may act as relay. We have written our own C++ custom code and run them on a `GNU` 4.8 compiler on Intel core $i7$ machine. We run our experiments for around 6000 runs and take average results per run and per hop for the packet loss, end to end (E2E) delay per packet, and throughput. E2E delay is the total time (in seconds) to send a packet successfully from source UE to the destination UE including time it takes to explore and switch to newly selected relay links. New relays are selected during exploration based

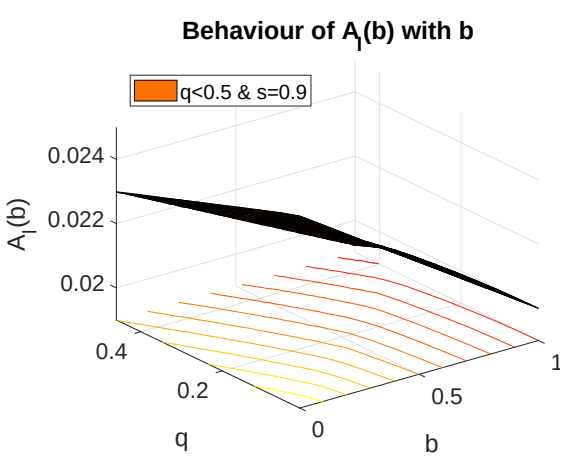

Figure 6.22: Behaviour of $A_l(b)$ with b fixing s=0.9

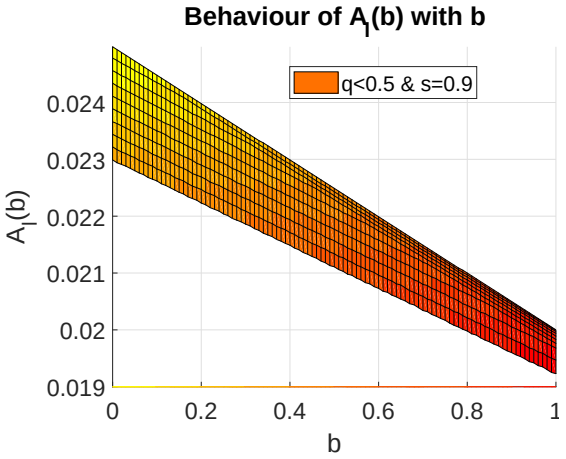

Figure 6.23: $Z - X$ axis view of $A_l(b)$ with b fixing s=0.9

on the highest received signal strength. The throughput is defined total packets delivered successfully per unit time. We have given two proposed approaches respectively for i) $q > s$ and ii) $q < s$ (for both cases $q \geq 0.5$ and $s \leq 0.5$) based on the analysis and method presented in the previous section. We are comparing the results of our proposed approach with two existing approaches: 1) an approach which selects relay link based on received signal strength (`RSS Based`) and 2) an approach which selects relay link based on maximum overall throughput (`Throughput Based`) [34] which utilizes parameter q in computing the throughput. We show the impact of varying number of static and dynamic obstacles on aforementioned parameters. Also, effect on percentage of total links where explorations and continuing decisions are optimal on varying ζ, is also shown. The parameter ζ is lying in the set $\{0, 0.25C, 0.5C, 0.75C, C, 1.25C, 1.5C, 1.75C, 2C\}$. The cost C is taken to be penalty of one slot duration δ=10 ms.

Simulation Results & Analysis

For Figures 6.4-6.6, ζ=C and the number of static obstacles S is fixed at 32. Figure 6.4 shows the result of average packet loss over the number of dynamic obstacles. The packet loss increases with increasing in number of dynamic obstacles for the policy given for both cases where $q > s$, and $q < s$ (for both cases $q \geq 0.5$ and $s \leq 0.5$). As the number of dynamic obstacles increase, chance of more links getting blocked by these obstacles also increases. Our proposed methods outperform other algorithms because we learn the quality of D2D links based on ACK received and switch to another better relay when the quality of current D2D link deteriorates. While other algorithms, RSS based and Throughput based, only continue on the link initially provided by the BS. Hence, lot of packet loss occurs when link is blocked by dynamic obstacles. This explains the importance of deferring the communication to some other newly selected relay when several successive packet loss occurs on the current

link provided by the BS. Figures 6.5 and 6.6 capture the effect of the number of dynamic obstacles over average E2E delay per packet and average throughput respectively. As the number of dynamic obstacles increases, the delay increases and the throughput decreases. This is due to increased packet loss, since link blockage chance increases as obstacles increase as explained above. Here too our proposed method outperforms other algorithms since it learns the channel quality by utilizing the optimal policy analyzed in the paper. In all of figures 6.4-6.6, our approach for the case $q > s$ performs better than the case $q < s$ because of the nature of the transition probabilities. The chance of going from good state to good state is more as compared to that of going from bad state to good state for the case when $q > s$. Hence when a link is in good state, it implies that it transitioned from a good state with a higher probability. Hence most of the time the link resided in the good state and hence higher performance is observed.

The results mentioned in Figures 6.7-6.9 are capturing the effects of varying S on average packet loss, average E2E delay, and average throughput keeping $D = 0$ and ζ=C. Here the trends and explanations are similar to previous paragraph.

In rest of the Figures 6.10-6.15, we show the effect of varying the exploration cost ζ on various parameters and observe some insights for the case when $q > s$. Similar insights would follow for the other case ($q < s$ when (i) $q \geq 0.5$ and (ii) $s \leq 0.5$) as well. Figures 6.10-6.12 show the performance of our approach in terms of average packet loss, average E2E delay, and average throughput for varying ζ when $D = 48$ and S fixed at 32. In Figure 6.10, as ζ increases, the average packet loss first decreases slightly and then increases rapidly after ζ=C. For ζ=C, average packet loss is 11.41 and average packets transmitted successfully is 76.01. However, when ζ=0, upon packet loss, new links are explored instantaneously. Here average packet loss is 15.68 and average packets transmitted successfully is 82.44. We can see that average number of packets sent for data transmission when ζ=0 is 98.14 which is higher as compared to that of the case when ζ=C (87.42). This is because of lower exploration cost when ζ=0 and hence more slots are available for data transmission, hence lower chances of packet loss comparatively for ζ=C. Note that when ζ=0, the total packet transmitted is not 100% because for some time instants all neighbouring zones might be blocked due to blockage and no zones are available for data transmission after exploration. In Figure 6.11, average E2E delay increases with ζ. For ζ=C, average packets transmitted successfully in 1 second is 76.01. For ζ=0, this value is 82.44. Hence, the average E2E delay for the case when ζ=0 is lower compared to the case when ζ=C. Effects of ζ on average throughput in Figure 6.12 can be explained similar to previous result as more packets are transmitted for ζ=0 (82.44 packets) case as compared to that of ζ=C (76.01 packets) case.

Figure 6.13 shows the effect of varying ζ on total number of times communication is stopped on the current link and new explorations are performed in the given time horizon. We can observe that, as ζ increases, the frequency in exploration decreases. Higher values of ζ discourages explorations when packet loss occurs. Hence, number of times communica-

tion on current link is stopped and new explorations are performed also decreases. Lower exploration cost ζ makes more explorations and switching feasible when packet loss event occurs. As shown in the figure, when ζ=2C, the number of times new links are switched is almost 0, this causes the data transmission to be continued on current relay link selected by the BS for the whole time horizon even in case of longer successive ACK failures due to obstacles. This case is similar to that of RSS based approach. When ζ=0, the new relay links would be explored and switched every time there is a packet loss event and thereby causing excessive explorations. The value of ζ has a strong effect on the value of the derived scalar $\overline{\alpha}$. When ζ value is lesser, $\overline{\alpha}$ is closer to 0, indicating exploring for a new relay link is optimal during packet loss event. Similarly, for higher value of ζ, $\overline{\alpha}$ is closer to 1, indicating continuing on the current link is optimal during packet loss event. These results are shown respectively in figures 6.14-6.15. Figure 6.14 shows that the percentage of total available links where explorations are optimal decreases with ζ. Similarly, Figure 6.15 shows that the percentage of total available links where continuing on those links are optimal increase with ζ. Till ζ=C, it is 0% and then rapidly increases with ζ. At ζ=C, there are total of about 63% links where exploration is optimal (Figure 6.14) and 0% links where continuation is optimal (Figure 6.15), and for the rest 37% links there is a threshold based policy which is directly dependent on the derived scalar $\overline{\alpha}$.

We numerically checked Conjecture 6.3.1 by running 10000 simulation runs and varying q, s, and k, keeping ζ fixed at 1.5C. These results verify Conjecture 6.3.1. We are presenting few results in figures 6.16-6.23 where k=0.5 and l=N-3=97 for our simulation environment. In Figures 6.16 and 6.18, we have shown the behaviour of $A_l(b)$ keeping q fixed at 0.2 and 0.4 respectively and varying s in range $(0.5, 1.0)$. Figures 6.17 and 6.19 show the view of $X - Z$ axis, corresponding to Figures 6.16 and 6.18 respectively. Similarly, Figures 6.20 and 6.22, we have shown the behaviour of$A_l(b)$ keeping s fixed at 0.7 and 0.9 respectively varying q in range $(0, 0.5)$. Figures 6.21 and 6.23 show the view of $X - Z$ axis corresponding to Figures 6.20 and 6.22 respectively. These results are consistent with Conjecture 6.3.1.

6.5 Conclusion

The unpredictable fluctuations in D2D channel quality due to presence of dynamic obstacles may cause severe packet loss and hence delay. The problem of making decision to stop communication via current relay in the event of successive packet loss considering substantial exploration cost is modeled as a finite horizon POMDP framework at each UE locally. An optimal threshold policy that maps belief to action is derived for both positively ($q > s$) and negatively ($q < s$) correlated links. We conjectured that $A_l(b)$ is non-increasing in b for the negatively correlated links when $q < 1/2$ & $s > 1/2$. We then provided a simple stationary policy for positively correlated links which tells UE to make decision locally by counting the number of ACK failures. Similarly, a strategy based on scalar $\overline{\alpha}$ is also devised

for negatively correlated links. Both of these strategies are simple and easy to implement. Through simulations, we showed that our approach captures the effects of dynamic obstacles and outperforms other state of art algorithms.

Chapter 7

Local Relay Selection during Exploration time in Presence of Dynamic Obstacles in Millimeter Wave D2D Communication

Much of the content of this chapter is copied from my own paper[5] *with the permission of my co-authors Arpan Chattopadhyay and Sasthi C. Ghosh. Even though the paper can be found in the literature, it is copied here so that I can make minor changes and clarifications for the convenience of the reader.*

In the previous chapter, we described the local sequential decision problem at each UE, i.e., whether stop communication on a chosen mmWave D2D relay link in case of successive packet losses *or* whether to continue the transmission over it, by considering the directional search costs for the new relay. The next problem which follows is: How to locally guarantee that the chosen relay is itself free of dynamic obstacles and it would not cause frequent relay switching. Note that frequent relay switching might occur if the newly chosen relay is also going to get blocked by dynamic obstacles in local time instants when it was selected. This has very high overhead because the directional search of mmWave D2D relay has some significant cost in terms of exploration time. The new relaying UE must be chosen carefully during exploration time (ranging from few microseconds to 10 ms [15]), because it may get blocked during data transmission time (100-1000 times higher than exploration time) due to presence of dynamic obstacles, even when the source and relay beams are perfectly aligned as was shown in figure 1.2.

In this chapter, we have investigated the idea of reducing frequency in relay switching and thus average end-to-end (E2E) delay at the expense of additional exploration time during beam alignment. Here we have considered the fact that exploration has a substantial

[5]D. Singh, A. Chattopadhyay, and S. C. Ghosh. Local relay selection in presence of dynamic obstacles in millimeter wave d2d communication. In IEEE International Conference on Communications (ICC), pages 1–6, 2021.

delay. We have modeled the problem as a finite horizon POMDP. The states are the D2D relay link qualities which are not observable at the current time instant. It can only be observed after receiving the acknowledgements (ACKs) of the probe packets which are sent in order to access a link. *Even the ACKs can get lost due to presence of dynamic obstacles.* Information about dynamic obstacles are *not* known at BS a priori and it can only be learned through ACKs of probe packets. The goal is to take decision of whether selecting or not selecting a relay which minimizes packet loss and in-turn delay by sending additional exploration probe packets to learn the channel quality. Optimal threshold policies have been derived which maps the belief to a set of actions. By exploiting the derived policy structure, we have obtained a stationary policy which tells the UE during exploration that after how many successive ACK successes or ACK failures to take the decision of whether selecting or not selecting the relay respectively. Our optimal policy can be implemented locally at each UE, thereby facilitating distributed implementation. Theoretical analysis is validated through extensive simulation.

The organization of the chapter is as follows. System model is described in section 7.1. The POMDP formulation is provided in section 7.2. Optimal policy structure is derived in section 7.3. Numerical results are provided in section 7.4, followed by the conclusions in section 7.5.

7.1 System Model

We are considering the device-tier of 5G D2D architecture mentioned in [1], where devices or UEs can communicate among themselves with or without the help from BS. The service region is discretized into various *zones* or *grids* as shown in figure 7.1(a) with one BS. Each zone may have many UEs and is assumed to have at least one D2D device which is ready to take part in D2D communication as a relay or source/destination node. A zone i containing the source UE may form connection to a UE of another zone $j \in \mathbb{U}^i$, where $\mathbb{U}^i$ is the *viable* relay zones of the zone i which is given by the BS. A viable relaying zone of zone i is one which is nearer to the zone containing the destination UE and is in the communication range of the zone i. When the source UE in the fixed zone i forms a connection with another UE of zone $j \in \mathbb{U}^i$, then the link formed between zones i and j is termed as link j. Link is formed between UEs of two zones when they are in communication range of each other and the received signal strength is sufficient for the required data rate.

Time is discretized as $t, t+1, \cdots$ as shown in figure 6.2 with time duration Δt between two consecutive time instants. Duration Δt is further sub-divided into various smaller time duration of value δ. We denote each such smaller time duration by l which takes integer values in $[0, N-1]$, where N is represents a positive integer such that $\Delta t = N\delta$. Here δ is the smaller discretized time slot when the UEs transmit packets locally. It is assumed that δ (for each $l \in [0, N-1]$) is large enough to send one packet of size L_s bytes. Here,

instants $t, t+1, \cdots$ represent the moments when global decisions is given by the BS. At these time instant BS takes the channel state information from all UEs in the service region and gives the decision of best relaying UE of a given zone for a given source UE. Hence, in between two consecutive time instants when BS can make global decision, a UE can send at-most N packets of size L_s to another UE. Note that at time $l = 0$, the UE chooses the relay link suggested by the BS and at time $l \in \{1, 2, \cdots, N-1\}$, UEs do not get channel state information from the BS. At global time instants, BS sends two types of information to UEs, i) the best relaying UE for a given source UE and ii) viable relaying zones $\mathbb{U}^i$ for given source zone i, hence the zone i may choose an appropriate zone for relaying data from the set $\mathbb{U}^i$ by undergoing exploration. Each UE can communicate with one another on

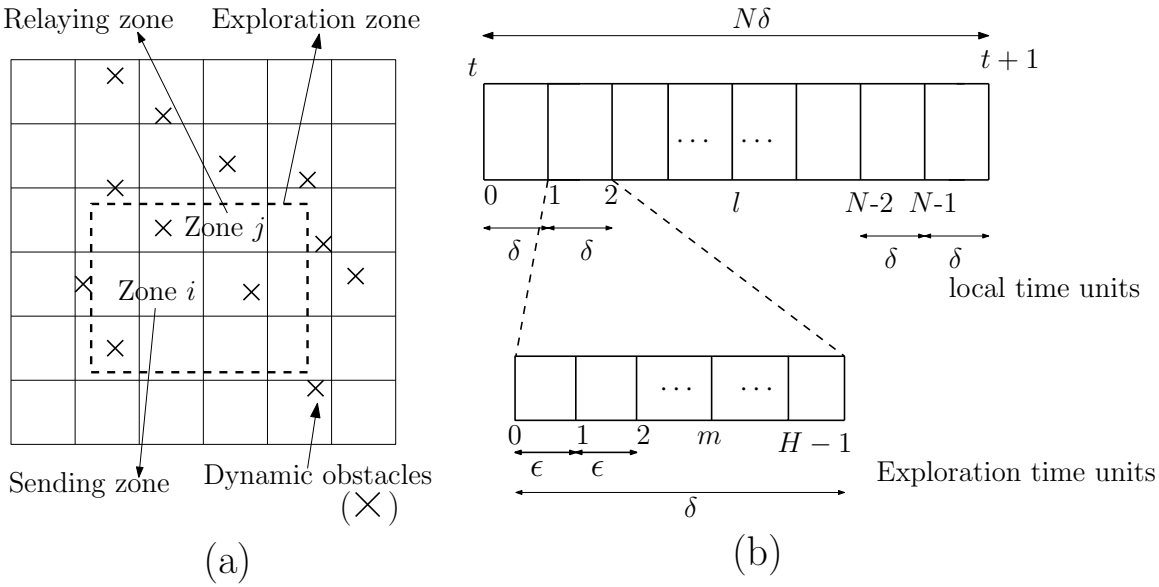

Figure 7.1: (a) Service region divided into zones along with dynamic obstacles. (b) Discretized time slots with exploration time unit.

mmWave channels using directional antennas. The received signal strength (Q_{ij}^l) at time l on zone j from zone i is modeled as [34]:

$$Q_{ij}^l = \psi \cdot P_i^l \cdot G_t \cdot G_r \cdot PL_{ij}^l \tag{7.1.1}$$

where, ψ is the shadowing random variable, P_i^l is the transmit power of the UE in zone i at instant l, G_t & G_r are transmit and receive beam-forming gains respectively. PL_{ij}^l is the distance dependent path loss function between zone i and zone j.

Exploration: When the current link quality is not good enough then source UE locally explores for an appropriate relaying UE from given viable set. One of the basic procedure in the exploration phase involves sequentially searching space in all directions to align transmitter and receiver beams (beam alignment). The quality of link is piggy-back to the sending UE. This overall process of beam alignment is termed as the exploration phase.

Any of the state of art approaches mentioned in [18] can be applied for the exploration phase. We have considered an abstraction of this phase and thus it is considered as a black box. It is assumed that the beams are perfectly aligned after the exploration phase and thus we focus on the effects of dynamic obstacle's blockage on a given D2D link. This exploration by source UE in zone i is done for UEs belonging only in the set $\mathbb{U}^i$ to find out the best relaying zone for that time instant. Note that the UE is using directional mmWave antennas for exploring the neighbors and hence explorations cause some significant delay. Each exploration time duration is denoted by $\epsilon < \delta$ as shown in figure 7.1(b). In a given duration δ, we can perform a number of explorations. Each of the time instants during exploration time of duration ϵ is denoted by $m \in \{0, 1, \cdots, H-1\}$, where $H = \lfloor \delta/\epsilon \rfloor$. The overall exploration time is bounded by the maximum value M which can be more than H. It is assumed that once exploration is complete, switching takes negligible time.

There are static and dynamic obstacles in the service region. There is *no* external facility like radars or vision cameras available at BS to track them. The behavior of dynamic obstacles are not known a priori and need to be learned from the received ACKs of probe packets during exploration phase in an online fashion. Since mmWaves are highly susceptible to obstacles and suffer from severe penetration losses, we assume that even a single moving or static obstacle may break an already established D2D link and can cause packet loss.

7.2 Problem Formulation as POMDP

Zone i containing source UE forms a link with an UE (relay or destination) of some other zone $j \in \mathbb{U}^i$. Global decision for the best relay is given by the BS at the time instant t to relay data packet till $t+1$ time instant. The quality of link given by the BS may deteriorate due to presence of dynamic obstacles resulting in link outage and a new relay link needs to be explored from the viable set $\mathbb{U}^i$ locally. A newly found relay link might provide very good data rate initially during exploration phase, but it may gradually deteriorate in future data transmission time because of dynamic obstacles. This problem is subtle due to the fact that exploration time is very small (ranging from few microseconds to 10 ms [15]) in contrast to the data transmission time which is in order of seconds (usually 100-1000 times more than search time). The main idea is to reduce the E2E delay on the cost of sending additional probe packets till decision of whether selecting or not selecting a given relay for data transmission considering dynamic obstacles can be learned. This process is limited upto maximum M exploration time units where each exploration time duration is of ϵ time. If the given relay is not selected within this time then the exploration process again starts for another possible relaying UE in a zone belonging to $\mathbb{U}^i$.

We model this problem of relay selection during exploration as that of POMDP considering uncertainty in relay link quality. We will define the POMDP as follows: For all the possible links $j \in \mathbb{U}^i$, the state is written as $y_m^j \in \{0, 1\}$ for exploration time instant m.

Values 1 and 0 signify if relay link j is in a good or a bad state respectively. Good and bad notion denotes that whether the given link will be formed successfully or not respectively. State represented by G and $\overline{G}$ respectively denote the good and bad state as shown in figure 7.2. The action set is defined as {do not select relay link, select relay link, decision cannot be made thus continue sending probe packets}. The first action signifies that the current link is bad, hence stop exploring it and start a new exploration. The second action signifies that the current link being explored is of good quality, hence choose it for data transmission. The third action signifies that the decision of relay selection cannot be made and exploration should continue for another ϵ unit of time to learn the relay link quality. The action is denoted by a_m^j for link j at time instant m. The link quality is observed by the ACKs of the received probe packet signal. The ACK test for link j at time m is denoted as $w_m^j \in \{0, 1\}$ for a given state y_m^j and action a_m^j, may also be uncertain due to the unpredictable channel condition. In figure 7.2, A and $\overline{A}$ denotes whether ACKs are received successfully or not respectively.

Figure 7.2 represents the probabilistic structure of the problem as shown below.

$$P(w_m^j = 1|y_m^j = 1) = k; P(w_m^j = 0|y_m^j = 1) = 1 - k$$

$$P(w_m^j = 1|y_m^j = 0) = g; P(w_m^j = 0|y_m^j = 0) = 1 - g$$

However, note that the ACK piggyback in current time instant will show quality of the channel for probe packet sent in previous time instant. Hence a transition probability of g is introduced above. The probabilistic structure assumed for the system state transition is given below. We have assumed that $q > s$ and $k > g$ which signify respectively that the probability of a link becoming good from previous good state is higher than that of previous bad state and probability of successful ACK from good state is higher than that of bad state.

$$P(y_{m+1}^j = 1|y_m^j = 1) = q; P(y_{m+1}^j = 0|y_m^j = 1) = 1 - q$$

$$P(y_{m+1}^j = 1|y_m^j = 0) = s; P(y_{m+1}^j = 0|y_m^j = 0) = 1 - s$$

For a given relaying zone j, let us define the information vector available locally to the

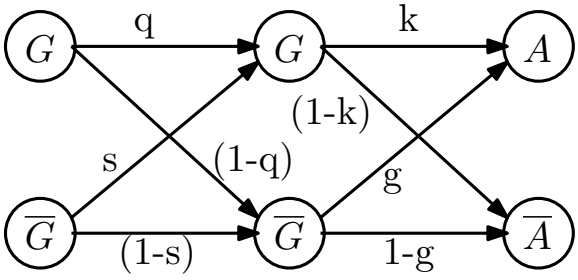

Figure 7.2: Probabilistic structure of the exploration problem at a UE locally.

zone i till time instant m as $\mathbb{H}_m^j = (w_0^j, w_1^j, \cdots, w_m^j)$. The sufficient statistics or belief [44] (chapter 5) for this problem is defined locally for a relaying zone j as:

$$b_m^j = P(y_m^j = 1 | \mathbb{H}_m^j) \tag{7.2.1}$$

This equation gives the probability that a relaying link/zone is in good state given the previous history of information. The estimator function for the local system can be defined as:

$$b_{m+1}^j = \Phi'(b_m^j, w_{m+1}^j). \tag{7.2.2}$$

Using Baye's rule we get,

$$b_{m+1}^j = \begin{cases} \frac{(qb_m^j + (1-b_m^j)s)k}{(qb_m^j + (1-b_m^j)s)k + (b_m^j(1-q) + (1-b_m^j)(1-s))g}, & \text{if } w_{m+1}^j = 1 \\ \frac{(qb_m^j + (1-b_m^j)s)(1-k)}{(qb_m^j + (1-b_m^j)s)(1-k) + (b_m^j(1-q) + (1-b_m^j)(1-s))(1-g)}, & \text{if } w_{m+1}^j = 0 \end{cases} \tag{7.2.3}$$

Cost structure: The cost for stopping the exploration for both cases when link cannot be and can be formed is 0. However, if the link which seems to be good and selected, may become bad in upcoming time instants and thus causes packet loss. So it will incur D_2 cost to compensate for the packet loss. Similarly, the link which was bad and not selected could have been a good relay link in upcoming time instants. Then it will incur some cost D_1 in order to compensate for further exploration. If decision of relay selection cannot be made in current time instant, then probe packets are sent for another ϵ time unit to continue the exploration. The cost incurred here is c_ϵ. This will go on till time M which is the upper bound on the exploration time for a single link. The objective is to derive a decision criterion, whether to select or not select the given relay link, or if this decision cannot be made then continue learning the current relay link quality. The expected cost is formulated as a dynamic program. At the end of the $(M-1)th$ period, the expected cost is:

$$J_{M-1}^j(b) = \min\{bD_1, (1-b)D_2\} \tag{7.2.4}$$

where b is a variable denoting belief. For the time instant $m = M-2$, we have,

$$J_{M-2}^j(b) = \min\{bD_1, (1-b)D_2, c_\epsilon + \mathbb{E}[J_{M-1}^j(b)] \tag{7.2.5}$$

where $\mathbb{E}[\cdot]$ is the mathematical expectation over the observations. Here the first term in minimization expression denotes the expected cost $(bD_1 + (1-b)0)$ incurred when the learning of the current link being explored is stopped since it was in the bad state. The second term denotes the expected cost for selecting the current relay link being explored. The third cost is the expected cost for continuing exploring the current relay link for another

round of ϵ unit of time. We can write a general expression as:

$$J_m^j(b) = \min\{bD_1, (1-b)D_2, c_\epsilon + \mathbb{E}[J_{m+1}^j(\Phi'(b,w))]\} \tag{7.2.6}$$

where $w \in \{0,1\}$ is a variable denoting ACKs failure/success. Note that the notation w_m^j defined earlier denotes the ACK failure/success of link j at time instant m, whereas w is used to denote a general variable for ACK failure/success. We will derive the optimal policy for this problem in section 7.3.

7.3 Derivation of the Optimal Policy in Exploration Phase

Properties of $J_m^j(b)$

The general expression for time instant m as mentioned in equation (7.2.6), can be written equivalently as:

$$J_m^j(b) = \min\{bD_1, (1-b)D_2, A_m^j(b)\} \tag{7.3.1}$$

where,

$$A_m^j(b) = c_\epsilon + P(w=1|b)J_{m+1}^j(\Phi'(b,1)) + P(w=0|b)J_{m+1}^j(\Phi'(b,0)) \tag{7.3.2}$$

For notation simplicity we will now remove the superscript j from each of the respective notations, e.g., we will write $A_m^j()$ as $A_m()$. Hence $A_m^j(b)$ can now be denoted as $A_m(b)$. Now equation (7.3.2) can be further reduced as:

$$\begin{aligned} A_m(b) = c_\epsilon + & \\ & \big((qb + (1-b)s)k + (b(1-q) + (1-b)(1-s))g\big)J_{m+1}(\Phi'(b,1)) + \\ & \big(1 - \big((qb + (1-b)s)k + (b(1-q) + (1-b)(1-s))g\big)\big)J_{m+1}(\Phi'(b,0)) \end{aligned} \tag{7.3.3}$$

The expected cost for the base case at the end of $(M-1)th$ period is mentioned in equation (7.2.4). We now show some of the properties of $A_m(b)$.

Proposition 7.3.1. *$A_m(b)$ is piece-wise linear and concave in b.*

Proof. We will prove this by first showing that $J_m(b)$ is piece-wise linear and concave for each m using induction. Then we prove our proposition. For time instant $(M-1)$, we have,

$$J_{M-1}(b) = \min\{bD_1, (1-b)D_2\}$$

which is piece-wise linear and concave. For time instant $(M-2)$, we have,

$$J_{M-2}(b) = \min\{bD_1, (1-b)D_2, A_{M-2}(b)\}$$

where,

$$A_{M-2}(b) = c_\epsilon + \min\big\{\big(qb + s(1-b)\big)kD_1, \big(b(1-q) + (1-s)(1-b)\big)gD_2\big\} + \min\big\{\big(qb + s(1-b)\big)\big(1-k\big)D_1, \big(b(1-q) + (1-s)(1-b)\big)\big(1-g\big)D_2\big\}.$$

This overall equation is also piece-wise linear and concave.

Assuming $J_{m+1}(b)$ is piece-wise linear and concave in b, we can say that for some suitable scalars, $\eta_1, \eta_2, \cdots, \eta_n$ and $\beta_1, \beta_2, \cdots, \beta_n$, $J_{m+1}(b)$ can be written as:

$$J_{m+1}(b) = \min\{\eta_1 + \beta_1 b, \eta_2 + \beta_2 b, \cdots, \eta_n + \beta_n b\}. \tag{7.3.4}$$

We can write,

$$J_m(b) = \min\{bD_1, (1-b)D_2, A_m(b)\}.$$

Expanding above using equation (7.3.3), we get:

$$J_m(b) = \min\Bigg\{bD_1, \big(1-b\big)D_2, c_\epsilon + \Big(\big(bq + (1-b)s\big)k + \big(b(1-q) + (1-b)(1-s)\big)g\Big) \times J_{m+1}\Bigg(\frac{\big(bq + (1-b)s\big)k}{\big(bq + (1-b)s\big)k + \big(b(1-q) + (1-b)(1-s)\big)g}\Bigg) + \Big(1 - \big((bq + (1-b)s)k + (b(1-q) + (1-b)(1-s))g\big)\Big) \times J_{m+1}\Bigg(\frac{\big(bq + (1-b)s\big)\big(1-k\big)}{\big(1 - ((bq + (1-b)s)k + (b(1-q) + (1-b)(1-s))g)\big)}\Bigg)\Bigg\}. \tag{7.3.5}$$

Let us substitute Y for $((bq + (1-b)s)k + (b(1-q) + (1-b)(1-s))g)$ to simplify the

calculations. Now using equation (7.3.4), the equation (7.3.5) is reduced as:

$$\begin{aligned}J_m(b)=\min\Big\{&bD_1,(1-b)D_2,c_\epsilon+\\&Y\min\big\{\eta_1+\beta_1\frac{(qb+s(1-b))k}{Y},\\&\eta_2+\beta_2\frac{(qb+s(1-b))k}{Y},\cdots,\eta_n+\beta_n\frac{(qb+s(1-b))k}{Y}\big\}+\\&(1-Y)\min\big\{\eta_1+\beta_1\frac{(qb+s(1-b))(1-k)}{(1-Y)},\eta_2+\\&\beta_2\frac{(qb+s(1-b))(1-k)}{(1-Y)},\cdots,\\&\eta_n+\beta_n\frac{(qb+s(1-b))(1-k)}{(1-Y)}\big\}\Big\}\end{aligned}\tag{7.3.6}$$

We can further reduce above equation as:

$$\begin{aligned}J_m(b)=\min\big\{&bD_1,(1-b)D_2,c_\epsilon+\min\{(Y)\eta_1+\\&\beta_1(qb+s(1-b))k,(Y)\eta_2+\beta_2(qb+s(1-b))k,\cdots,\\&(Y)\eta_n+\beta_n(qb+s(1-b))k\}+\min\{(1-Y)\eta_1+\\&\beta_1(qb+s(1-b))(1-k),(1-Y)\eta_2+\beta_2(qb+s(1-b))(1-k),\\&\cdots,(1-Y)\eta_n+\beta_n(qb+s(1-b))(1-k)\}\big\}\end{aligned}\tag{7.3.7}$$

This is again piece-wise linear and concave in b. Thus the induction is complete.

Now we will show that $A_m(b)$ is also piece-wise linear and concave in b:

$$A_m(b)=c_\epsilon+(Y)J_{m+1}(\Phi'(b,1))+(1-Y)J_{m+1}(\Phi'(b,0))\tag{7.3.8}$$

The first term c_ϵ is constant. For the next two terms $(Y)J_{m+1}(\Phi'(b,1))$ and $(1-Y)J_{m+1}(\Phi'(b,0))$, by expanding them using equation (7.3.4), we get,

$$\begin{aligned}&(Y)J_{m+1}(\Phi'(b,1))+(1-Y)J_{m+1}(\Phi'(b,0))=\\&(Y)\min\Big\{\eta_1+\beta_1\frac{(qb+s(1-b))k}{Y},\eta_2+\beta_2\frac{(qb+s(1-b))k}{Y},\\&\cdots,\eta_n+\beta_n\frac{(qb+s(1-b))k}{Y}\Big\}+(1-Y)\min\Big\{\eta_1+\\&\beta_1\frac{(qb+s(1-b))(1-k)}{1-Y},\eta_2+\beta_2\frac{(qb+s(1-b))(1-k)}{1-Y},\\&\cdots,\eta_n+\beta_n\frac{(qb+s(1-b))(1-k)}{1-Y}\Big\}\end{aligned}\tag{7.3.9}$$

We can reduce above to:

$$\begin{aligned}(Y)J_{m+1}(\Phi'(b,1)) + (1-Y)J_{m+1}(\Phi'(b,0)) = \\ \min\big\{\eta_1(Y) + \beta_1(qb+s(1-b))k, \eta_2(Y) + \beta_2(qb+s(1-b))k, \cdots, \\ \eta_n(Y) + \beta_n(qb+s(1-b))(1-k)\big\} + \min\big\{\eta_1(1-Y) + \\ \beta_1(qb+s(1-b))(1-k), \eta_2(1-Y) + \beta_2(qb+s(1-b))(1-k), \cdots, \\ \eta_n(1-Y) + \beta_n(qb+s(1-b))(1-k)\big\}. \quad (7.3.10)\end{aligned}$$

Since minimum of finite number of concave function is concave, $A_m(b)$ is piece-wise linear and concave in b. □

Proposition 7.3.2. *$\forall b \in [0,1]$,*

$$A_{m-1}(b) \leq A_m(b) \leq A_{m+1}(b)$$

Proof. We will first prove $J_m(b) \geq J_{m+1}(b)$, then we will use this to prove $A_m(b) \geq A_{m+1}(b)$. First we start for base case $m = M-1$ and the first term in recursion $m = M-2$:

$$J_{M-1}(b) = \min\{bD_1, (1-b)D_2\}$$

and

$$J_{M-2}(b) = \min\{bD_1, (1-b)D_2, A_{M-2}(b)\}$$

respectively. We can easily see that $J_{M-1}(b) \geq J_{M-2}(b)$. We now prove it for first two terms of the recursion $J_{M-2}(b)$ and $J_{M-3}(b)$. Let's denote $Y = (bq + (1-b)s)k + (b(1-q) + (1-b)(1-s))g$, we can write $J_{M-3}(b)$ as:

$$\begin{aligned}J_{M-3}(b) &= \min\{bD_1, (1-b)D_2, c_\epsilon + (Y)J_{M-2}(\Phi'(b,1)) + \\ &\qquad (1-Y)J_{M-2}(\Phi'(b,0))\} \\ &\leq \min\{bD_1, (1-b)D_2, c_\epsilon + (Y)J_{M-1}(\Phi'(b,1)) + \\ &\qquad (1-Y)J_{M-1}(\Phi'(b,0))\} \\ &= J_{M-2}(b)\end{aligned}$$

Hence $J_{M-2}(b) \geq J_{M-3}(b)$. Similarly it proceeds for other m and hence $J_{m+1}(b) \geq J_m(b)$. Now let us see this for $A_m(b)$ using previous proof for $J_m(b)$:

$$\begin{aligned}A_m(b) &= c_\epsilon + (Y)J_{m+1}(\Phi'(b,0)) + (1-Y)J_{m+1}(\Phi'(b,0)) && (7.3.11)\\ &\leq c_\epsilon + (Y)J_{m+2}(\Phi'(b,0)) + ((1-Y)J_{m+2}(\Phi'(b,0)) && (7.3.12)\\ &= A_{m+1}(b) && (7.3.13)\end{aligned}$$

Hence $A_{m+1}(b) \geq A_m(b)$.

□

Policy Structure

The structure of an optimal policy for our POMDP problem is provided in the following theorem.

Theorem 7.3.1. *The optimal policy for exploration in POMDP problem is a threshold policy. At any time instant $m \in \{0, 1, \cdots, M-1\}$, the optimal action is to stop exploration on current relay link and start exploring other relay links from $\mathbb{U}^i$ if $b_m \leq \alpha_m$, or stop exploration on current relay link and choose it for data transmission if $b_m \geq \beta_m$, otherwise continue sending probe packet once more on the current relay link which is being explored to check the link quality if $\alpha_m < b_m < \beta_m$. Here α_m, β_m are appropriate constants. Also, we can say for the thresholds: $\cdots \geq \alpha_m \geq \alpha_{m-1} \geq \cdots \geq \alpha_1$ and similarly $\cdots \leq \beta_m \leq \beta_{m-1} \leq \cdots \leq \beta_1$.*

Proof. For the last time period $M-1$, there exists $\rho = \frac{D_2}{D_1+D_2}$ such that stop exploration on current link and start exploring other links from $\mathbb{U}^i$ if $b < \rho$, otherwise stop exploration on current link and choose it for data transmission if $b \geq \rho$. At ρ, $J_{M-1}(\rho)$ attains it maximum value of $\frac{D_2D_1}{D_1+D_2}$.

For general time instants m, we can say that $A_m(0) > c_\epsilon$ and $A_m(1) > c_\epsilon$. Using this fact, proposition 7.3.1 and proposition 7.3.2, we can say that if for some b', $A_{M-2}(b') < \frac{D_2D_1}{D_1+D_2}$, then $A_{M-2}(b)$ and subsequent $A_m(b)$ will intersect $\min\{bD_1, (1-b)D_2\}$ at two points. Hence we can say that for general time instant m we will get an optimal policy as: stop exploration on current link and start exploring other links from $\mathbb{U}^i$ if $b_m \leq \alpha_m$, or stop exploration on current link and choose it for data transmission if $b_m \geq \beta_m$, otherwise continue sending probe packet once more on the current link which is being explored to check the link quality if $\alpha_m < b_m < \beta_m$. Here α_m and β_m are found by satisfying the corresponding equations: $\alpha_m D_1 = A_m(\alpha_m)$ and $(1-\beta_m)D_2 = A_m(\beta_m)$.

If for all b', $A_{M-2}(b') > \frac{D_2D_1}{D_1+D_2}$, then terms bD_1 and $(1-b)D_2$ will contribute to the single threshold ρ which is trivial for time instant $M-2$ due to proposition 7.3.1. In this case, using proposition 7.3.1 and proposition 7.3.2 one can have either single or two thresholds for other time instants m depending upon whether $A_m(b)$ intersects $\min\{bD_1, (1-b)D_2\}$ at two or no points as shown in figure below.

For the second part, using proposition 7.3.2 and if $A_{M-2}(\rho) < \frac{D_2D_1}{D_1+D_2}$, we can say that $\alpha_{M-2} < \rho < \beta_{M-2}$. This is easy to see because $J_{M-1}(b)$ first increases till ρ and then decreases. Also,

$$J_{M-1}(b) \geq J_{M-2}(b) = \min\{J_{M-1}(b), A_{M-2}(b)\}$$

and $\alpha_{M-1} = \beta_{M-1} = \rho$. Hence, $\alpha_{M-2} \leq \alpha_{M-1}$ and $\beta_{M-1} \leq \beta_{M-2}$. Similarly, using proposition 7.3.2 we can say this for other instants m that $\alpha_m \leq \alpha_{m+1}$ and $\beta_m \geq \beta_{m+1}$.

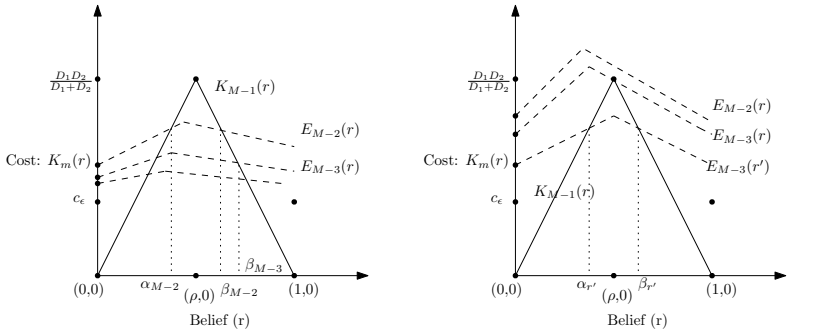

(a) Cost structure when $E_{M-2}(r) < \frac{D_1D_2}{D_1+D_2}$

(b) Cost structure when $E_{M-2}(r) > \frac{D_1D_2}{D_1+D_2}$

Figure 7.3: Cost structure of the problem for two cases.

Hence we can say that with respect to m:

$$\cdots \geq \alpha_m \geq \alpha_{m-1} \geq \cdots \geq \alpha_1$$

and similarly

$$\cdots \leq \beta_m \leq \beta_{m-1} \leq \cdots \leq \beta_1.$$

□

Using above result, we can say as $m \to \infty$, α_m and β_m converges to some scalar $\overline{\alpha}$ and $\overline{\beta}$ respectively. This is because β_m is bounded below and α_m is bounded above. Hence, for very large horizon length M, the optimal policy can be approximated by a stationary threshold policy with a time-invariant threshold $\overline{\alpha}$ and $\overline{\beta}$. In this case we can say that at time instant m, if $b_m \leq \overline{\alpha}$ then stop exploration on current link and start exploring other links from $\mathbb{U}^i$, if $b_m \geq \overline{\beta}$ then stop exploration on current link and choose it for data transmission, otherwise if $\overline{\alpha} < b_m < \overline{\beta}$ then continue sending probe packet once more on the current link which is being explored to check the link quality.

It is easy to check that $\Phi(b, w)$ is a non-decreasing function in b. Let us denote b_0 as the prior belief. We can say that, when prior belief satisfies $b_0 > \Phi(b_0, w) = b_1$, then $b_2 = \Phi(b_1, 0) < \Phi(b_0, 0) = b_1$ and $b_2 = \Phi(b_1, 1) < \Phi(b_0, 1) = b_1$. Proceeding in this way, we can show that b_m strictly decreases with m whenever we observe several successive ACK failures/successes. Similarly, when the prior belief satisfies $b_0 < \Phi(b_0, w) = b_1$, then we can say that $b_2 = \Phi(b_1, 0) > \Phi(b_0, 0) = b_1$ and $b_2 = \Phi(b_1, 1) > \Phi(b_0, 1) = b_1$. Proceeding in this way, we can show that b_m strictly increases with m whenever we observe several successive ACK failures/successes. For getting x successive ACK failures, we can define recursively a probability π_x as: $\pi_1 = \Phi(b_0, \overline{A})$, $\pi_2 = \Phi(\pi_1, \overline{A})$, $\cdots$, $\pi_x = \Phi(\pi_{x-1}, \overline{A})$ with $\pi_0 = b_0$. Similarly, for getting x successive ACK successes, we can define recursively a probability π'_x as: $\pi'_1 = \Phi(b_0, A)$, $\pi'_2 = \Phi(\pi'_1, A)$, $\cdots$, $\pi'_x = \Phi(\pi'_{x-1}, A)$ with $\pi'_0 = b_0$. Let c and d be the smallest integer such that $\pi_c \leq \overline{\alpha}$ and $\pi'_d \geq \overline{\beta}$ respectively. We can further simplify the stationary threshold policy as follows.

Corollary 7.3.1. *Using theorem 7.3.1, we can simplify the optimal policy further as follows. Let c and d be the smallest integer such that $\pi_c \leq \overline{\alpha}$ and $\pi'_d \geq \overline{\beta}$ respectively. If there are c successive ACK failures, stop exploring on current relay link being explored and start exploring some other relay link. If there are d successive ACK successes, stop exploring on current relay link being explored and choose it for data transmission. Otherwise, decision cannot be made and more probe packets are needed to be sent to learn the link quality.*

7.4 Simulation and Results

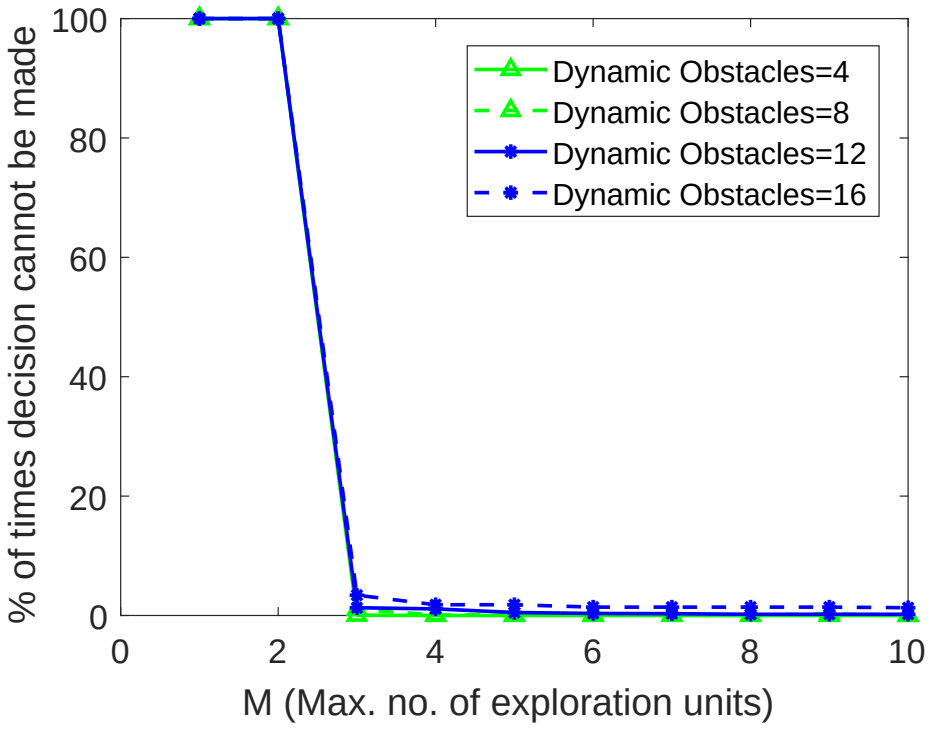

Figure 7.4: M vs % of times no decision can be made

Service region of dimension 100 $m \times 100$ m is divided into grid zones each of dimension 10 $m \times 10$ m. We have taken $\delta = 100$ ms and $\epsilon = 1$ ms. UEs are using directional transmitter and receiver antennas for 60 GHz frequency with $G_r = G_t = 6$ dB. LOS path loss exponent is 2.5 and zero mean log-normal shadowing random variable with standard deviation 3.5 [10, 106]. Thermal noise density is -174 dBm/Hz and devices are using 24 dBm transmit power. Capacity of each link (i, j) is $B \log_2(1 + S_{ij})$ $bits/sec$, where $B = 20$ MHz [102] is bandwidth and S_{ij} is the received signal to noise ratio. The packet length is fixed and of size 65535 *bytes*. A source UE in a grid zone i can transmit data to a maximum of 24 grids surrounding it ($|\mathbb{U}^i| \leq 24$). There are maximum of 16 static and D dynamic obstacles present in these 24 grids surrounding the source UE, where $D \in \{0, 4, 8, 12, 16\}$. Each static obstacle is placed uniformly in the service region. Each dynamic obstacles is moving

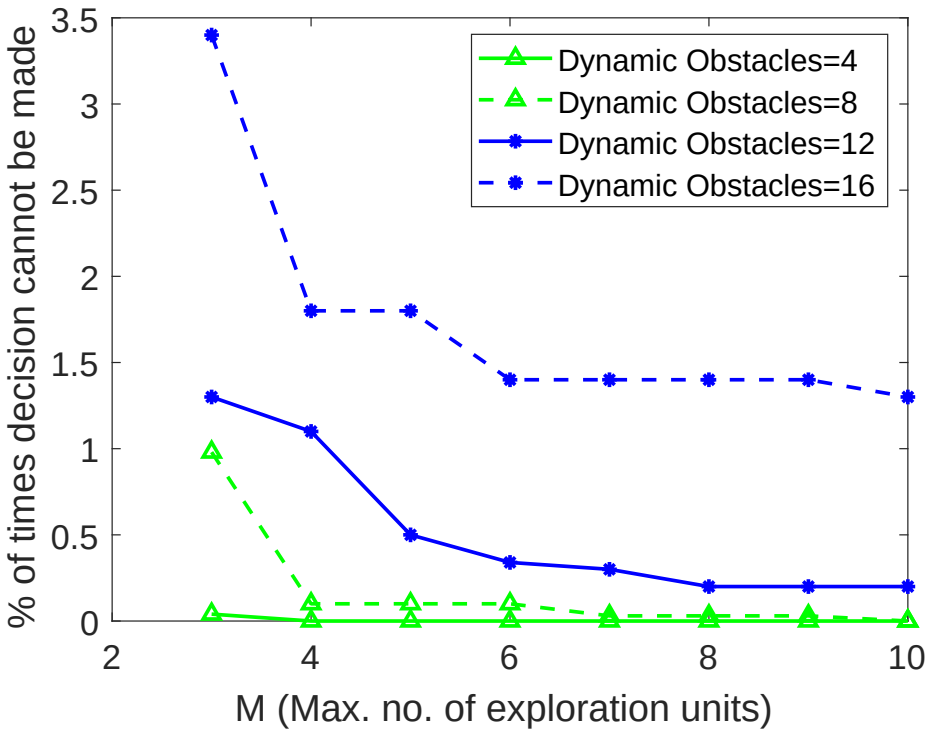

Figure 7.5: M vs % of times no decision can be made when $M \geq 3$

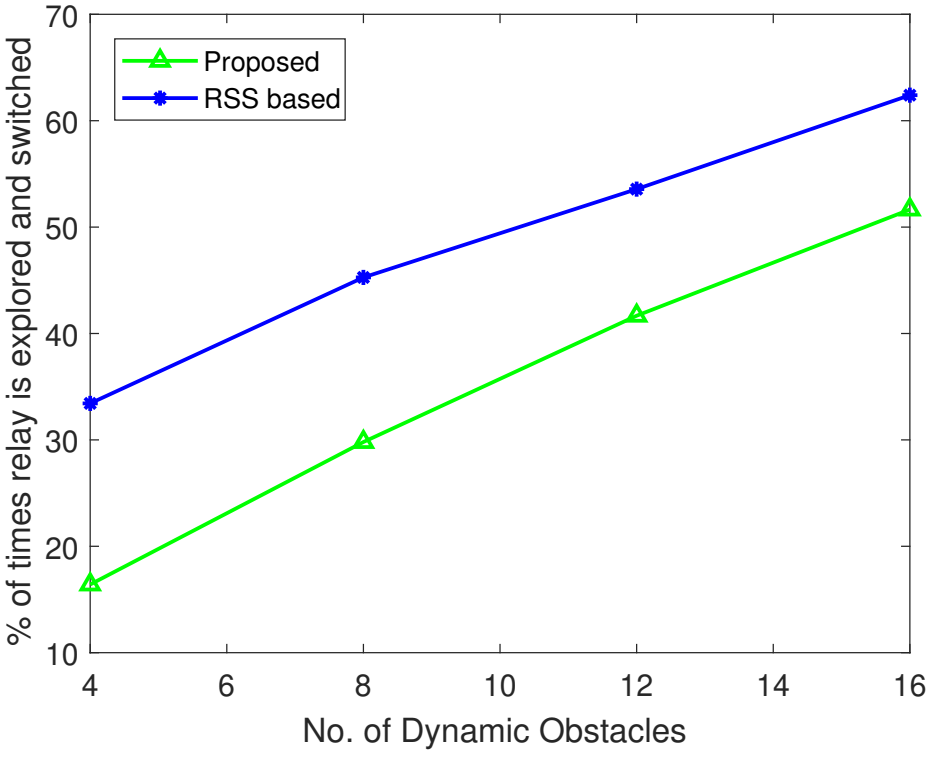

Figure 7.6: No. of times relay are explored and switched with dynamic obstacles.

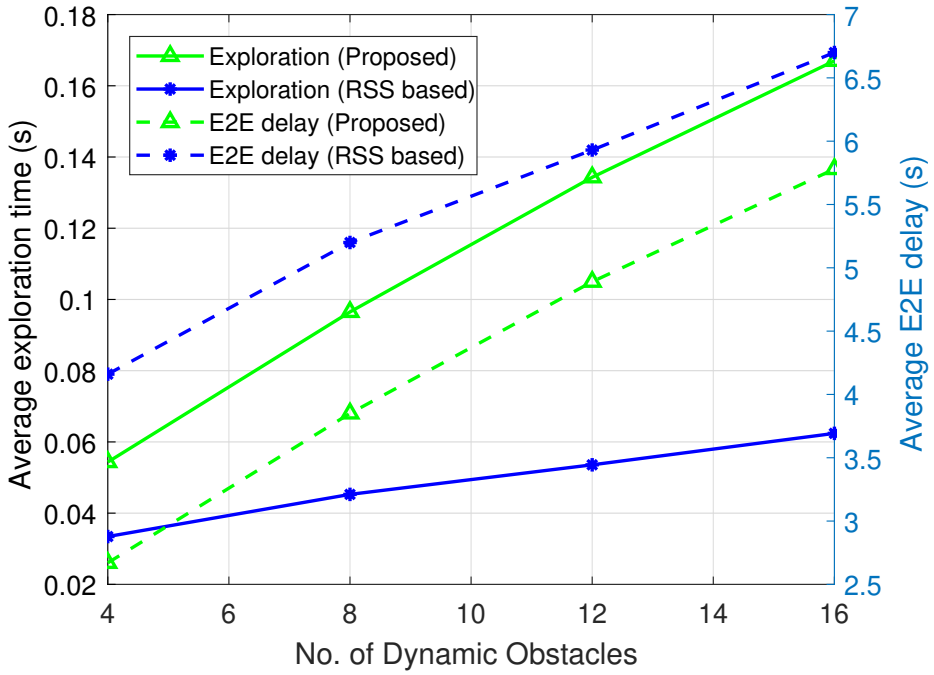

Figure 7.7: Trade-off for average exploration time and average E2E delay.

randomly and independently of each other and following a simple blockage model such that with probability 0.5 it will block a given link otherwise it will not block the link. A single source-destination pair is assumed for simplicity and all other devices in a given zone may act as relay. We have written our own C++ custom code and run them on a `GNU` 4.8 compiler on Intel core $i7$ machine and average of 1000 runs are taken. The average exploration time and E2E delay for sending 100 packets are the main parameters considered. We have compared our results with the received signal strength (`RSS Based`) approach which is most commonly used for relay selection during exploration after transmitter and receiver beams are perfectly aligned.

Value of M is derived experimentally in figure 7.4. This value should not be too small, otherwise there won't be sufficient exploration to lead to a decision. Also M should not be too big, otherwise a lot of time would be wasted in exploration. Figure 7.4 shows the percentage of time the decision could not be made on varying values of M for different D. It is clear that for almost all values of D, decision cannot be made when M is 1 and 2. For $D = 16$ and $M = 3$, for around 3.5% of cases decision cannot be made a shown in figure 7.5. This figure shows that with dynamic obstacles, no. of times the decision of relay selection cannot be made, also increases. We have chosen $M = 4$ for performing further simulations.

Figure 7.6 shows the effect of dynamic obstacles on percentage of times new relays are explored and switched. With dynamic obstacles, the probability of link breakage increases and thus number of times new relays are explored and switched also increases. Our approach outperforms the RSS based approach because it chooses the link by learning dynamic obsta-

cle's presence while RSS based approach greedily chooses a link based on best RSS values which might have higher chance of blockage. Figure 7.7 shows following results: first with dynamic obstacles, average E2E delay is increased which follows from previous result of figure 7.6. Since higher number of dynamic obstacles will have higher chance of breaking a link and thus causes increase in E2E delay. Similarly, following the argument of previous result of figure 7.6, our approach outperforms RSS based approach. Secondly, with dynamic obstacles, average exploration time is increased because higher link breakage with dynamic obstacles would cause more exploration and switching of relays. Here RSS based approach performs better since it always takes one time unit of exploration, whereas our approach takes additional exploration time units to learn the quality of link considering dynamic obstacles. Thirdly, it can be seen from above two results that, average exploration time is higher in our approach at the cost of reducing the cost of average E2E delay significantly compared to the RSS based approach. This describes the trade-off of additional exploration time over the average E2E delay.

7.5 Conclusion

The problem of selecting a given relay during exploration is investigated taking into account presence of dynamic obstacles. We have modeled this problem as a finite horizon POMDP framework at each UE. Using this model, an optimal threshold policy is derived for each UE which is then simplified to a stationary policy. This policy governs the source UE to take decisions based on successive ACK failures or success on the current relay link under exploration. Through simulations, the trade-off between average exploration time and E2E delay is shown, where our approach captures the effects of dynamic obstacles significantly compared to the RSS based approach.

Chapter 8

Conclusion and Future Directions

In this thesis, we have looked into the relay selection problem in D2D communication. We first considered the mobility of UEs which brings uncertainty in network parameters which in turn may lead to exponential performance degradation of the network. In order to capture the mobility of UEs we develop a SIP model which is later reduced to equivalent deterministic MINLP model whose hardness result is proved. We then utilized the constraints of the developed MINLP model to derive a greedy metric which is computed locally, hence utilising the distributed nature of D2D link quality. The metric efficiently captures the variations in the SINR of D2D link due to mobility of UEs. *Perceived graph* is constructed using the greedy metric which is then used to develop both network assisted and operator control algorithms for data transmission. Then, while selecting a relay, we considered the problem of the presence of dynamic obstacles which may cause unprecedented outage of D2D links since mmWaves are suffers from severe penetration losses and hence susceptible to blockage from obstacles. In this case too, we considered both network assisted and device controlled scenarios. We developed probabilistic model in network assisted scenario where geometry was used to analyse the blockage probability of dynamic obstacles considering both cases when the orientation of dynamic obstacles are known as well as *unknown*. Using the analysis we devised relay selection algorithms. For the device controlled scenario, the first problem was to decide locally at each UE, whether i) to stop communication on the current relay link and go for exploration of some other new relay link, or ii) to continue the communication on the current relay link itself, in case packet loss occurs considering the fact that exploration phase has significant delay overhead. The second problem was to ensure that the newly selected relay link during exploration is free from dynamic obstacles in near future during *local* time instants if it is chosen for data transmission. This follows after the decision in earlier problem was "to stop communication on the current relay link and go for exploration of some other new relay link". Here we want to minimize the frequent relay switching of newly explored relays, otherwise it would cost significant delay overhead. Here we are considering the fact that those newly explored relay links are to be chosen during the exploration phase which minimizes the packet loss and in turn delay due to blockage from

dynamic obstacles on the D2D relay link under exploration. For the second problem also, the UE has to locally make the decision: whether i) to discard the relay link under exploration and go for exploration of some other new relay link, or ii) to choose the current link under exploration for data transmission, or iii) to send more probe packets as a decision cannot be made and go for exploring that same relay for further exploration time units. For both of these problems, we modeled the uncertainty caused due to presence of dynamic obstacles in a given mmWave D2D link using the POMDP framework locally at the UEs. The link quality is observed using the information of ACKs which themselves are vulnerable to blockage. Optimal threshold policy is derived for both of these problems. Later, we gave easy to use stationary policies, which is based on counting number of successive ACK successes or ACK failures to arrive at a decision.

We found through simulations that dynamic obstacles have significant effects on a given relay link in terms of blockages. Hence their effects are required to be captured while selecting a relay. We demonstrated that our relay selection algorithms captures the presence of obstacles effectively and hence incorporate their effects on D2D relay links appropriately. Our algorithms outperform various other classical and state of the art approaches.

For future directions related to our thesis, we are thinking of further working on these major topics:

- To devise a relay selection algorithm for the case where the orientation in motion for both UEs and dynamic obstacles are *unknown*, by leveraging the ideas presented in Chapters 4 and 5
- To further study the *Perceived graph* for the underlay scenario of D2D communication which takes into account the interference from cellular users as well.
- Also, the *Perceived graph* can be further utilized to arrive on devising some channel allocation strategies, especially in unlicensed band, as it inherently takes into account the interference caused due to neighbouring nodes communicating on the same channel.

Bibliography

[1] Mohsen Nader Tehrani, Murat Uysal, and Halim Yanikomeroglu. Device-to-device communication in 5g cellular networks: challenges, solutions, and future directions. *IEEE Communications Magazine*, 52(5):86–92, 2014.

[2] Daquan Feng, Lu Lu, Yi Yuan-Wu, Geoffrey Ye Li, Shaoqian Li, and Gang Feng. Device-to-device communications in cellular networks. *IEEE Communications Magazine*, 52(4):49–55, 2014.

[3] J. Qiao, X. S. Shen, J. W. Mark, Q. Shen, Y. He, and L. Lei. Enabling device-to-device communications in millimeter-wave 5g cellular networks. *IEEE Communications Magazine*, 53(1):209–215, January 2015.

[4] M. Iwamura. NGMN view on 5G architecture. In *81st IEEE Vehicular Technology Conference*, pages 1–5, May 2015.

[5] Chih-Lin I, Corbett Rowell, Shuangfeng Han, Zhikun Xu, Gang Li, and Zhengang Pan. Toward green and soft: a 5G perspective. *IEEE Communications Magazine*, 52(2):66–73, 2014.

[6] G. Fodor, S. Parkvall, S. Sorrentino, P. Wallentin, Q. Lu, and N. Brahmi. Device-to-device communications for national security and public safety. *IEEE Access*, 2:1510–1520, 2014.

[7] Patrick Kwadwo Agyapong, Mikio Iwamura, Dirk Staehle, Wolfgang Kiess, and Anass Benjebbour. Design considerations for a 5G network architecture. *IEEE Communications Magazine*, 52(11):65–75, 2014.

[8] C. Hoymann, W. Chen, J. Montojo, A. Golitschek, C. Koutsimanis, and X. Shen. Relaying operation in 3gpp lte: challenges and solutions. *IEEE Communications Magazine*, 50(2):156–162, 2012.

[9] G. H. Sim, A. Loch, A. Asadi, V. Mancuso, and J. Widmer. 5g millimeter-wave and d2d symbiosis: 60 ghz for proximity-based services. *IEEE Wireless Communications*, 24(4):140–145, Aug 2017.

[10] N. Deng and M. Haenggi. A fine-grained analysis of millimeter-wave device-to-device networks. *IEEE Transactions on Communications*, 65(11):4940–4954, Nov 2017.

[11] H. Zhao, R. Mayzus, S. Sun, M. Samimi, J. K. Schulz, Y. Azar, K. Wang, G. N. Wong, F. Gutierrez, and T. S. Rappaport. 28 ghz millimeter wave cellular communication measurements for reflection and penetration loss in and around buildings in new york city. In *2013 IEEE International Conference on Communications (ICC)*, pages 5163–5167, June 2013.

[12] Z. Pi and F. Khan. An introduction to millimeter-wave mobile broadband systems. *IEEE Communications Magazine*, 49(6):101–107, June 2011.

[13] M. Gapeyenko, A. Samuylov, M. Gerasimenko, D. Moltchanov, S. Singh, M. R. Akdeniz, E. Aryafar, N. Himayat, S. Andreev, and Y. Koucheryavy. On the temporal effects of mobile blockers in urban millimeter-wave cellular scenarios. *IEEE Transactions on Vehicular Technology*, 66(11):10124–10138, 2017.

[14] Y. Koda, K. Nakashima, K. Yamamoto, T. Nishio, and M. Morikura. Handover management for mmwave networks with proactive performance prediction using camera images and deep reinforcement learning. *IEEE Transactions on Cognitive Communications and Networking*, 6(2):802–816, 2020.

[15] M. Giordani, M. Mezzavilla, and M. Zorzi. Initial access in 5g mmwave cellular networks. *IEEE Communications Magazine*, 54(11):40–47, 2016.

[16] H. Soleimani, R. Parada, S. Tomasin, and M. Zorzi. Fast initial access for mmwave 5g systems with hybrid beamforming using online statistics learning. *IEEE Communications Magazine*, 57(9):132–137, 2019.

[17] M. Zhang, M. Mezzavilla, R. Ford, S. Rangan, S. Panwar, E. Mellios, D. Kong, A. Nix, and M. Zorzi. Transport layer performance in 5g mmwave cellular. In *2016 IEEE Conference on Computer Communications Workshops (INFOCOM WKSHPS)*, pages 730–735, 2016.

[18] M. Giordani, M. Polese, A. Roy, D. Castor, and M. Zorzi. A tutorial on beam management for 3gpp nr at mmwave frequencies. *IEEE Communications Surveys Tutorials*, 21(1):173–196, 2019.

[19] Gábor Fodor, Erik Dahlman, Gunnar Mildh, Stefan Parkvall, Norbert Reider, György Miklós, and Zoltán Turányi. Design aspects of network assisted device-to-device communications. *IEEE Communications Magazine*, 50(3):170–177, 2012.

[20] Shanzhi Chen and Jian Zhao. The requirements, challenges, and technologies for 5g of terrestrial mobile telecommunication. *IEEE Communications Magazine*, 52(5):36–43, 2014.

[21] W. Lee, J. Kim, and S. W. Choi. New D2D peer discovery scheme based on spatial correlation of wireless channel. *IEEE Transactions on Vehicular Technology*, 65(12):10120–10125, Dec 2016.

[22] N. Bhushan, J. Li, D. Malladi, R. Gilmore, D. Brenner, A. Damnjanovic, R. T. Sukhavasi, C. Patel, and S. Geirhofer. Network densification: the dominant theme for wireless evolution into 5G. *IEEE Communications Magazine*, 52(2):82–89, February 2014.

[23] F. Jameel, Z. Hamid, F. Jabeen, S. Zeadally, and M. A. Javed. A survey of device-to-device communications: Research issues and challenges. *IEEE Communications Surveys Tutorials*, 20(3):2133–2168, 2018.

[24] N. Chakchouk. A survey on opportunistic routing in wireless communication networks. *IEEE Communications Surveys Tutorials*, 17(4):2214–2241, 2015.

[25] A. Orsino, A. Samuylov, D. Moltchanov, S. Andreev, L. Militano, G. Araniti, and Y. Koucheryavy. Time-dependent energy and resource management in mobility-aware D2D-empowered 5G systems. *IEEE Wireless Communications*, 24(4):14–22, Aug 2017.

[26] A. Orsino, D. Moltchanov, M. Gapeyenko, A. Samuylov, S. Andreev, L. Militano, G. Araniti, and Y. Koucheryavy. Direct connection on the move: Characterization of user mobility in cellular-assisted D2D systems. *IEEE Vehicular Technology Magazine*, 11(3):38–48, Sept 2016.

[27] S. Wu, R. Atat, N. Mastronarde, and L. Liu. Improving the coverage and spectral efficiency of millimeter-wave cellular networks using device-to-device relays. *IEEE Transactions on Communications*, 66(5):2251–2265, May 2018.

[28] A. Omri and M. O. Hasna. A distance-based mode selection scheme for D2D-enabled networks with mobility. *IEEE Transactions on Wireless Communications*, 17(7):4326–4340, July 2018.

[29] A. Orsino, A. Ometov, G. Fodor, D. Moltchanov, L. Militano, S. Andreev, O. N. C. Yilmaz, T. Tirronen, J. Torsner, G. Araniti, A. Iera, M. Dohler, and Y. Koucheryavy. Effects of heterogeneous mobility on D2D- and drone-assisted mission-critical MTC in 5G. *IEEE Communications Magazine*, 55(2):79–87, February 2017.

[30] T. Bai, R. Vaze, and R. W. Heath. Analysis of blockage effects on urban cellular networks. *IEEE Transactions on Wireless Communications*, 13(9):5070–5083, Sept 2014.

[31] T. Bai and R. W. Heath. Coverage and rate analysis for millimeter-wave cellular networks. *IEEE Transactions on Wireless Communications*, 14(2):1100–1114, Feb 2015.

[32] B. Xie, Z. Zhang, and R. Q. Hu. Performance study on relay-assisted millimeter wave cellular networks. In *2016 IEEE 83rd Vehicular Technology Conference (VTC Spring)*, pages 1–5, May 2016.

[33] S. Biswas, S. Vuppala, J. Xue, and T. Ratnarajah. An analysis on relay assisted millimeter wave networks. In *2016 IEEE International Conference on Communications (ICC)*, pages 1–6, May 2016.

[34] N. Wei, X. Lin, and Z. Zhang. Optimal relay probing in millimeter-wave cellular systems with device-to-device relaying. *IEEE Transactions on Vehicular Technology*, 65(12):10218–10222, Dec 2016.

[35] Durgesh Singh and Sasthi C. Ghosh. A distributed algorithm for D2D communication in 5g using stochastic model. In *16th IEEE International Symposium on Network Computing and Applications, NCA 2017, Cambridge, MA, USA, October 30 - November 1, 2017*, pages 459–466, 2017.

[36] D. Singh and S. C. Ghosh. Network-assisted d2d relay selection under the presence of dynamic obstacles. In *2019 IEEE 44th Conference on Local Computer Networks (LCN)*, pages 129–132, 2019.

[37] J. Park and R. W. Heath. Analysis of blockage sensing by radars in random cellular networks. *IEEE Signal Processing Letters*, 25(11):1620–1624, Nov 2018.

[38] M. Alrabeiah, A. Hredzak, and A. Alkhateeb. Millimeter wave base stations with cameras: Vision-aided beam and blockage prediction. In *2020 IEEE 91st Vehicular Technology Conference (VTC2020-Spring)*, pages 1–5, 2020.

[39] G. H. Sim, S. Klos, A. Asadi, A. Klein, and M. Hollick. An online context-aware machine learning algorithm for 5g mmwave vehicular communications. *IEEE/ACM Transactions on Networking*, 26(6):2487–2500, 2018.

[40] H. Zhang, S. Chong, X. Zhang, and N. Lin. A deep reinforcement learning based d2d relay selection and power level allocation in mmwave vehicular networks. *IEEE Wireless Communications Letters*, 9(3):416–419, 2020.

[41] L. Kong, L. Ye, F. Wu, M. Tao, G. Chen, and A. V. Vasilakos. Autonomous relay for millimeter-wave wireless communications. *IEEE Journal on Selected Areas in Communications*, 35(9):2127–2136, 2017.

[42] M. Abu Alsheikh, D. T. Hoang, D. Niyato, H. Tan, and S. Lin. Markov decision processes with applications in wireless sensor networks: A survey. *IEEE Communications Surveys Tutorials*, 17(3):1239–1267, thirdquarter 2015.

[43] K. Kaza, R. Meshram, and S. N. Merchant. Relay employment problem for unacknowledged transmissions: Myopic policy and structure. In *2017 IEEE International Conference on Communications (ICC)*, pages 1–7, May 2017.

[44] Dimitri P. Bertsekas. *Dynamic Programming and Optimal Control, Vol. I, 4th Edition.*

[45] M. Johnston and E. Modiano. Wireless scheduling with delayed csi: When distributed outperforms centralized. *IEEE Transactions on Mobile Computing*, 17(11):2703–2715, 2018.

[46] A. Asadi, Q. Wang, and V. Mancuso. A survey on device-to-device communication in cellular networks. *IEEE Communications Surveys Tutorials*, 16(4):1801–1819, 2014.

[47] G. Yu, L. Xu, D. Feng, R. Yin, G. Y. Li, and Y. Jiang. Joint mode selection and resource allocation for device-to-device communications. *IEEE Transactions on Communications*, 62(11):3814–3824, Nov 2014.

[48] M. Belleschi, G. Fodor, and A. Abrardo. Performance analysis of a distributed resource allocation scheme for D2D communications. In *IEEE GLOBECOM Workshops*, pages 358–362, Dec 2011.

[49] A. Al-Hourani, S. Kandeepan, and A. Jamalipour. Stochastic geometry study on device-to-device communication as a disaster relief solution. *IEEE Transactions on Vehicular Technology*, 65(5):3005–3017, May 2016.

[50] Scott Fowler, Yuan Li, Alberto Pollastro, and Stefano Napoli. Simple network design and power allocation for 5G device-to-device communication. In *19th IEEE International Workshop on Computer Aided Modeling and Design of Communication Links and Networks*, pages 203–207, Dec 2014.

[51] R. Ma, Y. Chang, H. Chen, and C. Chiu. On relay selection schemes for relay-assisted D2D communications in LTE-A systems. *IEEE Transactions on Vehicular Technology*, 66(9):8303–8314, Sept 2017.

[52] S. Dang, G. Chen, and J. P. Coon. Outage performance analysis of full-duplex relay-assisted device-to-device systems in uplink cellular networks. *IEEE Transactions on Vehicular Technology*, 66(5):4506–4510, May 2017.

[53] Y. Yang, Y. Zhang, L. Dai, J. Li, S. Mumtaz, and J. Rodriguez. Transmission capacity analysis of relay-assisted device-to-device overlay/underlay communication. *IEEE Transactions on Industrial Informatics*, 13(1):380–389, Feb 2017.

[54] L. Blackmore, M. Ono, and B. C. Williams. Chance-constrained optimal path planning with obstacles. *IEEE Transactions on Robotics*, 27(6):1080–1094, Dec 2011.

[55] Alexei A Gaivoronski. Stochastic optimization problems in telecommunications. *Applications of stochastic programming*, 5:669–704, 2005.

[56] R. Verdone and A. Zanella. On the effect of user mobility in mobile radio systems with distributed DCA. *IEEE Transactions on Vehicular Technology*, 56(2):874–887, March 2007.

[57] J. Harri, F. Filali, and C. Bonnet. Mobility models for vehicular ad hoc networks: a survey and taxonomy. *IEEE Communications Surveys Tutorials*, 11(4):19–41, 2009.

[58] D. Wu, L. Zhou, Y. Cai, R. Q. Hu, and Y. Qian. The role of mobility for D2D communications in LTE-advanced networks: energy vs. bandwidth efficiency. *IEEE Wireless Communications*, 21(2):66–71, April 2014.

[59] Ó. Helgason, S. T. Kouyoumdjieva, and G. Karlsson. Opportunistic communication and human mobility. *IEEE Transactions on Mobile Computing*, 13(7):1597–1610, July 2014.

[60] O. N. C. Yilmaz, Zexian Li, K. Valkealahti, M. A. Uusitalo, M. Moisio, P. Lundén, and C. Wijting. Smart mobility management for D2D communications in 5G networks. In *IEEE Wireless Communications and Networking Conference Workshops*, pages 219–223, April 2014.

[61] R. Wang, J. Zhang, S. H. Song, and K. B. Letaief. Mobility-aware caching in D2D networks. *IEEE Transactions on Wireless Communications*, 16(8):5001–5015, Aug 2017.

[62] Y. Han, H. Wu, Z. Yang, and D. Li. A new data transmission strategy in mobile D2D networks-deterministic, greedy, or planned opportunistic routing? *IEEE Transactions on Vehicular Technology*, 66(1):594–609, Jan 2017.

[63] Kwang Mong Sim and Weng Hong Sun. Ant colony optimization for routing and load-balancing: survey and new directions. *IEEE Transactions on Systems, Man, and Cybernetics - Part A: Systems and Humans*, 33(5):560–572, Sept 2003.

[64] C. E. Perkins and E. M. Royer. Ad-hoc on-demand distance vector routing. In *Second IEEE Workshop on Mobile Computing Systems and Applications*, pages 90–100, Feb 1999.

[65] R. Tang, J. Zhao, H. Qu, and Z. Zhang. User-centric joint admission control and resource allocation for 5G D2D extreme mobile broadband: A sequential convex programming approach. *IEEE Communications Letters*, 21(7):1641–1644, July 2017.

[66] J. G. Andrews, S. Singh, Q. Ye, X. Lin, and H. S. Dhillon. An overview of load balancing in hetnets: old myths and open problems. *IEEE Wireless Communications*, 21(2):18–25, April 2014.

[67] J. Ye, X. Ge, G. Mao, and Y. Zhong. 5G ultradense networks with nonuniform distributed users. *IEEE Transactions on Vehicular Technology*, 67(3):2660–2670, March 2018.

[68] H. Ding, D. B. da Costa, J. Coon, and Y. Chen. Relay when blocked: A hop-by-hop mmwave cooperative transmission protocol. *IEEE Communications Letters*, 22(9):1894–1897, 2018.

[69] S. Xu, N. Yang, B. He, and H. Jafarkhani. Coverage analysis of relay assisted millimeter wave cellular networks with spatial correlation. In *2020 IEEE Wireless Communications and Networking Conference (WCNC)*, pages 1–8, 2020.

[70] S. Sarkar and S. C. Ghosh. Relay selection in millimeter wave d2d communications through obstacle learning. In *2020 International Conference on COMmunication Systems NETworkS (COMSNETS)*, pages 468–475, 2020.

[71] X. Wang, L. Kong, F. Kong, F. Qiu, M. Xia, S. Arnon, and G. Chen. Millimeter wave communication: A comprehensive survey. *IEEE Communications Surveys Tutorials*, 20(3):1616–1653, 2018.

[72] W. Kim, J. Song, and S. Baek. Relay-assisted handover to overcome blockage in millimeter-wave networks. In *2017 IEEE 28th Annual International Symposium on Personal, Indoor, and Mobile Radio Communications (PIMRC)*, pages 1–5, Oct 2017.

[73] Feng Lu, Diba Mirza, and Curt Schurgers. D-sync: Doppler-based time synchronization for mobile underwater sensor networks. In *Proceedings of the Fifth ACM International Workshop on UnderWater Networks*, WUWNet '10, pages 3:1–3:8, New York, NY, USA, 2010. ACM.

[74] Qifan Pu, Sidhant Gupta, Shyamnath Gollakota, and Shwetak Patel. Whole-home gesture recognition using wireless signals. In *Proceedings of the 19th Annual International Conference on Mobile Computing & Networking*, MobiCom '13, pages 27–38, New York, NY, USA, 2013. ACM.

[75] Fadel Adib, Zachary Kabelac, and Dina Katabi. Multi-person localization via rf body reflections. In *Proceedings of the 12th USENIX Conference on Networked Systems Design and Implementation*, NSDI'15, pages 279–292, Berkeley, CA, USA, 2015. USENIX Association.

[76] Y. Shih, A. Pang, and P. Hsiu. A doppler effect based framework for wi-fi signal tracking in search and rescue operations. *IEEE Transactions on Vehicular Technology*, 67(5):3924–3936, May 2018.

[77] C. Jiao, Z. Zhang, C. Zhong, and Z. Feng. An indoor mmwave joint radar and communication system with active channel perception. In *2018 IEEE International Conference on Communications (ICC)*, pages 1–6, May 2018.

[78] R. Heckel. Super-resolution mimo radar. In *2016 IEEE International Symposium on Information Theory (ISIT)*, pages 1416–1420, July 2016.

[79] M. Pauli, B. Göttel, S. Scherr, A. Bhutani, S. Ayhan, W. Winkler, and T. Zwick. Miniaturized millimeter-wave radar sensor for high-accuracy applications. *IEEE Transactions on Microwave Theory and Techniques*, 65(5):1707–1715, May 2017.

[80] B. Ma, H. Shah-Mansouri, and V. W. S. Wong. Full-duplex relaying for d2d communication in millimeter wave-based 5g networks. *IEEE Transactions on Wireless Communications*, 17(7):4417–4431, 2018.

[81] M. Ibrahim, W. Hamouda, and S. Muhaidat. Spectral efficiency of multi-hop millimeter wave networks using nth best relay routing technique. *IEEE Transactions on Vehicular Technology*, pages 1–1, 2020.

[82] R. T. Rakesh, G. Das, and D. Sen. An analytical model for millimeter wave outdoor directional non-line-of-sight channels. In *2017 IEEE International Conference on Communications (ICC)*, pages 1–6, 2017.

[83] Durgesh Singh and Sasthi C Ghosh. Mobility-aware relay selection in 5g d2d communication using stochastic model. *IEEE Transactions on Vehicular Technology*, 68(3):2837–2849, 2019.

[84] Y. Liu, X. Fang, M. Xiao, and S. Mumtaz. Decentralized beam pair selection in multi-beam millimeter-wave networks. *IEEE Transactions on Communications*, 66(6):2722–2737, 2018.

[85] M. Feng, S. Mao, and T. Jiang. Dealing with link blockage in mmwave networks: D2d relaying or multi-beam reflection? In *2017 IEEE 28th Annual International Symposium on Personal, Indoor, and Mobile Radio Communications (PIMRC)*, pages 1–5, 2017.

[86] Danlu Zhang and K. M. Wasserman. Transmission schemes for time-varying wireless channels with partial state observations. In *Proceedings.Twenty-First Annual Joint Conference of the IEEE Computer and Communications Societies*, volume 2, pages 467–476, 2002.

[87] A. Laourine and L. Tong. Betting on gilbert-elliot channels. *IEEE Transactions on Wireless Communications*, 9(2):723–733, 2010.

[88] A. K. Karmokar, D. V. Djonin, and V. K. Bhargava. Pomdp-based coding rate adaptation for type-i hybrid arq systems over fading channels with memory. *IEEE Transactions on Wireless Communications*, 5(12):3512–3523, 2006.

[89] M. Kashef and A. Ephremides. Optimal packet scheduling for energy harvesting sources on time varying wireless channels. *Journal of Communications and Networks*, 14(2):121–129, 2012.

[90] D. Dzung, R. Guerraoui, D. Kozhaya, and Y. Pignolet. To transmit now or not to transmit now. In *2015 IEEE 34th Symposium on Reliable Distributed Systems (SRDS)*, pages 246–255, 2015.

[91] M. Johnston, I. Keslassy, and E. Modiano. Channel probing in opportunistic communication systems. *IEEE Transactions on Information Theory*, 63(11):7535–7552, 2017.

[92] Dacfey Dzung, Rachid Guerraoui, David Kozhaya, and Yvonne Anne Pignolet. Source routing in time-varing lossy networks. pages 200–215, 01 2015.

[93] B. R. Badrinath and P. Sudame. To send or not to send: implementing deferred transmissions in a mobile host. In *Proceedings of 16th International Conference on Distributed Computing Systems*, pages 327–333, 1996.

[94] Mohd Naseem and Chiranjeev Kumar. Congestion-aware fibonacci sequence based multipath load balancing routing protocol for MANETs. *Wireless Personal Communications*, 84(4):2955–2974, Oct 2015.

[95] In Keun Son and Shiwen Mao. An reformulation-linearization technique-based approach to joint topology design and load balancing in FSO networks. In *Proceedings of the Global Communications Conference*, pages 1–6, 2010.

[96] B. B. Nandi, A. Banerjee, S. C. Ghosh, and N. Banerjee. Stochastic VM multiplexing for datacenter consolidation. In *Ninth IEEE International Conference on Services Computing*, pages 114–121, June 2012.

[97] Athanasios Papoulis and S. Unnikrishna Pillai. *Probability, Random Variables, and Stochastic Processes*. McGraw Hill, Boston, fourth edition, 2002.

[98] Michael R. Garey and David S. Johnson. *Computers and Intractability; A Guide to the Theory of NP-Completeness*. W. H. Freeman & Co., New York, NY, USA, 1990.

[99] Andrea Goldsmith. *Wireless Communications*. Cambridge University Press, 2005.

[100] S. Sun, T. S. Rappaport, M. Shafi, P. Tang, J. Zhang, and P. J. Smith. Propagation models and performance evaluation for 5g millimeter-wave bands. *IEEE Transactions on Vehicular Technology*, 67(9):8422–8439, Sept 2018.

[101] R. Congiu, H. Shokri-Ghadikolaei, C. Fischione, and F. Santucci. On the relay-fallback tradeoff in millimeter wave wireless system. In *2016 IEEE Conference on Computer Communications Workshops (INFOCOM WKSHPS)*, pages 622–627, April 2016.

[102] Akram Al-Hourani, Sathyanarayanan Chandrasekharan, and Sithamparanathan Kandeepan. Path loss study for millimeter wave device-to-device communications in urban environment. In *Communications Workshops (ICC), 2014 IEEE International Conference on*, pages 102–107. IEEE, 2014.

[103] J. Lianghai, A. Klein, N. Kuruvatti, and H. D. Schotten. System capacity optimization algorithm for d2d underlay operation. In *2014 IEEE International Conference on Communications Workshops (ICC)*, pages 85–90, June 2014.

[104] M. Dong and T. Kim. Reliability of an urban millimeter wave communication link with first-order reflections. In *2016 IEEE Global Communications Conference (GLOBECOM)*, pages 1–6, Dec 2016.

[105] S. Wu, R. Atat, N. Mastronarde, and L. Liu. Coverage analysis of d2d relay-assisted millimeter-wave cellular networks. In *2017 IEEE Wireless Communications and Networking Conference (WCNC)*, pages 1–6, March 2017.

[106] T. S. Rappaport, G. R. MacCartney, M. K. Samimi, and S. Sun. Wideband millimeter-wave propagation measurements and channel models for future wireless communication system design. *IEEE Transactions on Communications*, 63(9):3029–3056, Sep. 2015.

[107] K. Belbase, Z. Zhang, H. Jiang, and C. Tellambura. Coverage analysis of millimeter wave decode-and-forward networks with best relay selection. *IEEE Access*, 6:22670–22683, 2018.

[108] Holger Füßler, Jörg Widmer, Michael Käsemann, Martin Mauve, and Hannes Hartenstein. Contention-based forwarding for mobile ad hoc networks. *Ad Hoc Networks*, 1(4):351 – 369, 2003.

[109] Liyan Su, Chenyang Yang, Zhikun Xu, and Andreas F. Molisch. Energy-efficient downlink transmission with base station closing in small cell networks. In *2013 IEEE International Conference on Acoustics, Speech and Signal Processing*, pages 4784–4788, 2013.

[110] Takehiro Nakamura, Satoshi Nagata, Anass Benjebbour, Yoshihisa Kishiyama, Tang Hai, Shen Xiaodong, Yang Ning, and Li Nan. Trends in small cell enhancements in lte advanced. *IEEE Communications Magazine*, 51(2):98–105, 2013.